Numéro d'ordre : 110 - 2014 Année 2014

Université Claude Bernard Lyon 1
Institut Camille Jordan - UMR 5208
École doctorale InfoMaths

Thèse de l'Université de Lyon
pour l'obtention du
Diplôme de Doctorat

Spécialité : Mathématiques
(arrêté du 7 août 2006)

Présentée par
Benoît Laslier

Dynamique stochastique d'interface discrète et modèles de dimères

Thèse dirigée par Fabio Toninelli,
soutenue publiquement le 2 juillet 2014,
devant un jury composé de :

Thierry Bodineau	CNRS et École Polytechnique	Rapporteur
Cedric Boutillier	Université Paris 6	Examinateur
Giambattista Giacomin	Université Paris 7	Examinateur
Fabio Martinelli	Universita di Roma Tre	Rapporteur
Christophe Sabot	Université Lyon 1	Examinateur
Fabio Toninelli	CNRS et Université Lyon 1	Directeur

Résumé

Nous avons étudié la dynamique de Glauber sur les pavages de domaines finies du plan par des losanges ou par des dominos de taille 2×1. Ces pavages sont naturellement associés à des surfaces de $\mathbb{R}^3$, qui peuvent être vues comme des interfaces dans des modèles de physique statistique. En particulier les pavages par des losanges correspondent au modèle d'Ising tridimensionnel à température nulle. Plus précisément les pavages d'un domaine sont en bijection avec les configurations d'Ising vérifiant certaines conditions au bord (dépendant du domaine pavé). Ces conditions forcent la coexistence des phases $+$ et $-$ ainsi que la position du bord de l'interface.

Dans la limite thermodynamique où L, la longueur caractéristique du système, tend vers l'infini, ces interfaces obéissent à une loi des grand nombre et convergent vers une forme limite déterministe ne dépendant que des conditions aux bord.

Dans le cas où la forme limite est planaire et pour les losanges, Caputo, Martinelli et Toninelli [CMT12] ont montré que le temps de mélange T_{mix} de la dynamique est d'ordre $O(L^{2+o(1)})$ (scaling diffusif). Dans le chapitre 3 nous avons généralisé ce résultat aux pavages par des dominos, toujours dans le cas d'une forme limite planaire. Nous avons aussi prouvé une borne inférieure $T_{\text{mix}} \geq cL^2$ qui améliore d'un facteur log le résultat de [CMT12].

Dans le cas où la forme limite n'est pas planaire, elle peut être analytique ou bien contenir des parties "gelées" où elle est en un sens dégénérée. Dans le cas où elle n'a pas de telle partie gelée, et pour les pavages par des losanges, nous avons montré que la dynamique de Glauber devient "macroscopiquement proche" de l'équilibre en un temps $L^{2+o(1)}$ (chapitre 2).

Mots clés : Temps de mélange, dynamique de Glauber, pavage par des losanges, pavage par des dominos, mouvement par courbure moyenne.

Abstract

We studied the Glauber dynamics on tilings of finite regions of the plane by lozenges or 2×1 dominoes. These tilings are naturally associated with surfaces of $\mathbb{R}^3$, which can be seen as interfaces in statistical physics models. In particular, lozenge tilings correspond to three dimensional Ising model at zero temperature. More precisely, tilings of a finite regions are in bijection with Ising configurations with some boundary conditions (depending on the tiled domain). These boundary conditions impose the coexistence of the $+$ and $-$ phases, together with the position of the boundary of the interface.

In the thermodynamic limit where L, the characteristic length of the system, tends toward infinity, these interface follow a law of large number and converge to a deterministic limit shape depending only on the boundary condition.

When the limit shape is planar and for lozenge tilings, Caputo, Martinelli and Toninelli [CMT12] showed that the mixing time of the dynamics is of order $L^{2+o(1)}$ (diffusive scaling). In the chapter 3 we generalized this result to domino tilings, always in the case of a planar limit shape. We also proved a lower bound $T_{\text{mix}} \geq cL^2$ which improve on the result of [CMT12] by a log factor.

When the limit shape is not planar, it can either be analytic or have some "frozen" domains where it is degenerated in a sense. When it does not have such frozen region, and for lozenge tilings, we showed that the Glauber dynamics becomes "macroscopically close" to equilibrium in a time $L^{2+o(1)}$.

Key words : Mixing time, Glauber dynamics, lozenge tiling, domino tiling, mean curvature motion.

Remerciements

Je remercie infiniment mon directeur Fabio Toninelli. Il restera toujours un mentor pour moi. Merci de m'avoir fait découvrir un très beau sujet et de m'y avoir guidé avec beaucoup de tact.

Je remercie chaleureusement les rapporteurs Thierry Bodineau et Fabio Martinelli d'avoir accepté d'évaluer mon travail. Un grand merci aussi à Thierry pour m'avoir conseillé dans le choix de mon directeur de thèse, je n'aurai pas pu espérer de meilleurs conseils. Je remercie aussi les autres membres du jury, Cédric Boutillier, Giambatista Giacomin et Christophe Sabot.

Merci à tous les membres de l'ICJ qui ont fait de ces années un vrai plaisir, en particulier le groupe de 11h38, Adrianne, Blanche, Colin, Coline, Corentin, Élodie, François D, François V, Hugo, Luigia, Mathias, Niccolò, Quentin, Thomas, Xiaolin, sans oublier les pièces rapportées, les deux Céciles, François L, Fred. Merci à Damien pour sa compagnie au laboratoire de Physique. Un très grand merci aussi à Adrianne pour son travail de relecture.

Je n'oublie pas ma famille. Je leur dois bien sûr plus que je ne saurais le dire.

Enfin un très grand merci à Rafael et Alejandro pour avoir supporté notre cohabitation.

Table des matières

Chapitre 1

Introduction

1.1 Motivations physiques

1.1.1 La physique statistique, notre cadre général

Notre étude se place dans le cadre de la physique statistique. On peut considérer que l'observation fondamentale à l'origine de ce domaine est que la physique habituelle à l'échelle macroscopique, en particulier la thermodynamique, donne une description très satisfaisante des phénomènes physiques que l'on observe sous des conditions "habituelles". Ainsi il est presque toujours possible d'ignorer la structure infinitésimale discrète des objets physiques macroscopiques et de les décrire par des modèles effectifs n'ayant que peu de variables. Bien que présente au quotidien, cette simplification n'a rien a priori d'évident et est même plutôt étonnante. En effet d'un point de vue microscopique rigoureux, un système physique macroscopique est extrêmement complexe : il a un nombre considérable de variables en interactions et des comportements très chaotiques. Il est donc naturel de s'interroger sur les raisons pour lesquelles une telle réduction peut se produire.

Bien évidemment, cette question a été amplement étudiée par la communauté physique, et on peut dire qu'elle est globalement très bien comprise au niveau phénoménologique. Cependant il reste des difficultés à plusieurs niveaux. En particulier même si l'on dispose d'idées générales et d'une compréhension intuitive relativement précise de comment une physique macroscopique "simple" apparaît comme résultat d'interactions microscopiques complexes, il est souvent difficile d'appliquer ces idées à des systèmes physiques réalistes car des obstacles techniques importants arrivent rapidement. Par ailleurs, d'un point de vue mathématique, déduire un comportement macroscopique à partir d'une description microscopique utilisant des lois connues est un problème bien posé. Il s'est ainsi développé une littérature mathématique importante (physique statistique rigoureuse) visant notamment à justifier (et vérifier) de manière complètement rigoureuse les résultats et les intuitions des physiciens.

Notons que la physique statistique ne se restreint pas à l'étude de systèmes à l'équilibre thermodynamique mais aussi à des systèmes stationnaires hors équilibre et à des systèmes non stationnaires. La différence entre l'équilibre et la simple stationnarité est qu'un état d'équilibre doit pouvoir être stable de manière autonome alors que dans un état stationnaire il peut y avoir des apports constants de l'extérieur. Une autre manière de voir la différence est qu'un système à l'équilibre doit être invariant par renversement du temps contrairement à un état seulement stationnaire. En particulier dans une situation stationnaire hors équilibre il y a a priori une production constante d'entropie qui rend l'évolution irréversible. Un exemple typique d'état stationnaire hors équilibre est l'écoulement de l'eau dans un tube entre deux réservoirs (supposés infinis) de pression différente. Le système n'est pas à l'équilibre car le flux de matière ne se maintient que par l'action continue des réservoirs. Remarquons que la physique statistique hors équilibre est en général beaucoup plus complexe que le cas de l'équilibre.

Dans cette thèse nous ne considérerons toutefois que des systèmes à l'équilibre ou des systèmes non stationnaires mais qui convergent vers une situation d'équilibre. En particulier les dynamiques que nous considérerons seront toujours réversibles par rapport à leur mesure invariante, ce qui correspond à la symétrie par renversement du temps évoquée plus haut.

1.1.2 Le système physique étudié

La situation physique à laquelle nous nous intéresserons est l'interface entre deux phases thermodynamiques en coexistence.

Par phase thermodynamique nous entendons bien sûr les trois états de la matière, solide, liquide, gazeuse, mais aussi n'importe quelle situation où un système physique "choisit" une forme d'organisation parmi plusieurs possibilités. Par exemple dans un aimant (en dessous de la température de Curie), chaque direction moyenne d'aimantation correspond à une phase, même si ces phases ne diffèrent que par le choix d'une orientation. Dans un mélange d'eau et de sel, le sel peut apparaître soit dissout dans l'eau soit sous forme de cristal, ce qui représente deux phases correspondant à des organisations qualitativement différentes, comme dans le cas des états de la matière.

Lorsque deux phases distinctes se trouvent en contact, deux situations très différentes peuvent se présenter. La plus habituelle est celle où l'une des phases est instable et vouée à disparaître, par exemple un glaçon déposé dans de l'eau maintenue à température positive. Cependant ici nous étudierons le cas d'une interface entre deux phases stables, c'est-à-dire le mélange eau-glace à exactement 0°C. En termes de fonctions thermodynamiques, cela correspond au fait que les énergies libres des deux phases (dans le "bulk") soient égales. Dans ce cas il est plus difficile de voir qu'il y a bien une évolution macroscopique à partir de l'expérience quotidienne car les mouvement

se font à des échelles de temps sont beaucoup plus longues. Par ailleurs il est clair par symétrie qu'une interface plane infinie n'aura pas de mouvement macroscopique donc que les situations les plus simples peuvent effectivement être statiques. On peut néanmoins se convaincre qu'il doit exister une évolution en remarquant que l'interface doit avoir un coût énergétique. En effet, si ce n'était pas le cas, des interfaces se créeraient spontanément à partir d'une phase homogène et on ne parlerait pas de deux phases distinctes mais d'une seule correspondant au mélange. Par conséquent les situations où l'interface a une grande surface sont défavorables énergétiquement et devraient donc disparaître avec le temps. Ainsi, une interface plane devrait être stable mais une interface très irrégulière devrait être "lissée" avec le temps (phénomène de "coarsening") et avoir une dynamique non triviale. Notons par ailleurs que dans certains systèmes, par exemple pour les aimants, l'existence de plusieurs phases stables est très commune dans des conditions physiques réalistes.

Un point important est que nous ne considérerons que des situations où il n'y a pas de paramètre d'ordre conservé, c'est-à-dire que chacune des phases peut librement croître ou diminuer. C'est clairement le cas dans un mélange eau/glace ou dans un aimant mais pas pour le cas eau/sel puisque le nombre d'atomes de sel est conservé (cependant voir la partie 1.2.2).

1.1.3 Théorie phénoménologique de l'équilibre

Comme indiqué dans la partie 1.1.1, on comprend assez bien le comportement macroscopique de l'interface en utilisant les principes généraux de la physique statistique à un niveau non rigoureux. On obtient ainsi une théorie phénoménologique que nous présentons maintenant.

La remarque fondamentale est que l'interface est une forme de défaut et a donc un coût en énergie libre que l'on appelle habituellement énergie d'interface ou tension superficielle. Il est naturel, sous des hypothèses de localité des interactions, de supposer que cette tension dépend uniquement de la pente locale et que le coût total d'une interface dont la forme globale est une surface S est :

$$E(S) = \int_S \sigma(\vec{n}_S(x))d\Sigma,$$

avec avec $\vec{n}_S(x)$ le vecteur normal à S au point x et $d\Sigma$ l'élément infinitésimal d'aire. On peut identifier $\sigma(\vec{n})$ en considérant le cas d'une surface plane : c'est la différence entre le coût énergétique proprement dit et le gain d'entropie dû à l'interface (en pratique, dans notre application, seul le terme entropique contribuera). On peut aussi décrire $\sigma(\vec{n})$ comme la différence d'énergie libre entre le système avec une interface de pente $\vec{n}$ d'aire 1 et un système, de même volume, avec une seule phase.

Si le système est invariant par rotation (par exemple pour une interface liquide-liquide), alors σ doit l'être aussi et $E(S)$ devient simplement proportionnelle à l'aire de S. Quand le système a une orientation privilégiée (par exemple les axes du réseau des atomes dans un aimant), σ est a priori non triviale. Par contre, des principes généraux de thermodynamique impliquent que σ sera toujours convexe. Plus précisément si $\tilde{\sigma}(\vec{n}) = \sigma(\frac{\vec{n}}{\|\vec{n}\|})$ étend σ à tous les vecteurs non nuls, alors $\tilde{\sigma}$ est convexe.

Une première conséquence triviale de ce coût associé à l'interface est que dans un système "libre" il n'y a pas d'interface, ce qui est cohérent avec la notion de phase. Cependant il est possible de forcer un système à l'équilibre à avoir une interface en imposant des contraintes au bord. Dans ce travail, nous nous intéresserons à une boîte finie dont les bords sont arbitrairement contraints à rester indéfiniment dans une phase ou l'autre selon qu'ils sont au-dessus ou en dessous d'une certaine courbe qui détermine donc la position de l'interface au bord du domaine (voir figure 1.1). On s'attend alors à ce que l'interface adopte à l'équilibre une forme minimisant la tension superficielle parmi toutes les surfaces compatibles avec les conditions au bord. Si le bord de l'interface est inclus dans un plan, alors la convexité de la tension superficielle σ implique que la forme optimale est plate. Par contre, dans le cas général, ces formes sont complexes : même dans le cas invariant par rotation, on obtient la surface d'aire minimale de bord donné qui n'est pas particulièrement simple. Remarquons que l'existence de formes macroscopiques non triviales à l'équilibre ne peut pas être capturée par un modèle en deux dimension. En effet, la courbe minimisant la tension de surface à bord (i.e. extrémités) fixé est toujours le segment reliant les extrémités qui est macroscopiquement plat.

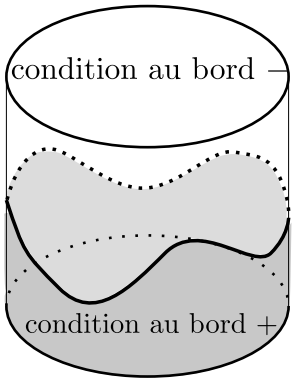

FIGURE 1.1: Conditions au bord utilisées pour forcer l'existence d'une interface s'appuyant sur une courbe donnée.

On s'attend à observer de petites fluctuations thermiques de l'interface autour de sa forme moyenne. Pour déterminer heuristiquement leur ordre de grandeur, imaginons que l'interface se comporte comme une membrane élastique, qui a une configuration d'équilibre déterminée par les conditions au bord et telle qu'un petit déplacement par rapport à l'équilibre ait un coût énergétique proportionnel à l'intégrale du carré du gradient de la perturbation. Cette simplification amène à s'attendre à ce que dans un cadre tridimensionnel (surface à deux dimension dans $\mathbb{R}^3$) les fluctuations soient logarithmiques en la taille du système, comme dans un champ libre gaus-

sien (voir dans partie 1.3.2, après la conjecture 1.3.6). Par contre pour des courbes d'interface dans $\mathbb{R}^2$ ces fluctuations devraient être d'ordre racine (comme la hauteur d'un pont brownien par exemple).

1.1.4 Théorie phénoménologique hors équilibre

Si l'on considère un système présentant initialement une interface macroscopique dans une position ne minimisant pas l'énergie (bulle d'une phase dans une autre, surface non minimale), on s'attend à observer une évolution macroscopique déterministe. Puisque le système cherche à minimiser l'énergie, une première intuition sur la forme que devrait prendre cette évolution est qu'elle devrait être un flot gradient par rapport à l'énergie $E(S)$. Le système devrait évoluer en cherchant à tout instant à minimiser la tension de surface le plus rapidement possible, comme une goutte de miel sur une surface courbée dont la vitesse est toujours dans la direction de plus grande pente.Remarquons cependant que l'interface vit dans un espace de dimension infinie, ce qui rend le processus plus compliqué. Localement, l'interface peut s'écrire comme le graphe d'une fonction h et la dynamique s'écrie sous forme d'équation différentielle :

$$\frac{\mathrm{d}h}{\mathrm{d}t} = \sum_{i,j\in\{1;2\}} \left((\partial^2_{ij}\tilde{\sigma}) \circ \nabla h\right) \partial^2_{ij} h$$

où $\tilde{\sigma}$ est la forme de σ après le changement de variable, et où $(\partial^2_{ij}\tilde{\sigma}) \circ \nabla h$ est simplement la fonction $\partial^2_{ij}\tilde{\sigma}$ appliquée au point ∇h. Dans le cas invariant par rotation, cette équation devient celle du *mouvement par courbure moyenne*, et dans le cas général on peut simplement penser à une variante non linéaire de celui-ci.

Cependant, l'équation ci-dessus est incomplète dans la mesure où elle ne prend pas en compte la nature de la dynamique ! En pratique, il n'y a aucune raison de supposer que la vitesse à laquelle la dynamique peut faire diminuer la tension de surface est invariante par rotation. Il est donc nécessaire d'ajouter un facteur, dit de *mobilité*, μ pour prendre en compte cette dépendance. De même que l'énergie ne dépend que de la pente de la surface, il est naturel de supposer que c'est aussi le cas de la mobilité. Par ailleurs, puisqu'il s'agit de représenter le fait que le temps caractéristique d'évolution dépend de la pente, ce terme doit être ajouté comme un facteur global. On obtient donc, toujours en coordonnées locales :

$$\frac{\mathrm{d}h}{\mathrm{d}t} = \tilde{\mu}(\nabla h) \sum_{i,j\in\{1;2\}} \left((\partial^2_{ij}\tilde{\sigma}) \circ \nabla h\right) \partial^2_{ij} h. \tag{1.1}$$

Le facteur μ est en général difficile à connaître précisément. Dans le cadre de la théorie de la réponse linéaire, on peut écrire (voir [Spo93]) une formule de type Green-Kubo qui exprime $\mu(\vec{n})$ en fonction de corrélations

à l'équilibre mais qui n'est calculable que dans des cas particuliers. En effet la formule est une intégrale sur les corrélations spatio-temporelles, c'est-à-dire des lois de probabilité jointes pour des événements se passant en des points et à des instants différents, pour la dynamique qui part de son état d'équilibre avec une interface infinie et plane.

Enfin le dernier élément fondamental dans la définition de l'évolution générale est l'échelle de temps globale en fonction de la taille du système. Dans notre cadre de phases en coexistence, on s'attend à ce que les mouvements macroscopiques se produisent à une échelle L^2, où L est la longueur caractéristique du système. On parle "d'échelle diffusive" ou plus habituellement en anglais de "diffusive scaling". On peut justifier cette échelle par un argument de cohérence dans le cas d'un système invariant par rotation évoluant selon un mouvement par courbure moyenne. La vitesse de disparition pour une grande bulle de rayon L ne doit pas dépendre de l'échelle choisie pour la description macroscopique. Sachant que pour un mouvement par courbure moyenne, une bulle de rayon r met un temps r^2 à disparaître, on constate facilement que L^2 est la seule normalisation possible du temps.

Une autre justification, plus microscopique, de l'échelle diffusive L^2 sera donnée dans la partie 1.2.4 et elle fera intervenir le fait que l'évolution de l'interface se produit grâce à un processus de diffusion de ses gradients microscopiques.

1.2 Modélisation mathématique

Comme nous l'avons dit plus haut, notre objectif est de prouver que la théorie phénoménologique ci dessus est correcte en partant d'une description microscopique. Malheureusement il n'est pas possible de traiter la véritable dynamique physique et nous nous concentrons donc sur un modèle effectif simplifié.

1.2.1 Les pavages par des losanges, un modèle effectif d'interface

Notre modèle principal pour les interfaces sera les bords d'empilements de cubes, voir figure 1.2 pour un exemple. On remarque immédiatement que le dessin d'un empilement définit un pavage par des losanges d'une région du plan. La forme globale et la structure locale du bord de cette région définissent une courbe dans l'espace sur laquelle s'appuie l'interface. Elle correspond à la courbe définissant les conditions au bord dans la figure 1.1. Par ailleurs, l'empilement est forcément "plein" ou "monotone", c'est-à-dire que l'on peut s'imaginer que les cubes sont en équilibre sous l'effet de la gravité (les cubes sont orientés avec une grande diagonale dans l'axe vertical donc ont un sommet pointé vers le bas ; en d'autres termes la gravité est orientée dans la direction $(-1, -1, -1)$).

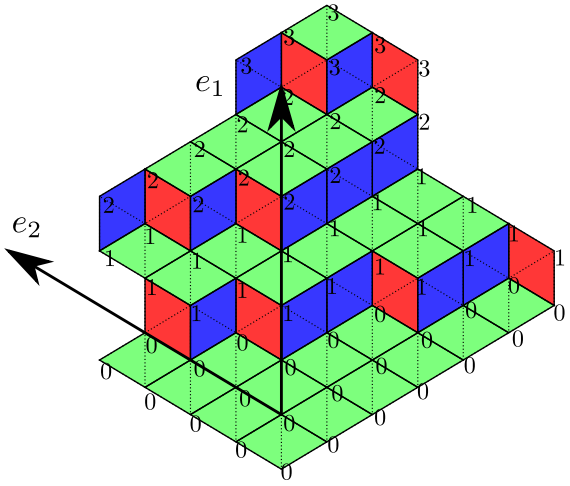

FIGURE 1.2: Un exemple d'empilement de cube représenté en perspective par un pavage par des losanges. La "fonction de hauteur" correspondante est indiquée.

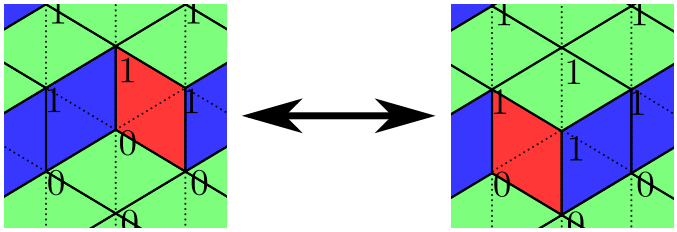

FIGURE 1.3: Un mouvement élémentaire de la dynamique. En termes de pavages on fait une rotation de trois losanges, en terme d'empilement on ajoute ou enlève un cube et en terme de modèle d'Ising on change le signe d'un site.

Ces interfaces apparaissent naturellement dans le cadre du modèle d'Ising sur $\mathbb{Z}^3$ à température nulle. En effet dans le modèle d'Ising à plus proches voisins, à chaque site de $\mathbb{Z}^3$ est associé un signe "+" ou "−" et l'énergie d'une configuration est simplement le nombre de désaccords entre voisins. À température nulle, les phases stables sont triviales : tout les site + ou −. Il est assez simple de voir que les surfaces que nous considérons correspondent exactement aux états d'énergie minimum pour le modèle d'Ising avec des conditions au bord fixées comme dans la figure 1.1. À température nulle, la mesure d'Ising devient la mesure uniforme sur toutes ces configurations et il est donc naturel d'appeler *mesure d'équilibre* la mesure uniforme sur les pavages.

La dynamique que nous considérerons est très simple : à chaque endroit où l'on peut ajouter ou retirer un cube et pour chaque intervalle de temps

infinitésimal $\mathrm{d}t$, on fait un mouvement avec probabilité $\mathrm{d}t$, indépendamment de tous les autres endroits (plus rigoureusement on utilise des processus de Poisson indépendants, voir la partie 2.3 pour une définition précise). Elle est appelée *dynamique de Glauber*. Il est clair que la dynamique est irréductible, récurrente et que la mesure uniforme est réversible, c'est-à-dire que pour chaque paire de pavages (P, P'), la probabilité de voir une transition de P à P' est la même que celle de voir une transition de P' à P. La réversibilité de la mesure uniforme justifie a posteriori le fait de la considérer comme l'équilibre du système.

1.2.2 Hypothèses et simplifications du modèle

Le modèle de pavage par des losanges est clairement très loin d'une description exacte d'un système physique. Il contient un certain nombre de simplifications ou d'approximations par rapport à la réalité que nous présentons ici. Notons qu'il ne s'agit pas du tout du seul modèle effectif d'interface bien défini mathématiquement et que la plupart des approximations détaillées ici concernent aussi les autres modèles que nous mentionnerons dans la partie 1.2.3.

La première simplification fondamentale du modèle est le fait de ne regarder que l'interface et d'oublier complètement la structure microscopique de l'intérieur des deux phases. Plus précisément l'interaction entre les phases est résumée par les mouvements aléatoires de l'interface. Remarquons que la modélisation par des variables aléatoires d'un système dont l'état microscopique est inconnu est un des fondements de la physique statistique qu'il serait vain de rediscuter ici. Enfin, remarquons qu'indépendamment de la nature physique du système que l'on considère, comme nous nous plaçons à l'équilibre l'interface doit avoir autant de chance de se déplacer dans les deux directions.

Une deuxième simplification est de considérer une dynamique microscopique markovienne (i.e. sans mémoire) et dont la loi ne dépend pas de l'état global de l'interface mais seulement de la structure locale. Physiquement cela correspond à dire que les mouvements de l'interface ne modifient pas la structure des deux phases. Dans certains cas, comme celui d'un aimant, cette hypothèse est physiquement raisonnable : il paraît peu probable qu'un changement d'orientation pour un spin à l'interface modifie l'alignement des spins loin de l'interface. Dans des systèmes où une quantité est conservée, on peut parfois retrouver la même simplification quand le système est grand. En particulier pour la dissolution du sel, en toute rigueur, dans un volume d'eau fini, si des fluctuations amènent le cristal de sel à un volume particulièrement petit, alors elles ont aussi rendu l'eau trop riche en sel et le cristal n'est plus à l'équilibre mais doit grossir. Cependant, si le volume d'eau est très grand par rapport au volume du cristal (et si la mise à l'équilibre de la densité de sel est assez rapide), on peut supposer la densité de sel constante et retrou-

ver notre hypothèse. Le fait de considérer une chaîne de Markov correspond à une hypothèse de séparation des échelles de temps. Les mouvements de l'interface sont relativement lents alors que dans le bulk, la relaxation vers l'équilibre est très rapide donc on peut négliger tout régime transitoire dans le bulk et supposer qu'il est toujours à l'équilibre.

La troisième simplification, et certainement celle qui s'éloigne le plus de la réalité, est de considérer que l'interface ne produit jamais de structure complexe comme des surplombs ou des îlots, et qu'elle n'a pas d'épaisseur. Remarquons que cette simplification est implicite dès lors que l'on décrit la surface par un pavage par des losanges dans la mesure où les empilements de cubes pouvant être représentés par un pavage sont justement ceux qui n'ont pas de telle complication. Physiquement, cette hypothèse peut se justifier dans une limite de température nulle. En effet, il est naturel de considérer qu'il y a un coût énergétique associé à l'interface qui croît avec la surface de celle-ci. Les surplombs sont donc énergétiquement défavorables et doivent disparaître à température nulle. Cette limite de température nulle appelle quelques commentaires. Premièrement elle signifie seulement que les énergies d'interactions dominent les fluctuations thermiques $k_B T$. Selon les systèmes étudiés cela peut être le cas même à température ambiante (la physique des semi conducteur étant un exemple classique). Deuxièmement on voit souvent un système à température nulle comme complètement figé. En réalité, même à température strictement nulle, il peut y avoir une évolution à condition que le minimum d'énergie soit atteint en plusieurs états, comme c'est le cas dans notre modèle d'empilement de cube (si l'on considère que le coût énergétique de l'interface est directement donné par sa surface).

Enfin les dernières simplifications majeures sont : une description classique et non quantique de la matière, la discrétisation de l'espace et le fait de ne considérer que des mouvements d'un site à la fois. Remarquons cependant que le choix de la dynamique n'influe pas sur les résultats d'équilibre et qu'il est nécessaire de faire un choix arbitraire dans la définition de la dynamique.

Même si les simplifications présentées ci-dessus sont radicales et ne s'appliquent probablement qu'à peu de systèmes physiques, il faut noter qu'elles sont nécessaires pour obtenir un modèle à la fois bien posé et assez simple pour pouvoir être étudié finement au niveau mathématique. En particulier, le fait de se placer à température nulle est fondamental pour notre étude car nous utiliserons des résultats exacts de nature combinatoire qui s'effondrent complètement sans cette hypothèse (voir partie 1.3.1).

1.2.3 Autres modèles effectifs d'interface

Le modèle de pavage du plan par des losanges n'est pas le seul modèle effectif d'interface étudié d'un point de vue mathématique.

Un autre modèle très proche des pavages par des losanges est les pavages

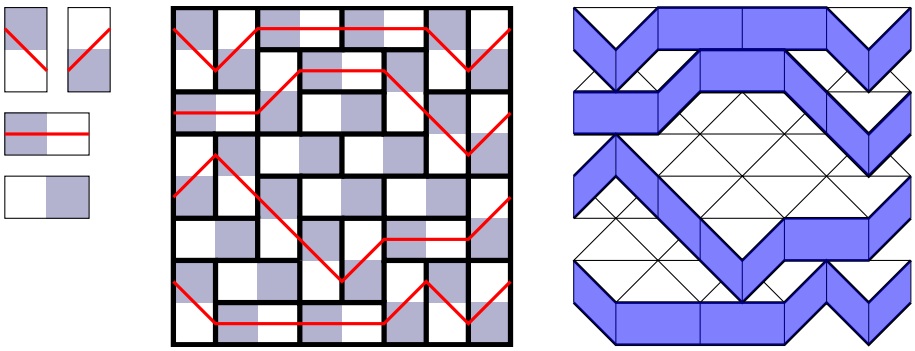

FIGURE 1.4: La construction de la fonction de hauteur pour les pavages par des dominos. Les lignes rouges pleine sont obtenues en dessinant un trait indépendamment dans chaque domino selon les règles données à gauche. Pour passer du pavage à la représentation en perspective, on ne conserve que les chemins que l'on trace comme des bandes. Il est clair que le dessin à droite est une représentation en perspective d'un empilement de prismes à base triangulaire. Les trais fins représentent les bords de ces prismes.

par des rectangles de taille 2×1 (ou "domino"). Bien que cela ne soit pas directement visuel comme dans le cas des losanges, on peut aussi associer à chaque pavage par des dominos une fonction de hauteur et ainsi l'interpréter comme une interface dans $\mathbb{R}^3$ (voir figure 1.4). On peut considérer que la principale différence entre ces deux modèles est l'utilisation d'une discrétisation différente de l'espace.

On peut encore généraliser ces deux modèles pour obtenir la classe des modèles de dimères sur des réseaux bipartis, qui sera le cadre le plus général que nous considérerons dans ce travail. Dans ces modèles, on fixe un graphe biparti infini périodique puis on considère l'ensemble des *appariements parfaits* où *recouvrement par des dimères* d'un sous-graphe fini G. Par appariement parfait, nous entendons un ensemble de paires de sommets de G tel que d'une part, deux sommets associées soient toujours voisins dans G et d'autre part, chaque sommet soit associé à exactement un autre. On peut aussi le voir comme un ensemble E d'arêtes tel que chaque sommet soit l'extrémité d'une et d'une seule arête de E. Rappelons qu'un graphe est dit biparti si ses sommets peuvent être colorié de deux couleurs (noir et blanc) de sorte à ce que deux sommets voisins soient toujours de couleur différente. Il est facile de vérifier (voir figure 1.5) que les pavages par des losanges correspondent au réseau hexagonal et que les pavages de dominos correspondent au réseau carré. Ces modèles peuvent aussi être interprétés comme des surfaces dans $\mathbb{R}^3$, même si la construction est trop longue pour être exposée ici (voir partie 4.4.1), et forment un cadre naturel pour beaucoup des méthodes combinatoires que nous utiliserons ici.

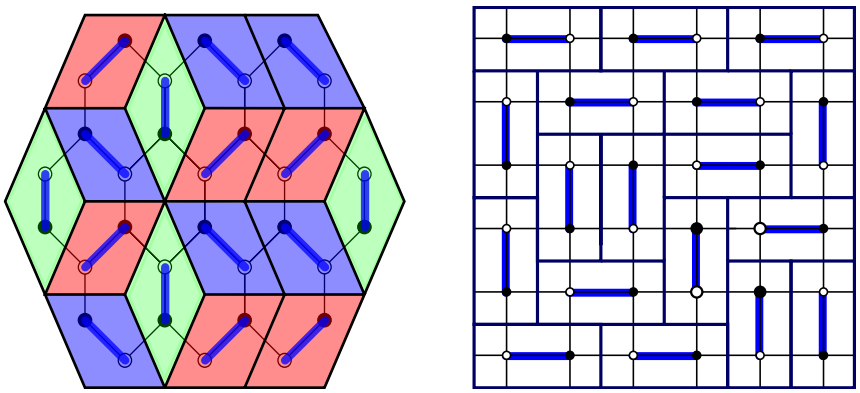

FIGURE 1.5: Illustration de la bijection entre pavage par des losanges ou des dominos et dimères sur les réseaux hexagonal et carré.

Un autre modèle effectif d'interface important est le *modèle de Ginzburg-Landau*. Dans ce modèle, on considère un graphe fini G planaire ou bien dessiné sur un tore. On identifie G à l'ensemble de ses sommets et on définit pour toute fonction ϕ de G dans $\mathbb{R}$ une énergie

$$H(\phi) = \sum_{s \text{ voisin de } s'} V(\phi(s) - \phi(s'))$$

où V est une fonction *strictement convexe* symétrique donnée appelée potentiel d'interaction.

Physiquement, on interprète ϕ comme une surface dans $\mathbb{R}^3$ paramétrée par la distance à un plan de référence où est dessiné G. L'espace est discrétisé dans les deux directions de ce plan mais la hauteur est continue. La forme de l'énergie est telle que les gradients importants coûtent cher. Étant donné que la hauteur est continue, il est naturel d'introduire une dynamique sur ces fonctions sous forme d'une équation différentielle stochastique avec un terme brownien. L'idée phénoménologique que la dynamique cherche à minimiser son énergie conduit à considérer l'évolution :

$$d\phi(s) = -\sum_{s' \text{ voisin de } s} V'(\phi(s') - \phi(s))dt + \sqrt{2}dB_t^s$$

où les B^s sont des mouvements browniens indépendants. En d'autre termes $\phi(s)$ est attirée par ses voisins avec une force donnée par la dérivée de V' tout en étant perturbée par un bruit aléatoire indépendant de tout le reste.

Pour considérer la mesure d'équilibre du processus, il est naturel de fixer la valeur de ϕ sur le bord de G, ce qui revient à considérer des conditions au bord similaire à celles pour les losanges (figure 1.1). Il est alors assez facile de voir que la mesure d'équilibre s'écrit

$$\mu(d\phi) = \frac{1}{Z} e^{-H(\phi)} d\Lambda$$

où Z, qui dépend des conditions au bord, est la constante de normalisation pour que μ soit une probabilité et Λ est la mesure de Lebesgue sur les fonctions de G dans $\mathbb{R}$. Le facteur $\sqrt{2}$ devant le brownien sert à éviter d'avoir un préfacteur devant H dans la mesure invariante.

Nous évoquerons à nouveau ce modèle dans la partie 1.4.3 sur l'historique. En effet pour ce modèle nous sommes capable de dériver assez complètement la théorie phénoménologique à l'équilibre comme hors équilibre. En particulier la convergence de la dynamique vers un mouvement par courbure moyenne anisotrope y est connue.

1.2.4 Dérivation des équations phénoménologiques dans un cas simplifié

Si pour les modèles d'interface bidimensionnelle plongée dans $\mathbb{R}^3$ les résultats de la partie 1.1.4 sont très difficile à obtenir, on peut les justifier assez facilement pour des modèles dans $\mathbb{R}^2$. Nous présentons ici le cas du modèle d'Ising sur $\mathbb{Z}^2$ à température nulle.

Rappelons que le modèle de pavage par des losanges est équivalent au modèle d'Ising à température nulle sur $\mathbb{Z}^3$ avec condition au bord fixée. De manière analogue il devrait être clair d'après la figure 1.6 que le modèle d'Ising à température nulle sur $\mathbb{Z}^2$ et avec des conditions au bords du type de celles de la figure 1.1 est équivalent à la marche aléatoire simple.

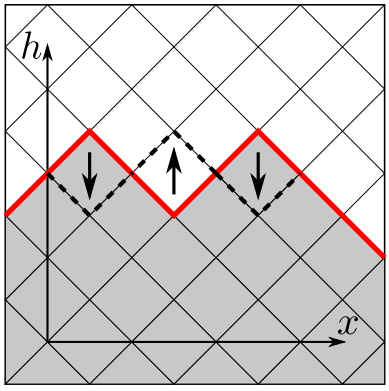

FIGURE 1.6: Correspondance entre interface dans le modèle d'Ising sur $\mathbb{Z}^2$ à température nulle et marche aléatoire simple. Les carrés gris représentent des sites $+$ et les carrés blancs des sites $-$. Les carrés pas complet sur le bord sont fixe et définissent des conditions aux bords analogue à celles de la figure 1.1. La courbe rouge épaisse est clairement une trajectoire de marche aléatoire simple à extrémités fixées. Les flèches et les pointillés indiquent les trois mouvements possibles.

L'équivalent de notre dynamique dans ce cadre est clair. En terme de modèle d'Ising : à taux un et indépendamment en chaque site, un carré comptant dans ses voisins exactement 2 blancs et deux noirs peut changer de couleur. En terme de marche, si $h(x)$ est un minimum (resp. maximum) local, on modifie h de $+2$ (resp. -2).

Notons que cette dynamique est aussi associée à un processus de particules, dit *processus d'exclusion simple symétrique*. Dans cette description nous considérons une pente ascendante comme une particule et une pente

descendante comme un trous. Pour la dynamique, chaque particule peut avancer ou reculer avec probabilité $1/2$ à condition que son site d'arrivée soit libre, où en d'autre terme une particule peut échanger sa place avec un trou. Cette description est en un sens l'équivalent pour le modèle 2D des pavages.

Ce modèle est très simple, et on peut y calculer explicitement les valeurs de tous les termes dans l'équation phénoménologique du mouvement macroscopique (équation 1.1). Pour un domaine de longueur L et où les conditions au bord sont $h(0) = a$ et $h(L) = b$, on a exactement $\binom{L}{\frac{L+b-a}{2}}$ marches possibles. Par définition $\sigma(s)$ est la limite de l'entropie pour des domaines tels que $b - a = Ls$ donc

$$\sigma(s) = \lim_{L\to\infty} \frac{1}{L} \log \binom{L}{\frac{L(1+s)}{2}} = -\frac{1+s}{2} \log \frac{1+s}{2} - \frac{1-s}{2} \log \frac{1-s}{2}$$

où pour des raisons géométriques évidentes $s \in [0, 1]$. Pour la mobilité, l'intégrale de type Green-Kubo sur des corrélations spatio-temporelle se simplifie exactement et il ne reste qu'un terme simple

$$\mu(s) = \lim_{L\to\infty} \mathbb{P}_L(\text{un mouvement est possible en } L/2) = \frac{1-s^2}{2}$$

où la probabilité $\mathbb{P}_L$ est la mesure uniforme sur toutes les trajectoires vérifiant $h(0) - h(L) = \lfloor Ls \rfloor$. Notons qu'en fait la mesure $\mathbb{P}_L$ converge vers la loi d'une marche aléatoire ayant une probabilité $\frac{1+s}{2}$ de monter et $\frac{1-s}{2}$ de descendre et qu'on aurait donc pu prendre n'importe quel point dans la définition de μ. En remplaçant dans les équations phénoménologiques, on s'attend donc à observer à grande échelle un mouvement donné par :

$$\frac{\partial h}{\partial t}(x,t) = \frac{1}{2} \frac{\partial^2 h}{\partial x^2}(x,t)$$

après une mise à l'échelle diffusive. Remarquons que la de la dérivée seconde de σ est compensée exactement par le fait que la mobilité tend vers zéro quand $|s|$ tend vers 1.

Pour justifier la convergence on passe l'équation sous forme faible

$$\frac{\partial}{\partial t} \int \phi(x) h(x,t) \, \mathrm{d}x = \int \frac{1}{2} \frac{\partial^2 \phi}{\partial x^2}(x) h(x,t) \, \mathrm{d}x.$$

On change la normalisation du système discret par $1/L$ de sorte à ce que la marche aléatoire soit définie sur $[0, 1]$ et ait des pas de taille $1/L$ et on peut donc discrétiser l'intégrale de gauche en posant

$$I\phi(t) = \sum_{i=1}^{L} \phi(\frac{i}{L}) h(\frac{i}{L}).$$

On remarque par ailleurs que les positions auxquelles un mouvement augmentant h de $1/L$ sont possibles sont exactement celles où $\Delta h = h(\frac{i-1}{L}) + h(\frac{i+1}{L}) - 2h(\frac{i}{L}) = \frac{2}{L}$. De même les mouvements pouvant faire décroître h de $1/L$ sont possibles exactement là où $\Delta h = -2/L$ et aucun mouvement n'est possible aux endroits où $\Delta h = 0$. L'espérance de la variation de $I\phi$ pour un intervalle de temps $\mathrm{d}t$ est donc

$$\begin{aligned}\mathrm{d}I\phi &= \frac{1}{L}\sum \phi(\frac{i}{L})\frac{1}{2}\Delta h(\frac{i}{L})\mathrm{d}t \simeq \frac{1}{2L}\sum(\Delta\phi(\frac{i}{L}))h(\frac{i}{L})\mathrm{d}t \\ &\simeq \frac{1}{2}I\frac{1}{L^2}\frac{\partial^2\phi}{\partial x^2}\mathrm{d}t.\end{aligned}$$

Dans la première ligne nous avons fait une intégration par partie discrète et négligé les termes de bords. Dans la deuxième ligne nous avons écrit que le laplacien discret de ϕ (qui est bien $\mathcal{C}^2$) approxime sa dérivée seconde avec un préfacteur $1/L^2$. On voit directement qu'il faut normaliser le temps par L^2 pour compenser ce $1/L^2$ et qu'après cette normalisation les sommes de Riemann dans la deuxième ligne devraient converger vers la forme faible de l'équation de la dynamique macroscopique.

En terme de système de particule, on constate que si l'on "marque" les particules initiales et si on autorise deux particules voisine à échanger leurs positions alors chaque particule effectue une marche simple. Comme les particules correspondent aux gradients de la hauteur h, on peut interpréter l'évolution comme un processus de diffusion des gradients. L'échelle L^2 apparaît alors une nouvelle fois comme l'échelle naturelle pour pouvoir observer cette diffusion.

Remarquons que la méthode précédente ne peut pas être généralisée au cas des pavages par des losanges. En effet le passage sous forme faible est indispensable pour faire apparaître le comportement à grande échelle de l'interface qui devrait être régulier au lieu de ses dérivées discrètes qui ne peuvent pas converger dans un espace de fonction. Or, dans le cas des losanges, si l'on décrit en terme de hauteur les endroits où un mouvement est possible, on obtient une sorte de laplacien discret non linéaire que l'on ne peut pas du tout sommer par partie. On ne peut pas non plus se ramener à deux direction indépendantes.

1.3 Résultats mathématiques

1.3.1 Combinatoire exacte, théorie de Kasteleyn

La propriété fondamentale des pavages par des losanges ou plus généralement des modèles de dimères bipartis est leur côté "exactement soluble". C'est par ailleurs pour cette propriété que nous avons travaillé sur ces modèles précisément.

Fixons pour cette partie un domaine borné du plan U, pavable par des losanges. U peut être vu comme un ensemble fini de faces d'un réseau triangulaire infini $\mathcal{T}$, où chaque losange recouvre exactement deux faces. On remarque aussi que les faces de $\mathcal{T}$ peuvent être coloriées en noir et blanc de sorte que deux faces ayant un coté commun soient toujours de couleur différente. On associe au domaine U la matrice K (matrice de Kasteleyn), dont les lignes sont indexées par les faces blanches de U et les colonnes par les faces noires, en posant $K(w,b) = 1$ si les faces w et b ont un côté commun et $K(w,b) = 0$ sinon. On a le théorème fondamental suivant, dû à Kasteleyn.

Théorème 1.3.1. *[Kas61] Le nombre de pavages de U par des losanges est* $|\det(K)|$.

Par un choix approprié de l'ordre dans lequel les sites blancs et noirs sont étiquetés, on peut faire en sorte que le déterminant soit positif (changer l'ordre des sites correspond a permuter l'ordre des lignes et des colonnes dans la matrice K) et nous supposerons dans la suite que ce choix a été fait.

Ce théorème a des conséquences très importantes car il permet aussi d'estimer des probabilités sous la mesure uniforme $\mu = \mu_{U_L}$. Plus précisément, soient $l_1 = (w_1, b_1), \ldots, l_n = (w_n, b_n)$ des positions possibles pour des losanges (i.e. des paires de triangles adjacents) ; on peut obtenir une formule close pour la probabilité $\mu(l_1, \ldots, l_n)$ d'avoir des losanges à toutes ces positions. On note $U' = U \setminus \bigcup l_i$ et K' la matrice de Kasteleyn correspondante. En appliquant le théorème à la fois aux domaines U et à U', on obtient :

$$\mu(l_1, \ldots, l_n) = \frac{\det(K')}{\det(K)}.$$

De plus on constate que $\det(K')$ est un mineur de K. On a donc

$$\det(K') = \det(K) \prod_k K(w_k, b_k) \det(K^{-1}(b_i, w_j))_{1 \leq i,j \leq n}$$

où $\det(K^{-1}(b_i, w_j))_{1 \leq i,j \leq n}$ est le déterminant de la sous-matrice de K^{-1} correspondant aux lignes w_i et aux colonnes b_i. Finalement on trouve

Corollaire 1.3.2. *La probabilité que les losanges* $l_1 = (w_1, b_1), \ldots, l_n = (w_n, b_n)$ *apparaissent dans un pavage tiré uniformément est*

$$\mu(l_1, \ldots, l_n) = \left(\prod_k K(w_k, b_k) \right) \det(K^{-1}(b_i, w_j))_{1 \leq i,j \leq n}.$$

La quasi-totalité des résultats mathématiques sur la mesure d'équilibre se base sur ce corollaire et fonctionne par des estimations de la matrice K^{-1}.

Remarque 1.3.3. *Dans le cadre que nous avons précisé, le produit qui apparaît avant le déterminant est trivialement égal à* 1. *Cependant il est intéressant de garder la formule sous cette forme car elle s'étend directement à des cas plus généraux (notamment aux pavages par dominos) où K prend des valeurs différentes de* 0 *et* 1.

On rappelle la définition des modèles de dimères sur réseau biparti donné dans la partie 1.2.3 comme ensemble d'appariements sur un graphe biparti G. Le théorème 1.3.1, ainsi que son corollaire, se généralisent très facilement à ce cadre. La matrice de Kasteleyn K est alors une version de la matrice d'adjacence de G, avec des lignes indexées par les sommets blancs et des colonnes indexées par les sommets noirs. La seule différence est qu'il faut multiplier les éléments non nuls de la matrice d'adjacence par des nombres complexes appropriés, de norme 1.

Le corollaire 1.3.2 est extrêmement utile car il permet de ramener presque toute les questions sur la mesure uniforme à des estimations de K^{-1}. Par exemple, la différence de hauteur entre deux points x et y de U_L dans la même colonne verticale du réseau triangulaire $\mathcal{T}$ est donnée simplement en termes de l'espérance du nombre de losanges horizontaux croisés par un chemin vertical qui va de x à y (voir figure 1.2). Grâce au corollaire 1.3.2, ceci n'est autre que la somme des $K^{-1}(b_i, w_i)$, où les (b_i, w_i) sont les arêtes horizontales croisées par ce chemin.

1.3.2 Propriétés asymptotiques de la mesure d'équilibre

Historiquement, les études sur les pavages par des losanges (et plus généralement sur les modèles de dimères) se sont principalement concentrées sur l'équilibre (i.e. la mesure uniforme) et nous en avons maintenant une vision relativement précise.

Dans la suite, quand nous voudrons parler en termes d'interface dans $\mathbb{R}^3$ il sera pratique de fixer une convention de paramétrisation. Premièrement, nous identifierons le plan où sont dessinés les losanges au plan de vecteur normal $(1, 1, 1)$ de l'espace (passant par l'origine). Ensuite, sur l'ensemble des sommets des losanges (qui forment un réseau triangulaire $\mathcal{T}$), nous définissons la *fonction de hauteur* $h(s)$ comme la coordonnée z de l'unique point de l'interface se projetant sur s (voir figure 1.2 pour un exemple). On étend naturellement la construction aux surfaces continues pouvant être approchées par une suite d'empilements de cubes.

Limite d'échelle

Le cadre que nous considérons est une suite de domaines U_L, bornés, simplement connexes et pavables par des losanges de taille $1/L$. Pour ces losanges de taille $1/L$, nous considérerons que l'empilement correspondant contient des cubes de taille $1/L$ Par conséquent la fonction de hauteur est définie sur le réseau triangulaire réechelonné $(1/L)\mathcal{T}$ et ses incréments seront de $\pm 1/L$. À la limite $L \to \infty$, on suppose que

- le domaine U_L tend vers un domaine U_∞ de bord suffisamment "lisse"
- la hauteur au bord de U_L (qui est une fonction de ∂U_L à valeurs dans $\mathbb{Z}/L$) tend vers une fonction de hauteur limite h^∂_∞ à valeurs réelles et

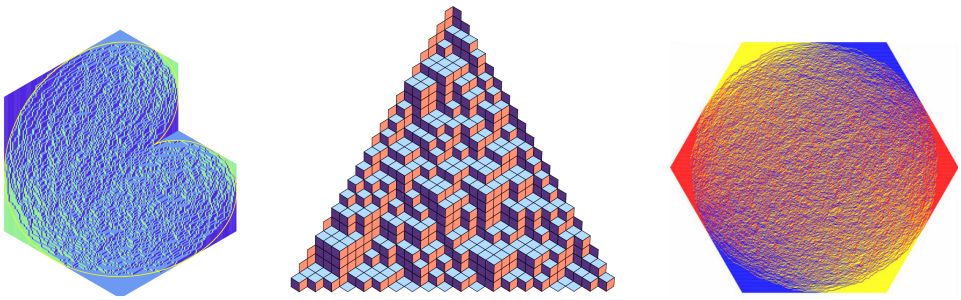

FIGURE 1.7: Exemples de pavage aléatoire uniforme pour de grands domaines. Dans le premier et le troisième exemple la hauteur au bord n'est pas planaire et on voit clairement des parties gelées. Au milieu par contre le bord est dans le plan $(1,1,1)$ et la hauteur à l'intérieur approxime ce plan.

définie sur le bord ∂U_∞. Le graphe de la hauteur au bord h^∂_∞ définit une courbe $\mathcal{C}$ dans $\mathbb{R}^3$.

Il est important de noter que la courbe $\mathcal{C}$ n'est pas déterminée par le bord de U_∞, donc que la deuxième condition n'est pas une conséquence de la première.

Forme macroscopique

Pour ce qui est de la forme macroscopique et de la minimisation d'une tension d'interface, on peut considérer le travail comme achevé avec le résultat suivant (valable aussi pour les pavages par des dominos) :

Théorème 1.3.4. *[CKP01] On se place dans la cadre ci-dessus. Pour chaque U_L, on tire un pavage uniformément indépendamment et on note h_L les fonctions de hauteur correspondantes. On a presque sûrement et pour la norme infinie sur les hauteurs :*

$$h_L \to h_\infty,$$

où $h_\infty : U_\infty \to \mathbb{R}$ est une fonction de hauteur continue déterministe. De plus, h_∞ est l'unique minimiseur de la fonctionnelle

$$E(h) = \int_{U_\infty} \sigma(\nabla h(x)) d^2x$$

avec condition au bord $h_\infty|_{\partial U_\infty} = h^\partial_\infty$. La fonction σ est une fonction strictement convexe explicite (entropie). Son expression est donnée dans le théorème 2.2.12 pour le cas des losanges.

La fonction σ est la tension de surface, c'est-à-dire l'excès d'énergie libre lié à la présence de l'interface. Pour nos modèles à température nulle, il n'y a pas de contribution d'énergie donc $\sigma(s,t)$ est (à une normalisation par la

surface près) le logarithme du nombre de pavages correspondant à la pente paramétrée par (s,t). Plus précisément, pour une suite de domaines telle que la courbe limite $\mathcal{C}$ soit dans un plan de pente (s,t), le logarithme du nombre de pavages par des losanges de taille $1/L$ est asymptotiquement équivalent à $\mathcal{A}(U_\infty)\sigma(s,t)L^2$, où $\mathcal{A}(U_\infty)$ est l'aire de U_∞.

Remarque 1.3.5. *Dans la partie 1.1.3 σ était définie sur les vecteurs normaux mais avec notre paramétrisation il est plus naturel de changer de convention et d'utiliser le gradient comme variable.*

La forme macroscopique h_∞ n'est pas forcément régulière partout. Dans beaucoup d'exemples naturels (comme dans la figure 1.7) le domaine de U_∞ peut être séparé en une partie "gelée", où h_∞ est affine ou affine par morceaux, et une partie "liquide" où c'est une fonction analytique non triviale. Sur la frontière entre ces sous-domaines, h_∞ ou ses dérivées deviennent singulières. En termes de losanges, le pavage typique de U_L apparaît qualitativement très différent dans les deux régions (voir la discussion des structures locales ci-dessous pour plus de détails). La présence de régions gelées est souvent appelée "phénomène du cercle arctique".

Dans le domaine liquide la forme macroscopique h_∞ satisfait l'équation aux dérivées partielles naturellement associée au problème de minimisation $\mathrm{div}(\nabla\sigma \circ \nabla h) = 0$ soit en développant :

$$\sum_{ij} (\partial^2_{ij}\sigma) \circ (\nabla h_\infty)\partial^2_{ij} h_\infty = 0$$

où les dérivées de σ sont bien sûr par rapport à ses deux variables de pentes et où $\partial^2_{ij}\sigma$ sont évaluées au point ∇h_∞. Puisque σ est strictement convexe et analytique, c'est une équation elliptique non linéaire dont les coefficients dépendent analytiquement de ∇h_∞. Par conséquent, h_∞ est $\mathcal{C}^\infty$ et même analytique à l'intérieur du domaine liquide.

Fluctuations

Outre la forme macroscopique, une deuxième question naturelle concerne, dans le même contexte, les fluctuations de h_L autour de h_∞. Cette question est nettement plus difficile et nous ne disposons que de résultats partiels et de conjectures. Nous présentons ici les conjectures "optimales" et donnerons l'énoncé des résultats connus aujourd'hui à la partie 1.4 où nous donnerons l'historique du modèle. Par ailleurs dans le cas d'un bord général, l'énoncé même des conjectures est difficile donc nous serons volontairement approximatifs.

Conjecture 1.3.6. *On se place dans le cadre du théorème 1.3.4 et on suppose en plus que la courbe limite $\mathcal{C}$ est incluse dans un plan de pente (s,t). Dans ce cas h_∞ est simplement une application affine de gradient (s,t).*

Il existe alors une application linéaire ℓ, dépendant de (s,t) mais pas du domaine U_∞, telle que

$$L(h_L - h_\infty) \to GFF \circ \ell.$$

où GFF désigne le champ libre gaussien avec condition au bord nulle sur le domaine $\ell(U)$.

Rappelons que le champ libre gaussien est une distribution aléatoire gaussienne (i.e. son intégrale contre toute fonction test est une variable aléatoire gaussienne) dont la covariance est la fonction de Green, $G(x,y) = \frac{1}{4\pi}\log(x^2+y^2)$.

Dans le cas général, on peut formuler une conjecture similaire mais la transformation à appliquer n'est plus linéaire, elle dépend de la forme limite de manière complexe. Nous énonçons seulement un résultat plus simple sur les fluctuations en un point

Conjecture 1.3.7. *Dans le cadre du théorème 1.3.4, pour tout $x \in U_\infty$, il existe v_x tel que*

$$L\frac{h_L(x) - \mathbb{E}[h_L(x)]}{\sqrt{\log L}} \to \mathcal{N}(0, v_x)$$

où $\mathcal{N}(0,v_x)$ est une loi normale de variance v_x.

Remarquons que la normalisation $\sqrt{\log L}$ est attendue pour le champ libre gaussien : en effet puisque la fonction de Green diverge en log à l'origine, la variance de la hauteur en un point x doit se comporter comme $\log L/L^2$.

Structure locale et mesures de Gibbs ergodiques

Enfin une dernière question naturelle est la structure locale de la surface, i.e. la probabilité d'observer un motif fini particulier contenant plusieurs losanges. L'exemple typique est la probabilité qu'une rotation augmentant la hauteur soit possible autour d'un point x, donc la probabilité de voir trois losanges disposés comme dans la partie gauche de la figure 1.3. Plus généralement il s'agit ici de déterminer les corrélations à portée finie alors que les fluctuations de hauteur exprimaient des corrélations à longue portée dans le système (rappelons que la hauteur en un point x au milieu de U_L dépend de l'état de tous les losanges croisés par un chemin allant du bord à x).

Puisque dans cette section nous nous intéressons à la structure locale des surfaces, nous ne rééchelonnerons pas l'espace par $1/L$, c'est-à-dire que les losanges seront de taille 1 et, par abus de notation, U_L dénotera le domaine $L\,U_L$.

Remarquons que quand L tend vers l'infini, la loi qui décrit la statistique locale de l'interface autour d'un point fixé de U_L doit tendre vers une loi sur les pavages du réseau infini $\mathcal{T}$. En effet, elle doit décrire la loi jointe de

configurations arbitrairement grandes. Les candidats naturels pour décrire cette mesure limite sont les mesures de Gibbs ergodiques. Il s'agit de mesures de probabilité sur les pavages de $\mathcal{T}$, avec les propriétés suivantes.

- La loi dans un domaine fini U conditionnellement à une configuration ω sur le reste de l'espace est la mesure uniforme sur tous les pavages pouvant se prolonger au plan entier par ω (equation DLR, pour Dobrushin-Lanford-Ruelle). Cette propriété doit être valable puisque c'est toujours le cas pour la mesure uniforme μ_{U_L}
- La loi est invariante et ergodique par translations de $\mathbb{Z}^2$.

Les mesures de Gibbs ergodiques sont classifiées par le théorème 1.3.8 ci-dessous. Pour le formuler, fixons d'abord un choix de coordonnes sur le réseau triangulaire $\mathcal{T}$. Nous utilisons les vecteurs e_1 et e_2 représentés sur la figure 1.2 comme vecteurs de base. Ainsi tous les sommets de losanges ont des coordonnées multiples de $1/L$.

Théorème 1.3.8. *[She05] Soit N le triangle de sommets $(0,0),(1,1)$ et $(1,0)$. Pour tout (s,t) dans son intérieur $\mathring{N}$, il existe une unique mesure de Gibbs ergodique $\mu_{s,t}$ de pente (s,t), i.e. pour tout $x=(x_1,x_2)$ et $y=(y_1,y_2)$ dans $\mathcal{T}$, $\mu_{s,t}[h(x)-h(y)] = s(x_1-y_1)+t(x_2-y_2)$. Pour $(s,t)\in\partial N := N\setminus \mathring{N}$, il existe une mesure invariante et satisfaisant les équations DLR par translation mais elle n'est pas forcément unique.*

On peut aussi exprimer ces mesures comme des processus déterminantaux, d'une manière similaire au théorème 1.3.1

Théorème 1.3.9. *[KOS06] Pour tout $(s,t)\in\mathring{N}$, on peut construire trois réels positifs a,b,c et une matrice infinie K_{st}^{-1}, indexée par les faces noires et blanches du réseau triangulaire infini $\mathcal{T}$, permettant d'exprimer les probabilités d'événements finis pour μ_{st} de la manière suivante. On définit une matrice infinie K_{st}, aussi indexée par les faces de $\mathcal{T}$, par $K_{st}(b,w)=a$ (resp. b,c) si b et w sont voisins et forment un losange horizontal (resp. orienté "\" et "/"). On a alors, si $l_1=(b_1,w_1),\dots,l_n=(b_n,w_n)$ désignent des positions possibles pour des losanges,*

$$\mu_{st}(l_1,\dots,l_n) = \left(\prod_k K_{st}(w_k,b_k)\right)\det(K_{st}^{-1}(b_i,w_j))_{1\le i,j\le n}.$$

Par ailleurs, les matrices K_{st} et K_{st}^{-1} sont inverses l'une de l'autre, $K_{st}K_{st}^{-1} = K_{st}^{-1}K_{st} = Id$. Enfin K_{st}^{-1} est bornée et a un développement asymptotique connu. Il existe α,β,γ tels que $a\alpha+b\beta+c\gamma=0$. Pour tout couple de sommet blanc et noir, on note (m,n) les coordonnées de la différence entre $w-b$, on a alors le développement asymptotique suivant :

$$K_{st}^{-1}(b,w) = \frac{1}{\pi}\Im\left(\frac{\alpha^{1-n}\beta^{m+n}\gamma^{-m}}{a\alpha-c\gamma}\right) + O\left(\frac{1}{\|w-b\|^2}\right)$$

Ces mesures sont invariantes sous l'effet de la dynamique (par la propriété de Gibbs) et décrivent donc des interfaces macroscopiquement planes infinies à l'équilibre. La valeur de $\sigma(s,t)$ est exactement l'entropie (par unité d'aire) de μ_{st} et on conjecture que ces mesures définissent bien la structure locale de l'interface.

Conjecture 1.3.10. *Dans le cadre du théorème 1.3.4, soit $x \in U_\infty$ tel que h_∞ soit différentiable en x et soit $(s,t) = \nabla h_\infty(x)$. Pour toute configuration C fixée d'un nombre fini de losange (avec des distances finies), la probabilité (sous la mesure uniforme μ_{U_L}) d'observer C autour du point x dans U_L converge vers $\mu_{st}(C)$ quand $L \to \infty$.*

Classification des phases

Les mesures correspondant à des pentes dans l'intérieur de N et celles correspondant au bord de N sont qualitativement très différente.

À l'intérieur de N, on parle de *phase liquide*. On observe des corrélations à longue portée, qui décroissent comme l'inverse du carre de la distance. Par exemple, si A_x est l'événement "un losange horizontal est présent autour du point x", on a

$$\mu_{s,t}(A_x A_y) - \mu_{s,t}(A_x)\mu_{s,t}(A_y) = \mu_{s,t}(A_x A_y) - \mu_{s,t}(A_x)^2 \approx |x-y|^{-2}.$$

La mesure est aussi "vraiment aléatoire", au sens où toute configuration finie pouvant être complétée en un pavage du plan a une probabilité strictement positive d'apparaître autour de tout point du graphe. On peut prouver qu'à grande échelle, la hauteur se comporte comme un champ libre gaussien (sans bord). En particulier, la covariance de la hauteur en deux points à distance L se comporte logarithmiquement en la distance et la variance de la hauteur en un point à distance L de l'origine (où l'on doit fixer la hauteur de manière déterministe) croît comme $\frac{1}{\pi^2}\log L$.

Si par contre (s,t) appartient au bord de N, on parle de *phase solide ou gelée* car il existe des chemins infinis le long desquels la position de tous les losanges est déterministe sous la mesure $\mu_{s,t}$. Les configurations de part et d'autre d'un de ces chemins sont indépendantes. Les mesures correspondant aux trois sommets du triangle N sont même entièrement déterministes et tous les losanges y sont alignés. Pour les mesures correspondant aux bords du triangle, la situation est plus complexe : il n'y a plus unicité des mesures de Gibbs invariantes par translation et le système peut se comporter comme s'il avait une dimension de moins (voir figure 1.8).

Il convient aussi de mentionner ici le troisième type de phase pouvant apparaître dans des modèles de dimères, dit *gazeuse*. Cette phase n'existe pas dans les modèles les plus simples comme les pavages par des losanges ou par des dominos, qui, rappelons-le, correspondent aux appariements parfaits des réseaux hexagonal et carré (cf figure 1.5). Par contre, elle apparaît

pour des appariements parfaits de graphes sous-jacents G plus complexes, par exemple le réseau carré-octogone représenté à la figure 3.1. Comme les phases solides, les phases gazeuses correspondent à une condition "singulière" sur la pente : une phase gazeuse peut exister seulement quand deux composantes de (s,t) sont entières et est dans l'intérieur de N_G, l'ensemble des pentes possibles pour des appariements de G. Les phases gazeuses sont cependant qualitativement très différentes des phases solides puisqu'elles correspondent à une limite "presque iid" : les corrélations entre dimères décroissent exponentiellement et non pas algébriquement avec la distance. Quand aux fluctuations de hauteur, elles ne sont pas bornées de façon déterministe, mais ont une variance finie et leur covariance décroît aussi exponentiellement avec la distance. En termes de fonction thermodynamique, une phase gazeuse correspond à une singularité (plus précisément un "cusp") dans la tension de surface σ. Notons que nous ne disposons d'aucun résultat sur la dynamique dans le cas d'un modèle pouvant faire apparaître une phase gazeuse. Nous supposons que cette absence de résultat est due à des raisons fondamentales, voir la discussion dans la partie 3.5.1.

Les notions de phase gelée et de phase liquide, que nous avons définies dans le cadre des mesures de Gibbs ergodiques dans le plan entier, peuvent être étendues au cas des pavages d'un domaine fini, dans la limite d'échelle où les losanges ont taille $1/L \to 0$. On se place dans le cadre du théorème 1.3.4 avec une courbe de hauteur de bord $\mathcal{C}$ pas nécessairement planaire. On appelle *domaine gelé* de la forme limite h_∞ l'ensemble des points de U_∞ tels que $\nabla h_\infty \in \partial N$ et *domaine liquide* les points tels que $\nabla h_\infty \in \overset{\circ}{N}$.

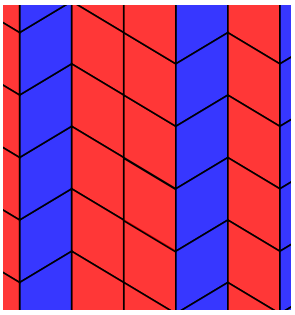

FIGURE 1.8: Exemple de loi se comportant comme un système unidimensionnel. Pour chaque bande verticale, on tire de manière i.i.d. si l'on place les losanges en position "/" ou "\". La mesure obtenue a une pente $(1, \frac{1}{2})$, satisfait les équations DLR mais est équivalente à une marche aléatoire simple.

Le domaine gelé est parfois non trivial, même si la condition qui le définit semble être de mesure nulle. Dans les domaines représentés sur la figure 1.7 par exemple, le domaine gelé occupe tout le bord de U_∞ et est d'intérieur non vide. Par ailleurs, les pentes correspondantes sont exactement les trois pentes extrémales associées aux sommets de N. Dans un tel cas où les pentes sont associées aux sommets, d'après les simulations de la figure 1.7 on s'attend à ce que la hauteur n'ait aucune fluctuation dans le domaine gelé. Malheureusement, on ne connaît pas de critère simple sur la condition au bord $\mathcal{C}$ pour l'existence d'un domaine gelé.

Au niveau microscopique, on voit que la configuration dans le domaine liquide est "véritablement" aléatoire. Comme évoqué plus haut, les fluctuations de hauteur à l'intérieur du domaine liquide devraient être gaussiennes, et plus précisément une variante de champ libre gaussien. Enfin, à la frontière entre les domaines gelés et non gelés, la forme limite h_∞ peut perdre en régularité (dans l'hexagone, sur des points typiques de la frontière elle est seulement $\mathcal{C}^2$). Les fluctuations de cette frontière ne sont pas connues en général mais on a des conjectures sur leur forme et des preuves dans certains cas particuliers, comme pour les fluctuations de hauteur dans le domaine liquide (par exemple dans [Pet12a]).

1.3.3 Dynamique de Glauber et résultats principaux de la thèse

Les travaux sur la dynamique du modèle sont beaucoup moins nombreux et nous sommes encore loin de pouvoir faire un lien complet entre les équations macroscopiques phénoménologiques et le modèle discret. En pratique nous n'avons étudié ici que la plus élémentaire des questions, à savoir quel est le temps total nécessaire pour que la dynamique arrive à l'équilibre.

Remarquez que cette question est importante du point de vue de l'informatique théorique puisqu'elle garantie la convergence et donne la complexité de l'algorithme "Monte Carlo Markov Chain" de génération d'un pavage aléatoire consistant à simuler la dynamique pendant assez longtemps pour qu'elle atteigne l'équilibre. Elle permet aussi d'obtenir la complexité d'une variante de l'algorithme précédent, *le couplage par le passé*, qui permet de générer sans aucun biais lié au manque de convergence un pavage aléatoire. Notons cependant que d'autres méthodes de génération "directe" d'un pavage aléatoire plus efficaces (mais plus complexes à implémenter) existent (voir dans la discussion de la partie 3.1.1. Du point de vue physique, il est aussi important de connaître la vitesse de retour à l'équilibre du système, ne serait ce que parce que cela permet d'identifier la normalisation que l'on doit appliquer au temps pour espérer voir une dynamique macroscopique non triviale.

Notre premier résultat donne une réponse à cette question de la vitesse de convergence vers l'équilibre pour le modèle de pavage par des losanges.

Théorème 1.3.11. *On se place dans le cadre du théorème 1.3.4 : on a une suite de domaines U_L, pavables par des losanges de taille $1/L$ et tels que la hauteur au bord (vue dans $\mathbb{R}^3$) converge vers une courbe $\mathcal{C}$. On note h_∞ la forme limite associée à $\mathcal{C}$ et on suppose que h_∞ ne contient pas de domaine gelé, c'est-à-dire que ∇h_∞ est dans l'intérieur de N en tout point de U_∞. On note $h(t)$ la fonction de hauteur au temps t. Alors, pour tous $\epsilon > 0$, $n, k \in \mathbb{N}$ et pour L assez grand (dépendant de $\epsilon, n, k, \mathcal{C}$), il existe T d'ordre*

$L^{2+o(1)}$ *tel que, indépendamment des conditions initiales,*

$$\mathbb{P}\left[\forall t \in [T, L^n], \|h(t) - h_\infty\|_\infty \leq \epsilon\right] \geq 1 - O(L^{-k}).$$

Autrement dit, après un temps d'ordre $L^{2+o(1)}$*, la surface devient* macroscopiquement *indistinguable de la forme limite.*

Les points forts du résultat sont la précision de l'estimation du temps (les bornes supérieures et inférieures ne différent que par un facteur $L^{o(1)}$ très petit devant le terme l'ordre dominant L^2) et surtout le cadre assez général dans lequel il s'applique. Par contre la notion de convergence utilisée est assez faible et il ne s'applique pas à certains des domaines les plus naturels, en particulier les hexagones.

On considère que la convergence au sens de la norme infinie des fonctions de hauteur normalisées est assez faible car elle ne donne aucune information sur la structure microscopique de l'interface. Ainsi une approximation déterministe de h_∞ sera très proche de l'équilibre au sens de la norme des fonctions de hauteur mais très différente pour les notions de convergence probabiliste classiques. Le théorème 1.3.16 ci-dessous fournit une borne inférieure pour le temps d'approche à la forme macroscopique.

Nos autres résultats utilisent une notion de convergence beaucoup plus forte, la distance en variation totale, mais sont plus limités dans les domaines qu'ils considèrent.

Définition 1.3.12. *Soit* μ *et* ν *deux mesures de probabilité sur un ensemble* M*. Soit* $\mathcal{C}$ *l'ensemble des couplages de* μ *et* ν*, c'est-à-dire les mesure de probabilité sur* M^2 *telles que, si* (X, Y) *désigne la variable aléatoire associée,* X *soit de loi* μ *et* Y *soit de loi* ν*. La* distance en variation totale *entre* μ *et* ν *est :*

$$\|\mu - \nu\| = \inf_{\mathcal{C}} \mathbb{P}(X = Y).$$

On a aussi les relations

$$\|\mu - \nu\| = 2 \sum_{E \subset M} |\mu(E) - \nu(E)|$$

et si μ *et* ν *sont toutes deux absolument continues par rapport à une certaine mesure* λ*, de densités respectives* f *et* g*, alors*

$$\|\mu - \nu\| = \|f - g\|_1 = \int |f - g| \mathrm{d}\lambda.$$

Définition 1.3.13. *On considère un domaine fixé pavable* U_L*. On note* μ_{U_L} *la mesure uniforme sur les pavages de ce domaine. Pour toute condition initiale* h*, on note* μ_t^h *la loi de l'état du système au temps* t *pour la dynamique commencée en* h*. On définit le* temps de mélange *par :*

$$T_{\text{mix}} = \inf\{t > 0 : \max_h \|\mu_t^h - \mu_{U_L}\| < 1/(2e)\}$$

Le choix de la constante dans la définition de T_{mix} est arbitraire. Prendre $1/(2e)$ permet d'avoir pour tout t, $\|\mu_t^h - \mu_{U_L}\| \leq e^{-\lfloor \frac{t}{T_{\text{mix}}} \rfloor}$.

On s'attend à ce que, dans le cadre du théorème 1.3.11, le temps de mélange soit de l'ordre $L^2 \log L$. Remarquons que ce logarithme est en accord avec l'existence d'une dynamique macroscopique à l'échelle L^2. En effet, le temps de mélange devrait correspondre au temps nécessaire pour que la dynamique macroscopique arrive à la hauteur des fluctuations typiques, soit $\frac{\log L}{L}$. Puisque la dynamique macroscopique ralentit quand elle s'approche de l'équilibre, ce temps peut être divergent avec L, et, dans le cas du mouvement par courbure moyenne ou de l'équation de la chaleur, on trouve bien le facteur $\log L$. En présence de phase gelée, la situation est moins claire. Il ne serait pas surprenant d'obtenir une convergence en $L^2 \log^C L$ pour $C > 1$ et on ne peut même pas vraiment garantir que l'on conserve une forme $L^{2+o(1)}$.

On peut maintenant énoncer nos autres résultats principaux :

Théorème 1.3.14. *Considérons une suite H_L de domaines hexagonaux dans le réseau triangulaire $(1/L)\mathcal{T}$, dont les bords (vu dans $\mathbb{R}^3$ toujours) convergent vers six arêtes d'un parallélépipède rectangle (voir figure 1.12). On note h_∞ la forme limite et D son domaine liquide. Soit $U \Subset D$ et soit U_L une suite de domaines qui convergent vers U et tels que la hauteur au bord converge vers $h_\infty|_{\partial U}$. Pour la dynamique dans les domaines U_L on a $T_{\text{mix}} = L^{2+o(1)}$.*

Notons que le résultat $T_{\text{mix}} = L^{2+o(1)}$ a été obtenu aussi dans [CMT12], sous l'hypothèse que les conditions au bord soient telles que la courbe $\mathcal{C}$ soit incluse dans un plan.

Ces résultats suggèrent que la convergence dans le cas d'un bord général devrait bien avoir lieu en variation totale en un temps $L^{2+o(1)}$ et que la faiblesse de la topologie utilisée dans 1.3.11 est une limitation technique. Par ailleurs, la seule différence fondamentale entre les preuves des théorèmes 1.3.11 et 1.3.14 est la précision des estimations sur les fluctuations à l'équilibre utilisées. Le théorème 1.3.14 montre donc que c'est le manque de connaissance de l'équilibre dans un cadre général qui limite la force de la convergence dans le théorème 1.3.11.

Nous nous sommes aussi intéressés au temps de mélange pour d'autres modèles d'interfaces que les pavages par des losanges, en particulier pour les pavages par des dominos (cf. figure 1.4 pour la vision d'un tel pavage comme surface). Sur ces pavages, nous considérons une dynamique très similaire au cas des losanges : indépendamment en chaque site et à taux 1, si deux dominos accolés forment un carré (de côté 2), on les tourne de 90°. On peut par exemple faire une rotation dans le coin en haut à gauche du pavage de la figure 1.4 et cela correspond à enlever un prisme.

Théorème 1.3.15. *On considère, comme dans le cadre standard des losanges, une suite U_L de domaines pavables par des dominos de taille $1/L$ et*

dont la hauteur de bord (vue dans $\mathbb{R}^3$) converge vers une courbe $\mathcal{C}$. Si $\mathcal{C}$ est incluse dans un plan, alors on a $T_{\text{mix}} = L^{2+o(1)}$.

Ce résultat a été obtenu avant les théorèmes 1.3.11 et 1.3.14. Au vu de la méthode utilisée pour les preuves de ces théorèmes, il est clair que pour traiter des bords non planaires dans le cas des dominos, il "suffirait" d'obtenir des estimations sur les fluctuations à l'équilibre avec des bords non planaires, plus précisément un analogue du lemme 1.3.21.

Enfin, après toutes ces bornes supérieures, nous passons à notre résultat sur la borne inférieure. Notons qu'il est suffisamment fort pour s'appliquer à toutes les situations précédentes et n'est en un sens même pas asymptotique. Il améliore d'un facteur log la borne inférieure connue dans le cas des bords planaires pour les losanges [CMT12].

Théorème 1.3.16. *Pour les modèles de pavages par des losanges ou des dominos, soit U_L un domaine pavable par des "tuiles" de taille $1/L$. Pour tout ϵ, il existe c_ϵ, ne dépendant de U que par son diamètre, tel que :*

$$\mathbb{P}[\|h(0) - h(c_\epsilon L^2)\|_\infty \leq \epsilon] > 1/2$$

où $h(t)$ désigne la fonction de hauteur au temps t. En d'autre termes, après un temps $c_\epsilon L^2$ la dynamique est encore macroscopiquement proche de son état initial.

Pour finir, nous présentons maintenant les résutats obtenus avant cette thèse sur la dynamique.

Spohn [Spo93] a développé, dans le cadre de la théorie de la réponse linéaire, la théorie phénoménologique générale des interfaces entre phases thermodynamiques et a traité mathématiquement certains cas simples. Il a en particulier établi pourquoi la dynamique à grande échelle devrait obéir à une variante non linéaire de mouvement par courbure moyenne ainsi qu'une expression de type Green-Kubo (une intégrale sur les corrélations spatio-temporelle à l'équilibre) pour la mobilité.

Pour les modèles de dimères, il paraît très difficile aujourd'hui de prouver la validité de cette théorie phénoménologique mais cela a été largement fait pour le modèle de Ginzburg-Landau. Ces résultats seront évoqué dans la partie 1.4 avec le reste des considérations historiques.

Pour les pavages par des losanges ou des dominos, un premier ensemble de résultats date de la deuxième moitié des années 1990. Luby, Randall et Sinclair ont introduit dans [LRS01] des dynamiques pour les losanges et les dominos, différentes de celles étudiées ici mais similaires, et ont prouvé une borne polynomiale ($O(L^6)$ avec nos conventions de temps continu) sur leur temps de mélange. Au même moment la technique de comparaison de chaînes de Randall et Tetali [RT00] a permis de déduire relativement simplement une borne en $O(L^{10})$ sur le temps de mélange de la dynamique de Glauber.

Pour le cas des losanges, Wilson [Wil04] a ensuite amélioré l'estimation du temps de mélange de la chaîne de Luby, Randall et Sinclair et obtenu l'ordre optimal : $cL^2 \log L \leq T_{\text{mix}} \leq CL^2 \log L$. La même technique de comparaison donne alors une borne $O(L^6 \log L)$ sur le temps de mélange de notre dynamique dans le cas des losanges. Notons que la méthode de Wilson ne s'étend pas simplement au cas des dominos (voir remarque 3.4.12 pour une discussion détaillée).

Notons par ailleurs que la motivation principale dans [LRS01] était de nature algorithmique, plus précisément la génération de pavage aléatoire par la méthode Markov Chain Monte Carlo évoquée au début de cette section. Ceci explique pourquoi ils ont introduit et étudié une chaîne qui n'a pas de signification physique particulière.

Après ces premiers résultats, la question des bornes optimales est restée ouverte pendant longtemps. Ce n'est que peu de temps avant le début de cette thèse que Caputo, Martinelli, Simenhaus et Toninelli ont développé une méthode permettant de capturer la bonne puissance L^2. Puisque c'est aussi celle que nous utilisons ici, elle sera présentée de manière assez détaillée dans la prochaine partie (1.3.4).

Plus précisément, dans [CMST10], ils ont d'abord étudié la vitesse de disparition d'une "bulle" de rayon L pour le modèle d'Ising à température nulle sur $\mathbb{Z}^3$. Rappelons qu'il s'agit du même modèle et de la même dynamique que pour les pavages par des losanges mais que les conditions au bord sont modifiées. Le fait de considérer une bulle ajoute des complications dans la paramétrisation et oblige à traiter séparément les points où la tangente à la bulle est dans un plan du réseau.

L'équivalent du théorème 1.3.15 (avec une borne supérieure $L^2 \log^C L$ au lieu de $L^{2+o(1)}$) pour les pavages par des losanges a été obtenu juste après par les trois premiers auteurs [CMT12]. Les principaux éléments nouveaux par rapport à [CMST10] sont le traitement du bord du domaine et la gestion du fait que l'interface devienne de plus en plus plate et la dynamique de plus en plus lente quand on s'approche de l'équilibre.

1.3.4 Methode de preuve

Comme nous l'avons indiqué ci-dessus dans la discussion sur les résultats connus avant le début de cette thèse, les preuves de nos trois théorèmes 1.3.11, 1.3.14 et 1.3.15 reposent sur une même méthode fondamentale. Nous allons maintenant présenter cette méthode de manière semi-rigoureuse de manière à en faire ressortir les idées principales.

L'interprétation des pavages comme des surfaces permet de définir un ordre partiel naturel sur les configurations : un pavage P est plus grand qu'un pavage P' si sa fonction de hauteur est partout plus grande, i.e. pour tout v, $h_P(v) \geq h_{P'}(v)$. La propriété fondamentale de notre dynamique est de conserver cet ordre partiel.

Proposition 1.3.17 (Monotonie)**.** *Soit $h \geq h'$ deux fonctions de hauteurs. On note h_t et h'_t les dynamiques commencées respectivement en h et h'. Il existe un couplage des processus h_t et h'_t tel que, pour tout t, $h_t \geq h'_t$. On peut même coupler en même temps les trajectoires partant de tous les états possibles en conservant l'ordre. On appellera cela un* grand couplage monotone*.*

Une première conséquence simple de la monotonie est qu'il suffit de contrôler les évolutions partant de l'état maximal et de l'état minimal pour contrôler le temps de mélange. En effet, considérons un grand couplage monotone et notons h_t^+ et h_t^- les dynamiques partant des états extrémaux. Si à un temps T, pour une certaine réalisation, on a $h_T^+ = h_T^-$ alors par monotonie toutes les trajectoires ont coalescé au temps T, en particulier une trajectoire commencée dans un état tiré de la mesure d'équilibre. Par conséquent, pour un temps t fixé, si on a $\mathbb{P}(h_t^+ = h_t^-) \geq 1 - 1/2e$ alors on a aussi, avec probabilité supérieure à $1/2e$, un couplage avec la mesure uniforme donc T_{mix} est inférieur à t.

La méthode générale que nous utilisons pour contrôler l'évolution de la dynamique se base sur deux lemmes principaux dépendant des détails du modèle considéré puis sur une construction "macroscopique" valable aussi bien pour les losanges et les dominos.

Le premier lemme concerne le temps de mélange du modèle dans le cas où l'état initial est déjà très proche de l'équilibre et où il est contraint arbitrairement à le rester indéfiniment. Plus précisément, on considère deux fonctions réelles $\bar{h}$ et $\underline{h}$ définies sur les sommets du réseau triangulaire $(1/L)\mathcal{T}$ (ce ne sont pas forcément des hauteurs correspondant à des pavages) et on considère une dynamique modifiée où tous les mouvements qui briseraient l'inégalité $\underline{h} \leq h_t \leq \bar{h}$ sont supprimés. On appelle, pour des raisons évidentes, $\bar{h}$ le "plafond" et $\underline{h}$ le "plancher" et on définit leur distance comme $\sup(\bar{h}(v) - \underline{h}(v))$.

Dans le cas des pavages par des losanges, les résultats de Wilson [Wil04] et de Randall et Tetali [RT00] permettent d'obtenir relativement simplement :

Lemme 1.3.18. *[CMST10] Soit U_L un domaine pavable par des* losanges *de taille $1/L$. Pour la dynamique contrainte entre un plafond et un plancher à distance H/L (i.e. H en nombre de losanges), on a*

$$T_{\text{mix}} = O(L^2 H^2 \log^2 L).$$

Pour les pavages par des dominos, les résultats de Wilson sur lesquels s'appuie la preuve du lemme ne s'appliquent plus. Nous avons donc dû trouver une preuve alternative, qui donne un résultat plus faible mais équivalent pour notre application dans la mesure où H sera toujours de la forme L^ϵ.

Lemme 1.3.19. *Soit U_L un domaine pavable par des* dominos *de taille $1/L$. Pour la dynamique contrainte entre un plafond et un plancher à distance H/L (i.e. H en nombre de dominos), on a*

$$T_{\text{mix}} = O(L^2 H^9 \log^4 L).$$

La preuve de ce résultat se trouve dans [LT12] , voir chapitre 3. On commence par introduire une dynamique markovienne auxiliaire bien choisie. Cette nouvelle dynamique est non locale (i.e. chaque mise à jour entraîne la rotation d'un nombre a priori arbitrairement grand de dominos ou de losanges) et est définie en utilisant une représentation du modèle de pavages en termes d'un modèle "de bille" (voir [Bou09]). Pour cette dynamique modifiée, introduite à l'origine dans [LRS01], on peut montrer que le volume V_t compris entre h_t^+ et h_t^- est une sur-martingale positive. Remarquons que la définition de cette dynamique auxiliaire dépend du modèle et que c'est cette définition que nous ne sommes pas capable de généraliser à des modèles de dimères plus généraux et qui limite donc le cadre du théorème 1.3.15. On montre ensuite qu'en présence d'un plafond et d'un plancher, on peut contrôler la variance de V_t essentiellement par V_t lui-même. Un argument standard de martingale permet alors de contrôler le temps nécessaire pour atteindre $V_t = 0$, c'est-à-dire le temps de coalescence pour la dynamique auxiliaire. Enfin, un argument de Peres et Winkler [PW11] permet de comparer la vraie dynamique à l'auxiliaire, toujours en utilisant l'existence des contraintes et on obtient que leurs temps de mélange sont au plus dans un rapport $H^2 \log L$.

Remarquons que la structure globale de cette preuve est identique à celle de la preuve du fait que $T_{\text{mix}} \leq L^{10}$ obtenue en combinant [LRS01] et [RT00]. La différence principale est que nous utilisons la présence du plafond et du plancher pour minorer la variance alors que dans [LRS01] les auteurs devaient se contenter d'une borne triviale sur celle-ci.

Le deuxième lemme fondamental concerne les fluctuations de domaines finis, qui s'avéreront être de taille mésoscopique $L^{-1/2+\delta}$ dans l'application. Pour les domaines planaires on a

Lemme 1.3.20. *[LT12] On considère soit des pavages par les losanges, soit des pavages par des dominos. On fixe $\alpha > -1$ arbitraire (même $\alpha \geq 0$) et on considère un domaine de taille L^α, pavé par des tuiles de taille $1/L$ avec des conditions au bord planaires. Pour tous ϵ et n, on a*

$$\mathbb{P}(\exists v : \ |h(v) - h_\infty(v)| \geq \frac{L^\epsilon}{L}) = O(L^{-n}).$$

Remarquons que d'après la conjecture 1.3.6, on s'attend à ce que la plus grande fluctuation soit similaire à celle d'un champ libre gaussien, c'est-à-dire de hauteur $\frac{\log L}{L}$. Ce lemme est une conséquence simple (par monotonie)

de la convergence vers le champ libre gaussien, au sens des moments, des fluctuations de hauteur dans les mesures invariantes ergodiques. Celle-ci s'obtient relativement simplement à partir du développement asymptotique de la matrice de Kasteleyn inverse donné dans [KOS06] et en suivant les idées de [KOS06, Ken07].

Nous avons obtenu, dans le cas des losanges, un analogue du lemme 1.3.20 dans le cas de conditions au bord non planaires. Rappelons que le domaine liquide de la forme limite h_∞ (dans un domaine U_∞ avec hauteur au bord fixée) est la région de U_∞ ou la pente ∇h_∞ n'est pas extrémale. On a

Lemme 1.3.21. *Fixons un point x dans l'intérieur du domaine liquide de h_∞. Soit V_L un domaine, pavable par par des losanges de taille $1/L$, centré en x et de rayon $L^{-1/2+\delta}$ pour $0 < \delta < 1/6$. On suppose que la hauteur au bord $h_{\partial V_L}$ coïncide, à une erreur $O(1/L)$ près, avec la hauteur $h_\infty|_{\partial V_L}$. Pour tous ϵ et n, on a*

$$\mu_{V_L}(\exists v : \ |h(v) - h_\infty(v)| \geq L^{-1+\epsilon}) = O(L^{-n}).$$

La preuve de ce résultat est nettement plus difficile que celle de l'équivalent planaire, malgré la limitations dans la taille des domaines considérés. Elle se base sur les estimations très précises de fluctuations de hauteur pour les pavages de domaines hexagonaux prouvées dans [Pet12a, Pet12b], ainsi que sur l'existence d'une formule explicite pour la forme limite dans ces domaines.

L'élément nouveau est le passage des domaines hexagonaux au cas général. On remarque premièrement que pour les petits domaines V_L du lemme 1.3.21 on peut approcher la forme limite à l'ordre 2 :

$$h_{\infty V_L}(x_1, x_2) = \partial_1 h_\infty x_1 + \partial_2 h_\infty x_2 + \frac{1}{2}\sum_{ij} \partial^2_{ij} h_\infty x_i x_j$$

où l'on a centré le repère au centre de V_L. Par ailleurs, on rappelle que dans le domaine liquide, h_∞ satisfait une EDP non linéaire

$$\sum_{ij} \partial^2_{ij}\sigma(\nabla h_\infty)\partial^2_{ij} h_\infty = 0, \tag{1.2}$$

qui donne une relation entre le gradient de h_∞ et sa hessienne. Il est donc naturel d'introduire l'ensemble

$$\mathcal{A} = \{(s,t) \in \overset{\circ}{\mathrm{N}}, M \in \mathcal{M}_2^{\mathrm{sym}}(\mathbb{R}) | \sum_{ij} \partial^2_{ij}\sigma(s,t) M_{ij} = 0\}$$

des couples gradients-hessiennes a priori possibles pour une forme limite.

Soit $\mathcal{W}$ l'ensemble des couples gradients-hessiennes apparaissant dans les formes limites de domaines hexagonaux (voir la figure 1.12 pour une définition précise),

$$\mathcal{W} = \left\{ \left(\nabla h_{abc}(x_1, x_2), \left(\partial^2_{ij} h_{abc}(x_1, x_2) \right)_{1 \leq i,j \leq 2} \right) \text{ pour } a, b, c > 0, (x_1, x_2) \in \mathcal{E}_{abc} \right\}.$$

Les résultats de Petrov impliquent assez simplement (par monotonie) le lemme 1.3.21 quand l'on considère des formes limites venant de domaines hexagonaux. Pour passer au cas général, nous avons en fait montré que tous les $((s,t), M) \in \mathcal{A}$ peuvent être obtenus dans les formes limites de domaines hexagonaux, i.e. $\mathcal{A} = \mathcal{W}$, ce qui suffit puisque seuls les deux premiers ordres du développement de Taylor sont significatif dans la condition au bord. La preuve de ce résultat utilise la formule explicite pour les formes limites h_{abc} dans les hexagones de côtés a, b, c puis des considérations géométriques pour garantir l'existence de solutions du système non linéaire

$$\begin{aligned} \nabla h_{abc}(x_1, x_2) &= (s, t), \\ \partial^2_{ij} h_{abc}(x_1, x_2) &= M_{ij} \end{aligned}$$

sans avoir à inverser explicitement.

Enfin le cœur de la méthode de preuve des théorèmes 1.3.11, 1.3.14 et 1.3.15 est l'utilisation des deux lemmes pour contrôler la dynamique sans contrainte. Comme nous l'avons vu ci-dessus, par monotonie et par symétrie, on peut s'intéresser uniquement à la majoration de la dynamique commencée dans l'état maximal. Notre but est de prouver que la dynamique reste (avec très grande probabilité) toujours inférieure à une fonction C_t évoluant de manière déterministe et s'approchant de h_∞ en temps $L^{2+o(1)}$. Dans la suite nous désignerons souvent C_t par le terme de *coupole*. Cette évolution sera choisie de sorte à pouvoir propager la domination itérativement. Rappelons que le domaine est de taille $O(1)$ et les losanges de taille $1/L$ donc qu'un mouvement élémentaire modifie la hauteur de $\pm 1/L$.

Nous présenterons dans un premier temps la méthode de [CMT12], c'est-à-dire avec un bord planaire comme dans le théorème 1.3.15 mais en montrant seulement comment amener la coupole à distance ϵ fixée de h_∞, dans l'esprit du théorème 1.3.11. Nous présenterons ensuite les modifications à apporter pour obtenir des résultats plus forts en termes de temps de mélange ou de bords non planaires. Pour simplifier l'exposition, nous ne préciserons pas explicitement les termes $o(1)$ et nous ferons comme si les estimations vraies avec proba $1 - L^{-n}$ étaient déterministes.

Pour définir notre majoration déterministe, nous considérons le plan P sur lequel se trouve la courbe $\mathcal{C}$ correspondant à la hauteur au bord de U. Dans P, nous fixons un disque $\mathcal{V}$ de rayon R assez grand et tel que $\mathcal{C}$ soit au milieu de $\mathcal{V}$. À l'instant initial, nous considérons une calotte sphérique C_0

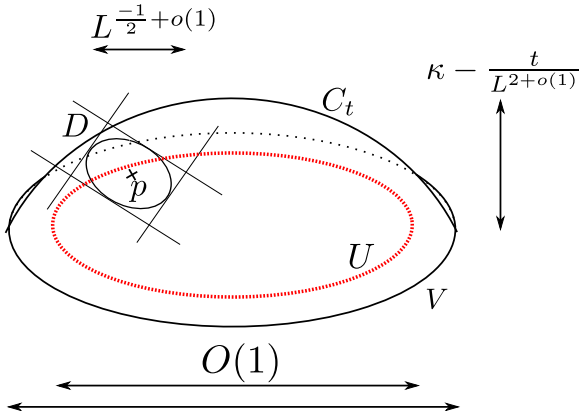

FIGURE 1.9: Dessin en 3D montrant la calotte sphérique que l'on découpe par un plan pour obtenir le domaine D.

s'appuyant sur le bord de $\mathcal{V}$. Soit V la projection de $\mathcal{V}$ sur le plan $(1,1,1)$, qui rappelons est identifié au plan où sont dessinés les losanges. Par abus de notation, nous identifierons C_t à sa fonction de hauteur (définie de V dans $\mathbb{R}$). On note κ la hauteur de C_0 au centre de V et on prend R et κ assez grands pour que la configuration de losanges maximale dans U soit inférieure à C_0. Pour les temps ultérieurs, C_t reste une calotte sphérique s'appuyant sur le même bord $\partial\mathcal{V}$ mais de hauteur au centre $\kappa_t = \kappa(1 - \frac{t}{L^{2+o(1)}})$.

On considère l'hypothèse de récurrence suivante, où h_t désigne la fonction de hauteur associée à la configuration de losanges au temps t et l'état initial n'a pas d'importance :

$$\text{HRt : sauf avec proba } L^{-n},\ \forall u \in [t, L^5],\ h_u \leq C_t.$$

Le terme L^5 est juste un temps très grand.

L'initialisation de la récurrence est triviale puisque nous avons choisi C_0 de sorte à avoir $h \leq C_0$ pour toute configuration de losanges dans U.

Pour la récurrence, nous fixons un point p dans U et nous allons montrer

$$\text{But : sauf avec proba } L^{-n},\ \forall u \in [t + L^{1+o(1)}, L^5],\ h_u(p) \leq C_t(p) - \frac{1}{L}.$$

En effet, une fois que nous aurons ce résultat, il suffira de le répéter en chaque point pour obtenir l'hypothèse de récurrence au temps $t + L^{1+o(1)}$. Ensuite il suffira de faire $O(L)$ pas de temps pour amener C_t à distance ϵ de h_∞. Nous donnons maintenant les étapes successives pour prouver ce résultat.

Majoration par une dynamique contrainte. Soit $\hat{h}_t$ la hauteur maximale dans V telle que $\hat{h}_t \leq C_t$. On définit $(\hat{h}_u)_{u \geq t}$ comme la dynamique partant de $\hat{h}_t$ contrainte par un plafond C_t, c'est-à-dire utilisant les mêmes mouvements

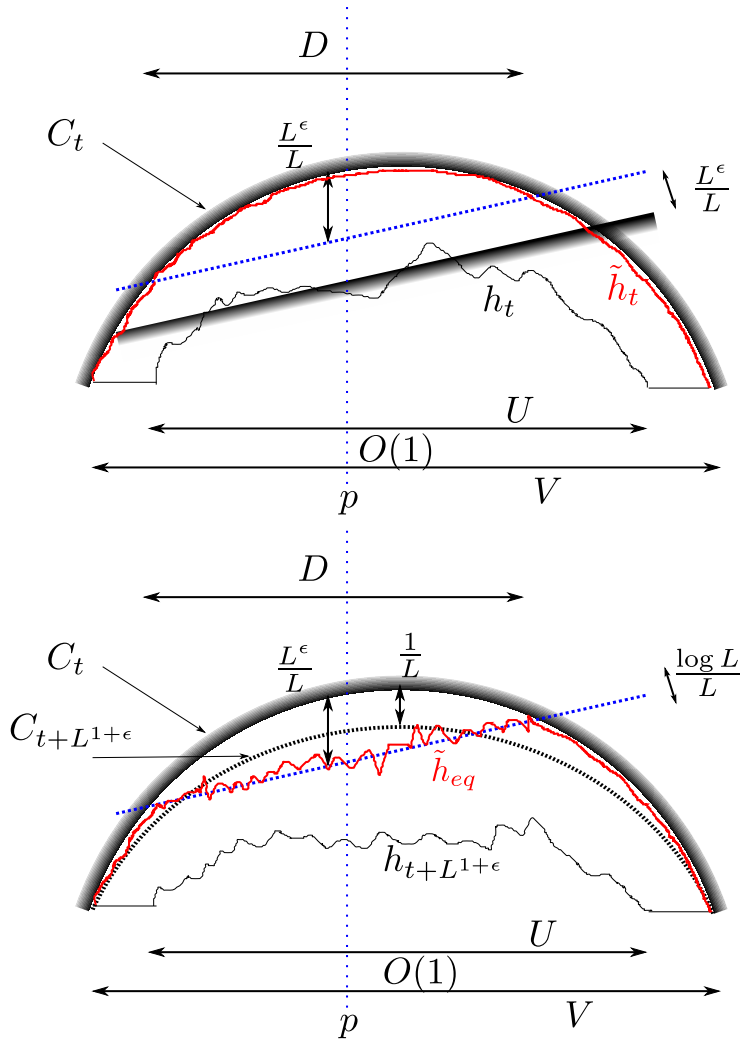

FIGURE 1.10: Dessins en coupe de la situation au temps t (en haut) et $t+L^{1+\epsilon}$ (en bas). Les ϵ désignent de petites quantités et sont tous différents entre eux. Les contraintes de plafond et de plancher sur $\tilde{h}$ sont indiquées par des dégradés. La droite pointillée bleue représente le plan par lequel est découpé la coupole C_t. La forme de $\tilde{h}$ est indiquée en rouge et en traits épais tandis que h est en traits fins noirs.

que pour h_u sauf ceux qui rompraient l'inégalité $\hat{h}_u \leq C_t$. Par monotonie et par l'hypothèse de récurrence on a, pour tout $u \geq t$, $h_u \leq \hat{h}_u$. Soit D un disque de rayon $L^{-\frac{1}{2}+o(1)}$ centré en p et soit $\tilde{h}_u$ la dynamique n'évoluant que dans D et avec un plancher à distance $L^{-1+o(1)}$. Par monotonie on a $\hat{h}_u \leq \tilde{h}_u$ et donc

$$\forall u \geq t,\ h_u \leq \tilde{h}_u.$$

Réduction à un problème d'équilibre. La dynamique $\tilde{h}_u$ évolue dans un domaine de rayon $L^{-\frac{1}{2}+o(1)}$ et est contrainte par un plancher et un plafond à distance $L^{-1+o(1)}$ (voir paragraphe suivant pour ce calcul géométrique). D'après le lemme 1.3.18, le temps de mélange de $\tilde{h}_u$ est donc d'ordre $L^{1+o(1)}$. Après le temps de mélange, étant donnée notre précision en temps, on peut considérer $\tilde{h}$ comme complètement à l'équilibre donc

$$\forall u \geq t + L^{1+o(1)}, h_u \leq \tilde{h}_{eq}.$$

Contrôle en espérance. Notre but est de pouvoir remplacer $\tilde{h}_{eq}$ ci dessus par $C_{t+L^{1+o(1)}}$. Nous commençons par contrôler $\mathbb{E}[\tilde{h}_{eq}]$. Par définition C_t est une calotte sphérique s'appuyant sur un cercle de rayon R et de hauteur au centre $\kappa_t = \kappa(1 - \frac{t}{L^{2+o(1)}})$ que nous pouvons supposer supérieure à ϵ. Son rayon de courbure est donc par des calculs géométriques triviaux $\rho_t = \frac{R^2+\kappa_t^2}{2\kappa_t}$, qui est borné tant que κ_t ne tend pas vers 0. Puisque les conditions au bord pour $\tilde{h}_{eq}$ sont planaires, les mêmes calculs montrent que, si on note r_D le rayon de D,

$$C_t(p) - \mathbb{E}[\tilde{h}_{eq}] = \frac{r_D^2}{2\rho_t} + o\left(\frac{r_D^2}{2\rho_t}\right) = \frac{L^{o(1)}}{L}.$$

Fluctuations de $\tilde{h}_{eq}$. Pour conclure, il nous suffit maintenant de montrer qu'avec grande probabilité, $\tilde{h}_{eq}$ n'est pas à plus de $\frac{L^{o(1)}}{2L}$ de son espérance. C'est exactement ce que nous donne le lemme 1.3.20.

La preuve du théorème dans le cas planaire demande d'abaisser la coupole à une hauteur $L^{-1+o(1)}$, et pas ϵ, pour pouvoir conclure à l'aide du lemme 1.3.18. La principale difficulté vient de ce que le rayon de courbure ρ_t diverge quand on s'approche de l'équilibre. Pour compenser cette divergence, on augmente le rayon r_D des disques D avec le temps de sorte à conserver un ordre $\frac{L^{o(1)}}{L}$ dans le contrôle en espérance. On vérifie facilement que cela ne fait pas trop augmenter la taille des pas de temps et qu'il suffit toujours d'un temps $L^{2+o(1)}$ pour atteindre une hauteur $L^{-1+o(1)}$.

Pour le cas non planaire, la principale difficulté (une fois admis le lemme 1.3.21) réside dans le choix de la dynamique auxiliaire déterministe C_t qui doit permettre de contrôler $C_t(p) - \mathbb{E}[\tilde{h}_{eq}(p)]$. Le problème est que, quand la coupole devient très proche de h_∞, C_t n'est plus concave ; au contraire le déterminant de sa hessienne devient partout négatif (voir l'équation (1.2) sur l'EDP vérifiée par h_∞). Par conséquent il n'est pas évident de comparer

C_t elle même à $\mathbb{E}[\tilde{h}_{eq}]$, la forme d'équilibre dans D avec condition au bord C_t, et en particulier de voir si $\mathbb{E}[\tilde{h}_{eq}(p)]$ est au dessus ou en dessous de $C_t(p)$. Par ailleurs, les fluctuations de $\tilde{h}_{eq}$ ne sont *pas* contrôlée par le lemme 1.3.21 car le couple $(\nabla C_t, (\partial^2_{ij} C_t))$ n'est pas dans $\mathcal{A}$.

Pour contrôler à la fois l'espérance et les fluctuations de $\tilde{h}_{eq}(p)$, on construit des conditions au bord h' sur ∂D, le bord de D, compatibles avec le lemme 1.3.21 (i.e. pouvant apparaître comme restriction à ∂D d'une forme macroscopique d'équilibre h' d'un plus grand domaine), et telles que $h'(p) \leqslant C_t(p) - \frac{L^{o(1)}}{L}$ et que $h' \geqslant C_t$ sur ∂D. En d'autres termes, on trouve une configuration à l'équilibre (forme macroscopique) h' sur D qui soit à la fois supérieure à C_t sur le bord de D et inférieure au milieu. En effet si h' est une telle configuration, sur ∂D on a $h' \geq C_t = \tilde{h}_{eq}$ donc par monotonie $\tilde{h}_{eq} \leq h'$ sur tout D, ce qui donne le résultat voulu $\tilde{h}_{eq}(p) \leqslant C_t(p) - \frac{L^{o(1)}}{L}$ en p.

On constate facilement que pour qu'un tel h' existe, il suffit que C_t vérifie

$$\sum_{ij} \partial^2_{ij} \sigma(\nabla C_t) \partial^2_{ij} C_t < 0.$$

Si l'on écrit $C_t = h_\infty + \psi_t$ et que l'on développe au premier ordre en ψ_t (on a dit que la difficulté apparaît quand C_t est proche de h_∞), on obtient :

$$\sum_{ij} \nabla \left(\partial^2_{ij} \sigma(\nabla h_\infty) \right) . \nabla \psi_t \partial^2_{ij} h_\infty + \sum_{ij} \partial^2_{ij} \sigma(\nabla h_\infty) \partial^2_{ij} \psi_t < 0.$$

On constate que le deuxième terme est bien négatif si ψ_t est concave. On contourne le manque d'information sur premier terme en prenant ψ_t tellement concave que sa dérivée seconde dans le deuxième terme écrase la dérivée première du premier terme (voir la partie 2.6 et plus précisément la remarque 2.6.4 pour le choix précis de ψ). Remarquons que la concavité de ψ_t ne contredit pas le manque de concavité de $C_t = h_\infty + \psi_t$ puisque ψ_t est seulement une petite perturbation de h_∞.

1.4 Historique

Les pavages par des losanges sont étudiés depuis très longtemps, en particulier en combinatoire. On trouve dans [Mac15], il y a presque un siècle, une formule sur le nombre de pavages par des losanges de l'hexagone de côté a, b, c (voir définition dans la figure 1.12) :

$$M(a,b,c) = \prod_{i=1}^{a} \prod_{j=1}^{b} \prod_{k=1}^{c} \frac{i+j+k-1}{i+j+k-2}.$$

Beaucoup plus pertinente pour notre étude, la méthode de dénombrement des pavages pour des domaines généraux exposée dans la partie 1.3.1

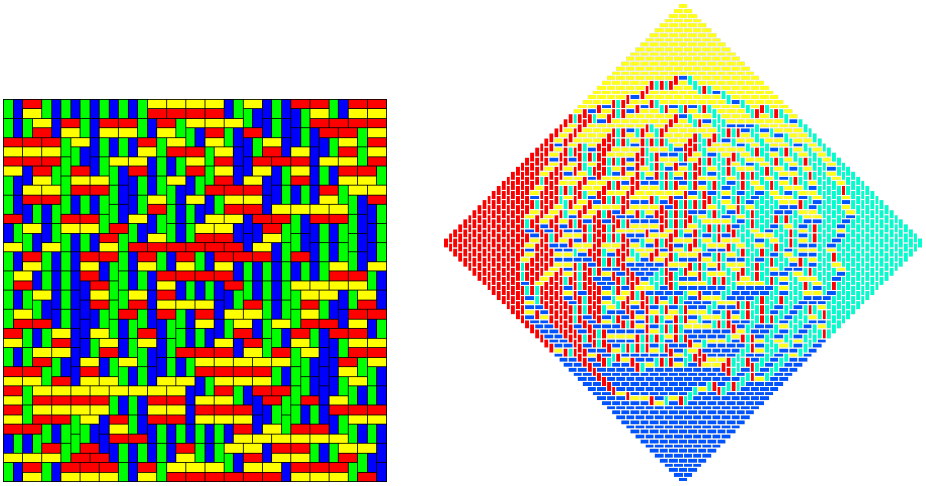

FIGURE 1.11: Les deux types de domaines les plus étudiés dans le cas des dominos, avec des pavages tirés aléatoirement uniformément. Les quatre couleurs correspondent aux quatre dessins de chemins dans les dominos de la figure 1.4 qui servaient à définir la hauteur. À gauche, le pavage semble spatialement homogène alors qu'à droite, on voit des parties gelées dans les coins. Dans la suite comme dans la littérature, les termes de *carré* et *rectangles* seront réservés aux cas où les axes sont parallèles au réseau comme à gauche et le domaine de droite sera appelé *diamant aztèque*.

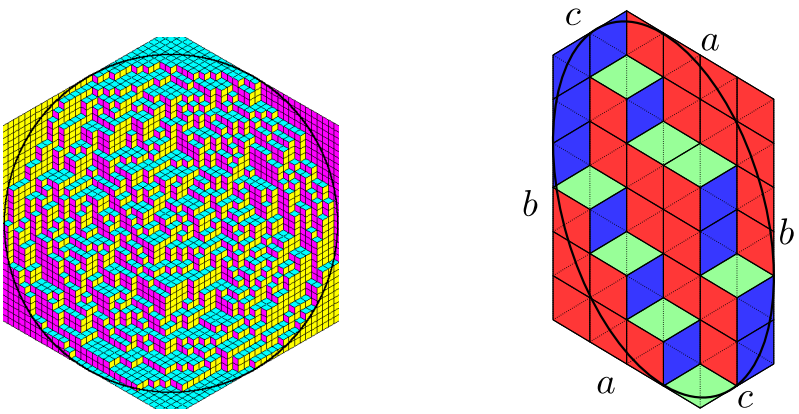

FIGURE 1.12: Deux exemples de domaines hexagonaux, l'un régulier l'autre non. Le pavage de l'hexagone régulier a été tiré uniformément, mais pas celui de l'hexagone irrégulier. Les limites asymptotiques des domaines gelés (cercle et ellipse inscrites) sont dessinées en noir. Dans la suite, le terme de domaine hexagonal désignera toujours ce type de domaine dont les côtés sont alignés avec le réseau triangulaire et dont la hauteur au bord correspond à six côtés d'un parallélépipède. On note $\mathcal{E}_{abc}$ l'ellipse inscrite dans l'hexagone de cotés a, b, c et h_{abc} sa forme limite.

remonte à Kasteleyn [Kas61] qui l'a utilisée pour estimer asymptotiquement le nombre de pavages d'un rectangle (voir figure 1.11) par des dominos. Temperley et Fisher ont obtenu les mêmes résultats que Kasteleyn dans [TF61] mais il n'est pas clair que leur méthode puisse être généralisée pour donner les résultats de la partie 1.3.1. Notons que leurs motivations était très différentes de celle présentée ici, bien qu'aussi inspirée de la physique statistique. Leur but était de comprendre le modèle "monomères-dimères" où l'on autorise certains sommets à ne pas être appariés. En termes de pavage, cela correspond à autoriser les "trous" dans le pavage (mais toujours pas les recouvrements). Ce modèle monomère-dimères était utilisé pour décrire un gaz contenant deux types de particules de taille différente ou l'adsorption de molécules sur une surface.

Nous omettons le reste de la littérature des années 60 à 90 pour passer directement aux résultats pouvant s'interpréter en termes de forme limite.

1.4.1 Résultats sur la forme limite

Pendant longtemps, les études ont été limitées aux domaines sur lesquels on peut disposer de résultats combinatoires exacts, en particulier les hexagones (pour les pavages par des losanges), les rectangles et le diamant aztèque (pour les pavages par des dominos), voir les figures 1.11 et 1.12. Il est facile

de voir que les rectangles ont des conditions au bord planaires et que leur pente est exactement au centre de l'ensemble des pentes possibles (le point $(\frac{1}{2}, \frac{1}{2})$ dans la figure 3.1). C'est la pente d'entropie maximale. Le diamant aztèque et les hexagones ont par contre des bords non planaires et font apparaître des parties gelées dans les simulations.

Les rectangles sont les premiers domaines pour lesquels la structure d'un pavage typique a été étudié. Burton et Pemantle [BP93] ont prouvé que la structure d'un pavage typique y est homogène, ce qui correspond, avec nos notations, à une preuve du théorème 1.3.4 et de la conjecture 1.3.10. Notons qu'ils ont aussi pour cela défini et montré l'unicité de la mesure sur les pavages du plan entier d'entropie maximale.

Sur le diamant aztèque, les premiers travaux se sont concentrés sur le phénomène de "cercle arctique", c'est-à-dire, en terme modernes, sur l'existence d'un domaine gelé et sur le fait que sa frontière soit le cercle tangent aux quatre côtés. Ces résultats ont d'abord été prouvés par Jockusch, Propp et Shor [JPS95]. Peu après, Cohn, Elkies et Propp [CEP96] ont trouvé une nouvelle preuve donnant l'existence et une expression pour toute la forme limite. Par ailleurs, les auteurs y conjecturent le théorème 1.3.4, l'unicité des mesures invariantes du théorème 1.3.8 ainsi qu'une version de la conjecture 1.3.10.

Enfin, pour les hexagones, l'existence d'une forme limite a été prouvée dans [CLP98] par Cohn, Larsen et Propp.

Le théorème 1.3.4 pour des bords généraux a finalement été prouvé par Cohn, Kenyon et Propp [CKP01], cinq ans après sa conjecture dans [CEP96]. Leur méthode suit l'intuition physique derrière le principe variationnel puisqu'ils montrent que le logarithme du nombre de pavages approchant toute forme macroscopique h fixée est bien L^2 fois l'intégrale de $\sigma(\nabla h)$. Ils obtiennent ainsi, en plus de l'existence de la forme limite, l'expression explicite de la tension de surface et des estimations de grandes déviations. On peut donc considérer leur théorème comme essentiellement optimal pour ce qui est de la forme macroscopique.

Les résultats plus récents sur la forme limite traitent de formes particulières pour lesquelles on peut résoudre le problème variationnel.

Dans [KO07], une famille de conditions au bord a été introduite pour laquelle la forme limite peut être décrite en terme algébrique. En particulier, pour ces domaines la frontière du domaine gelée est une courbe algébrique explicitement calculable, par exemple une cardioïde dans le cas de la partie gauche de la figure 1.7. Cette famille inclue notamment le domaine de la partie gauche de la figure 1.7. La forme limite à l'intérieur du domaine est paramétrée à l'aide d'une équation de Burgers, encore en termes algébriques. Dans [Pet12a, Pet12b], une autre famille de domaines polygonaux est étudiée pour laquelle la forme limite est aussi reliée à une équation de Burgers.

1.4.2 Résultats sur les fluctuations ou la structure locale

En ce qui concerne les conjectures 1.3.6 et 1.3.10, les cas de différents domaines particuliers où l'on peut utiliser des résultats combinatoires sont connus.

Le premier résultat sur les fluctuations de hauteur se trouve dans [Ken00]. Pour les dominos, la convergence des fluctuations vers un champ libre gaussien (conjecture 1.3.6) y est prouvée pour des conditions au bord particulières dite "de Temperley". Remarquons que ces conditions généralisent en un sens les rectangles. En effet, la hauteur au bord y est aussi planaire et de même pente que pour les rectangles. Par contre elles ne contraignent pas la forme générale du domaine (qui peut même ne pas être simplement connexe).

En ce qui concerne la structure locale, le théorème 1.3.8 à propos de l'existence et l'unicité des mesures de Gibbs sur le plan entier a été prouvé par Sheffield dans sa thèse [She05].

Ces mesures de Gibbs en domaine infini ont ensuite été décrites précisément dans [KOS06] par Kenyon, Okounkov et Sheffield. On y trouve en particulier le théorème 1.3.8 avec la formule asymptotique pour K^{-1}, la définition des différentes phases, le critère pour l'existence d'une phase gazeuse, le calcul de la tension de surface pour les mesures infinies et enfin les fondements de la méthode d'estimation des fluctuations dans les phases liquides. De manière remarquable, tous les résultats y sont valables pour le cadre le plus général des dimères sur réseau biparti présenté dans la partie 1.2.3.

Plus tard dans [Ken07], une méthode générale d'estimation des fluctuations a été proposée. Celle-ci permet de ramener l'étude des fluctuations à celle des fonctions harmoniques discrètes sur un graphe auxiliaire (voir partie 1.5). Malheureusement, ce graphe auxiliaire étant complexe (en particulier déterministe mais apériodique), ces fonctions harmoniques discrètes sont encore mal connues. Le chapitre 4 de cette thèse est une étape vers une meilleur compréhension de ces fonctions. Notons que ces graphes auxiliaires avaient été initialement introduit dans le cadre d'une bijection entre arbre couvrant et modèle de dimères, découverte par Temperley dans [Tem74] pour les pavages par des dominos des rectangles, puis étendue à des cas généraux dans [KPW00] et [KS04].

Enfin, dans le cas non planaire, les principaux résultats connus ont été obtenus par Petrov dans [Pet12a, Pet12b]. Pour des domaines "polygonaux", en particulier pour les hexagones, il a démontré l'équivalent non planaire de la conjecture 1.3.6, i.e. la loi jointe des fluctuations dans le domaine liquide, ainsi que la conjecture 1.3.10. On peut noter qu'il a aussi obtenu une description des fluctuations du bord du domaine gelé.

1.4.3 Autres modèles d'interface

Nous avons déjà évoqués dans la partie 1.3.3 l'historique des résultats à propos de la dynamique sur les pavages qui, même après cette thèse, sont encore très partiels. Par contre, pour d'autres modèles, en particulier le modèle d'Ising sur $\mathbb{Z}^2$ à température nulle et le modèle de Ginzburg-Landau, la situation est nettement plus claire.

Rappelons que les pavages par des losanges correspondent aux interfaces du modèle d'Ising sur $\mathbb{Z}^3$ à température nulle. Le cas de $\mathbb{Z}^2$, toujours à température nulle, a aussi été étudié récemment. Lacoin, Simenhaus et Toninelli [LST11, LST13] ont prouvé que la disparition d'une "goutte" macroscopique de $+$ au milieu d'un océan de $-$ se produit bien selon un mouvement par courbure moyenne (aussi appelé mouvement par réduction de la longueur) anisotrope avec une échelle de temps L^2. Ils ont ainsi confirmés la description phénoménologique de la partie 1.1.4. Rappelons (voir partie 1.2.4) que pour ce modèle dans $\mathbb{Z}^2$, quand on fixe des conditions au bord de manière similaire à la dimension 3, le problème se ramène au cas très bien connu de l'exclusion simple symétrique, c'est-à-dire à la marche aléatoire simple conditionnée sur ses deux extrémités.

Pour les modèles de surfaces dans $\mathbb{R}^3$, le seul cas, à notre connaissance, où l'on sache dériver la dynamique macroscopique est le modèle de Ginzburg-Landau défini dans la partie 1.2.3. La littérature sur ce modèle est trop vaste pour être détaillée précisément ici, citons seulement que la dynamique macroscopique en a été obtenue par Funaki et Spohn [FS97]. Elle est bien de type "mouvement par courbure moyenne anisotrope" à l'échelle L^2 comme attendu. Notons que pour ce modèle, nous pouvons même aller plus loin dans la validation de la description phénoménologique. Par exemple, nous connaissons les grandes déviations de la dynamique et nous savons décrire les fluctuations dynamiques autour de l'équilibre comme un processus stationnaire. On peut aussi traiter certaines contraintes comme la présence d'un mur. Pour une présentation et des références complètes, on peut se référer au cours [Fun03].

1.5 Les T-graphes

1.5.1 Motivations

L'un des principaux problèmes aujourd'hui concernant les modèles de dimères est l'estimation des fluctuations dans des domaines finis. Comme indiqué plus haut, la plupart des résultats connus reposent sur des formules combinatoires que nous n'espérons pas pouvoir généraliser à des domaines généraux. Nous nous sommes donc intéressés à la méthode de Kenyon [Ken07] que nous présentons maintenant.

Premièrement rappelons (c.f partie 1.3.1), qu'il "suffit" d'avoir de bonnes

estimations sur la matrice K^{-1} d'un domaine fini pour connaître les fluctuations sur ce domaine. Par ailleurs on constate que, pour un sommet blanc w fixé, $b \to K^{-1}(b, w)$ est une fonction analytique discrète en un certain sens (sa divergence est nulle autour de tout sommet blanc sauf w). Il est donc naturel de chercher la limite de K^{-1} comme une fonction analytique. Malheureusement, les conditions au bord vérifiées par K^{-1} sont très difficiles à manipuler et nous n'espérons pas pouvoir les faire passer à la limite continue.

La méthode de [Ken07] consiste à réécrire K^{-1} comme une fonction analytique discrète sur un nouveau graphe où les conditions au bord sont beaucoup plus simples. Plus précisément, dans le cas planaire, pour toute pente fixée (s, t), on introduit un graphe auxiliaire infini T_{st} (voir figure 1.13), que nous appelerons un T-graphe. Ce graphe est muni d'une notion naturelle de marche aléatoire permettant de définir l'harmonicité discrète d'une fonction. Sur T_{st}, la relation $KK^{-1} = Id$ est équivalente au fait que K^{-1} soit la dérivée discrète d'une fonction harmonique discrète G^* sur les sommets de T_{st}. L'intérêt de la construction est que les sous-graphes finis de T_{st} correspondent à des domaines pavables de hauteur au bord planaire de pente (s, t) et que les conditions au bord pour G^* sont de type Dirichlet. On peut donc espérer passer au continu sur G^* de manière assez précise pour pouvoir dériver et obtenir K^{-1}. Notons que les conditions au bord obtenues à partir de T_{st} généralisent les conditions de Temperley au cas des losanges et de pentes générales.

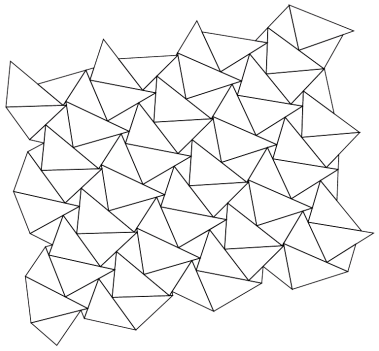

FIGURE 1.13: Un exemple de graphe T_{st}.

Notre résultat est un premier pas dans la mise en œuvre de cette technique.

Théorème 1.5.1. *Pour toute pente (s, t) non extrémale, la marche aléatoire à temps continu sur T_{st} converge en loi vers un mouvement brownien de covariance proportionnelle à l'identité.*

Remarque 1.5.2. *En fait, le résultat est légèrement moins fort. La convergence n'est prouvée que pour presque tout choix d'un paramètre auxiliaire (qui en un sens correspond au point de départ de la marche) dans la construction de T_{st}.*

Ce théorème implique la convergence des fonctions harmoniques discrètes

vers des fonctions harmoniques continues, avec la définition usuelle du laplacien puisque la covariance est proportionnelle à l'identité. Malheureusement, il n'est pas suffisant pour estimer K^{-1}, qui est une dérivée, car il nous faudrait des estimations sur la vitesse de convergence.

Corollaire 1.5.3. *Soit U un domaine ouvert régulier de $\mathbb{R}^2$ et soit h une fonction harmonique sur U qui s'étend continûment sur ∂U. Soit $(s,t) \in \mathring{N}$ une pente, T_{st} le graphe associé et T_n le graphe obtenu en rééchelonnant T_{st} par $1/n$. Soit $U_n = U \cap T_n$ et soit ∂U_n l'ensemble des points de T_n adjacents à U_n mais pas dans U_n. Soit h_n la solution du problème de Dirichlet :*

- *h_n est harmonique discrète dans U_n*
- *$h_n = h$ sur ∂U_n.*

La suite (h_n) converge alors ponctuellement vers h.

1.5.2 Méthode de preuve

Notre méthode de preuve s'inspire de la théorie des marches aléatoires symétriques en milieu aléatoire, et plus précisément d'une preuve de Lawler [Law82]. On commence par considérer la marche aléatoire non pas comme une particule se déplaçant dans un graphe fixé mais comme une particule fixe sur un graphe se déplaçant dans le temps. C'est ce qu'on appelle l'environnement vu de la particule. Avec ce point de vue, on introduit une topologie naturelle (de type convergence locale) sur l'ensemble E des états possibles de la marche qui le rend compact (plus précisément, pour un graphe T fixé, l'espace est précompact mais on construit simplement son adhérence). La structure de E est telle que l'on peut facilement le munir d'une mesure invariante par translation et ergodique. On peut aussi construire sans difficultés par compacité une mesure $\mathbb{Q}$ invariante pour la marche.

Le deuxième point consiste à montrer que $\mathbb{Q}$ est absolument continue par rapport à $\mathbb{P}$. Pour cela, on prouve des équivalents discrets d'inégalités fonctionnelles. C'est principalement dans ces preuves qu'intervient la forme précise de la marche aléatoire, et en particulier, une propriété d'*uniforme ellipticité* disant que la marche a toujours une probabilité uniformément minorée de se déplacer dans n'importe quelle direction. Enfin, une fois que l'on a prouvé l'absolue continuité de $\mathbb{Q}$ par rapport à $\mathbb{P}$, des arguments assez généraux permettent de montrer que $\mathbb{P}$ et $\mathbb{Q}$ sont équivalentes puis de "transporter" l'ergodicité de $\mathbb{P}$ pour les translations en ergodicité de la marche aléatoire commencée selon la mesure stationnaire $\mathbb{Q}$. Le théorème ergodique permet alors de contrôler la variance de la marche. Comme la marche est une martingale, cela suffit à appliquer le principe d'invariance pour prouver la convergence vers un mouvement brownien.

Remarquons cependant que le schéma ci-dessus ne donne aucune information sur la matrice de covariance du mouvement brownien limite. En effet,

la mesure $\mathbb{Q}$ est obtenue de manière non constructive (par compacité). Pour prouver que la covariance limite est bien proportionnelle à l'identité, nous utilisons une méthode indépendante. L'idée de base en est que le lien avec les dimères nous donne un développement asymptotique pour une fonction harmonique discrète particulière G^* : il existe une fonction f $\mathcal{C}^2$ explicite telle que $G^*(x) = f(x) + O(1/x)$. On peut alors identifier la covariance C (à une constante près) comme étant la seule matrice symétrique pour laquelle $\sum_{ij} C_{ij}\partial^2_{ij} f = 0$.

1.6 Perspectives

Nous présentons maintenant quelques pistes d'étude pour de futurs travaux.

Pour la dynamique de Glauber sur les pavages, la question la plus intéressante dans l'état actuel des choses me paraît être celle des phases gelées. Plus précisément la limitation aux domaines non gelés dans le théorème 1.3.11 est-elle uniquement technique ou correspond-elle à un véritable changement de comportement du modèle ?

On sait que quand la pente tend vers le bord de N, la mobilité μ tend vers 0 (à une vitesse inconnue) et les dérivées secondes de la tension de surface σ tendent vers l'infini. Par conséquent même la description phénoménologique devient problématique. Par ailleurs dans nos théorèmes les états initiaux peuvent être largement gelés donc nous savons qu'un domaine gelé peut avoir un mouvement macroscopique à l'échelle $L^{2+o(1)}$ tant qu'il est assez loin de l'équilibre. En conclusion, il paraît raisonnable de supposer que le temps de mélange dans ce cas est toujours d'ordre $L^{2+o(1)}$ mais il ne serait pas étonnant que l'ordre précis du temps de mélange ne soit pas $L^2 \log L$ comme attendu dans le cas liquide. Toute question plus fine est très ouverte, nous ne risquerons pas ici à hasarder des conjectures.

Notons qu'en présence de domaine gelé, toutes les étapes de notre méthodes s'effondrent, à la fois les lemmes 1.3.18 et 1.3.21 et la majoration par la coupole. L'étude de ce cas demandera donc certainement des idées vraiment nouvelles.

Les autres limitations du théorème 1.3.11 par contre semblent moins dues à un manque de compréhension de la dynamique que de l'équilibre. Comme nous l'avons noté précédemment, la raison pour laquelle nous n'avons pas pu obtenir un temps de mélange est que nous ne pouvons pas contrôler les fluctuations pour des domaines généraux. Pour ce qui est de l'extension à d'autres modèles de dimères, en particulier les dominos, aussi il devrait suffire de contrôler les fluctuations d'équilibres pour que tout le reste de la méthode fonctionne.

Pour l'étude de l'équilibre, comme nous l'avons indiqué dans la partie 1.5.1, il parait intéressant de prolonger le travail de la partie 4 et de l'article [Li13] pour exploiter la méthode de [Ken07]. Il parait très raisonnable

d'espérer une preuve de la conjecture 1.3.6 par cette méthode voire de sa variante non planaire.

Il y a aussi des questions très intéressantes sur des modèles reliés.

Pour la dynamique de Luby, Randall et Sinclair [LRS01] mentionné plus haut, Fabio Toninelli et moi espérons montrer prochainement la convergence vers une dynamique déterministe conformément à la théorie phénoménologique de la partie 1.1.4. Pour cette dynamique en effet, il paraît possible de suivre la méthode exposée dans la partie 1.2.4 puisque l'on peut faire une sommation par partie discrète.

Enfin une question très naturelle est celle d'interface à température positive sous-critique. En effet les pavages par des losanges correspondent au modèle d'Ising avec interaction plus proche voisin sur $\mathbb{Z}^3$ à température nulle. En particulier pour le modèle d'Ising avec interaction à plus proche voisin le comportement devrait être qualitativement identique à température positive et à température nulle. L'étude mathématique est cependant considérablement plus difficile et les résultats sont aujourd'hui limités à une borne "quasi-polynomiale" $T_{\text{mix}} = O(L^{\log L})$ en dimension 2 et à $T_{\text{mix}} = O(e^{cL})$ en dimension 3.

1.7 Organisation du reste de la thèse

Le reste de la thèse reprend les articles que j'ai écrit ou coécrit avec mon directeur.

Le chapitre 2 correspond à l'article [LT12], avec Fabio Toninelli. Il traite du modèle de pavage par hexagone et du cas des bords non planaire. Il contient la preuve des théorèmes 1.3.11 et 1.3.14 ainsi que du lemme 1.3.21. Notez que le lemme n'est pas explicitement donné mais apparaît seulement dans la preuve du théorème principal. La preuve du théorème 1.3.14 se trouve dans la partie 2.9 qui n'apparaît pas dans l'article originel.

Le chapitre 3 correspond à l'article [LT13], aussi avec Fabio Toninelli, qui est à paraître dans la revue "Probability Theory and Related Fields". Il contient une présentation générale des modèles de dimères bipartite ainsi que les preuves du théorème 1.3.15 et des lemmes 1.3.20 et 1.3.19. Notons que ces résultats sont en fait antérieurs à ceux du chapitre 2.

Enfin le chapitre 4 correspond à l'article [Las13]. Il traite des T-graphes présentés dans la partie 1.5 et contient la preuve du théorème 1.5.1. Il est très indépendant du reste de la thèse.

Chapter 2

Pavage par des losanges de domaines à bord non planaire

2.1 Introduction

Random lozenge tilings and their Glauber dynamics are a very natural object in mathematical physics, probability, combinatorics and theoretical computer science. Let $\mathcal{T}_L$ be the triangular lattice of mesh $1/L$ and call the union of two adjacent triangular faces a "lozenge". A region of $\mathcal{T}_L$ is called tileable if it can be covered by non-overlapping lozenges, so that no hole is left, cf. Figure 2.2. Typically, the number of possible tilings of a tileable region grows like the exponential of L^2 time its area, when the lattice mesh tends to zero. To a lozenge tiling is naturally associated a height function, so that a tiling can be seen as a discrete interface, see again Figure 2.2. When the mesh tends to zero and the height function at the boundary of the domain tends to some well-defined boundary height φ, the height function of a random tiling sampled from the uniform measure tends in probability to a certain limit shape $\bar{\phi}$. This limit shape minimizes the surface energy functional defined in formula (2.2), compatibly with the boundary height. According to the choice of the boundary height, $\bar{\phi}$ is either analytic, with $\nabla\bar{\phi}$ contained in the interior of a bounded set $\mathbb{T}$ of "allowed slopes" ($\mathbb{T}$ is a triangle, see later) or it can show coexistence of analytic portions ("liquid phase") and "frozen regions" or facets where $\nabla\bar{\phi}$ is on the boundary of $\mathbb{T}$ (facets correspond microscopically to regions where at least one of the three types of lozenges has vanishing probability of being present). For special boundary heights, $\bar{\phi}$ can happen to be non-frozen and flat (with constant slope in the interior of $\mathbb{T}$).

The Glauber dynamics on lozenge tilings is a natural Markov process whose updates consist in rotating by an angle 180° three lozenges that share

a vertex, see Figure 2.1. Such dynamics received a lot of attention in the-

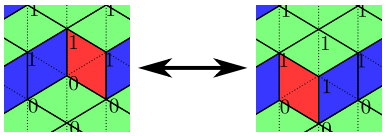

Figure 2.1: The allowed updates.

oretical computer science [LRS01, Wil04, RT00] since it is a conceptually and algorithmically simple way of sampling a random tiling in the long-time limit (the invariant measure of the process is the uniform one)[1]. In this context, a natural question that was investigated in the mentioned works was, how long one should run the dynamics before the uniform measure is reached. The Glauber dynamics is an even more natural stochastic process in mathematical physics: In the height function representation, lozenge dynamics is equivalent to the zero-temperature dynamics of interfaces, separating "+" and "−" spins, for the *three-dimensional* Ising model. Then, the question of convergence to equilibrium takes a rather different flavor: how long does it take before the interface, started far from equilibrium, approximates the macroscopic shape? Does the stochastic evolution converge to a deterministic, macroscopic evolution under suitable time rescaling?

It is widely believed that the time to reach equilibrium should scale like $L^{2+o(1)}$: actually, one expects that under diffusive scaling of time (i.e. setting $\tau = t/L^2$) the limiting deterministic evolution of the height function ϕ should roughly be the gradient flow associated to the surface energy functional,

$$\frac{d}{d\tau}\phi = \mu(\nabla\phi)\mathcal{L}\phi. \tag{2.1}$$

Here $\mathcal{L}$, directly related to the first variation of the surface energy functional, is the non-linear elliptic operator defined in (2.4), while $\mu(\nabla\phi)$ is a "mobility coefficient". See [Spo93] for an illuminating discussion of these issues. For $\tau \gg 1$ (i.e. $t \gg L^2$) the interface should asymptotically reach the macroscopic shape, characterized by $\mathcal{L}\bar{\phi} = 0$. This belief is supported by numerical simulations (for this and related models, see [Des02] and references in [Wil04, Hen97]), heuristic arguments [Hen97] and partial mathematical results [Wil04, CMT12].

Let us also mention that, for the zero-temperature *two-dimensional* (and not three-dimensional) Ising model, convergence of the evolution of spin droplets to a deterministic equation of anisotropic mean-curvature type under diffusive scaling has been achieved very recently [LST11, LST13]. The limit equation is somewhat the analog of (2.1), with the notable difference

[1]Let us mention that there are alternative, algorithmically more efficient, ways to sample uniform random tilings, see for instance [Wil96, KPW00] or [MS06].

that in that case ϕ describes a curve in the plane and not a surface in three-dimensional space. What helps in the two-dimensional case is that, as observed in [Spo93], the stochastic interface evolution can be locally mapped to well-studied interacting particle processes like one-dimensional symmetric simple exclusion and zero-range processes. None of these mappings holds in the three-dimensional case (i.e. for lozenge dynamics) and a host of new ideas is called for.

The main result of the present work is a mathematical confirmation of the $L^{2+o(1)}$ scaling of the time to reach the macroscopic shape:

Theorem 1 (Informal version)**.** *If the macroscopic shape $\bar{\phi}$ contains no frozen region then, whatever the initial condition of the dynamics, at time $L^{2+o(1)}$ the height function is with high probability at distance $o(1)$ from $\bar{\phi}$.*

See Theorem 2.3.3 for a precise formulation. Some previous results in this direction are reviewed in Section 2.3.1.

It is at present unclear to us whether the restriction to non-frozen macroscopic shapes is just a technical limitation or if something deeper happens. Frozen regions reflect the singularities of the surface tension functional and it is a priori possible that such singularities might have a drastic effect on dynamics. For the two-dimensional Ising model at zero temperature, singularities of the surface tension do not modify the time scaling L^2, but they have the effect that the deterministic macroscopic interface evolution one obtains in the diffusive limit is not smooth: the curvature of the interface is in general not differentiable in space [LST11, Section 2.2.2].

An obvious difficulty in attacking the lozenge dynamics problem is that we have no *a priori* knowledge of the non-equilibrium interface fluctuations during the evolution (before the equilibrium state is reached), or even of their order of magnitude. A natural idea is to look at the system on mesoscopic regions, sufficiently small so that macroscopic properties of the interface (slope, curvature, ...) are almost constant but much larger than the lattice spacing so that statistical fluctuations are small. More precisely one might expect that, if at some time t the interface approximates some smooth height function ϕ_t, then locally in the neighborhood of a point where the normal vector to ϕ_t is $\mathbf{n}$, the statistics of the interface will be determined by the infinite-volume, translation invariant Gibbs state of slope $\mathbf{n}$ [KOS06]. This reasoning would suggest height fluctuations of order $\sqrt{\log L}/L$. "Local equilibrium" ideas of this type are rather classical in physics, for the macroscopic derivation of the equations of fluid dynamics from microscopic particle systems.

In our case, this intuition seems extremely difficult to substantiate mathematically, yet we do use it somehow. Indeed the route we follow to prove Theorem 1 is to show that, if time is rescaled a bit more than diffusively (by setting $\tau = t/L^{2+\epsilon}$ with $\epsilon > 0$ arbitrarily small), then the interface

is bounded above and below by two evolving surfaces, both converging to the macroscopic shape, that follow an auxiliary deterministic equation that morally looks like (2.1). Via this auxiliary, slowed down, evolution we are able to make use of the "local equilibrium" intuition mentioned above.

We will not try to explain in detail the idea of the proof of Theorem 1 in this introduction. At this stage, let us just point out that one of the main difficulties we have to overcome is to precisely estimate average height and height fluctuations in mesoscopic regions of size $L^{-1/2+\delta}$ with δ small, for a rather large class of boundary heights. In [CMT12] the analog of Theorem 1 in the special case where the macroscopic shape is flat (i.e. $\bar{\phi}$ is an affine function) was proven: there, the problem of controlling equilibrium fluctuations in finite domains was bypassed since it was possible to reduce to fluctuation estimates in the translation invariant infinite-volume Gibbs states mentioned above. In the present case, this trick cannot work.

In general, it is only for special domains and boundary conditions that precise estimates on height fluctuations and on the finite-L corrections to the average height w.r.t. to the macroscopic limit $\bar{\phi}$ are known in the literature. See for instance [Ken00] for domino tilings. More relevant for us are the works [Pet12a, Pet12b] by L. Petrov. There, the author considers uniform random tilings of a hexagon $\hexagon_{abc}$ of sides a, b, c. In this case, the macroscopic shape (that is not flat) can be written down "explicitly" [CLP98] (cf. also Sections 2.3.2 and 2.4 below) and the equilibrium measure has an exact determinantal representation [Pet12a, Pet12b] which allows for precise asymptotic analysis.

One of the main new ideas of our work is that, locally in regions of size $\approx L^{-1/2+\delta}$, we can compare the height of the randomly evolving interface with the random *equilibrium* height of lozenge tilings in a hexagonal region $\hexagon_{abc}$ with suitably chosen, time-dependent parameters a, b, c. Technically, one key result we prove, which might be of interest by itself, is the following:

Theorem 2 (Informal version)**.** *Given a macroscopic shape $\bar{\phi}$ in a domain U, if $\bar{\phi}$ is smooth in the neighborhood of a point $u \in U$, then the Taylor expansion of $\bar{\phi}$ around u coincides up to second order with the Taylor expansion of the macroscopic shape associated to some hexagon $\hexagon_{abc}$.*

We will call the second-order Taylor expansion of $\bar{\phi}$ at a given point a "local structure". We would like to emphasize that Theorem 2 is *a priori* not obvious: As we will see in Section 2.4, the set of all admissible local structures associated to arbitrary macroscopic shapes is parametrized by four variables (two for the slope and two for the Hessian matrix), while "hexagonal" local structures are parametrized by a different set of four variables with a rather different meaning (two for the side-lengths of the hexagon and two for the coordinates of a point inside the hexagon). We have then to check that a certain explicit but complicated function from $\mathbb{R}^4$ to $\mathbb{R}^4$ is surjective (actually it turns out to be a bijection).

Theorem 2 would be false if "second order" were replaced, say, by "third order" (it would require surjectivity of a function from $\mathbb{R}^4$ to $\mathbb{R}^n$ for some $n > 4$). Remarkably, for the proof of Theorem 1 the second-order comparison provided by Theorem 2 is sufficient. The basic reason is that, in regions of size $L^{-1/2+\delta}$, third- or higher-order terms in the expansion of the macroscopic shape give negligible contributions of order $L^{-3/2+3\delta}$, much smaller than the minimal significant length-scale of the model, which is the lattice spacing $1/L$.

2.2 Random lozenge tilings and height function

2.2.1 Monotone surfaces and height functions

Let L be an integer, that will be taken large later. Closed squares in $\mathbb{R}^3$ of side $1/L$, with the four vertices in $(\mathbb{Z}/L)^3$, will be called *faces of* $(\mathbb{Z}/L)^3$.

Definition 2.2.1. *A discrete (or stepped) monotone surface Σ_L is a connected union of faces of $(\mathbb{Z}/L)^3$ that projects bijectively on the* 111 *plane P_{111}.*

Look at Figure 2.2: the projection of each square face of Σ_L is a lozenge with angles 60° and 120° and three possible orientations: horizontal, south-east and south-west, according to whether the normal vector to the square face of Σ_L is $(0, 0, 1)$, $(1, 0, 0)$ or $(0, 1, 0)$. The projection of Σ_L gives therefore a lozenge tiling of P_{111} with these three types of tiles. Vertices of the lozenges are the vertices of a triangular lattice $\mathcal{T}_L$ of side *const.*$/L$. Via a suitable choice of coordinates, we will set the constant to be 1 below.

Definition 2.2.2. *A continuous monotone surface Σ in $\mathbb{R}^3$ is a two-dimensional connected surface such that:*

1. *Σ projects bijectively on P_{111};*
2. *the normal vector to Σ, assumed to be defined almost everywhere, points in $\mathbb{R}^3_{\geqslant 0}$.*

Note that injectivity of the orthogonal projection of Σ on P_{111} is a consequence of the assumption on the normal vector.

Definition 2.2.3 (Height function)**.** *To a continuous (resp. stepped) monotone surface Σ (resp. Σ_L) we associate a height function $\phi : P_{111} \to \mathbb{R}$ (resp. $h : \mathcal{T}_L \to \mathbb{Z}/L$) , as follows: $\phi(u)$ (resp. $h(u)$) equals the height with respect to the horizontal plane of the point $p \in \Sigma$ (resp. $p \in \Sigma_L$) whose orthogonal projection on P_{111} is u.*

Note that, for discrete monotone surfaces, heights are associated to vertices of lozenges, i.e. to vertices of $\mathcal{T}_L$. The definition can be extended to

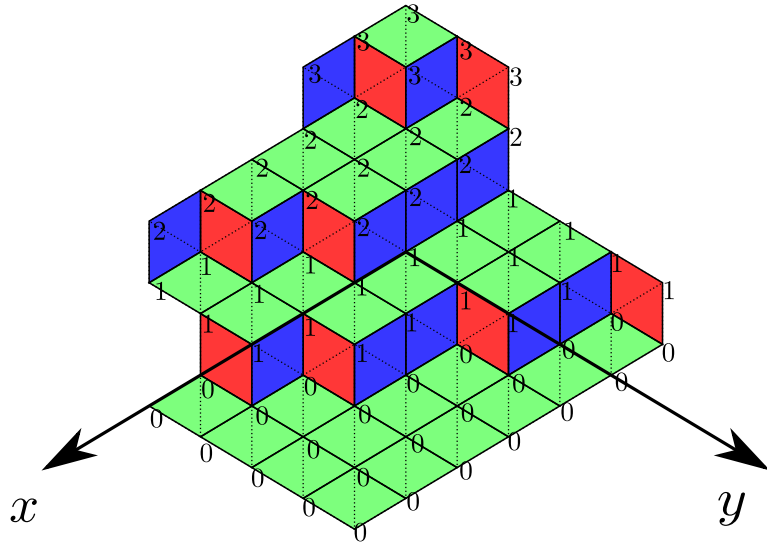

Figure 2.2: A portion of lozenge tiling associated to a stepped monotone interface. Next to each vertex of $\mathcal{T}_L$ is marked the value of the height function. The underlying triangular lattice is given by dotted lines.

obtain a real-valued height function h on the whole P_{111}, simply by establishing that the height is linear on triangular faces of $\mathcal{T}_L$.

On P_{111} introduce a coordinate frame (x, y) (see Figure 2.2) such that a given reference vertex $v_0 \in \mathcal{T}_L$ has coordinates $(0, 0)$ and the vertices of $\mathcal{T}_L$ that are nearest neighbors of v_0 in directions $e^{-5i\pi/6}$ (resp. $e^{-i\pi/6}$) have coordinates $(1/L, 0)$ (resp. $(0, 1/L)$). This choice of coordinates is convenient for stepped monotone surfaces, since the axes are along two of the directions of the triangular lattice $\mathcal{T}_L$. Note also that the x and y axes are along the P_{111} projections of the directions of the usual $\hat{e}_1$ and $\hat{e}_2$ coordinate axes of $\mathbb{R}^3$. Whenever convenient, we will implicitly identify the plane P_{111} with $\mathbb{R}^2$.

For continuous monotone interfaces, the condition that the normal vector points in $\mathbb{R}^3_{\geqslant 0}$ can be reformulated as follows: wherever defined, the gradient $\nabla\phi = (\partial_x\phi, \partial_y\phi)$ belongs to $\mathbb{T}$, where:

Definition 2.2.4. $\mathbb{T} \subset \mathbb{R}^2$ *is the triangle with vertices* $(0, 0), (0, -1), (-1, 0)$.

Remark 2.2.5. *When one moves by one lattice step in* $\mathcal{T}_L$ *along the* x *or* y *directions the height function of a stepped interface decreases by* $1/L$ *if one crosses a lozenge, and is unchanged if one moves along the edge of a lozenge. When instead one moves by a lattice step upward in the vertical direction (i.e. by* $(-1/L, -1/L)$ *in the* (x, y) *coordinates), the height function is unchanged if one crosses a lozenge, and increases by* $1/L$ *if one moves along the edge of a lozenge.*

While a discrete height function uniquely identifies a lozenge tiling, in view of Remark 2.2.5 a lozenge tiling identifies the height function h only modulo a global additive constant (the tiling identifies the height gradients). If however one fixes the height at some vertex, then the correspondence is bijective. In the following, the height along the boundary of a finite region will be fixed, so we will freely identify height functions and lozenge tilings.

Definition 2.2.6 (Domains)**.** *In the continuous surface setting, a domain U will denote a simply connected, bounded, closed subset of P_{111}, whose boundary ∂U is a piecewise C^∞ simple curve.*

In the discrete setting, a discrete domain U_L will be a simply connected, bounded union of closed triangular faces of $\mathcal{T}_L$. With some abuse of notation, we will often identify U_L with $U_L \cap \mathcal{T}_L$. The set of sites $v \in U_L \cap \mathcal{T}_L$ that are not on ∂U_L is denoted U_L^{int}, while $U_L^{ext} = \mathcal{T}_L \setminus U_L^{int}$.

Definition 2.2.7 (Non-extremal monotone surface)**.** *Let Σ be a continuous monotone surface, with height function ϕ, and U be a domain of P_{111}. We say that Σ is non-extremal in U if $\nabla\phi$ is defined everywhere in $\overset{\circ}{U}$ (the interior of U) and there exists $\epsilon > 0$ such that, for every $(x, y) \in \overset{\circ}{U}$, $\nabla\phi$ is at distance at least ϵ from the boundary of the triangle $\mathbb{T}$.*

In geometric terms, this means that all three components of the normal vector to Σ are larger than a constant times ϵ, at every point that projects on $\overset{\circ}{U}$.

Definition 2.2.8 (Continuous boundary heights)**.** *Given a domain $U \subset P_{111}$, a function $\varphi : P_{111} \setminus U \mapsto \mathbb{R}$ is called* (continuous) boundary height *if there exists a continuous monotone surface Σ whose height function ϕ coincides with φ on $P_{111} \setminus U$.*

Discrete boundary heights are defined similarly:

Definition 2.2.9 (Discrete boundary heights)**.** *Given a discrete domain U_L as in Definition 2.2.6, we call $\varphi_L : U_L^{ext} \mapsto \mathbb{Z}/L$ a* discrete boundary height *if there exists a stepped monotone surface Σ_L whose height coincides with φ_L on U_L^{ext}.*

Remark 2.2.10. *Boundary heights have been defined for technical reasons as height functions outside certain (continuous or discrete) domains. However, with some abuse of notation, we will often see φ_L and φ as functions on ∂U_L and ∂U, respectively (instead of functions on U^{ext} and $P_{111} \setminus U$). This makes sense because we will see (DLR equations below) that the statistical properties of the height function in a domain U_L are determined uniquely by the height on ∂U_L.*

We will be mostly interested in stepped monotone surfaces that approximate as $L \to \infty$ a continuous monotone surface:

Definition 2.2.11 (Discretizations)**.** *Consider a continuous monotone surface Σ, a domain U and, for $L \geqslant 1$, stepped monotone surfaces Σ_L and discrete domains U_L. We say that $(\Sigma_L, U_L)_{L\geqslant 1}$ is a discretization of (Σ, U) if, for some constant C independent of L:*

1. *the boundary ∂U_L is within Hausdorff distance C/L from ∂U;*
2. *for every $u \in U_L \cap U$, one has $|h(u) - \phi(u)| \leqslant C/L$.*

The restriction φ_L of h (the height function of Σ_L) to U_L^{ext} is said to be a discretization of the boundary height $\varphi = \phi|_{P_{111}\setminus U}$.

Given (Σ, U), one can always find a discretization $(\Sigma_L, U_L)_{L\geqslant 1}$: just take Σ_L as the boundary of the union of all closed cubes with vertices in $(\mathbb{Z}/L)^3$ that are below Σ, and U_L as the union of triangular faces of $\mathcal{T}_L$ contained in U.

2.2.2 Uniform measure, DLR equations and macroscopic shape

Given a discrete domain U_L and a discrete boundary height φ_L as in Definition 2.2.9, we let $\pi_{U_L}^{\varphi_L}$ denote the uniform measure over the set Ω_{U_L,φ_L} of all stepped monotone surfaces whose height on U_L^{ext} is φ_L (by definition, there is at least one of them).

The measure $\pi_{U_L}^{\varphi_L}$ satisfies the so-called DLR equations. If V_L is a subdomain of U_L, then under the law $\pi_{U_L}^{\varphi_L}$, conditioned to the event that the height on V_L^{ext} is a certain boundary height ψ_L, the height function in V_L has the uniform law $\pi_{V_L}^{\psi_L}$.

The following well-known theorem states that, if the boundary condition φ_L is the discretization of a continuous boundary height φ, with high probability under the uniform measure $\pi_{U_L}^{\varphi_L}$ the stepped interface Σ_L approximates a certain macroscopic shape $\bar{\phi}$, that solves a variational principle.

Theorem 2.2.12. *[CKP01] Let U and φ be a domain and a continuous boundary height, satisfying the properties specified in Definitions 2.2.6 and 2.2.8.*

1. *There exists a unique minimizer $\bar{\phi}$, among continuous monotone surfaces with boundary height φ, of the surface tension functional*

$$\Psi(\phi) = \int_U \sigma(s(u), t(u)) d^2u = \int_U \sigma(\nabla\phi) d^2u \tag{2.2}$$

where

$$\sigma(s,t) = -\frac{1}{\pi}\left[\Lambda(\pi s) + \Lambda(\pi t) + \Lambda(\pi(-1-s-t))\right] \tag{2.3}$$

and

$$\Lambda(\theta) = -\int_0^{-\theta} \log(2\sin(t))dt$$

(observe that $-\theta \geqslant 0$*, since* $s, t, -1-s-t \leqslant 0$ *if* $(s,t) \in \mathbb{T}$*).*

2. *Let* $(\varphi_L, U_L)_{L\geqslant 1}$ *be a discretization of the boundary condition* (φ, U) *and* Σ_L *be distributed according to the uniform measure* $\pi_{U_L}^{\varphi_L}$*. Then, as* $L \to \infty$*,* Σ_L *tends in* $\pi_{U_L}^{\varphi_L}$*-probability to* $\bar{\phi}$*: for every* $\epsilon > 0$*,*

$$\pi_{U_L}^{\varphi_L}\left(\exists u \in U_L : |h(u) - \bar{\phi}(u)| \geqslant \epsilon\right) \to 0.$$

The Euler-Lagrange equation associated to the variational principle is the non-linear elliptic PDE in "divergence form"

$$\begin{aligned}\mathcal{L}\bar{\phi} &:= \partial_x(\partial_s\sigma(\nabla\bar{\phi})) + \partial_y(\partial_t\sigma(\nabla\bar{\phi})) \\ &= a_{11}(\nabla\bar{\phi})\partial_x^2\bar{\phi} + a_{22}(\nabla\bar{\phi})\partial_y^2\bar{\phi} + 2a_{12}(\nabla\bar{\phi})\partial_{x,y}^2\bar{\phi} = 0 \quad (2.4)\end{aligned}$$

with

$$a_{11}(\nabla\bar{\phi}) = \frac{1}{\tan(-\pi\partial_x\bar{\phi})} + \frac{1}{\tan(\pi(1+\partial_x\bar{\phi}+\partial_y\bar{\phi}))} \quad (2.5)$$

$$a_{22}(\nabla\bar{\phi}) = \frac{1}{\tan(-\pi\partial_y\bar{\phi})} + \frac{1}{\tan(\pi(1+\partial_x\bar{\phi}+\partial_y\bar{\phi}))} \quad (2.6)$$

$$a_{12}(\nabla\bar{\phi}) = a_{21}(\nabla\bar{\phi}) = \frac{1}{\tan(\pi(1+\partial_x\bar{\phi}+\partial_y\bar{\phi}))}. \quad (2.7)$$

The matrix $\mathbf{a}(s,t) = \{a_{ij}((s,t))\}_{i,j=1,2}$ is strictly positive definite in $\mathring{\mathbb{T}}$, as a consequence of strict convexity of the surface tension functional Ψ (positive definiteness can also be checked by hand; in particular, the determinant of $\mathbf{a}(s,t)$ is 1). In $\mathring{\mathbb{T}}$ the matrix elements $a_{ij}((s,t))$ are analytic and the diagonal elements $a_{ii}(s,t)$ are strictly positive. When instead (s,t) approaches $\partial\mathbb{T}$, the matrix $\mathbf{a}(s,t)$ becomes singular.

Assume that $\bar{\phi}$ is non-extremal in U (its gradient is bounded away from the boundary of the set of allowed slopes). Then, $\bar{\phi}$ is real analytic in $\mathring{U}$ (see for instance [Gia83, Ch. II.2 and Ch. VI.3]) and solves (2.4) everywhere in $\mathring{U}$.

It can however happen, even for some natural boundary conditions (U, φ) (see Section 2.3.2), that in some subset $\hat{U} \subset U$ with non-empty interior the gradient $\nabla\bar{\phi}$ belongs to $\partial\mathbb{T}$. Such regions $\hat{U}$ are called *frozen regions*.

2.3 Dynamics, conjectures and main result

The Glauber dynamics is defined as a Markov process $(h_t^\eta)_{t\geqslant 0}$ on the set Ω_{U_L,φ_L}, with η denoting the initial condition. To each site $v \in U_L^{int}$ such

that all six neighbors of v are in U_L, we associate a mean-one Poisson clock. Clocks at different sites are independent. When the clock at v rings, if in the present lozenge configuration v belongs to exactly three lozenges, then we turn the three lozenges by an angle π. See Figure 2.1. In terms of height function, an update corresponds to increasing by $+1/L$ or decreasing by $-1/L$ the height $h_t^\eta(v)$ with rate 1, with the constraint that h_t^η remains a stepped monotone surface in Ω_{U_L,φ_L} at all times.

We denote μ_t^η the law of h_t^η and $\mathbb{P}$ the law of the entire process. The dynamics is reversible and its unique invariant measure is the uniform measure $\pi_{U_L}^{\varphi_L}$.

As we mentioned in the introduction, the dynamics is expected to converge to equilibrium in a time of order L^2 times sub-leading corrections. More precisely:

Conjecture 2.3.1. *Let U, φ and its discretizations $(U_L, \varphi_L)_{L\geqslant 1}$ be as above. For every $\delta > 0$ there exists $c(\delta) < \infty$ such that, whatever the initial condition η, at times $t > c(\delta)L^{2+\delta}$ the following holds with probability tending to 1 as $L \to \infty$: for every vertex $v \in U_L$*

$$|h_t^\eta(v) - \bar{\phi}(v)| = o(1). \tag{2.8}$$

In other words, within time $L^{2+o(1)}$ the interface macroscopically approximates the equilibrium shape to any pre-assigned precision.

Actually, we believe that more should be true: at time $L^{2+o(1)}$, the law μ_t^η should be very close to the equilibrium measure $\pi_{U_L}^{\varphi_L}$. More precisely, define the mixing time of the dynamics as

$$T_{\text{mix}} = T_{\text{mix}}(U_L, \varphi_L) = \inf\{t : \max_\eta \|\mu_t^\eta - \pi_{U_L}^{\varphi_L}\| \leqslant 1/(2e)\}, \tag{2.9}$$

with $\|\mu - \nu\|$ the total variation distance between two probability measures μ, ν. Then:

Conjecture 2.3.2. *In the same setting of Conjecture 2.3.1, it is expected that $T_{\text{mix}} = O(L^{2+o(1)})$.*

Thanks to the classical inequality

$$\max_\eta \|\mu_t^\eta - \pi_{U_L}^{\varphi_L}\| \leqslant e^{-\lfloor t/T_{\text{mix}}\rfloor}, \tag{2.10}$$

this would say that, at time of order $L^{2+o(1)}\log(1/\delta)$, μ_t^η is within variation distance δ from equilibrium, for any arbitrary δ.

Our main results is a proof of Conjecture 2.3.1 under the assumption that the macroscopic shape has no frozen regions (Theorem 2.3.3). As mentioned at the end of Section 2.3.2, the methods we develop in this work allow also to prove the stronger Conjecture 2.3.2 for a rather special class of boundary conditions (Theorem 2.3.8; details will be given in a forthcoming publication).

Theorem 2.3.3. *Let the domain U and the boundary condition φ satisfy the assumptions of Definitions 2.2.6 and 2.2.8. Assume in addition that the associated macroscopic shape $\bar{\phi}$ is non-extremal in U and let $(\varphi_L, U_L)_{L\geqslant 1}$ be a discretization of (φ, U). Consider the Glauber dynamics in U_L with boundary height φ_L and initial condition η. There exists a sequence ϵ_L tending to zero and, for each $\delta > 0$, a constant $c(\delta) < \infty$ such that, with $T_L = c(\delta)L^{2+\delta}$,*

$$\max_{\eta} \sup_{t>T_L} \mathbb{P}(\exists v \in U_L : |h_t^\eta(v) - \bar{\phi}(v)| \geqslant \epsilon_L) \to 0 \quad \text{as} \quad L \to \infty. \tag{2.11}$$

It is important to emphasize that, except for the δ in the exponent of T_L, this result is optimal. Indeed, it is known that there exist initial conditions η such that, for times smaller than aL^2 with $a > 0$ small (how small, depending on the domain U and on the boundary height φ), $\max_v |h_t^\eta(v) - \bar{\phi}(v)|$ is still bounded away from zero. This is proven in [LT12, Section 10] in the special case where the macroscopic shape $\bar{\phi}$ is flat, but the proof extends with minor modifications to the case of non-extremal $\bar{\phi}$ considered here.

A slight generalization of Theorem 2.3.3 is the following:

Corollary 2.3.4. *The same statement as in Theorem 2.3.3 holds without the assumption that $\bar{\phi}$ is non-extremal, if the following holds: there exists a sequence $(\varphi^{(n)})_{n\geqslant 1}$ of continuous boundary heights on $P_{111} \setminus U$ such that:*

- $\max_{x\in\partial U} |\varphi(x) - \varphi^{(n)}(x)|$ *tends to zero as $n \to \infty$;*
- *for every n, the macroscopic shape $\bar{\phi}^{(n)}$ corresponding to boundary conditions $(U, \varphi^{(n)})$ is non-extremal.*

In other words, the claim of Theorem 2.3.3 holds if $\bar{\phi}$ can be approximated by a sequence of non-extremal macroscopic shapes. A typical application is given in Section 2.3.2 below.

2.3.1 Previous results

The first mathematical estimate we are aware of on the relaxation time of the Glauber dynamics for lozenge tilings is in the work of Luby, Randall and Sinclair [LRS01]. These authors actually introduced and studied an *ad-hoc* modified, highly non-local Markov dynamics, such that the number of lozenges that can be updated in a single step is unbounded (when L grows). Recall that, by constrast, for the local Glauber dynamics we study here, updates consist in rotating only three lozenges at the time. The result of [LRS01] is *rapid mixing*: the mixing time $T^\star_{\text{mix}}$ of the non-local dynamics grows *at most* like some polynomial of the graph-distance diameter of U_L. A few years later, D. Wilson [Wil04] proved the $O(L^2 \log L)$ scaling for $T^\star_{\text{mix}}$, always for the non-local dynamics.

Via known comparison arguments for Markov chains [DSC93], Wilson's result implies [RT00] a non-optimal polynomial upper bound $T_{\text{mix}} = O(L^6 \log L)$ for the mixing time of the local Glauber dynamics (actually the log factor can be removed by going through the spectral gap of the non-local chain, see [Wil04, Section 5]). This result is quite far from the expected behavior $T_{\text{mix}} = L^{2+o(1)}$, but we emphasize that the methods of [LRS01, Wil04, RT00] require essentially no conditions on the boundary height (in particular, the possible presence of frozen regions in the macroscopic shape plays no role at all).

Both [LRS01] and [Wil04] are based on clever path-coupling arguments. The reason why they cannot catch the right scaling $\approx L^2$ for the time the local Glauber dynamics takes to approach the equilibrium shape is, in our opinion, that they do not use any input from the knowledge of the macroscopic shape and of height fluctuations properties of the equilibrium measure.

A first mathematical confirmation of the $L^{2+o(1)}$ scaling for the time of convergence to equilibrium for the local Glauber dynamics came in [CMT12], where it was proven that $T_{\text{mix}} = O(L^{2+o(1)})$, under the strongly limiting assumption that the boundary height is such that the macroscopic shape ϕ is flat (i.e. an affine function). The same result was proven later, with a somewhat different method, for more general tilings (e.g. domino tilings) [LT12].

Going beyond the flat case, as we do in the present work, requires many novel mathematical ideas.

2.3.2 Hexagonal regions

A crucial role in our work is played by some special boundary heights, of "hexagonal type". This may look at first surprising since the associated macroscopic shape is not at all non-extremal, in contrast with the requirements of Theorem 2.3.3. Such boundary conditions have played an extremely important role in the understanding of random tilings: in particular, this is the first case where the occurrence of frozen region and of the "arctic circle phenomenon" was discovered [CLP98] (see also the earlier work [JPS95] for domino tilings). Also, the uniform law on lozenge tilings has in this case an explicit determinantal representation. This allows to extract sharp estimates, as $L \to \infty$, on height fluctuations, on the finite-size corrections to the average height with respect to the macroscopic shape $\bar{\phi}$, and to prove convergence of height fluctuations to the Gaussian Free Field [Pet12a, Pet12b].

Let the monotone surface Σ be the boundary of $(\mathbb{R}^+)^3$, the positive octant of $\mathbb{R}^3$ and let the half-infinite lines $\hat{e}_1, \hat{e}_2, \hat{e}_3$ be the 111 projection of the positive coordinate axes of $\mathbb{R}^3$, see Figure 2.3. Given $a, b, c > 0$ let $\hexagon_{abc}$ be the hexagon in P_{111} with angles of 120° and with sides a, b, c, a, b, c, such that three of the vertices are on the lines $\hat{e}_i$. The sides of length a are

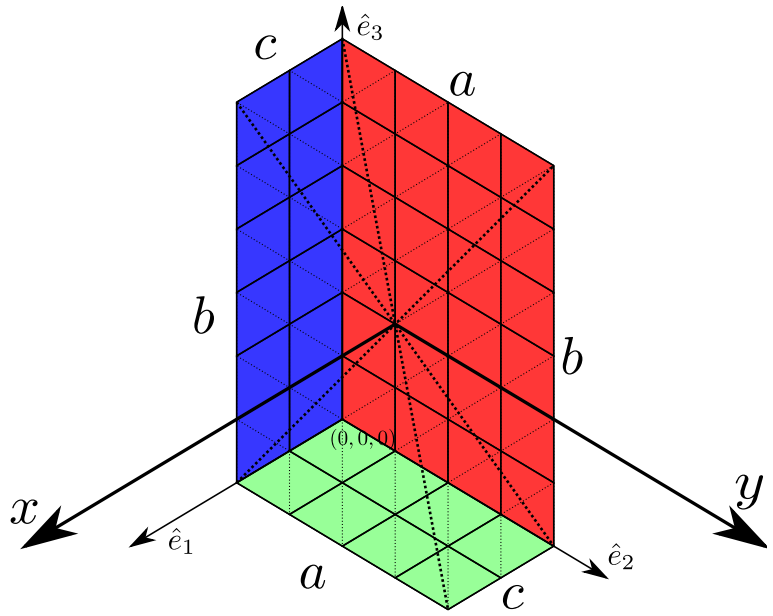

Figure 2.3: The hexagon $\hexagon_{abc}$. The origin of (x, y) is set at the center of the hexagon, where the three diagonals (dotted lines) meet. The lines $\hat{e}_i$ are the 111 projections of the positive coordinate axes of $\mathbb{R}^3$.

parallel to the y axis and those of length c to the x axis (recall that the x and y axes are not orthogonal). See again Figure 2.3. Without loss of generality, we will assume that $a + b + c = 1$.

We let $\bigcirc_{abc}$ be the open ellipse inscribed in $\hexagon_{abc}$, and φ_{abc} the boundary height of Σ restricted to $\partial\hexagon_{abc}$.

This is the prototypical case where the macroscopic shape contains frozen regions:

Theorem 2.3.5. *[CLP98] Call $\bar{\phi}_{abc}$ the macroscopic shape when $U = \hexagon_{abc}$ and $\varphi = \varphi_{abc}$. In $\bigcirc_{abc}$, $\bar{\phi}_{abc}$ is analytic and its gradient $\nabla\bar{\phi}_{abc}$ is in $\mathring{\mathbb{T}}$. On $\hexagon_{abc} \setminus \bigcirc_{abc}$, $\nabla\bar{\phi}_{abc} \in \partial\mathbb{T}$. More precisely, remove from $\hexagon_{abc} \setminus \bigcirc_{abc}$ the six points of contact between $\bigcirc_{abc}$ and the boundary of the hexagon and consider the six connected components of the set thus obtained. On the components that touch sides ac (resp. ab, resp. bc) the gradient is $(0, 0)$ (resp. $(-1, 0)$, resp. $(0, -1)$).*

The ellipse $\bigcirc_{abc}$ is called the "smooth region" or "liquid region", while $\hexagon_{abc} \setminus \bigcirc_{abc}$ is the "frozen region".

A discretization of $(\hexagon_{abc}, \varphi_{abc})$ is simply obtained as $(\hexagon_{a_L b_L c_L}, \varphi_{a_L b_L c_L})_{L \geqslant 1}$ where

$$a_L = (1/L)\lfloor aL \rfloor, b_L = (1/L)\lfloor bL \rfloor, c_L = (1/L)\lfloor cL \rfloor.$$

To simplify formulas we will always pretend that aL, bL, cL are even integers, in which case $\hexagon_{a_L b_L c_L}$ and $\varphi_{a_L b_L c_L}$ exactly coincide with $\hexagon_{abc}, \varphi_{abc}$, and the center of the hexagon is a vertex of $\mathcal{T}_L$, that will be chosen by convention as the origin of P_{111}. For lightness of notations, we write simply π_L^{abc} for the uniform measure $\pi^{\varphi_{a_L b_L c_L}}_{\hexagon_{a_L b_L c_L}}$.

We already know from Theorem 2.2.12 that, under the measure π_L^{abc}, the typical height function is macroscopically close to $\bar{\phi}_{abc}$. The following theorem makes this claim much sharper, but the statements hold only in the liquid region:

Theorem 2.3.6. *For every $v, u \in \hexagon_{abc}$*

$$|(\pi_L^{abc}(h(u)) - \pi_L^{abc}(h(v))) - (\bar{\phi}_{abc}(u) - \bar{\phi}_{abc}(v))| \leqslant K|u-v|/L \qquad (2.12)$$

where $K = K(a,b,c,u,v)$ is bounded as long as

$$\min(a, b, c, dist(u, \partial\hexagon_{abc}), dist(v, \partial\hexagon_{abc}))$$

is bounded away from zero.

For every $u \in \hexagon_{abc}$, $n > 0$ and $\epsilon > 0$,

$$\pi_L^{abc}\left(|h(u) - \pi_L^{abc}(h(u))| > L^{-1+\epsilon}\right) = O(L^{-n}) \qquad (2.13)$$

(again, the error term is uniform in a, b, c, u if $\min(a, b, c, dist(u, \partial\hexagon_{abc}))$ is bounded away from zero).

The first claim is proven in Appendix 2.A, following methods of [Pet12a, Pet12b]. The second one follows directly from [Pet12b, Lemma 5.6], where it is proven that $\pi_L^{abc}(L^n|h(v) - \pi_L^{abc}(h(v))|^n) = O(L^\epsilon)$, plus Tchebyshev's inequality. Uniformity of the error term is not stated explicitly in [Pet12b], but it can be easily extracted from the proof).

Let us state and prove a simple consequence of Theorem 2.3.6, that we need in Section 2.7.

Proposition 2.3.7. *Let as above $a, b, c > 0$ with $a + b + c = 1$ and D_L be a discrete domain contained in $\hexagon_{abc}$, whose distance from $\partial\hexagon_{abc}$ is at least $\delta > 0$ independent of L. Let further φ_L be a boundary height on ∂D_L such that, for some $C > 0$,*

$$|\varphi_L(v) - \pi_L^{abc}(h(v))| \leqslant C/L \quad \text{for every} \quad v \in \partial D_L.$$

Then, for every $\epsilon > 0$ and $n < \infty$,

$$\sup_{v \in D_L} \pi_{D_L}^{\varphi_L}(|h(v) - \pi_L^{abc}(h(v))| \geqslant L^{-1+\epsilon}) \leqslant c(\delta, n, \epsilon) L^{-n}. \qquad (2.14)$$

Proof of Proposition 2.3.7. The arguments are rather standard, so let us be sketchy. Suppose for instance we want to upper bound

$$\sup_v \pi_{D_L}^{\varphi_L}\left(h(v) - \pi_L^{abc}(h(v)) \geqslant L^{-1+\epsilon}\right). \tag{2.15}$$

Define $\varphi'_L = \varphi_L - L^{-1+\epsilon}/2$. From (2.13) we see that, under the measure π_L^{abc}, except with probability $O(L^{-n})$ one has $h(v) \geqslant \varphi'_L$ for every $v \in \partial D_L$. Therefore,

$$\begin{aligned}
&\sup_v \pi_{D_L}^{\varphi_L}\left(h(v) - \pi_L^{abc}(h(v)) \geqslant L^{-1+\epsilon}\right) \\
&\qquad = \sup_v \pi_{D_L}^{\varphi'_L}\left(h(v) - \pi_L^{abc}(h(v)) \geqslant L^{-1+\epsilon}/2\right) \\
&\qquad \leqslant \sup_v \pi_L^{abc}\left(h(v) - \pi_L^{abc}(h(v)) \geqslant L^{-1+\epsilon}/2\right) + O(L^{-n}).
\end{aligned} \tag{2.16}$$

In the last step we used monotonicity (the increasing event $h(v) - \pi_L^{abc}(v) \geqslant L^{-1+\epsilon}/2$ becomes more likely if we replace φ'_L with a higher boundary condition, see Section 2.5) and the DLR equations. Then, Eq. (2.13) implies directly (2.15) (estimates are uniform in v because we assumed that all $v \in D_L$ are uniformly bounded away, by at least δ, from $\partial \bigcirc_{abc}$.)

□

Dynamics with hexagonal boundary height

Let $U = \bigcirc_{abc}$ and the boundary condition φ be the restriction of $\bar{\phi}_{abc}$ to ∂U. The macroscopic shape $\bar{\phi}$ is *not* non-extremal in U since, while the gradient $\nabla\bar{\phi}$ is well-defined and belongs to $\mathring{\mathbb{T}}$ everywhere in $\mathring{U}$, it approaches $\partial\mathbb{T}$ when the boundary of U is approached. However, Corollary 2.3.4 is applicable in this case, implying the estimate (2.11) on the time when the equilibrium shape is reached. Just take some sequence $u^{(n)} > 0$ tending to zero, define

$$a^{(n)} = a(1+u^{(n)}), b^{(n)} = b(1+u^{(n)}), c^{(n)} = c(1+u^{(n)})$$

and let $\varphi^{(n)}$ be the restriction to $\partial\bigcirc_{abc}$ of the macroscopic shape $\bar{\phi}_{a^{(n)}b^{(n)}c^{(n)}}$ corresponding to the expanded hexagon $\hexagon_{a^{(n)}b^{(n)}c^{(n)}}$. Since $\bigcirc_{a^{(n)}b^{(n)}c^{(n)}}$ contains $U = \bigcirc_{abc}$ strictly, the macroscopic shape $\bar{\phi}^{(n)} = \bar{\phi}_{a^{(n)}b^{(n)}c^{(n)}}$ is non-maximal in U.

The sharp control of the equilibrium measure provided by Theorem 2.3.6, together with the methods developed in the proof of Theorem 2.3.3, allow to prove the stronger result $T_{\text{mix}} \approx L^{2+o(1)}$ (Conjecture 2.3.2) in the case where U is a closed, simply connected subset of the open ellipse $\bigcirc_{abc}$ and the boundary height φ is the restriction of $\bar{\phi}_{abc}$ to ∂U.

Theorem 2.3.8. *Fix a, b, c with $a + b + c = 1$ and $a > 0, b > 0, c > 0$. Let U be a closed domain contained in $\bigcirc_{abc}$. Let φ be the restriction of $\bar{\phi}_{abc}$ to ∂U and let $(\varphi_L, U_L)_{L\geqslant 1}$ a discretization of (φ, U). Then, $T_{\text{mix}} \leqslant c(\delta)L^{2+\delta}$ for every $\delta > 0$.*

The proof of the theorem will be given in section 2.9.

2.4 Local structures of macroscopic shapes

In this section we formalize and prove Theorem 2.

Let $\bar{\phi}$ be the macroscopic shape in some domain U with some boundary height φ. Consider a point $(x, y) \in \overset{\circ}{U}$ where $\bar{\phi}$ is at least twice differentiable, and such that $\nabla\bar{\phi} \in \overset{\circ}{\mathbb{T}}$; let $H^{\bar{\phi}}$ be the 2×2 Hessian matrix of $\bar{\phi}$ at (x, y). We call $\{\nabla\bar{\phi}, H^{\bar{\phi}}\}$, the *local structure of* $\bar{\phi}$ *at* (x, y). We are excluding points (x, y) where the gradient of $\bar{\phi}$ is in $\partial\mathbb{T}$, or where $\bar{\phi}$ is non-smooth: in any case, our Theorem 2.3.3 involves only domains where the macroscopic shape is non-extremal and in particular is C^∞.

Recall that, if $\nabla\bar{\phi} \in \overset{\circ}{\mathbb{T}}$, the components of the Hessian $H^{\bar{\phi}}$ verify Eq. (2.4), i.e. for any local structure $\nabla\bar{\phi}$ and $H^{\bar{\phi}}$ are related by

$$\sum_{i,j=1}^{2} a_{ij}(\nabla\bar{\phi}) H^{\bar{\phi}}_{ij} = 0. \tag{2.17}$$

Therefore, to identify a local structure it is sufficient to know the gradient of $\bar{\phi}$ and two elements of the Hessian matrix, say the ∂^2_x and ∂^2_{xy} components (i.e. the (11) and (12) = (21) matrix elements). In view of this, we define

$$\mathcal{A} = \{z = (z_1, z_2, z_{11}, z_{12}) \in \mathbb{R}^4 : (z_1, z_2) \in \overset{\circ}{\mathbb{T}}\} \tag{2.18}$$

which should be seen as *the set of all a priori admissible local structures*. Note that it is not guaranteed that every $z \in \mathcal{A}$ can be actually realized as the local structure for some boundary condition.

Let us also define the open set

$$W = \{w = (a, b, x, y) \in \mathbb{R}^4 : a > 0, b > 0, a + b < 1, (x, y) \in \bigcirc_{abc}\}$$

where as usual it is understood that $c = c(a, b) = 1 - a - b$. This is the set parametrizing points in ellipses of the type $\bigcirc_{abc}$.

Remark 2.4.1. *The allowed values of* (a, b) *belong to the interior of triangle* $\mathbb{V} = -\mathbb{T}$*, with* $\mathbb{T}$ *as in Definition 2.2.4.*

We introduce a map $f : W \mapsto \mathcal{A}$ as follows:

$$f(a, b, x, y) = z = (z_1, z_2, z_{11}, z_{12}) \in \mathbb{R}^4$$

with (z_1, z_2) the slope $\nabla\bar{\phi}_{abc}$ at (x, y) (with $\bar{\phi}_{abc}$ the macroscopic shape corresponding to the hexagon $\hexagon_{abc}$, as in Theorem 2.3.5) and

$$(z_{11}, z_{12}) = (\partial^2_x\bar{\phi}_{abc}, \partial^2_{xy}\bar{\phi}_{abc}) \in \mathbb{R}^2$$

with the derivatives computed at (x, y). Note that $f(W)$ is the set of all local structures arising from macroscopic shapes with boundary heights of "hexagonal type". A priori it could be that $f(W)$ is a proper subset of $\mathcal{A}$, and even that $f(W)$ has topological dimension smaller than 4. Indeed, hexagonal boundary conditions look very special in the class of all admissible boundary heights. However, Theorems 2.4.2 and 2.4.4 below exclude these possibilities.

Let the 4×4 matrix

$$Df(w) = \begin{pmatrix} \partial_a z_1 & \partial_b z_1 & \partial_x z_1 & \partial_y z_1 \\ \partial_a z_2 & \partial_b z_2 & \partial_x z_2 & \partial_y z_2 \\ \partial_a z_{11} & \partial_b z_{11} & \partial_x z_{11} & \partial_y z_{11} \\ \partial_a z_{12} & \partial_b z_{12} & \partial_x z_{12} & \partial_y z_{12} \end{pmatrix} \tag{2.19}$$

denote the derivative of f at $w \in W$. If, for some $w \in W$, $Df(w)$ has (maximal) rank 4, then f is locally bijective on $\mathcal{A}$: every point z in a suitable neighborhood $B(f(w), \epsilon) \cap \mathcal{A}$ (with $B(z_0, r)$ the ball of radius r centered at z_0) has a unique pre-image through f in W at distance $O(\epsilon)$ from w. We have

Theorem 2.4.2. *The rank of $Df(w)$ is 4 for every $w \in W$. More precisely, in compact subsets of W the determinant of $Df(w)$ is strictly negative.*

Proof of Theorem 2.4.2. Call simply $\bar{\phi}$ the macroscopic shape in the *abc* hexagon and recall that, here and in the following, $c = 1 - a - b$. The explicit expression for $\nabla\bar{\phi}$ is given in [CLP98][2]. Introduce the coordinates (u, v) and (u', v') as

$$u = u(x, y) = -x + \frac{y}{2}, \quad v = v(x, y) = -\frac{\sqrt{3}}{2} y \tag{2.20}$$

$$u' = u'(x, y) = y - \frac{x}{2} = u/2 - \frac{\sqrt{3}}{2} v, \quad v' = v'(x, y) = -\frac{\sqrt{3}}{2} x = \frac{\sqrt{3}}{2} u + \frac{v}{2}. \tag{2.21}$$

What one finds is then

$$z_1 = \partial_x \bar{\phi} = -\frac{1}{\pi} \cot^{-1} \left[\frac{Q_{bca}(u(x, y), v(x, y))}{\sqrt{E_{bca}(u(x, y), v(x, y))}} \right] \tag{2.22}$$

$$z_2 = \partial_y \bar{\phi} = -\frac{1}{\pi} \cot^{-1} \left[\frac{Q_{cab}(u'(x, y), v'(x, y))}{\sqrt{E_{cab}(u'(x, y), v'(x, y))}} \right] \tag{2.23}$$

$$Q_{abc}(u, v) = \frac{\sqrt{3}}{2} \left(\frac{4}{3} v^2 - 4u^2 + b^2 + ab + bc - ac \right), \tag{2.24}$$

$$\begin{aligned} E_{abc}(u, v) = 3abc - (3(a + c)^2 u^2 - 2\sqrt{3}(a + 2b + c)(a - c)uv \\ +((a + 2b + c)^2 - 4ac)v^2). \end{aligned} \tag{2.25}$$

[2]The authors of [CLP98] consider on P_{111} an orthogonal coordinate frame (u, v) that does not coincide with the non-orthogonal coordinate frame (x, y) we adopt here. The change of coordinates is given in (2.20).

For later convenience, let us point out also that

$$z_3 := -1 - z_1 - z_2 = -\frac{1}{\pi}\cot^{-1}\left[\frac{Q_{abc}(u''(x,y), v''(x,y))}{\sqrt{E_{abc}(u''(x,y), v''(x,y))}}\right] \tag{2.26}$$

with

$$\begin{aligned} u''(x,y) &= \frac{1}{2}x + \frac{1}{2}y = -\frac{u}{2} - \frac{\sqrt{3}}{2}v, \\ v''(x,y) &= -\frac{\sqrt{3}}{2}x + \frac{\sqrt{3}}{2}y = \frac{\sqrt{3}}{2}u - \frac{v}{2}. \end{aligned} \tag{2.27}$$

Let also $z_{11} = \partial_x z_1, z_{12} = \partial_y z_1 = \partial_x z_2$.

Remark 2.4.3. *The boundary of the ellipse $\bigcirc_{abc}$ corresponds to the set of zeros of $E_{bca}(u(x,y), v(x,y))$. One can also check that*

$$E_{bca}(u(x,y), v(x,y)) = E_{cab}(u'(x,y), v'(x,y)) = E_{abc}(u''(x,y), u''(x,y))$$

and formulas above are understood to hold inside $\bigcirc_{abc}$. From the explicit formulas (2.19) *and* (2.22) *one sees that both $f(w)$ and $Df(w)$ are C^∞ in W, with uniform bounds when w is in compact subsets of W.*

We have to prove that the determinant of the matrix Df is negative. Observe that, when we take derivatives with respect to a or b, we have to remember that c is a function of a, b. One can painfully check[3] that the determinant of Df equals

$$\det(Df) = \frac{1}{32\pi^4}\frac{N(x,y)}{D(x,y)} \tag{2.28}$$

$$\begin{aligned} N(x,y) = {} & (1-a)(1-b)(1-c) \\ & + 2(1-a^2)y^2 + 2(1-c^2)x^2 - 4(1-a)(a+b)xy \end{aligned} \tag{2.29}$$

$$\begin{aligned} D(x,y) = {} & \left(y^2 - \frac{(a+b)^2}{4}\right)\left(x^2 - \frac{(1-a)^2}{4}\right)^2 \\ & \times \left(x - (y - \frac{1-b}{2})\right)^2 \left(x - (y + \frac{1-b}{2})\right)^2. \end{aligned} \tag{2.30}$$

One easily sees that $D(x,y)$ vanishes exactly along the sides of the hexagon $\hexagon_{abc}$, and is negative inside the hexagon (since in the hexagon the y coordinate ranges between $-(a+b)/2$ and $+(a+b)/2$). As for the numerator, it vanishes for

$$y = -\frac{2(1-a)(a+b)x \pm \sqrt{2}\sqrt{(1-a)(1-b)(a+b)(-1+a^2-4x^2)}}{2(a^2-1)} \tag{2.31}$$

[3]It is immediate from Eqs. (2.22) that the matrix elements of Df, and therefore also the determinant, are rational functions of a, b, x, y. For the actual computation of the coefficients of the two polynomials we used Mathematica, in order to symbolically simplify otherwise intractable expressions.

Since $a < 1$, the square root is imaginary and therefore the numerator has no zeros. The numerator is clearly positive for $(x, y) = (0, 0)$, so it is positive everywhere. □

A key point for the following is that $f : W \mapsto \mathcal{A}$ is actually a bijection:

Theorem 2.4.4. *The application f is a diffeomorphism from W to $\mathcal{A}$. In particular, $f(W) = \mathcal{A}$.*

The non-trivial step is to prove that points on the boundary of W are mapped through f to points on the boundary of $\mathcal{A}$ (Proposition 2.4.5). Given this, the proof of Theorem 2.4.4 follows rather closely that of a theorem of Hadamard [Had06], that gives a necessary and sufficient condition for a smooth map from $\mathbb{R}^n$ to $\mathbb{R}^n$ to be a diffeomorphism, cf. for instance [Gor72].

Proposition 2.4.5 (Compact sets have compact pre-images)**.** *Let $\{w_n\}_{n\geqslant 1}$ be a sequence of points in W, that tends as $n \to \infty$ to a point $\bar{w}$ on the boundary of W. Then, none of the sub-sequential limits of the sequence $\{f(w_n)\}_{n\geqslant 1}$ is in $\mathcal{A}$.*

Proof of Proposition 2.4.5. Recall that, for $w \in W$, we write $w = (a, b, x, y)$ and $f(w) = (z_1, z_2, z_{11}, z_{12})$. Note that

$$\partial W = \{w : (a, b) \in \partial\mathbb{V}\} \cup \{w : (a, b) \in \overset{\circ}{\mathbb{V}}, (x, y) \in \partial\bigcirc_{abc}\}. \tag{2.32}$$

Therefore, if $\bar{w} = (\bar{a}, \bar{b}, \bar{x}, \bar{y}) = \lim_n w_n \in \partial W$, exactly one of these two conditions holds:

(A) $(\bar{a}, \bar{b}) \in \overset{\circ}{\mathbb{V}}$ and $(\bar{x}, \bar{y})$ is on the boundary of $\bigcirc_{\bar{a}\bar{b}\bar{c}}$;

(B) $(\bar{a}, \bar{b})$ is in $\partial\mathbb{V}$.

We have to prove that, in both cases, at least one of the following two options occurs:

(Option 1) (z_1, z_2) approaches the boundary of $\mathbb{T}$ as $n \to \infty$;

(Option 2) the directional derivative $|\partial_v z_i|$ diverges as $n \to \infty$, for some $i = 1, 2, 3$ and for some direction v in the plane. This implies that either (z_1, z_2) approaches $\partial\mathbb{T}$, or $z_{11}^2 + z_{12}^2$ diverges, in both cases implying the statement of the Proposition.

Indeed, recall that $z_3 = -1 - z_1 - z_2$ and observe that $\partial_v z_i$ is a linear combination of $\partial_x z_i$ and $\partial_y z_i$. If $|\partial_v z_i|$ diverges, then one among $z_{11} = \partial_x z_1$, $z_{12} = \partial_x z_2 = \partial_y z_1$ or $\partial_y z_2$ diverge. If either z_{11} or z_{12} diverges, we are done. So suppose instead that $\partial_y z_2$ diverges. Remember that

$$\begin{aligned} &a_{11}(z_1, z_2)\partial_x z_1 + 2a_{12}(z_1, z_2)\partial_x z_2 + a_{22}(z_1, z_2)\partial_y z_2 \\ &\qquad = a_{11}(z_1, z_2)z_{11} + 2a_{12}(z_1, z_2)z_{12} + a_{22}(z_1, z_2)\partial_y z_2 = 0 \end{aligned} \tag{2.33}$$

and that, when (z_1, z_2) is bounded away from $\partial\mathbb{T}$, a_{ij} are finite and a_{ii} are strictly positive. As a consequence, if $\partial_y z_2$ diverges then either (z_1, z_2) approaches $\partial\mathbb{T}$ or at least one among z_{11} and z_{12} also diverges.

In Case (A), it follows directly from Theorem 2.3.5 that the slope (z_1, z_2) approaches the boundary of $\mathbb{T}$, so Option 1 occurs.

In Case (B) we have to go back to formulas (2.22)-(2.26) for z_1, z_2 and $z_3 = -1 - z_1 - z_2$, that we rewrite compactly as

$$z_i(x,y) = -\frac{1}{\pi}\cot^{-1}\left[\frac{Q^{(i)}_{abc}(x,y)}{\sqrt{E^{(i)}_{abc}(x,y)}}\right], \quad i = 1,2,3 \tag{2.34}$$

(recall that actually $E^{(i)}_{abc}$ does not depend on i, so we will just write E_{abc}). The numerators $Q^{(i)}_{abc}$ are second-order polynomials in x, y, symmetric under $(x, y) \leftrightarrow (-x, -y)$. Let $Z^{(i)}_{abc}, i = 1, 2, 3$ be the respective level-zero sets on the (x, y) plane: they are hyperbolas, that can be degenerate (two straight lines intersecting at $(0, 0)$) for particular values of $a, b, c = 1 - a - b$. More precisely, $Z^{(i)}_{abc}$ is degenerate if and only if $Q^{(i)}_{abc}(0, 0) = 0$. It is however easy to check that there are no values $a, b, c = 1 - a - b$ for which the three hyperbolas are simultaneously degenerate: an explicit calculation shows that $\sum_{i=1}^{3} Q^{(i)}_{abc}(0, 0)$ is never zero. Therefore, for $n \to \infty$, at least one of the curves $Z^{(i)}_{a_n b_n c_n}$ tends to a non-degenerate hyperbola. To fix ideas, let us assume that this is the case for $i = 1$, i.e. that

$$\liminf_n |Q^{(1)}_{a_n b_n c_n}(0, 0)| > 0. \tag{2.35}$$

Then we proceed as follows. We first note that the sup-norm of $E_{a_n b_n c_n}$ on $\bigcirc_{a_n b_n c_n}$ is just $\delta_n := E_{a_n b_n c_n}(0, 0) = 3a_n b_n c_n = o(1)$ (the graph of E_{abc} is a concave paraboloid with gradient zero at $(0, 0)$ and vanishes at the boundary of $\bigcirc_{abc}$). The fact that $a_n b_n c_n = o(1)$ is because when (a_n, b_n) approaches $\partial\mathbb{V}$, at least one of the three values $a_n, b_n, 1 - a_n - b_n$ approaches zero. Given $(x_n, y_n) \in \bigcirc_{a_n b_n c_n}$, if for some $i = 1, 2, 3$

$$\left|\frac{Q^{(i)}_{a_n b_n c_n}(x_n, y_n)}{\sqrt{E_{a_n b_n c_n}(x_n, y_n)}}\right| \geqslant \frac{1}{\delta_n^{1/8}}$$

then, for $n \to \infty$, z_i approaches either 0 or 1 (according to the sign of $Q^{(i)}_{a_n b_n c_n}/\sqrt{E_{a_n b_n c_n}}$), and therefore Option 1 occurs.

Assume instead that at (x_n, y_n) one has

$$\max_i |Q^{(i)}_{a_n b_n c_n}/\sqrt{E_{a_n b_n c_n}}| \leqslant \frac{1}{\delta_n^{1/8}}. \tag{2.36}$$

Note that automatically (x_n, y_n) is bounded away from $(0,0)$, otherwise condition (2.36) would be violated, since one would have

$$\left| \frac{Q^{(1)}_{a_n b_n c_n}(x_n, y_n)}{\sqrt{E_{a_n b_n c_n}(x_n, y_n)}} \right| \geqslant \frac{\left|Q^{(1)}_{a_n b_n c_n}(x_n, y_n)\right|}{\sqrt{\delta_n}} \simeq \frac{\left|Q^{(i)}_{a_n b_n c_n}(0,0)\right|}{\sqrt{\delta_n}}$$

and $Q^{(1)}_{a_n b_n c_n}(0,0)$ is bounded away from zero for $n \to \infty$, cf. (2.35). We look at the derivative of z_i at (x_n, y_n) in the direction v tangent to the local level line of $E_{a_n b_n c_n}$: we get

$$\partial_v z_i = -\frac{1}{\pi} \frac{1}{1 + (Q^{(i)}_{a_n b_n c_n} / \sqrt{E_{a_n b_n c_n}})^2} \frac{\partial_v Q^{(i)}_{a_n b_n c_n}}{\sqrt{E_{a_n b_n c_n}}}.$$

Therefore,

$$|\partial_v z_i| \geqslant const. \times \delta_n^{2/8 - 1/2} |\partial_v Q^{(i)}_{a_n b_n c_n}| = const. \times \delta_n^{-1/4} |\partial_v Q^{(i)}_{a_n b_n c_n}|. \quad (2.37)$$

If we can prove that $|\partial_v Q^{(i)}_{a_n b_n c_n}|$ stays bounded away from zero as $n \to \infty$ for at least one value of i, we get that $|\partial_v z_i|$ diverges and we can conclude that Option 2 occurs. To control $|\partial_v Q^{(i)}_{a_n b_n c_n}|$, observe that

$$\begin{aligned} \nabla Q^{(1)}_{a_n b_n c_n} &= 2\sqrt{3}(-2x + y, x) \\ \nabla Q^{(2)}_{a_n b_n c_n} &= 2\sqrt{3}(y, -2y + x) \\ \nabla Q^{(3)}_{a_n b_n c_n} &= 2\sqrt{3}(-y, -x). \end{aligned} \quad (2.38)$$

From these explicit formulas it is immediate to check that, whenever $(x, y) \neq (0,0)$, all three gradients have non-zero norm and that there are at least two of them that are not colinear[4]. As a consequence (recalling that (x_n, y_n) is bounded away from $(0,0)$), for any given direction v one has that $|\partial_v Q^{(i)}_{a_n b_n c_n}|$ is bounded away from 0 for at least one value of i, as we wished to show.

□

Proof of Theorem 2.4.4. **Point (I): f is surjective ($f(W) = \mathcal{A}$).** Fix some $\bar{w} \in W$ and let $\bar{z} = f(\bar{w})$. We define on $\mathcal{A}$ the radial vector field $v(z) = \bar{z} - z$ that points everywhere towards $\bar{z}$. Given $z \in \mathcal{A}$, we let for $t \geqslant 0$

$$y^z(t) = \bar{z} + e^{-t}(z - \bar{z}), \quad (2.39)$$

that solves

$$\frac{d}{dt} y^z(t) = v(y^z(t)), \quad y^z(0) = z$$

[4] Just compute $\nabla Q^{(i)}_{a_n b_n c_n} \cdot [\nabla Q^{(j)}_{a_n b_n c_n}]^\perp$ for all $i \neq j$, with $v^\perp$ the vector v rotated by $\pi/2$, and check that only for $(x, y) = 0$ the three products vanish simultaneously.

and note that $\lim_{t\to\infty} y^z(t) = \bar{z}$. Thanks to Theorem 2.4.2, $\bar{z}$ is in the interior of $f(W)$, so there exists $0 \leqslant \tau^z < \infty$ such that $y^z(\tau^z) \in f(W)$. Let $w_{\tau^z} \in W$ be such that $f(w_{\tau^z}) = y^z(\tau^z)$. We let $w^z(t)$ be the solution of the differential equation on W

$$\begin{cases} \frac{d}{dt} w^z(t) = V(w^z(t)) \cdot v(f(w^z(t))) \\ w^z(\tau^z) = w_{\tau^z}, \end{cases} \tag{2.40}$$

where

$$V(w) = [Df(w)]^{-1}. \tag{2.41}$$

The existence of the inverse of the matrix $Df(w)$ is guaranteed by Theorem 2.4.2. The solution $w^z(t)$ exists at least locally around $t = \tau^z$.

Let I be the interval of definition of the solution, and $\underline{t} = \inf\{s : s \in I\}$. For every $t \in \mathbb{R}_+ \cap I$ we have $f(w^z(t)) = y^z(t)$ since, as one easily checks, both quantities verify the same differential equation and take the same value for $t = \tau^z$. We wish to show that $\underline{t} < 0$, so that $f(w^z(0)) = z$, i.e. $z \in f(W)$ and in turn (by the arbitrariness of z) this implies $f(W) = \mathcal{A}$.

Let us assume by contradiction that $\underline{t} \geqslant 0$. Recalling Remark 2.4.3 and Theorem 2.4.2, we have that $Df(w)$ is C^∞ (actually analytic) in W and $\det(Df(w))$ is bounded away from zero in compact subsets of W. Therefore, the vector field $V(w) \cdot v(f(w)) = [Df(w)]^{-1} \cdot v(f(w))$ is C^∞ and bounded, away from the boundary of W. As a consequence, we have that there exists a sequence $s_n \searrow \underline{t}$ such that $w^z(s_n)$ approaches ∂W as $n \to \infty$ (otherwise the solution could be extended to short times before $\underline{t}$). By Proposition 2.4.5, one deduces that the sequence $f(w^z(s_n)) = y^z(s_n)$ cannot have a limit in $\mathcal{A}$. However, from (2.39) such limit exists and is simply $\bar{z} + e^{-\underline{t}}(z - \bar{z})$, which belongs to $\mathcal{A}$ (recall that $z, \bar{z}$ are in $\mathcal{A}$, remark that $\mathcal{A}$ is convex and that $\bar{z} + e^{-\underline{t}}(z - \bar{z})$ is a convex combination of z and $\bar{z}$).

Point (II): f is bijective and a diffeomorphism. We know from point (I) that f is surjective, and from Theorem 2.4.2 that it is a local diffeomorphism. It remains only to prove that $f^{-1}(\bar{z})$ is uniquely defined for every $\bar{z} \in \mathcal{A}$ (injectivity). This is essentially identical to the proof of injectivity in Hadamard's theorem (cf. [Gor72, Theorem A]), so we will just sketch the main steps.

First, the set $f^{-1}(\bar{z}) = \{w \in W : f(w) = \bar{z}\}$ is finite: otherwise, by Proposition 2.4.5 (compact sets have compact pre-images) it would contain an accumulation point w_∞ in W. This would contradict Theorem 2.4.2, since the determinant of $Df(w_\infty)$ is non-zero, so that f is locally one-to-one in a neighborhood of w_∞.

Second, to each $w_i \in f^{-1}(\bar{z})$ is associated the set

$$W_i = \{w_0 \in W : \lim_{t\to\infty} w(t) = w_i\},$$

with $w(t)$ the solution of the Cauchy problem

$$\begin{cases} \frac{d}{dt}w(t) = V(w(t)) \cdot v(f(w(t))) \\ w(0) = w_0. \end{cases} \tag{2.42}$$

Recall that $f(w(t)) = y^{z_0}(t)$, with $y^{z_0}(t)$ defined in (2.39) and $z_0 = f(w_0)$. Since $y^{z_0}(t)$ stays in a compact set uniformly for $t \geqslant 0$, using again Proposition 2.4.5 we see that $w(t)$ exists for all positive times (it never approaches the boundary of W). But $y^{z_0}(t)$ converges to $\bar{z}$ as $t \to \infty$, so that $w(t)$ tends to an inverse of $\bar{z}$: thanks to the arbitrariness of w_0, this implies that $W = \cup_i W_i$. Moreover, each W_i is open, by continuity of solutions of (2.42) with respect to initial conditions. Given that the W_i are disjoint and that W is open and connected, one deduces that $f^{-1}(\bar{z})$ contains a single element. □

2.5 Monotonicity and constrained dynamics

As well as in previous works on lozenge dynamics [Wil04, CMST10, CMT12, LT12], monotonicity will play an important role. Let us briefly recall the basic idea.

In the set of stepped monotone interfaces we introduce a partial order where $h \leqslant h'$ if $h(v) \leqslant h'(v)$ for every v. It is well known that dynamics conserves the partial order: give a discrete domain U_L, it is possible to couple in the same probability space all the evolutions $h_t^{\eta;\varphi_L}$ with boundary height φ_L and initial condition $\eta \in \Omega_{U_L,\varphi_L}$ in such a way that, $\mathbb{P}$-almost surely,

$$h_t^{\eta,\varphi_L} \leqslant h_t^{\eta',\varphi'_L} \quad \text{for every} \quad t \geqslant 0, \quad \text{if } \eta \leqslant \eta' \text{ and } \varphi_L \leqslant \varphi'_L. \tag{2.43}$$

An immediate consequence on the equilibrium measures is that $\pi_{U_L}^{\varphi_L}$ is stochastically dominated by $\pi_{U_L}^{\varphi'_L}$.

Consider two stepped monotone surfaces with height functions h^-, h^+ such that $h^- \leqslant h^+$. Let moreover U_L be a discrete domain and φ_L be a boundary height such that $h^- \leqslant \varphi_L \leqslant h^+$ on U^{ext}. The dynamics in U_L with boundary height φ_L, "ceiling" h^+ and "floor" h^- is defined as the usual dynamics h_t, except that any updates that would lead to a violation of the inequalities

$$h^- \leqslant h_t \leqslant h^+$$

are discarded (censored). Of course, we will assume that the initial condition η does satisfy $h^- \leqslant \eta \leqslant h^+$. The invariant measure of the constrained dynamics is simply the uniform measure $\pi_{U_L}^{\varphi_L}$ conditioned on the interface being between floor and ceiling, i.e.

$$\pi_{U_L}^{\varphi_L}(\cdot | h^- \leqslant \cdot \leqslant h^+).$$

Define the distance between floor and ceiling as

$$\max_{v \in U_L} (h^+(v) - h^-(v)).$$

Then:

Lemma 2.5.1. *[CMT12, Theorem 4.3] The Glauber dynamics in a discrete domain U_L of diameter D in the graph-distance, with floor and ceiling at distance H/L, has $T_{\text{mix}} = O(D^2 H^2 (\log D)^2)$.*

Take U_L to be the discretization of a domain U, so that its graph-distance diameter D is of order L. Note that, if we let $h^\pm = \varphi_L \pm A$ with $A = O(1)$ sufficiently large then the constrained dynamics exactly coincides with the unconstrained one. This is simply because the height functions h and φ_L change by $\pm 1/L$ or 0 along edges of $\mathcal{T}_L$: if $u \in \partial U_L$ and $v \in U^{int}$ and u, v are at graph-distance $d(u, v)$, one has

$$h(v) \leqslant h(u) + d(u, v)/L$$

and

$$h^+(v) \geqslant h^+(u) - d(u, v)/L = \varphi_L(u) + A - d(u, v)/L.$$

Given that $h(u) = \varphi_L(u)$ on ∂U_L, we see that

$$h^+(v) \geqslant h(u) + A - d(u, v)/L \geqslant h(v) + A - 2d(u, v)/L.$$

If A is chosen larger than $2D/L = O(1)$ we have then $h(v) \leqslant h^+(v)$ (and analogously $h(v) \geqslant h^-(v)$) deterministically. Hence the floor/ceiling constraints are automatically satisfied by the unconstrained dynamics. On the other hand, if $h^\pm = \varphi_L \pm A$ then the distance between floor and ceiling is $2A$. Therefore, an immediate consequence of Lemma 2.5.1 is:

Corollary 2.5.2. *Let the discrete domain U_L be a discretization of a domain U. For any boundary height φ_L, the mixing time of the Glauber dynamics with neither floor nor ceiling is smaller than $C\, L^4 (\log L)^2$ for some constant C depending only on U.*

2.6 Proof of Theorem 2.3.3

Here we make a few comments about the idea of the proof and its structure. Recall from the introduction that we want to show that the interface stays with very high probability "trapped" between two deterministic surfaces that evolve on a time scale just slower than diffusive and both tend to the macroscopic shape. We will only consider the upper bound in the following because the proof of the lower bound is identical.

The first step, that does not require much work, is to realize that it is enough to prove that when the initial condition is at distance $2\epsilon_L$ from equilibrium (for some suitably small ϵ_L) then within time $L^{2+o(1)}$ the interface reaches distance ϵ_L (see Claim 2.6.1). To prove this, the key point is Claim 2.6.3, that says that the height function stays with high probability below the deterministically evolving interface

$$\tilde{\phi}_t := \bar{\phi} + \epsilon_L(1 - t/L^{2+o(1)})\psi,$$

with a well chosen function $\psi \geqslant 2$, until the time when $(1 - t/L^{2+o(1)})$ becomes sufficiently small. As mentioned in the introduction, we prove the bound by looking at "mesoscopic" regions of size $L^{-1/2+o(1)}$ and at time increments $L^{1+o(1)}$, that are small with respect to the diffusive time-scale L^2. The choice of ψ will be justified in Remark 2.6.4. In practice, one must guarantee that $\hat{\mathcal{L}}\psi$ (with $\hat{\mathcal{L}}$ the linearization of the elliptic operator in (2.4), that should determine the interface drift, see (2.1)) is comparable with $\Delta\psi$ (with Δ the usual Laplacian).

Here we start with the actual proof. For simplicity we will write π_L for the equilibrium measure $\pi_{U_L}^{\varphi_L}$ and as usual $\bar{\phi}$ denotes the macroscopic shape in U with boundary height φ.

Let $\epsilon_L = 1/\log L$. To prove Theorem 2.3.3 it is sufficient to prove that

$$\sup_{t>c(\delta)L^{2+\delta}} \mathbb{P}(\exists v \in U_L : h_t(v) - \bar{\phi}(v) > 2\epsilon_L) = o(1) \tag{2.44}$$

and

$$\sup_{t>c(\delta)L^{2+\delta}} \mathbb{P}(\exists v \in U_L : h_t(v) - \bar{\phi}(v) < -2\epsilon_L) = o(1), \tag{2.45}$$

with bounds uniform in the initial condition η (we omit for lightness the argument η in h_t^η). We will prove only (2.44), the proof of (2.45) being essentially identical.

Let G be a positive constant, independent of η and L, that will be fixed in a moment (it will depend only on the diameter of U). We have:

Claim 2.6.1. *For $i = 0, 1, \ldots, \lfloor G/\epsilon_L \rfloor - 1$,*

$$\mathbb{P}(h_t \leqslant G - i\epsilon_L + \bar{\phi} \text{ for every } t \in [T_i, L^5]) \geqslant 1 - i/L \tag{2.46}$$

where

$$T_i = L^{2+\delta/2}i.$$

When we write $h_t \leqslant g$ like in (2.46), what we mean exactly is that for every $u \in U_L \cap \mathcal{T}_L$ one has $h_t(u) \leqslant g(u)$.

Proof of (2.44) *given Claim 2.6.1.* For $i = \lfloor G/\epsilon_L \rfloor - 1$ we have

$$T_i = O(L^{2+\delta/2}/\epsilon_L) = O(L^{2+\delta/2} \log L) \ll c(\delta) L^{2+\delta}$$

and we obtain that

$$\mathbb{P}(h_t \leqslant \bar{\phi} + 2\epsilon_L \quad \text{for every } t \in [c(\delta)L^{2+\delta}, L^5]) = 1 + o(1). \tag{2.47}$$

On the other hand, we know from Corollary 2.5.2 that the mixing time of the dynamics is $T_{\text{mix}} = O(L^4(\log L)^2)$. Therefore, from (2.10) we see that for times larger than L^5 the system is at equilibrium (modulo a negligible error term $O(\exp(-L/(\log L)^2))$, uniform in time and in η) and we deduce that

$$\pi_L(h \leqslant \bar{\phi} + 2\epsilon_L) = 1 + o(1) \tag{2.48}$$

so that

$$\begin{aligned} \sup_{t > L^5} \mathbb{P}(h_t \leqslant \bar{\phi} + 2\epsilon_L) &= \pi_L(h \leqslant \bar{\phi} + 2\epsilon_L) + O(\exp(-L/(\log L)^2)) \\ &= 1 + o(1). \end{aligned} \tag{2.49}$$

Equations (2.47) and (2.49) imply (2.44). It will be clear from the proof of Claim 2.6.1 that in (2.46) we could have replaced L^5 with any other larger power of L. □

Proof of Claim 2.6.1. We prove (2.46) by induction on i. The functions h_t and $\bar{\phi}$ are uniformly 1-Lipschitz in space and they coincide on the boundary of U_L: therefore, Eq. (2.46) for $i = 0$ is trivially true (for every $t \geqslant 0$) if G is chosen large enough depending on the diameter of U.

Definition 2.6.2. *Set for* $(x, y) \in \mathbb{R}^2$

$$\psi(x, y) = \psi(0, 0) - e^{x/\xi} - e^{y/\xi} \tag{2.50}$$

with $\xi \ll 1$ *but independent of* L *and the constant* $\psi(0, 0)$ *chosen so that* $\inf\{\psi(x, y), (x, y) \in U\} = 2$. *Let* $\psi_{max} = \max\{\psi(x, y) : (x, y) \in U\}$ *and* $N \sim L(1 - 1/\psi_{max})$ *the smallest integer such that*

$$\left(1 - \frac{N}{L}\right) \psi_{max} \leqslant 1.$$

To prove (2.46) for $i + 1$ given the same statement for i, we proceed as follows. Since $\psi \geqslant 2$ in U, the inductive hypothesis (i.e. (2.46) for i) implies

$$\mathbb{P}(h_t \leqslant G - (i + 2)\epsilon_L + \bar{\phi} + \epsilon_L \psi, \text{ for every } T_i \leqslant t \leqslant L^5) \geqslant 1 - i/L. \tag{2.51}$$

Define

$$\gamma_{i,j} = G - (i + 2)\epsilon_L + \bar{\phi} + \epsilon_L (1 - j/L)\psi, \tag{2.52}$$

let $T_{i,j} = T_i + jL^{1+\delta/4}$ and $E_{i,j}$ be the event

$$E_{i,j} = \{h_t \leqslant \gamma_{i,j} \text{ for every } T_{i,j} \leqslant t \leqslant L^5\}. \tag{2.53}$$

We will prove:

Claim 2.6.3. *Fix $0 \leqslant i < \lfloor G/\epsilon_L \rfloor - 1$ and assume that (2.46) holds. For $j \leqslant N$,*

$$\mathbb{P}(E_{i,j}) \geqslant 1 - i/L - j/L^3. \tag{2.54}$$

Taking $j = N$, we obtain the claim (2.46) for $i+1$, since $T_{i,N} \leqslant T_{i+1}$,

$$\gamma_{i,N} \leqslant G - (i+1)\epsilon_L + \bar{\phi}$$

and

$$1 - i/L - N/L^3 \geqslant 1 - (i+1)/L.$$

This concludes the proof of Claim 2.6.1, assuming Claim 2.6.3.

□

Remark 2.6.4. *The choice of ψ, which might look at first sight rather arbitrary, is dictated by the following reasoning. At time T_i we have $h_t \leqslant \bar{\phi} + \epsilon_L\psi + c$, with c the constant $G - (i+2)\epsilon_L$. From the discussion in the Introduction, we expect the macroscopic evolution of the interface under diffusive time scaling to be given by (2.1). Linearizing the differential operator $\mathcal{L}$ around $\bar{\phi} + c$ and observing that $\mathcal{L}(\bar{\phi} + c) = 0$, we find that*

$$\mathcal{L}(\bar{\phi} + c + \epsilon_L\psi) = \epsilon_L\hat{\mathcal{L}}\psi + O(\epsilon_L^2)$$

with $\hat{\mathcal{L}}$ the linear elliptic operator

$$\begin{aligned}\hat{\mathcal{L}}\psi = &\sum_{i,j=1}^{2} a_{ij}(\nabla\bar{\phi})\partial_{ij}^2\psi \\ &+ \sum_{i,j=1}^{2}\left[(\partial_x\psi)\,\partial_s a_{ij}(s,t)|_{(s,t)=\nabla\bar{\phi}} + (\partial_y\psi)\,\partial_t a_{ij}(s,t)|_{(s,t)=\nabla\bar{\phi}}\right].\end{aligned} \tag{2.55}$$

Now observe that the Hessian matrix of our ψ is diagonal, with negative diagonal entries:

$$H^\psi = -\frac{1}{\xi^2}\begin{pmatrix} e^{x/\xi} & 0 \\ 0 & e^{y/\xi} \end{pmatrix}. \tag{2.56}$$

Therefore, the first sum in (2.55) is strictly and pointwise negative, uniformly in U (the diagonal elements a_{ii} are positive) and the second sum can be neglected, if ξ is small (because $|\partial_x\psi| \ll |\partial_x^2\psi|$ and similarly for the y

derivatives). In conclusion, with our choice of ψ, $\mathcal{L}(\bar\phi + c + \epsilon_L\psi)$ is everywhere negative, so the interface feels a negative drift that pushes it towards the equilibrium shape. The drift is of order $-L^{-2}$ (recall that, in (2.1), τ is the rescaled time $\tau = t/L^2$). This heuristic reasoning is what is behind Claim 2.6.3. Indeed, going from j to $j+1$ corresponds to lowering the interface by $\approx 1/L$, in a time $T_{i,j+1} - T_i \approx L$, i.e. corresponds to a negative drift of order $-1/L^2$.

Proof of Claim 2.6.3. We proceed by induction on j and we observe that for $j = 0$ the claim is trivial (it just reduces to (2.51), that is a consequence of (2.46) which we assumed to hold for the value i). We want to prove (2.54), given the same claim for $j-1$.

Let V be a shrinking of U by ϵ_L^2, i.e. let

$$V = U \setminus \cup_{x\in\partial U} B(x, \epsilon_L^2), \tag{2.57}$$

with $B(x,r)$ the ball of radius r centered at x.

Remark 2.6.5. *We claim first of all that it is sufficient to prove* (2.46) *at lattice sites $v \in V$. Indeed, recall that the height on ∂U_L is always fixed (for all times) to the boundary height φ_L. Since both the height function h_t and $\bar\phi$ are uniformly* 1*-Lipschitz in space and $|h_t - \bar\phi| \simeq |\varphi_L - \varphi| = O(1/L)$ at the boundary ∂U_L one deduces that,* deterministically*, $|h_t - \bar\phi| = O(\epsilon_L^2)$ in $U_L \setminus V$. On the other hand, for $i < \lfloor G/\epsilon_L\rfloor - 1$ and $j \leqslant N$*

$$\begin{aligned}\gamma_{i,j} - h_t &= \bar\phi - h_t + G - (i+2)\epsilon_L + (1 - j/L)\epsilon_L\psi \\ &\geqslant \bar\phi - h_t + \epsilon_L(1 - N/L)\psi_{max}\frac{\psi}{\psi_{max}} \geqslant \bar\phi - h_t + \epsilon_L/\psi_{max}\end{aligned} \tag{2.58}$$

since $\psi \geqslant 2$ and $(1 - N/L)\psi_{max} = 1 + o(1)$. We have seen that for the sites within distance ϵ_L^2 from ∂U one has $|\bar\phi - h_t| = O(\epsilon_L^2) \ll \epsilon_L/\psi_{max}$ deterministically, so the inequality $h_t \leqslant \gamma_{i,j}$ holds automatically.

In conclusion, we do not have to worry about lattice sites too close to the boundary ∂U, see also Remark 2.6.6.

One has

$$\begin{aligned}\mathbb{P}(E_{i,j}) &\geqslant \mathbb{P}(E_{i,j-1}) - \mathbb{P}(E_{i,j-1}; E_{i,j}^c) \\ &\geqslant 1 - \frac{i}{L} - \frac{j-1}{L^3} - \mathbb{P}(E_{i,j-1}; E_{i,j}^c).\end{aligned} \tag{2.59}$$

Next, via a union bound,

$$\mathbb{P}(E_{i,j-1}; E_{i,j}^c) \leqslant \sum_{u\in V} \mathbb{P}\left(E_{i,j-1}; h_t(u) > \gamma_{i,j}(u) \text{ for some } t \in [T_{i,j}, L^5]\right). \tag{2.60}$$

Since there are $O(L^2)$ sites $u \in V$, it is sufficient to prove

$$\mathbb{P}(E_{i,j-1}; h_t(u) > \gamma_{i,j}(u) \text{ for some } t \in [T_{i,j}, L^5]) \leqslant 1/L^6 \tag{2.61}$$

to deduce (2.54).

Let the stepped monotone interface $\gamma^{(L)}_{i,j-1}$ be a discretization of $\gamma_{i,j-1}$ such that

$$\gamma^{(L)}_{i,j-1} > \gamma_{i,j-1} \tag{2.62}$$

(strict inequality) and $\{\hat{h}_t\}_{t \geqslant T_{i,j-1}}$ be the Markov dynamics with (random) initial condition $h_{T_{i,j-1}}$ at time $T_{i,j-1}$, and such that:

- if $h_{T_{i,j-1}} \leqslant \gamma^{(L)}_{i,j-1}$, then $\hat{h}_t$ is the dynamics with ceiling $\gamma^{(L)}_{i,j-1}$;
- if instead $h_{T_{i,j-1}} \not\leqslant \gamma^{(L)}_{i,j-1}$, then $\hat{h}_t = h_{T_{i,j-1}}$ for every $t \geqslant T_{i,j-1}$.

Note that, on the event $E_{i,j-1}$, one has $h_{T_{i,j-1}} \leqslant \gamma^{(L)}_{i,j-1}$ and moreover the two dynamics h_t and $\hat{h}_t$ can be coupled so that they exactly coincide in the time interval $[T_{i,j-1}, L^5]$. In fact, from the definition of dynamics with ceiling (Section 2.5) the two dynamics coincide until the first time τ when $h_\tau(v) = \gamma^{(L)}_{i,j-1}(v)$ for some v; on the event $E_{i,j-1}$ one has $h_t \leqslant \gamma_{i,j-1} < \gamma^{(L)}_{i,j-1}$ up to time L^5 time and therefore $\tau \geqslant L^5$. Therefore, the probability in (2.61) can be upper bounded by

$$\mathbb{P}(\hat{h}_t(u) > \gamma_{i,j}(u) \text{ for some } t \in [T_{i,j}, L^5] | \hat{h}_{T_{i,j-1}} = h_{T_{i,j-1}} \leqslant \gamma^{(L)}_{i,j-1}). \tag{2.63}$$

Next, we want to reduce from the dynamics $\hat{h}_t$ in the whole U_L to a dynamics where only the height function in a much smaller domain D_u evolves. Given a lattice site $u \in V$ let D_u be a disk[5] of radius $L^{-1/2+\delta/100}$ centered at u: from the definition (2.57) of V, we see that the disk D_u is entirely contained in U, since $L^{-1/2+\delta/100} \ll \epsilon_L^2$.

We start by observing that, by monotonicity, since we want to upper bound (2.63), we are allowed to change the random configuration $\hat{h}_{T_{i,j-1}}$ at time $T_{i,j-1}$ to the deterministic configuration $\gamma^{(L)}_{i,j-1} \geqslant \hat{h}_{T_{i,j-1}}$, and to freeze $\hat{h}_t(v)$ to $\gamma^{(L)}_{i,j-1}(v)$ for times $t \geqslant T_{i,j-1}$ and sites v outside D_u. In words, we are pinning the height function to the ceiling outside D_u. Again by monotonicity, we impose that the evolution $\hat{h}_t$ has a "floor" constraint $\hat{h}_t(v) \geqslant \gamma^{(L)}_{i,j-1} - L^{-1+\delta/40}$. We still call $\{\hat{h}_t\}_{t \geqslant T_{i,j-1}}$ the dynamics after these two modifications, and we denote $\hat{\pi}_{i,j-1}$ its equilibrium measure (it is the uniform measure on stepped monotone interfaces in D_u, with boundary height $\gamma^{(L)}_{i,j-1}|_{\partial D_u}$, ceiling $\gamma^{(L)}_{i,j-1}$ and floor $\gamma^{(L)}_{i,j-1} - L^{-1+\delta/40}$).

[5]To be precise, D_u should be a discrete domain; take D_u as the union of triangles in $\mathcal{T}_L$ contained in such a disk. For lightness of exposition, we will overlook this minor detail and just call D_u a "disk".

Remark 2.6.6. *We have used crucially that $D_u \subset U$, more precisely that boundary sites on ∂D_u are in U_L to say that, on the event $E_{i,j-1}$, $h_t(v) < \gamma^{(L)}_{i,j-1}(v)$ for $v \in \partial D_u$ and $t \in [T_{i,j-1}, L^5]$. If we had to consider points much closer to the boundary, we would have to take a disk D_u of smaller diameter (so that it fits in U_L) and then the proof of Proposition 2.6.7 below would fail.*

Let us assume for the moment the following equilibrium estimate:

Proposition 2.6.7. *Let $j \leqslant N$ and $\hat{\pi}_{i,j-1}$ be as above. If ξ in (2.50) is smaller than some $\xi_0 > 0$ (that is independent of i, j, L) then*

$$\hat{\pi}_{i,j-1}\left[h(u) > \gamma_{i,j-1}(u) - L^{-1+\delta/60}\right] \leqslant L^{-20}. \tag{2.64}$$

Let us conclude the proof of the step $j-1 \to j$, given Proposition 2.6.7. By Lemma 2.5.1, since the graph-distance diameter of D_u is $O(L^{1/2+\delta/100})$ and the distance between floor $\gamma^{(L)}_{i,j-1} - L^{-1+\delta/40}$ and ceiling $\gamma^{(L)}_{i,j-1}$ is $L^{-1+\delta/40}$, the mixing time of the dynamics $\hat{h}_t$ is

$$O(L^{2(1/2+\delta/100)} L^{2\delta/40} (\log L)^2) \leqslant L^{1+\delta/8} \ll T_{i,j} - T_{i,j-1} = L^{1+\delta/4}.$$

Therefore, at time $T_{i,j}$ equilibrium $\hat{\pi}_{i,j-1}$ has been reached, up to a negligible variation distance error $O(\exp(-L^{\delta/8}))$. As a consequence,

$$\begin{aligned}
&\mathbb{P}(\hat{h}_t(u) > \gamma_{i,j}(u) \text{ for some } t \in [T_{i,j}, L^5]) \\
&\quad = \mathbb{P}^{\hat{\pi}_{i,j-1}}(\hat{h}_t(u) > \gamma_{i,j}(u) \text{ for some } t \in [T_{i,j}, L^5]) + O(\exp(-L^{\delta/8})) \\
&\qquad \leqslant L^7 \hat{\pi}_{i,j-1}(h(u) > \gamma_{i,j}(u)) + O(\exp(-L^{\delta/8})).
\end{aligned} \tag{2.65}$$

In the second line, $\mathbb{P}^{\hat{\pi}_{i,j-1}}$ denotes the law of the modified dynamics, with initial condition sampled from the equilibrium distribution $\hat{\pi}_{i,j-1}$; in the third line we used the standard fact that, for a continuous-time homogeneous Markov chain X_t with invariant measure π and any event A,

$$\mathbb{P}^{\pi}(\exists t \in [a,b] : X_t \in A) \leqslant |b-a| M \pi(X \in A)$$

with M the average number of updates per unit time. In our case M can be bounded by the number of lattice sites in D_u (since each site has a mean-one Poisson clock), which is much smaller than L^2.

Note that

$$\gamma_{i,j-1}(u) - L^{-1+\delta/60} < \gamma_{i,j}(u) : \tag{2.66}$$

just recall (2.52) and observe that $L^{-1+\delta/60} > \epsilon_L \psi(u)/L$. As a consequence, from Proposition 2.6.7,

$$\hat{\pi}_{i,j-1}(h(u) > \gamma_{i,j}(u)) \leqslant \hat{\pi}_{i,j-1}(h(u) > \gamma_{i,j-1}(u) - L^{-1+\delta/60}) \leqslant L^{-20} \tag{2.67}$$

and (2.61) follows from (2.63) and (2.65). The proof of Claim 2.6.3 is concluded. □

Remark 2.6.8. *The common points with the proof of [CMT12, Theorem 2] (that is the analog of Theorems 2.3.3 and 2.3.8 in the particular case of flat macroscopic shape) are the pervasive use of monotonicity and the idea of employing Lemma 2.5.1 on mesoscopic domains of size slightly larger than $L^{-1/2}$ (specifically, $L^{-1/2+\delta/100}$ here).*

2.7 Proof of Proposition 2.6.7

Since i and j are fixed in this section, we write for simplicity of notation

$$\gamma = \gamma_{i,j-1} = G - (i+2)\epsilon_L + \bar{\phi} + \kappa\epsilon_L\,\psi$$

with $\kappa = (1-(j-1)/L)$. Recall that $(j-1) < N$, with N as in Definition 2.6.2, so that

$$\kappa \in [(1+O(1/L))/\psi_{max}, 1]. \tag{2.68}$$

In fact, we will need that κ is bounded away from zero uniformly in L, i, j.

Recall that $u = (x,y) \in V$, $D_u \subset U$ is a disk centered at u, of radius $L^{-1/2+\delta/100}$ and that $\hat{\pi} := \hat{\pi}_{i,j-1}$ is the uniform measure over stepped interfaces in D_u, with boundary condition $\gamma^{(L)}_{i,j-1}|_{\partial D_u}$, ceiling $\gamma^{(L)}_{i,j-1}$ and floor $\gamma^{(L)}_{i,j-1} - L^{-1+\delta/40}$. Since we want to prove the *upper bound* (2.64), we can by monotonicity remove the ceiling.

The floor cannot be removed by monotonicity. However:

Lemma 2.7.1. *Let $\tilde{\pi}$ be obtained from $\hat{\pi}$ by eliminating the floor constraint $h \geqslant \gamma^{(L)}_{i,j-1} - L^{-1+\delta/40}$. We have $\|\hat{\pi} - \tilde{\pi}\| = O(L^{-n})$ for any given n.*

This will be proven at the end of this section. It is clear that it is sufficient to prove Proposition 2.6.7 with $\hat{\pi}$ replaced by $\tilde{\pi}$.

Call $\nabla\bar{\phi}(u) = (\partial_x\bar{\phi}(u), \partial_y\bar{\phi}(u))$ the slope of $\bar{\phi}$ at u and $H^{\bar{\phi}}(u)$ its 2×2 Hessian matrix. These are well-defined objects, since $\bar{\phi}$ is non-extremal and therefore infinitely differentiable, see Section 2.2.2. Similarly, call

$$\nabla\gamma(u) = (\partial_x\gamma(u), \partial_y\gamma(u)) = \nabla\bar{\phi}(u) + \kappa\epsilon_L\,\nabla\psi(u)$$

and

$$H^{\gamma}(u) = H^{\bar{\phi}}(u) + \kappa\epsilon_L\,H^{\psi}(u)$$

the slope and Hessian of γ. The argument u will be omitted unless needed for clarity. Note that $\nabla\gamma$ and H^{γ} do *not* in general satisfy (2.4), i.e. in general

$$\mathbf{a}(\nabla\gamma)\cdot H^{\gamma} := \sum_{i,j=1,2} a_{ij}(\nabla\gamma)H^{\gamma}_{ij} \neq 0, \tag{2.69}$$

because γ is *not* the equilibrium shape with some boundary height. In other words, $(\nabla\gamma, H^{\gamma})$ is *not* the local structure of any macroscopic shape.

Remark 2.7.2. *One has*

$$\nabla\psi = -\frac{1}{\xi}(\, e^{x/\xi}, e^{y/\xi}) \tag{2.70}$$

and

$$\|\nabla\gamma - \nabla\bar{\phi}\| = \kappa\epsilon_L\|\nabla\psi\| \leqslant \mathcal{K}(\xi,\kappa,\epsilon_L,u) := \sqrt{2}\frac{\kappa\epsilon_L}{\xi}\, e^{\max(x,y)/\xi}, \tag{2.71}$$

which is $o(1)$ when $L \to \infty$. In particular, since $\nabla\bar{\phi}$ is uniformly bounded away from $\partial\mathbb{T}$, so is $\nabla\gamma$.

Define then the 2×2 matrix

$$\bar{H} = H^{\bar{\phi}} - \frac{H^{\bar{\phi}} \cdot \mathbf{a}(\nabla\gamma)}{H^{\psi} \cdot \mathbf{a}(\nabla\gamma)} H^{\psi} \tag{2.72}$$

with H^{ψ} defined in (2.56). The denominator is non-zero always: recall from Section 2.2.2 that the diagonal elements a_{ii} given in (2.5) are positive away from $\partial\mathbb{T}$ and that H^{ψ} is diagonal, with negative diagonal entries, see (2.56). Remark also that, in contrast with (2.69),

$$\mathbf{a}(\nabla\gamma) \cdot \bar{H} = 0. \tag{2.73}$$

In other words, we have added the right correction to H^{γ} so that $(\nabla\gamma, \bar{H})$ is a local structure of a macroscopic shape. We further remark that

$$H^{\gamma} - \bar{H} = \left(\kappa\epsilon_L + \frac{H^{\bar{\phi}} \cdot \mathbf{a}(\nabla\gamma)}{H^{\psi} \cdot \mathbf{a}(\nabla\gamma)}\right) H^{\psi} = \kappa\epsilon_L(1 + O(\xi))H^{\psi}. \tag{2.74}$$

To see this, observe that for the denominator

$$|H^{\psi} \cdot \mathbf{a}(\nabla\gamma)| \geqslant \frac{c}{\xi^2} e^{\max(x,y)/\xi} \tag{2.75}$$

with $c = \min_{(x,y)\in U} \min(a_{11}(\nabla\gamma), a_{22}(\nabla\gamma)) > 0$; for the numerator,

$$H^{\bar{\phi}} \cdot \mathbf{a}(\nabla\gamma) = H^{\bar{\phi}} \cdot \mathbf{a}(\nabla\bar{\phi}) + H^{\bar{\phi}} \cdot (\mathbf{a}(\nabla\gamma) - \mathbf{a}(\nabla\bar{\phi})) \tag{2.76}$$

$$= 0 + H^{\bar{\phi}} \cdot (\mathbf{a}(\nabla\gamma) - \mathbf{a}(\nabla\bar{\phi})). \tag{2.77}$$

From (2.71) and (2.75) one deduces

$$\frac{H^{\bar{\phi}} \cdot \mathbf{a}(\nabla\gamma)}{H^{\psi} \cdot \mathbf{a}(\nabla\gamma)} = O\left(\kappa\epsilon_L\, \xi\right) \tag{2.78}$$

and (2.74) follows.

Let

$$z(u) = (\partial_x\gamma(u), \partial_y\gamma(u), \bar{H}_{11}(u), \bar{H}_{12}(u)) \in \mathcal{A}$$

and define

$$w(u) = (A(u), B(u), X(u), Y(u)) = f^{-1}(z(u)) \in W, \tag{2.79}$$

with $f : W \mapsto \mathcal{A}$ the function of Theorem 2.4.4. That is, recalling also (2.73), $(\nabla\gamma(u), \bar{H}(u))$ is the local structure of the macroscopic shape $\bar{\phi}_{A(u)B(u)C(u)}$ in the hexagon $\hexagon_{A(u)B(u)C(u)}$, with $C(u) = 1 - A(u) - B(u)$, at the point $(X(u), Y(u)) \in \bigcirc_{A(u)B(u)C(u)}$.

Remark 2.7.3. *Observe that, since $\bar{\phi}$ is non-extremal, the closure K of the set*

$$K' = \{(\partial_x\bar{\phi}(u), \partial_y\bar{\phi}(u), \partial^2_x\bar{\phi}(u), \partial^2_{xy}\bar{\phi}(u)),\ u \in U\}$$

is a compact subset of the open set $\mathcal{A}$. By Proposition 2.4.5, $f^{-1}(K)$ is a compact subset of the open set W. Next, note that

$$\sup_{u\in U} \|z(u) - (\partial_x\bar{\phi}(u), \partial_y\bar{\phi}(u), \partial^2_x\bar{\phi}(u), \partial^2_{xy}\bar{\phi}(u))\| = o(1) \tag{2.80}$$

when $L \to \infty$. Indeed, $\|\nabla\gamma - \nabla\bar{\phi}\|$ was bounded in (2.71)*, while*

$$\|\bar{H} - H^{\bar{\phi}}\| = \frac{|H^{\bar{\phi}} \cdot \mathbf{a}(\nabla\gamma)|}{|(H^{\psi}/\|H^{\psi}\|) \cdot \mathbf{a}(\nabla\gamma)|} = O(\sup_{u\in U} \mathcal{K}(\xi, \kappa, \epsilon_L, u)) = o(1) : (2.81)$$

for the numerator see (2.76) *and* (2.71)*, while the denominator is lower bounded by*

$$(1/\sqrt{2}) \times \min_{(x,y)\in U} \min(a_{11}(\nabla\gamma), a_{22}(\nabla\gamma))$$

which is positive, as discussed before.

As a consequence of (2.80) *and of Proposition 2.4.5, we see that $\{w(u), u \in U\}$ is contained in a compact subset of W. In other words, uniformly in $u \in U$, $A(u), B(u), C(u)$ are bounded away from zero and $(X(u), Y(u))$ is bounded away from $\partial\bigcirc_{A(u)B(u)C(u)}$. This remark is important to guarantee that, when one applies Theorem 2.3.6, estimates one obtains are uniform with respect to u. Uniformity will be not be recalled explicitly later.*

From now on, for lightness of notation we remove the argument u from $A(u), B(u), C(u)$. Call, as in Section 2.3.2, π_L^{ABC} the uniform measure in the hexagon $\hexagon_{A_LB_LC_L}$ (the discretization of $\hexagon_{ABC}$) and $\bar{\phi}_{ABC}$ the macroscopic shape. Translate $\hexagon_{A_LB_LC_L}$ in the P_{111} plane so that $u = (x, y)$ and $(X(u), Y(u))$ coincide, and add a suitable global constant to the boundary height $\varphi_{a_Lb_Lc_L}$ on $\partial\hexagon_{A_LB_LC_L}$, so that

$$\pi_L^{ABC}(h(u)) = \gamma(u). \tag{2.82}$$

We are at last in a position to prove the claim of Proposition 2.6.7, i.e. that

$$\tilde{\pi}(h(u) > \gamma(u) - L^{-1+\delta/60}) \leqslant L^{-20} \tag{2.83}$$

(recall that $\tilde{\pi}$ differs from $\hat{\pi}$ in that the floor constraint $h \geqslant \gamma^{(L)}_{i,j-1} - L^{-1+\delta/40}$ has been removed).

Recall that the boundary condition on ∂D_u (that is a disk of radius $L^{-1/2+\delta/100}$ centered at u), is $\gamma^{(L)}_{i,j-1}$, that is a discretization of $\gamma = \gamma_{i,j-1}$. We have for $v \in D_u$

$$\begin{aligned}\gamma^{(L)}_{i,j-1}(v) &= \gamma(v) + O(1/L)\\ &= \gamma(u) + (v-u)\cdot\nabla\gamma(u) + \frac{1}{2}(v-u)\cdot H^{\gamma}(u)\cdot(v-u) + O(1/L) \quad (2.84)\end{aligned}$$

where we used $\|u-v\| \sim L^{-1/2+\delta/100}$ and smoothness of γ to ignore higher-order terms in the Taylor expansion of γ around u. Next, write $H^{\gamma}(u) = \bar{H}(u) + (H^{\gamma}(u) - \bar{H}(u))$, with $\bar{H}$ defined in (2.72). From (2.74) and (2.56) we have for ξ small enough

$$(v-u)\cdot(H^{\gamma}(u) - \bar{H}(u))\cdot(v-u) \leqslant -C_1\epsilon_L\|u-v\|^2, \quad (2.85)$$

with $C_1(\xi,\kappa)$ a strictly positive constant, independent of L (recall from (2.68) that κ is bounded away from zero). Therefore,

$$\gamma^{(L)}_{i,j-1}(v) \leqslant \gamma(u) + (v-u)\cdot\nabla\gamma(u) + \frac{1}{2}(v-u)\cdot\bar{H}(u)\cdot(v-u) - C_1\epsilon_L\|u-v\|^2 + O(1/L). \quad (2.86)$$

Now recall that $\nabla\gamma(u)$ and $\bar{H}(u)$ are also the gradient and Hessian at u of $\bar{\phi}_{ABC}$, the macroscopic shape in the hexagon $\hexagon_{ABC}$. A second-order Taylor expansion and (2.82) give then

$$\begin{aligned}&\gamma^{(L)}_{i,j-1}(v) \leqslant (\gamma(u) - \bar{\phi}_{ABC}(u)) + \bar{\phi}_{ABC}(v) - C_1\epsilon_L\|u-v\|^2 + O(1/L)\\ &= (\pi_L^{ABC}(h(u)) - \bar{\phi}_{ABC}(u)) + \bar{\phi}_{ABC}(v) - C_1\epsilon_L\|u-v\|^2 + O(1/L). \quad (2.87)\end{aligned}$$

Thanks to Theorem 2.3.6 we have $(\pi_L^{ABC}(h(u)) - \bar{\phi}_{ABC}(u)) = (\pi_L^{ABC}(h(v)) - \bar{\phi}_{ABC}(v)) + O(1/L)$ and finally

$$\gamma^{(L)}_{i,j-1}(v) \leqslant \pi_L^{ABC}(h(v)) - C_1\epsilon_L\|u-v\|^2 + O(1/L). \quad (2.88)$$

Taking $v \in \partial D_u$, so that $\|u-v\| \sim L^{-1/2+\delta/100}$, we deduce that the boundary height $\gamma^{(L)}_{i,j-1}|_{\partial D_u}$ in the measure $\tilde{\pi}$ is lower than the function

$$\partial D_u \ni v \mapsto \pi_L^{ABC}(h(v)) - C_2\epsilon_L L^{-1+\delta/50}.$$

An immediate application of Proposition 2.3.7 gives that the $\tilde{\pi}$-probability that

$$h(u) > \gamma(u) - L^{-1+\delta/60} = \pi_L^{ABC}(h(u)) - L^{-1+\delta/60}$$

is $O(L^{-n})$ for any given n. Choosing $n > 20$ we get the desired result (2.83). □

Proof of Lemma 2.7.1. Observe that, with our usual notations, $\tilde{\pi} = \pi_{D_u}^{\gamma_{i,j-1}^{(L)}}$ and

$$\hat{\pi} = \tilde{\pi}(\cdot \mid \cdot \geqslant \gamma_{i,j-1}^{(L)} - L^{-1+\delta/40}),$$

from which it is immediate to deduce

$$\|\hat{\pi} - \tilde{\pi}\| \leqslant \frac{\tilde{\pi}(h \not\geqslant \gamma_{i,j-1}^{(L)} - L^{-1+\delta/40})}{1 - \tilde{\pi}(h \not\geqslant \gamma_{i,j-1}^{(L)} - L^{-1+\delta/40})},$$

where $h \not\geqslant \gamma_{i,j-1}^{(L)} - L^{-1+\delta/40}$ (violation of the floor constraint) is the event that there exists $v \in D_u$ such that $h(v) < \gamma_{i,j-1}^{(L)} - L^{-1+\delta/40}$.

It is not hard to see that $\tilde{\pi}(h \not\geqslant \gamma_{i,j-1}^{(L)} - L^{-1+\delta/40})$ is $O(L^{-n})$ for any given n. Indeed, analogously to (2.88) one has that, for $v \in \partial D_u$,

$$\gamma_{i,j-1}^{(L)}(v) \geqslant \pi_L^{ABC}(h(v)) - C_3 \epsilon_L L^{-1+\delta/50}. \tag{2.89}$$

From Proposition 2.3.7 one deduces that, except with $\tilde{\pi}$-probability $O(L^{-n})$,

$$h(v) \geqslant \pi_L^{ABC}(h(v)) - (1/2)L^{-1+\delta/40} \quad \text{for every} \quad v \in D_u.$$

On the other hand, from (2.88) we see that for every $v \in D_u$

$$\gamma_{i,j-1}^{(L)}(v) - L^{-1+\delta/40} \leqslant \pi_L^{ABC}(h(v)) - (3/4)L^{-1+\delta/40}.$$

□

2.8 Proof of Corollary 2.3.4

Let

$$\epsilon^{(n)} = \max_{x \in \partial U} |\varphi(x) - \varphi^{(n)}(x)| \tag{2.90}$$

and set

$$\tilde{\varphi}^{(n)} = \varphi^{(n)} - \min_{x \in \partial U} (\varphi^{(n)}(x) - \varphi(x))$$

(we are just adding a constant to the boundary height $\varphi^{(n)}$). Note that

$$\varphi \leqslant \tilde{\varphi}^{(n)} \leqslant \varphi + 2\epsilon^{(n)} \tag{2.91}$$

so that, if $\tilde{\phi}^{(n)}$ is the macroscopic shape in U with boundary height $\tilde{\varphi}^{(n)}$, one has

$$\bar{\phi} \leqslant \tilde{\phi}^{(n)} \leqslant \bar{\phi} + 2\epsilon^{(n)}. \tag{2.92}$$

If h_t^η and $\tilde{h}_t^\sigma$ denote respectively the dynamics with boundary heights $\varphi, \tilde{\varphi}^{(n)}$ and initial conditions η, σ, one has by monotonicity

$$\begin{aligned}\max_\eta \sup_{t>c(\delta)L^{2+\delta}} \mathbb{P}(\exists v \in U_L : h_t^\eta(v) > \bar{\phi}(v) + 3\epsilon^{(n)}) \\ \leqslant \max_\sigma \sup_{t>c(\delta)L^{2+\delta}} \mathbb{P}(\exists v \in U_L : \tilde{h}_t^\sigma(v) > \bar{\phi}(v) + 3\epsilon^{(n)}) \\ \leqslant \max_\sigma \sup_{t>c(\delta)L^{2+\delta}} \mathbb{P}(\exists v \in U_L : \tilde{h}_t^\sigma(v) > \tilde{\phi}^{(n)}(v) + \epsilon^{(n)}) \quad (2.93)\end{aligned}$$

where we used (2.92) in the second step. Theorem 2.3.3 says that the third line of (2.93) is some function $f(n, L)$ that vanishes as $L \to \infty$. It is then standard that one can choose some sequence $n(L)$ that diverges as $L \to \infty$ for which $f(n(L), L)$ still converges to zero. In conclusion, setting $\epsilon_L := \epsilon^{(n(L))}$, that tends to zero as $L \to \infty$, we have proven

$$\max_\eta \sup_{t>c(\delta)L^{2+\delta}} \mathbb{P}(\exists v \in U_L : h_t^\eta(v) > \bar{\phi}(v) + 3\epsilon_L) = o(1) \quad (2.94)$$

which is "half" of the claim (2.11). The other bound can be obtained similarly.

2.9 Hexagonal boundary

In this section we prove theorem 1.3.14. We will be sketchy because the proof is very similar to the proof of theorem 2.3.3. The main idea is that for hexagonal limit shapes, we are able to control fluctuations on domains larger than $L^{-1/2}$ and thus to keep the domination up to a time where the floor and ceiling are at distance L^δ/L. At that time, lemma 2.5.1 gives us the mixing time. In other words, we are able to push the control with non planar boundary condition to the same precision as in the planar case of [CMT12, LT12] given in chapter 3. We restate the theorem formally for convenience.

Theorem 2.9.1. *Let $a, b, c >$ with $a + b + c = 1$. Let U be an open simply connected domain with $\bar{U} \subset \bigcirc_{abc}$ (recall that by definition $\bigcirc_{abc}$ is the open ellipse so U does not go to the boundary of $\bigcirc_{abc}$). Let $(\varphi_L, U_L)_{L\geqslant 1}$ be a discretization of $(\bar{\phi}_{abc}, U)$, in other words consider the boundary condition induced on U by the limit shape in $\hexagon_{abc}$. Let $T_{\text{mix}}(L)$ denote the mixing time of the Glauber dynamics in U_L with boundary condition φ_L. For any $\delta > 0$, we have*

$$T_{\text{mix}} \leq C_\delta L^{2+\delta}.$$

Remark that the asymptotic height function in U is just $\bar{\phi}_{abc}$. Furthermore $\bar{U} \subset \bigcirc_{abc}$ so $\bar{\phi}_{abc}$ is non-extremal in U and theorem 2.3.3 applies. We

can thus assume in the proof of theorem 2.9.1 that the dynamics starts at distance ϵ from the limit shape and has a floor and ceiling at that height.

The proof will basically follow the second recursion (claim 2.6.3) from the proof of theorem 2.3.3 but we need slightly different technical choices at some points.

Let $\mathcal{O}$ be an open domain such that $U \subset \mathcal{O} \subset \bar{\mathcal{O}} \subset \circ_{abc}$. In section 2.6 we also used two domains (U and a shrinked $V \subset U$). Here we are able to enlarge U instead because we know how to extend the boundary condition. The advantage of enlarging the domain is that we will be able to control the height up to the boundary of U.

We define as above $\psi = \psi(0,0) - e^{x/\xi} - e^{y/\xi}$ with the constant $\psi(0,0)$ chosen such that $\inf_{\mathcal{O}} \psi = 2$ (ψ is controlled in the large domain).

The main step is, as above in claim 2.6.3, an induction with a moving ceiling. The difference is the growing size of the time steps.

Claim 2.9.2. *Let $\gamma_j = \bar{\phi} + (1 - j/L)\epsilon_L \psi$. Let T_j a sequence of time defined by $T_0 = 0$ and $T_{j+1} - T_j = L^{2+10\delta}/(L-j)$. For any $j \leq L - L^{10\delta}$, we let E_j be the event*

$$E_j = \{\forall t \in [T_j, L^5],\, h_t \leq \gamma_j\}$$

For $j \leq L - L^{10\delta}$, we have

$$\mathbb{P}(E_j) \geq 1 - \frac{j}{L^2}$$

Proof of theorem 2.9.1 given claim 2.9.2. We apply the claim for $j_0 = L - L^{10\delta}$. We have

$$T_j = L^{2+10\delta} \sum_{j=1}^{L-L^{10\delta}} \frac{1}{L-j} \tag{2.95}$$

$$= L^{2+10\delta} \sum_{k=L^{10\delta}}^{L-1} \frac{1}{k} \tag{2.96}$$

$$\leq C L^{2+11\delta} \tag{2.97}$$

On the event E_{j_0}, we can apply lemma 2.5.1 with floor and ceiling at distance $O(L^{-1+10\delta})$ to obtain the mixing time. □

The initialization is given by theorem 2.3.3.

For the recursion as in the proof of claim 2.6.3 we proceed separately for each lattice site $v \in U$ and use a union bound afterwards. We now assume that claim 2.9.2 holds for $j-1$ and we write for simplicity of notation

$$\gamma = \gamma_{j-1} = \bar{\phi}_{abc} + \kappa \epsilon_L \, \psi$$

with $\kappa = (1 - (j-1)/L)$. Remark that $\kappa \geq L^{-1+10\delta}$.

Let $v \in U$ and let D_v be a disk centered in v and of radius $R = \sqrt{L^{-1+\delta}/\kappa}$. As before, let $\hat{h}_t$ denote the dynamics pinned to the ceiling γ outside of D and with an additional floor constraint as in section 2.6. Let $\hat{\pi}_{j-1}$ be its equilibrium measure. Note that since $\kappa \geq L^{-1+10\delta}$, we have $R \leq L^{-9\delta/2} \ll 1$ so the disk D_v is always a subset of $\mathcal{O}$, even when v is on the boundary of U (this is why we enlarged U).

Note that by construction $T_j - T_{j-1} = L^2 R^2 L^{9\delta}$ which is by lemma 2.5.1 greater than the mixing time of $\hat{h}_t$. Therefore claim 2.9.2 follows, using the same proof as above, from the following equilibrium estimate (identical to proposition 2.6.7 except for the size of the disk D_v).

Proposition 2.9.3. *Let $j \leq L - L^{10\delta}$ and $\hat{\pi}_{j-1}$ defined as above. If ξ is smaller than some ξ_0 (independent of j and L), then*

$$\hat{\pi}_j \left[h(v) > \gamma - L^{-1+\delta/60} \right] \leq L^{-20}.$$

Recall that ξ appears in the definition of ψ.

Proof. Let $\tilde{\pi}$ be the uniform measure in D_v with boundary condition γ but no ceiling or floor constraint. We will prove the proposition for $\tilde{\pi}$ instead of $\hat{\pi}$, see lemma 2.7.1 for the proof that it is sufficient.

Let (A, B, X, Y) be defined as in section 2.7, equation (2.79), and let $\bar{\phi}_{ABC}$ be the corresponding height function. As in section 2.7 we translate the ABC hexagon so that v is at position (X, Y). We write for simplicity H^{abc} and H^{ABC} for the Hessian matrix of $\bar{\phi}_{abc}$ and $\bar{\phi}_{ABC}$.

We make a Taylor expansion at order 2 of $\gamma - \bar{\phi}_{ABC}$ around v :

$$\gamma(v') - \bar{\phi}_{ABC}(v') = \gamma(v) - \bar{\phi}_{ABC}(v) + \frac{1}{2}(v'-v) \cdot (H^{abc} - H^{ABC}) \cdot (v'-v) + \frac{1}{2}\epsilon\kappa(v'-v) \cdot H^{\psi} \cdot (v'-v) + \text{higher order} + O(1/L) \quad (2.98)$$

Remark that the higher order terms are of 2 sorts, either derivatives of $\epsilon\kappa\psi$ or derivative of $\bar{\phi}_{abc} - \bar{\phi}_{ABC}$. The former terms are obviously linear in κ but the latter are actually also controlled linearly by κ. Indeed the local structure is an explicit $\mathcal{C}^\infty$ function of the parameters of the hexagon with non zero determinant so, locally around the local structure at v, its inverse is also $\mathcal{C}^\infty$. Therefore A, B, X, Y and all the spatial derivatives of $\bar{\phi}_{abc} - \bar{\phi}_{ABC}$ are $\mathcal{C}^\infty$ functions of κ. For $\kappa = 0$ we have $(A, B, C) = (a, b, c)$ and the spatial derivatives of $\bar{\phi}_{abc} - \bar{\phi}_{ABC}$ are all 0 (remark that for a general limit shape as in theorem 2.3.3 only the first two orders are 0, the others do not vanish with κ). Via a Taylor expansion in κ they can therefore all be controlled linearly in κ and we can write the above expansion more precisely :

$$\gamma(v') - \bar{\phi}_{ABC}(v') = \gamma(v) - \bar{\phi}_{ABC}(v) + \frac{1}{2}(v'-v) \cdot (H^{abc} - H^{ABC}) \cdot (v'-v) + \frac{1}{2}\epsilon\kappa(v'-v) \cdot H^{\psi} \cdot (v'-v) + O(\kappa\|v'-v\|^3) + O(1/L). \quad (2.99)$$

Note that $\kappa R^3 = (L^{-1+\delta})^{3/2}/(\kappa)^{1/2} \leq L^{-1-2\delta}$ which is smaller than $1/L$, the smallest significant height difference in our model (recall that height function have discrete increments of $\pm 1/L$). Therefore we can completely drop the terms of order 3 and higher.

We add a global constant to $\bar{\phi}_{ABC}(\cdot)$ in order to have $\gamma(v) - \bar{\phi}_{ABC}(v) = L^{-1+\delta/2}$. As in section 2.7, the H^{ψ} term can be made to dominate the $H^{abc} - H^{ABC}$ term by taking ξ sufficiently small. We then have on the boundary of D_v :

$$\forall v' \in \partial D_v, \gamma(v') \leq \bar{\phi}_{ABC}(v') - C(\xi)L^{-1+\delta}.$$

Let π^{ABC} denote the equilibrium in D with boundary condition $\bar{\phi}_{ABC}$. Thanks to the above equation, $\tilde{\pi}$ the equilibrium in D with boundary γ is stochastically dominated by π^{ABC}. In particular at v,

$$\tilde{\pi}(h(v)) \leq \pi^{ABC}(h(v)) = \bar{\phi}_{ABC}(v) + O(1/L) \leq \gamma(v) - L^{-1+\delta/2}.$$

The same stochastic domination also gives a control of the fluctuations and therefore proves proposition 2.9.3.

□

2.A Proof of Eq. (2.12)

2.A.1 Mean height

We have to compute the average height difference between two lattice points u and v in $\mathcal{T}_L \cap \hexagon_{abc}$. Recall Remark 2.2.5: the height difference is directly related to the number of lozenges crossed by a lattice path from u to v (the height difference is independent of the chosen path). We will assume that the vector $u - v$ is along one of the three lattice directions of $\mathcal{T}_L$ (in the general case, we can always reduce to this situation by choosing the path from u to v as a concatenation of a L-independent number of straight paths along these directions) and by symmetry we consider only the case where $u - v$ is in the vertical direction, with v above u.

To avoid a plethora of $\lfloor \cdot \rfloor$, let us assume that

$$A = aL, B = bL, C = cL$$

are even integers. Recall our choice of (non-orthogonal) coordinates (x, y) for points in $\mathcal{T}_L$. In this Appendix, to fit better the notation of [Pet12a], it is convenient to translate the origin of the coordinates (that used to be in the center of the hexagon until now) in such a way that the center of the hexagon $\hexagon_{a_L b_L c_L}$ has coordinates

$$(-a - (b + c)/2 + 1/(2L), -(3/2)a - c - b/2 + 1/(2L)).$$

See Figure 2.4. Note that we translated the origin by a half-integer number of lattice steps in both directions x and y. Given a vertical edge in $\mathcal{T}_L$, let us label it with the coordinates (x, y) (that are now integers times $1/L$) of its mid-point. Again to stay closer to the notations of [Pet12a], here we assume that $a + c = 1$, instead of our usual normalization $a + b + c = 1$.

Recall that u and v are points in $\mathcal{T}_L$ related by a vertical segment and let $p_i, i = 0, \dots, n-1$ be the vertical lattice edges composing such segment (labeled say from below). Clearly, $n = L|v - u|$ (because each edge of $\mathcal{T}_L$ has length $1/L$). In this case from Remark 2.2.5 we see that

$$\pi_L^{abc}(h(v)) - \pi_L^{abc}(h(u)) = \frac{1}{L} \sum_{i=0}^{n-1} \left[1 - \pi_L^{abc}(\mathbf{1}_{p_i})\right] \quad (2.100)$$

with $\mathbf{1}_p$ the indicator function that the vertical edge p crosses a horizontal lozenge. We will prove the following estimate (which is a special case of estimates proved in [Pet12a, Section 7], except for the explicit control of the error term):

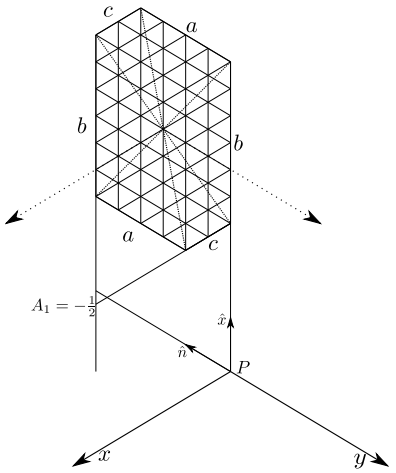

Figure 2.4: The coordinates we used until now (dotted axes) had the origin at the center of the hexagon. The coordinates we use in the Appendix are centered in P. The axes $\hat{n}, \hat{x}$ correspond to the the coordinates used in [Pet12a].

Proposition 2.A.1. *Let $p = (x, y)$ be a vertical edge contained in $\circlearrowright_{abc}$. One has*

$$\pi_L^{abc}(\mathbf{1}_p) = \Pi_\infty(x, y) + O(1/L) := \frac{1}{2\pi i} \int_{\bar{\mathrm{w}}_c}^{\mathrm{w_c}} \frac{(1 + y - x)}{(z + x)(z + y + 1)} dz + O(1/L) \quad (2.101)$$

where:

- *the $O(1/L)$ error is uniform for (x, y) in compact subsets of $\circlearrowright_{abc}$;*
- *$\mathrm{w_c} = \mathrm{w_c}(x, y, a, b, c)$ is the unique non-real critical point (w.r.t. w) of the function S, defined in equation (2.106), in the upper half complex plane and $\bar{\mathrm{w}}_c$ is the complex conjugate of w_c;*
- *the contour of integration in the complex plane intersects the real axis to the right of both poles.*

Now we can plug (2.101) into (2.100). After summation on i, the error term $O(1/L)$ gives an error term $O(n/L^2) = O(|u-v|/L)$. The main term $1 - \Pi_\infty$ gives as dominant term the line integral

$$\int_{\mathcal{C}(u,v)} (1 - \Pi_\infty)\, ds \tag{2.102}$$

(with $\mathcal{C}(u,v)$ the straight path from u to v) plus again an error $O(|u-v|/L)$ by Riemann approximation.

Finally we do *not* need to check that the line integral equals $\bar\phi_{abc}(v) - \bar\phi_{abc}(u)$: this follows from Theorem 2.3.5 on the existence of the limiting shape.

Our notations	Notations from [Pet12a]
-1/2	A_1
A	$B_1 - A_1$
B	$A_2 - B_1$
C	$B_2 - A_2$
x	$-x$
y	$-x - n$
L	N

Table 2.1: The correspondence between the two sets of notations, in the case where in [Pet12a] the origin is chosen such that $A_1 = -1/2$.

2.A.2 Correlation kernel

The proof of Proposition 2.A.1 is essentially identical to the proof of Theorem 2 of [Pet12a, Section 7], except that we keep track more precisely of the size of errors. Actually, Theorem 2 of [Pet12a] considers a much more general situation: first of all, the domain to be tiled is not simply a hexagon but a more general polygonal shape (the hexagon being a particular case). Secondly, Theorem 2 of [Pet12a] allows to get the asymptotics of the probability of any event involving a fixed number m of lozenges (say, the probability of the event $\mathbf{1}_{p_1} \cdots \mathbf{1}_{p_m}$). For simplicity of exposition, we will however restrict ourselves to the hexagonal region $\hexagon_{a_L b_L c_L}$ (which corresponds to the polygonal shape of [Pet12a] with the choice $k = 2$ there) and to the observable $\mathbf{1}_p$ we are interested in.

Let us introduce the Pochhammer symbol $(y)_m = y(y+1)\dots(y+m-1)$. The probability that the vertical edge $p = (x, y)$ crosses a horizontal lozenge can be read from formulas (2.5) and (2.6) of [Pet12a]: it is given by a double integral in the complex plane, with a L-dependent but explicit kernel. In our language, we have:

Theorem 2.A.2. *Let $p = (x, y)$ be a vertical edge in the hexagon. Define $X = Lx, Y = Ly$ (X, Y are automatically integers with the present conven-*

tion for coordinates). One has

$$\pi_L^{abc}(\mathbf{1}_p) = \frac{(L-X+Y)}{(2i\pi)^2} \times \oint dZ \oint dW \frac{(Z+X+1)_{L-X+Y-1}}{(W+X)_{L-X+Y+1}} \frac{1}{W-Z} \frac{(-W)_A}{(-Z)_A} \frac{(A+B-W)_C}{(A+B-Z)_C} \tag{2.103}$$

where the integration contours on Z and W have to chosen such that:

- *The Z contour runs counter-clockwise and includes the integer real points $-X, -X+1, ..., A+B+C$ and no other integer point of the real line;*
- *The W contour runs counter-clockwise; it contains the Z contour and also integer points $-Y-L, -Y-L+1, \ldots, -X$ (it may contain other integer points).*

We warn the reader who would like to find this formula in [Pet12a] that conventions in [Pet12a] are different from ours: the correspondence between the two sets of notations is conceptually trivial but a bit tricky as we need to rotate the hexagon and make an affine transformation to go from one setting to the other (compare for instance the shape of lozenges in our Figure 2.2 and in Figure 3 of [Pet12a]). We will not give details on the transformation but we summarize the correspondence in Table 2.1.

2.A.3 Contour changes

In this section we use upper-case letters for lengths and coordinates proportional to L and lower-case letters for the corresponding rescaled variables of order 1.

First we change the scale by the change of variable $Z \to Z/L = z$ and $W \to W/L = w$ and we reorder the resulting L-dependent factor to get:

$$\pi_L^{abc}(\mathbf{1}_p) = \frac{1}{(2\pi i)^2} \oint \oint \frac{1}{w-z} \frac{(1+y-x)}{(w+x)(w+y+1)} \frac{P_L(w,x,y)}{P_L(z,x,y)} dz\, dw \tag{2.104}$$

where

$$P_L(z,x,y) = \frac{(L+Ly-Lx-1)!}{(Lz+Lx+1)_{L+Y-X-1}} (-Lz)_A (A+B-Lz)_C.$$

The following approximation result can be extracted from [Pet12a, Lemma 7.4]:

$$P_L(w,x,y) = C_L \left(\frac{(w+x)(w+y+1)}{1+y-x} \right)^{1/2} \exp(LS(w;x,y) + O(1/L)) \tag{2.105}$$

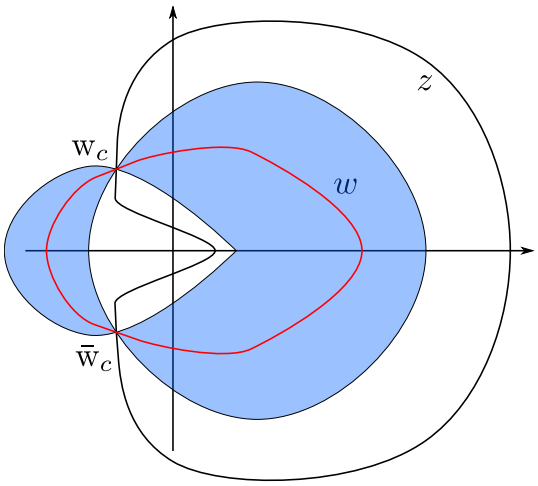

Figure 2.5: A schematic view of the new contours for z and w. The shaded region corresponds to $\{w \in \mathbb{C} : \Re(S(w) - S(\mathrm{w}_c)) < 0\}$. See also [Pet12a, Fig. 11].

where C_L may depend on A, B, C but not on w, x, y,

$$\begin{aligned} S(w;x,y) &= (w+x)\ln(w+x) - (w+y+1)\ln(w+y+1) \\ &+ (1+y-x)\ln(1+y-x) + (a-w)\ln(a-w) + (a+b+c-w)\ln(a+b+c-w) \\ &- (-w)\ln(-w) - (a+b-w)\ln(a+b-w) \end{aligned} \quad (2.106)$$

and the $O(1/L)$ terms can be taken uniform on the integration contours.

As proven in [Pet12a], if (x, y) is in the ellipse $\bigcirc_{abc}$ then S has two conjugate non-real critical points $\mathrm{w}_c, \bar{\mathrm{w}}_c$ (say with w_c in the upper half complex plane). Moreover, $S''(\mathrm{w}_c; x, y) \neq 0$.

Recall that the integration contour for w includes that for z. As explained in [Pet12a]:

Proposition 2.A.3. *One can move the integration contours so that:*

- *they cross exactly at the two points* $\mathrm{w}_c, \bar{\mathrm{w}}_c$*;*
- *the* w *contour lies in the region of the complex plane where* $\Re(S(w;x,y) - S(\mathrm{w}_c;x,y)) < 0$ *(except at* $\mathrm{w}_c, \bar{\mathrm{w}}_c$ *where the real part is obviously zero);*
- *the* z *contour lies in the region of the complex plane where* $\Re(S(z;x,y) - S(\mathrm{w}_c;x,y)) > 0$ *(except at* $\mathrm{w}_c, \bar{\mathrm{w}}_c$ *where it is zero);*
- *the contours avoid any poles of the integrand (that are on the real axis).*

See Figure 2.5. Of course, in the process of moving the contours some residue will appear, because there is a pole $1/(w - z)$ and the new contours

cross. As shown in [Pet12a, Lemma 7.9], the residue is exactly the single integral

$$\frac{1}{2\pi i}\int_{\bar{\mathrm{w}}_c}^{\mathrm{w}_c}\frac{(1+y-x)}{(z+x)(z+y+1)}\frac{P_L(z,y,x)}{P_L(z,y,x)}dz=\frac{1}{2\pi i}\int_{\bar{\mathrm{w}}_c}^{\mathrm{w}_c}\frac{(1+y-x)}{(z+x)(z+y+1)}dz$$

which is nothing but $\Pi_\infty(x,y)$. To prove (2.101) it remains therefore only to show that the double integral in the r.h.s. of (2.104), where now z and w run along the new contours, gives a contribution $O(1/L)$.

2.A.4 Integral approximations

For the double integral we use (2.105) to get

$$\frac{1}{(2i\pi)^2}\oint\oint\Big(\frac{(1+y-x)}{(z+x)(z+y+1)}\Big)^{\frac{1}{2}}\Big(\frac{(1+y-x)}{(w+x)(w+y+1)}\Big)^{\frac{1}{2}}\times\frac{1}{w-z}\exp L[S(w;x,y)-S(z;x,y)](1+O(1/L))dzdw \quad (2.107)$$

Recall the choice of the integration contours for z and w described in Proposition 2.A.3 and observe that along such contours the exponential in (2.107) is bounded by 1 in absolute value. Also, we choose the contours so that close to the critical points they are exactly linear.

We fix some small $\delta>0$ and we divide the integral into three regions:

Region 1 w,z are both within distance $L^{-1/2+\delta}$ from w_c or both within distance $L^{-1/2+\delta}$ from $\bar{\mathrm{w}}_c$;

Region 2 z is within distance $L^{-1/2+\delta}$ from w_c and w is within distance $L^{-1/2+\delta}$ from $\bar{\mathrm{w}}_c$, or viceversa;

Region 3 the rest of the integration contours.

Let us consider **Region 3** first, and assume that z is at distance at least $L^{-1/2+\delta}$ from both critical points. The first two factors in the integral are bounded (because the contours stay away from the poles). The factor $1/(w-z)$ can be upper bounded by $L^{1/2-\delta}$ in absolute value. The exponential is $O(\exp(-L^{2\delta}))$. Indeed, recall that $\Re(S(w;x,y)-S(\mathrm{w}_c;x,y))\leqslant 0$ while $\Re(S(z;x,y)-S(\mathrm{w}_c;x,y))>0$. More precisely, since $S''(\mathrm{w}_c,x,y)\neq 0$ and the third derivative is finite, one has $\Re(S(z;x,y)-S(\mathrm{w}_c;x,y))>L^{-1+2\delta}$ from a Taylor expansion. Finally the $O(1/L)$ term in (2.107) is bounded on the contour so it gives negligible contribution. In conclusion, the contribution from **Region 3** is $O(\exp(-L^{2\delta}))$.

Now let us consider **Region 2** and assume by symmetry that w is close to w_c and z is close to $\bar{\mathrm{w}}_c$. We can write $\Re(S(w;x,y)-S(\mathrm{w}_c;x,y))=-C_1|w-\mathrm{w}_c|^2+O(|w-\mathrm{w}_c|^3)$, $\Re(S(z;x,y)-S(\mathrm{w}_c;x,y))=-C_2|z-\bar{\mathrm{w}}_c|^2+O(|z-\bar{\mathrm{w}}_c|^3)$

for some $C_i > 0$. Furthermore since z and w are far from each other we can use a uniform bound on all terms outside the exponential and them we get a product of two Gaussian integrals, each of which gives a $O(1/\sqrt{L})$ contribution. Again the $O(1/L)$ term does not play any role.

Finally we consider **Region 1** which is more difficult because the $\frac{1}{w-z}$ term is singular. By symmetry we will only consider the case with both w and z close to w_c. Recall that the integration contours are linear near w_c, i.e. one has

$$w = \mathrm{w}_c + t\theta,\ t \in [-L^{-1/2+\delta}, L^{-1/2+\delta}], \quad z = \mathrm{w}_c + s\zeta,\ s \in [-L^{-1/2+\delta}, L^{-1/2+\delta}]$$

with θ, ζ two modulus-1 complex numbers.

The expression we have to control is then:

$$E = \int_{\mathrm{w}_c-\theta L^{-1/2+\delta}}^{\mathrm{w}_c+\theta L^{-1/2+\delta}} dw \int_{\mathrm{w}_c-\zeta L^{-1/2+\delta}}^{\mathrm{w}_c+\zeta L^{-1/2+\delta}} dz \left(\frac{(1+y-x)}{(z+x)(z+y+1)}\right)^{\frac{1}{2}}$$
$$\times \left(\frac{(1+y-x)}{(w+x)(w+y+1)}\right)^{\frac{1}{2}} \frac{1+O(1/L)}{w-z} \exp\left\{L[S(w;x,y) - S(z;x,y)]\right\}.$$

The first step is to get rid of the $\left(\frac{(1+y-x)}{(z+x)(z+y+1)}\right)^{\frac{1}{2}} \left(\frac{(1+y-x)}{(w+x)(w+y+1)}\right)^{\frac{1}{2}}$ factor. Remark that it has a non-zero limit when $w = z = \mathrm{w}_c$ and that we can use a Taylor expansion to approximate it by $a_0 + a_1(z - \mathrm{w}_c) + a_2(w - \mathrm{w}_c) + O(L^{-1+2\delta})$. Plugging this into the integral we get an expression of the form :

$$E = \iint dwdz \frac{a_0 + a_1(z-\mathrm{w}_c) + a_2(w-\mathrm{w}_c) + O(L^{-1+2\delta})}{w-z} \times \exp L[S(w;x,y) - S(z;x,y)] \quad (2.108)$$

where from now on $\iint dwdz$ means $\int_{\mathrm{w}_c-\theta L^{-1/2+\delta}}^{\mathrm{w}_c+\theta L^{-1/2+\delta}} dw \int_{\mathrm{w}_c-\zeta L^{-1/2+\delta}}^{\mathrm{w}_c+\zeta L^{-1/2+\delta}} dz$. Note that the $O(1/L)$ term has been absorbed into the $O(L^{-1+2\delta})$.

We start by looking at the most difficult term, the one proportional to a_0, call it E_0. Remark that we have :

$$\iint dwdz \frac{1}{w-z} \exp\left\{LS''(\mathrm{w}_c)[(w-\mathrm{w}_c)^2 - (z-\mathrm{w}_c)^2]\right\} = 0.$$

Indeed the integrand is an odd function of $(z - \mathrm{w}_c, w - \mathrm{w}_c)$ and we integrate on a symmetric domain (the integral is absolutely convergent). We can thus rewrite E_0 as

$$E_0 = a_0 \iint dwdz \frac{1}{w-z} \exp\left\{LS''(\mathrm{w}_c)[(w-\mathrm{w}_c)^2 - (z-\mathrm{w}_c)^2]\right\}$$
$$\times\left(-1 + \exp\left\{L\left[S(w;x,y) - S(z;x,y) - S''(\mathrm{w}_c)((w-\mathrm{w}_c)^2 - (z-\mathrm{w}_c)^2)\right]\right\}\right).$$

With a Taylor expansion on $\exp LS(w)$ we get

$$E_0 = a_0 \iint dwdz \frac{O\left(L|w-\mathrm{w}_c|^3 + L|z-\mathrm{w}_c|^3\right)}{w-z} \times \exp\left\{LS''(\mathrm{w}_c)[(w-\mathrm{w}_c)^2 - (z-\mathrm{w}_c)^2]\right\}. \quad (2.109)$$

Remark that this expansion is valid because $L|w-\mathrm{w}_c|^3 = O(L^{-1/2+3\delta}) = o(1)$. We take the absolute value inside the integral and change variables $\tilde{z} = \sqrt{L}(z-\mathrm{w}_c)$ and $\tilde{w} = \sqrt{L}(w-\mathrm{w}_c)$ to get

$$|E_0| \leq \frac{K}{L} \int_{-\theta L^\delta}^{\theta L^\delta} d\tilde{w} \int_{-\zeta L^\delta}^{\zeta L^\delta} d\tilde{z}\, \frac{|\tilde{z}|^3 + |\tilde{w}|^3}{|\tilde{z}-\tilde{w}|} \exp \Re[S''(\mathrm{w}_c)(\tilde{w}^2 - \tilde{z}^2)]$$

and we emphasize that both $S''(\mathrm{w}_c)\tilde{w}^2$ and $-S''(\mathrm{w}_c)\tilde{z}^2$ have negative real part. Finally since the linear integration contours for $\tilde{z}$ and $\tilde{w}$ are not colinear, we can lower bound $|\tilde{z}-\tilde{w}|$ by a constant times either $|\tilde{z}|$ or $|\tilde{w}|$ so we have

$$|E_0| \leq \frac{K'}{L} \int_{-\theta L^\delta}^{\theta L^\delta} d\tilde{w} \int_{-\zeta L^\delta}^{\zeta L^\delta} d\tilde{z}(|\tilde{z}|^2 + |\tilde{w}|^2) \exp \Re[S''(\mathrm{w}_c)(\tilde{w}^2 - \tilde{z}^2)]$$

and the Gaussian integral in the right hand side is bounded uniformly in L.

Let us go back to the integral E. The terms E_1, E_2 containing a_1 or a_2 can be treated similarly to E_0. They are actually easier since $(w-\mathrm{w}_c)$ or $(z-\mathrm{w}_c)$ produce a term $L^{-1/2}\tilde{w}$ or $L^{-1/2}\tilde{z}$: since $\tilde{w}/(\tilde{w}-\tilde{z})$ is bounded, one gets for $i = 1, 2$

$$\begin{aligned} |E_i| &\leq \frac{K''|a_i|}{L} \int_{-\theta L^\delta}^{\theta L^\delta} d\tilde{w} \int_{-\zeta L^\delta}^{\zeta L^\delta} d\tilde{z} \exp\left\{\Re[S''(\mathrm{w}_c)(\tilde{w}^2 - \tilde{z}^2)]\right\}(1 + o(1)) \\ &= O(1/L). \end{aligned}$$

Finally, the term E_R containing the $O(L^{-1+2\delta})$ error can be estimated once again with the same Taylor expansion of S and the same change of variables, and it turns out to be $O(L^{-3/2+2\delta})$. We just have to remark that the integral

$$\int_{-\theta L^\delta}^{\theta L^\delta} d\tilde{w} \int_{-\zeta L^\delta}^{\zeta L^\delta} d\tilde{z} \frac{1}{|\tilde{z}-\tilde{w}|} \exp \Re[S''(\mathrm{w}_c)(\tilde{w}^2 - \tilde{z}^2)]$$

does not diverge with L since the singularity $\frac{1}{|\tilde{z}-\tilde{w}|}$ is integrable in $\mathbb{R}^2$ (recall that even though $\tilde{z}$ and $\tilde{w}$ are complex they live on different lines so we are really integrating on a two dimensional box) and thus the Gaussian integral is bounded.

Overall we have proven that the double integral (2.107) is $O(1/L)$.

Chapter 3

Temps de mélange pour les pavages par des dominos

3.1 Introduction

Uniform random perfect matchings (or dimer coverings) of a bipartite, infinite, planar periodic graph G (e.g. $\mathbb{Z}^2$ or the hexagonal lattice $\mathcal{H}$) play a crucial role in statistical mechanics and combinatorics, and a vast literature exists on the subject (cf. for instance the classical papers [Kas61, TF61] and the much more recent [KOS06]). On one hand, thanks to the bijection between perfect matchings and discrete height functions (see Section 3.2.1), they provide natural and exactly solvable models of random $(2+1)$-dimensional interfaces (which can be thought of as simplified models for the interface separating two coexisting thermodynamic phases [Spo93]). On the other hand, thanks to their conformal invariance and Gaussian Free Field-like fluctuation properties in the scaling limit [Ken00, Ken01, KOS06], they belong, like the Ising model at $T = T_c$, to the family of critical two-dimensional systems.

In contrast, the study of stochastic dynamics of perfect matchings is a much less developed topic. Typically, one takes a large but finite portion G' of the graph G and defines a simple Glauber-type Markov chain such that each update locally modifies the matching within G'. The unique equilibrium measure is the uniform measure over perfect matchings of G'. From the point of view of theoretical computer science [LRS01, LPW08, Wil04, RT00], the interesting question is to understand how quickly, as a function of the size of G', the Markov chain approaches equilibrium (i.e. how quickly it samples reliably a uniformly chosen random perfect matching of G'). From the point of view of statistical physics, thanks to the above mentioned bijection between perfect matchings and height functions, this Markov chain can be seen as a dynamics for a $(2+1)$-dimensional interface and it is of interest to understand how the geometry of the interface evolves in time. For

instance, when $G = \mathcal{H}$ the evolution of the height function exactly coincides with the zero-temperature heat-bath dynamics for an interface, separating "$-$" from "$+$" spins, of the three-dimensional nearest-neighbor Ising model [CMST10].

Until recently, the best mathematical result on this dynamics issues was that, when $G = \mathbb{Z}^2$ or $G = \mathcal{H}$, the total-variation mixing time T_{mix} of the Markov chain is at most polynomial in the size of G'. See Section 3.1.1 for a short review. Results of this type are based on simple but effective coupling arguments that unfortunately have little chance of providing the sharp behavior of T_{mix}. (A notable exception is the work [Wil04], where sharp bounds on T_{mix} for $G = \mathcal{H}$ were given, but for a very particular, spatially non-local, dynamics).

In [CMT12], instead, in the case where $G = \mathcal{H}$ it was proven that, under a certain condition on the shape of the finite region G' ("almost planar boundary condition" assumption, see below), T_{mix} behaves like L^2, up to logarithmic corrections, if L is the diameter of G'. As we briefly explain in Section 3.1.2, going beyond the case of the hexagonal lattice $\mathcal{H}$ is a mathematical challenge, since certain exact identities that hold there do not survive on more general graphs. In this work we prove that, when $G = \mathbb{Z}^2$ (and in a few other cases, see below), again under the "planar boundary condition" assumption, $T_{\text{mix}} = L^{2+o(1)}$. We present this result, still informally but with a bit more of detail, in the next section.

The major improvement with respect to [LRS01, Wil04] is that both [CMT12] and the present work use the intuition that the height function should evolve, on a diffusive time-space scale, according to a deterministic, anisotropic mean-curvature type evolution [Spo93]. More precisely, call $h_t(X, Y)$ the height function at time t, with (X, Y) a bi-dimensional space coordinate on the lattice G. Then, one expects that under diffusive scaling (i.e. setting $\tau = t/L^2$, $(x, y) = (X, Y)/L$, $\phi_\tau(x, y) = L^{-1}h_{\tau L^2}(xL, yL)$ and letting $L \to \infty$) the limiting deterministic evolution of the height function ϕ should be of the type

$$\frac{d}{d\tau}\phi = \mu(\nabla\phi)\mathcal{L}\phi. \tag{3.1}$$

Here, $\mu(\nabla\phi)$ is a positive, slope-dependent "mobility coefficient" while $\mathcal{L}$, directly related to the first variation of the surface energy functional, is a non-linear elliptic operator of the type

$$\mathcal{L}\phi = a_{11}(\nabla\phi)\partial_x^2\phi + 2a_{12}(\nabla\phi)\partial_{xy}^2\phi + a_{22}(\nabla\phi)\partial_y^2\phi$$

where the matrix $\mathbf{a} = \{a_{ij}(\nabla\phi)\}_{i,j=1,2}$ (with $a_{21} = a_{12}$) is positive-definite. See [Spo93] for a discussion of these issues. Remark that $\mathcal{L}\phi$ is a linear combination (with slope-dependent coefficients) of the principal curvatures of the interface, hence the name "anisotropic mean-curvature evolution". By

the way, such intuition suggests the precise scaling $T_{\text{mix}} \sim const \times L^2 \log L$. Indeed, for $\tau \to \infty$ the solution of (3.1) approaches a "limit shape" $\bar{\phi}$ satisfying $\mathcal{L}\bar{\phi} = 0$, and one can consider that equilibrium is reached when

$$\|\phi_\tau - \bar{\phi}\|_\infty \approx (\log L)/L \tag{3.2}$$

(the typical equilibrium height fluctuations before space rescaling being expected to be $O(\log L)$, see Remark 3.2.10). Assume for simplicity that the matrix $\mathbf{a}$ is the identity and $\mu(\cdot)$ is constant: then, (3.1) is just the heat equation and (3.2) is satisfied as soon as τ is a suitable constant times $\log L$, i.e. t is some constant times $L^2 \log L$.

3.1.1 Informal presentation of the main result

A domino tiling of the plane is a covering of $\mathbb{R}^2$ with 2×1 non-overlapping vertical or horizontal rectangles (dominos), with vertices sitting at points of $(\mathbb{Z}^2)^* = \mathbb{Z}^2 + (1/2, 1/2)$. Domino tilings are in one-to-one correspondence with perfect matchings (or simply "matchings" in the following) of $G = \mathbb{Z}^2$, i.e. subsets of edges (called dimers) of $\mathbb{Z}^2$ such that each vertex is contained in exactly one dimer (to see the correspondence, just draw a segment of unit length inside each domino, parallel to its longer side, with endpoints on $\mathbb{Z}^2$). Similarly, tilings of a finite portion P of the plane correspond to matchings of a finite subset G' of $\mathbb{Z}^2$. From now on, we will abandon the tiling language and adopt the matching one. Typically, if the set G' does admit matchings (an obvious necessary condition is that its cardinality is even) and its area is large, the number $Z(G')$ of matchings grows like the exponential of a constant times its area. This is for instance the case when $G' = \{1, \dots, 2L\} \times \{1, \dots, 2L\}$, in which case $(1/L^2) \log Z(G') \sim 4K/\pi$, where $K \approx 0.916$ is Catalan's constant [Kas61, TF61].

A natural way to uniformly sample one among so many matchings (even if computationally not the most efficient, see Section 3.1.1) is to run a Markov chain where, with unit rate, two vertical dimers belonging to the same square face of $\mathbb{Z}^2 \cap G'$ are flipped to vertical, or vice-versa. The unique stationary (and reversible) measure is the uniform measure over all matchings of G' and a classical question in theoretical computer science [LRS01, LPW08, Wil04] is to evaluate how quickly the Markov chain reaches equilibrium, as a function of the diameter (call it L) of G'. This is measured for instance via the so-called total-variation mixing time T_{mix}, defined as the first time t such that, uniformly in the initial condition, the law of the chain at time t is within variation distance $1/(2e)$ from equilibrium (see Section 3.3 for a definition in formulas).

In the present work we prove that $T_{\text{mix}} = L^{2+o(1)}$, under a non-trivial restriction ("almost-planar boundary height" condition) on the shape of the region G', that we briefly introduce now. The lattice $\mathbb{Z}^2$ being a bipartite graph, it is possible to associate in a canonical way (see Section 3.2.1) a

discrete height function (defined on faces of G') to each matching of G'. The height along the boundary $\partial G'$ of G' is instead independent of the matching and depends only on the shape of G'. We say that *the boundary height of G' is "almost planar"* if the graph of the height function, restricted to $\partial G'$, is within distance of order 1 from some plane of $\mathbb{R}^3$. In this case, for L large the height function of a typical matching of G' (sampled from the uniform measure) is macroscopically planar not only along $\partial G'$ but also in the interior of G' (see Theorem 3.2.9).

The almost-planar boundary height hypothesis is verified for instance when G' is the $2L \times 2L$ square as above. More general domain shapes that verify this hypothesis are introduced in [Ken00] ("Temperley boundary conditions") and in that case the height function fluctuations are proven to converge to the Gaussian Free Field [Ken00, Ken01].

Our main result can be informally stated as follows (see Sections 3.2.1 and 3.3 for a precise statement of the hypothesis and of the result):

Theorem 3.1.1. *If the diameter of G' is L and the boundary height is almost planar then, as L goes to infinity,*

$$cL^2 \leq T_{\text{mix}} \leq L^{2+o(1)}. \tag{3.3}$$

The result holds also when $\mathbb{Z}^2$ is replaced by the hexagon or square-hexagon lattices of Fig. 3.1.

Based on the "mean curvature motion" heuristics mentioned above, we conjecture the true behavior to be $T_{\text{mix}} \sim const \times L^2 \log L$ for reasonably regular domains G'. The same conjecture was formulated in [Wil04, Section 5.6].

As we explain in Section 3.5.1, there are good reasons why we cannot consider general bipartite periodic planar graphs (for instance, why our method necessarily fails for the square-octagon graph of Fig. 3.1). This is related to the existence for such graphs of so-called "gaseous phases" in their phase diagram [KOS06]. In a gaseous phase, the height function looks qualitatively like a $(2+1)$-dimensional low temperature Solid-on-Solid interface (the interface is rigid, height fluctuations have bounded variance and their spatial correlations decay exponentially. In the scaling limit, the interface does not behave like the Gaussian Free Field in this case).

Review of previous results

The first mathematical result we are aware of on this problem is in [LRS01], where dynamics of perfect matchings of either $\mathbb{Z}^2$ or $\mathcal{H}$ are studied. There, the authors introduced and analyzed a non-local Markov dynamics whose updates can involve an unbounded number of dimer rotations (cf. Section 3.4.2). Via a coupling argument, they managed to prove that the mixing

time $T^{\star}_{\text{mix}}$ of such dynamics is $T^{\star}_{\text{mix}} \leqslant const \times L^6$ (no lower bound was given). Subsequently, in the case of the hexagonal lattice $\mathcal{H}$ this result was sharpened to $c_1 L^2 \log L \leqslant T^{\star}_{\text{mix}} \leqslant c_2 L^2 \log L$ by Wilson [Wil04]. Via the application of comparison arguments for Markov chains, these upper bounds for $T^{\star}_{\text{mix}}$ imply polynomial upper bounds on the mixing time T_{mix} of the local Glauber dynamics: indeed, it was deduced in [RT00] that $T_{\text{mix}} \leqslant L^C$ for some finite C. In this case, in the theoretical computer science language, the Markov chain is said to be "rapidly mixing" (slow mixing would correspond to T_{mix} being super-polynomial in L). In the particular case of the hexagonal lattice, using results of [Wil04] on the spectral gap of the non-local dynamics and the comparison arguments of [RT00], one obtains $T_{\text{mix}} \leqslant const \times L^6$. In [Wil04] computations are worked out for the hexagonal lattice (lozenge tilings) but it is claimed there that the method can be extended also to domino tilings.

The results we mentioned so far do not require any restriction on the boundary height. If instead one assumes the boundary height to be almost-planar, for the hexagonal lattice the upper bound in (3.3) was proven in [CMT12] (in the stronger form $T_{\text{mix}} = O(L^2(\log L)^{12})$), while the best known lower bound was $T_{\text{mix}} \geqslant L^2/(c \log L)$ (based on [CMST10]). We are not aware of previous results for the square-hexagon lattice.

Remark 3.1.2. *The main reason why in Theorem 3.1.1 we require the boundary conditions to be almost-planar is that in this case the height fluctuations at equilibrium (i.e. under the uniform measure) are well-controlled, see Theorems 3.2.8 and 3.2.9. In the case of general boundary conditions, only partial results are known (e.g. [Pet12b, Ken07]) and these are not sufficient to implement our scheme. We emphasize that instead the $T_{\text{mix}} = O(L^C)$ result of [LRS01] does not require boundary conditions to be almost-planar.*

Alternative ways of quickly sampling random perfect matchings

There are several known algorithms that sample uniform perfect matchings. The main reason why we focus on the Glauber algorithm is its above-mentioned connection with the three-dimensional zero temperature Ising dynamics and with interface motion in non-equilibrium statistical mechanics. However, there are more efficient algorithms in terms of running time.

Let us first of all observe that in algorithmic terms, our Theorem 3.1.1 says that the running time of the Glauber dynamics with almost-planar boundary conditions is $L^{4+o(1)}$, i.e. it requires at most that many updates to approach the uniform measure (our Markov chain was defined in continuous time, so that there are of order L^2 elementary updates per unit time). There are at least two families of more efficient methods to sample random perfect matchings.

In [MS06] (see also [Wil97]) it is proven that one can sample uniform perfect matchings of planar graphs G' in a time $O(L^{\omega})$, where $\omega \leq 2.376$

(matrix multiplication exponent) is the exponent of the running time of the best known algorithm to multiply two $L \times L$ matrices. In [MS06, Wil97] there is essentially no restriction on the domain G' (i.e. no assumption on the boundary height), apart from obviously requiring that the number of vertices is of order L^2. This algorithm can even be used to find a maximum matching for domains that do not admit perfect matchings. The starting point is a classical formula, the analog of the one in Theorem 3.2.4 but for finite domains, that expresses the probability of local dimer events in terms of minors of the adjacency matrix of the graph. In the proof of the $O(L^\omega)$ bound then [MS06] cleverly uses the planarity of the graph and the fact that the adjacency matrix is sparse, to efficiently compute the minors.

The second class of algorithms is based on the mapping between perfect matchings of G' and spanning trees of a related graph (T-graph) that has approximately the same size [KPW00, KS04]. Then one can sample a spanning tree using algorithms based on random walks [Wil96], whose running time is expressed in terms of the mean hitting time of the random walk. For reasonable domains (boundary heights) one can deduce a $O(L^2 \log L)$ bound on the algorithm running time. In the general case the same bound should still hold but it seems delicate to precisely estimate the mean hitting time in complete generality.

See also [Pro03] for algorithms to sample generalized domino shufflings.

3.1.2 Sketch of the proof and novelty

Here we briefly sketch how the proof of Theorem 3.1.1 works, and we point out the main novelties, especially with respect to [LRS01, Wil04, CMT12].

The idea of [CMT12] (see also [CMST10]) is to break the proof of the upper bound $T_{\text{mix}} \leqslant L^{2+o(1)}$ into two steps:

(i) first prove that $T_{\text{mix}} \leqslant c(\epsilon)L^{2+\epsilon}$ when the height function is constrained for all times between a "floor" and a "ceiling" that are at small mutual distance, say $L^{\epsilon/10}$. Here ϵ is an arbitrarily small, positive, L-independent constant;

(ii) then, via an iterative procedure that mimics the mean curvature motion that should emerge in the diffusive limit, deduce $T_{\text{mix}} \leqslant c(\epsilon)L^{2+\epsilon}$ for the unconstrained dynamics.

While this general scheme is robust and will be employed also here, step (i) is very much model-dependent. In particular, in [CMST10, CMT12] for the hexagonal graph $\mathcal{H}$ its implementation was based on the crucial observation (by D. Wilson [Wil04]) that, for the non-local dynamics introduced in [LRS01] (cf. Section 3.4.2), one can write explicitly an eigenfunction of the generator, and the evolution of the height function is controlled by the discrete heat equation. As we explain in Remark 3.4.12, this fact fails for graphs other than $\mathcal{H}$ and it has to be replaced by a more robust argument.

The "more robust argument" starts from the observation that, under the non-local dynamics, the mutual volume V_t between two evolving height functions, that can be seen as an integer-valued random walk, is on average non-increasing with time t. This was already realized in [LRS01], but without any further input this only implies a polynomial upper bound $O(L^{4+\epsilon})$ on the mixing time $T^{\star}_{\mathrm{mix}}$ of the non-local dynamics. The argument is as follows. The maximal volume between two configurations in a region of diameter L, constrained between floor and ceiling at mutual distance $L^{\epsilon/10}$, is of order $L^{2+\epsilon/10}$. The random walk V_t has non-positive drift and it is not hard to see that the variance increase $\lim_{\delta \searrow 0} \frac{1}{\delta}\mathbb{E}[(V_{t+\delta} - V_t)^2 | \mathcal{F}_t]$ is bounded away from zero as long as $V_t \neq 0$, where $\mathcal{F}_t$ is the sigma-algebra generated by the non-local dynamics up to time t. A simple martingale argument (see Lemma 3.5.2) implies then that V_t will hit the value 0 in a time of order $(L^{2+\epsilon/10})^2 \leqslant L^{4+\epsilon}$. When the volume is zero, the two configurations have coalesced and a simple coupling argument allows us to conclude that $T^{\star}_{\mathrm{mix}} \leqslant L^{4+\epsilon}$. The new input we provide for the proof of point (i) (see Section 3.5.1) is that $\lim_{\delta \searrow 0} \frac{1}{\delta}\mathbb{E}[(V_{t+\delta} - V_t)^2 | \mathcal{F}_t]$ can be *lower bounded* essentially by V_t itself: then, an iterative application of Lemma 3.5.2 allows to conclude that the coalescence time for the non-local dynamics is of the (essentially optimal) order $L^{2+\epsilon/2}$ and not $L^{4+\epsilon}$. Via a comparison argument that relates the mixing times for the local and non-local dynamics (Proposition 3.4.9) one finally deduces $T_{\mathrm{mix}} = O(L^{2+\epsilon})$ for the *local* dynamics (always constrained between "floor" and "ceiling" at distance $L^{\epsilon/10}$).

To prove the bounds on drift and variance of V_t, we introduce a mapping between perfect matchings and configurations of what we call a "bead model". This mapping turns out to be convenient in that it makes the proofs visually clear. In particular, the definition of the non-local dynamics looks somewhat more natural in this language than in the "non-intersecting-path" language [LRS01]. For the hexagonal lattice, the mapping was already used in the past literature, for instance by Propp.

A last comment concerns the mixing time lower bound in Theorem 3.1.1, which is better (by a factor $\log L$) than the lower bound $T_{\mathrm{mix}} \geqslant C\, L^2/\log L$ found in [CMT12] and based on an idea developed in [CMST10]. First of all, the proof of [CMST10] would not extend for instance to $G = \mathbb{Z}^2$, again because it is based on Wilson's eigenfunction argument that fails there. Moreover, even for $G = \mathcal{H}$ where Wilson's argument does work, removing the $\log L$ in the denominator involves a genuinely new idea, see Section 3.5.2: one needs to prove that the drift of the volume V_t under the non-local dynamics, which as we mentioned is non-positive, is not smaller than the size of the boundary of G', times some negative constant.

3.1.3 Organization of the paper

All the definitions and results the reader needs about perfect matchings, height functions and translation-invariant infinite measures of a given slope are in Section 3.2 (results are given for general periodic bipartite planar graphs and not just for the square, hexagon and square-hexagon graphs). The dynamics is precisely defined in Section 3.3 and its monotonicity properties are discussed in Section 3.3.1. In Section 3.4.1 we map height functions into the configurations of a "bead model". In Section 3.4.2 we rewrite the dynamics in terms of beads and we introduce two auxiliary, spatially non-local, dynamics, that are essential in proving the mixing time estimates of Theorem 3.1.1: the mixing time upper bound is proven in Section 3.5.1 and the lower bound in Section 3.5.2.

3.2 Some background on perfect matchings

3.2.1 Dimer coverings, height functions and uniform measures

We follow the notations of [KOS06]. Let $G = (V, E)$ be an infinite, $\mathbb{Z}^2$-periodic, bipartite planar graph. "Bipartite" means that its vertices can be colored black or white in such a way that white vertices have only black neighbors and vice-versa. $\mathbb{Z}^2$-Periodicity means that G can be embedded in the plane in such a way that $\mathbb{Z}^2$ acts as a color-preserving isomorphism. The dual graph of G, whose vertices are the faces f of G, is denoted G^*.

We let G_1 (the fundamental domain) denote $G/\mathbb{Z}^2$, which is a finite and periodic bipartite graph, embedded on the two-dimensional torus. See Fig. 3.1 for some classical examples (the square, hexagon, square-octagon and square-hexagon lattice) together with their fundamental domains.

Note that there is a certain degree of arbitrariness in the embedding of G in the plane and as a consequence a certain arbitrariness in the choice of the fundamental domain. For instance, in Fig. 3.1 the fundamental domain of $\mathbb{Z}^2$ contains two sites, but with a different embedding it could contain the four sites around a face (in this case the two axes of $\mathbb{Z}^2$ would be horizontal and vertical). In general, it is convenient to work with the smallest possible fundamental domain, as in Fig. 3.1.

A perfect matching of G is a subset of edges, $M \subset E$, such that each vertex of G is contained in one and exactly one edge in M. It is known that G admits a matching (which is implicitly assumed from now on) if and only if G_1 does, and Fig. 3.1 shows that the fundamental domains of the four graphs we mentioned do admit several matchings. We denote Ω the set of matchings of G.

Assumption 1. *To avoid trivialities, we will assume that for every edge e of G there exists $M \in \Omega$ such that $e \in M$ and $M' \in \Omega$ such that $e \notin M'$ (one*

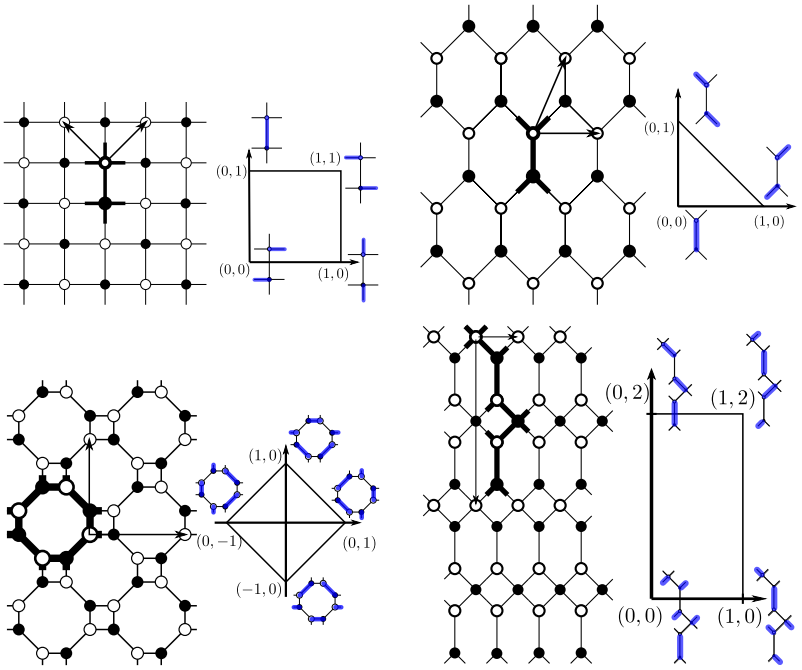

Figure 3.1: Some examples of $\mathbb{Z}^2$-periodic bipartite graphs (square, hexagon, square-octagon, square-hexagon) and their Newton polygons (cf. Theorem 3.2.3). The fundamental domain is indicated with thicker lines in the graph while the action of $\mathbb{Z}^2$ is represented by two arrows. Near each vertex of the Newton polygon is indicated the associated matching of the fundamental domain.

can easily construct pathological examples where this fails, but the edges in question can be simply removed and the matching problem is unchanged).

We will often refer to paths on the dual graph G^*:

Definition 3.2.1. *A path γ on G^* is a possibly infinite sequence $(\dots, f_{-1}, f_0, f_1, \dots)$ of faces of G, such that f_i is a neighbor of f_{i+1}. An infinite path γ is called periodic if there exists a finite path γ_0 and $v \in \mathbb{Z}^2$ such that γ is the concatenation of $\{T_{nv}\gamma_0\}_{n\in\mathbb{Z}}$, with T_v the translation by v.*

Height function and uniform measure

A flux is a function on the oriented edges of G, which is antisymmetric under the change of orientation of the edges. To each $M \in \Omega$ is associated a flux ω_M: edges contained in M carry unit flux, oriented from the white to the black vertex. Edges not contained in M carry zero flux. Note that the divergence of ω_M is 1 at white vertices and -1 at black vertices.

Fix now a reference matching M_0 (typically, a $\mathbb{Z}^2$-periodic matching, but the following definition would work for any flux of divergence $+1/-1$ at

white/black vertices). M_0 allows to associate to M a height function h_M on G^*, as follows. Fix some face $f_0 \in G^*$ ("the origin") and set $h_M(f_0)$ to some value, say 0. For every $f \neq f_0$, let γ be a path on G^* starting at f_0 and ending at f. Then, $h_M(f) - h_M(f_0)$ is the total flux of $\omega_M - \omega_{M_0}$ (say from right to left) across γ. Note that h_M does not depend on the choice of the path (because $\omega_M - \omega_{M_0}$ has zero divergence) and that the height difference between two matchings M, M' is independent of the choice of the reference matching M_0.

In the following, the set of perfect matchings Ω will denote equivalently the set of all admissible height functions (it is understood that M_0 and f_0 are fixed). For lightness of notation, we will often write h instead of h_M.

Definition 3.2.2. *Let U be a simply connected open subset set of $[-1/2, 1/2]^2$, $L > 0$ and $U_L = L\,U$. We let G' be the finite subset of G obtained by keeping all the vertices and edges belonging to faces which are entirely contained in U_L.*

Given $m \in \Omega$ (called the "boundary condition", with corresponding height function h_m) and $G' = (E', V')$ as in Definition 3.2.2, let

$$\Omega_{m,G'} = \left\{ M \in \Omega : M|_{G \setminus G'} = m|_{G \setminus G'} \right\} \tag{3.4}$$

be the finite collection of matchings that coincide with m outside of G'. Equivalently, we can identify $\Omega_{m,G'}$ as the set of height functions that coincide with h_m except on the faces of G'. We will implicitly assume (without loss of generality) that the reference face f_0 is *not* one of the faces of G'. Clearly, $\Omega_{m,G'}$ is non-empty (it includes at least m) and we will let $\pi_{m,G'}$ denote the uniform measure over $\Omega_{m,G'}$.

3.2.2 Pure phases

In this section we review known results about measures on the infinite graph G whose typical height functions are close to a plane. First we will identify the set of "natural" measures of fixed average slope, then give a classification into three "phases" with very different correlation properties, and finally give their "microscopic" behavior, i.e. the probabilities of events depending on a finite subset of edges. Most results come from [KOS06].

Ergodic Gibbs measure of fixed slope

Fix a reference matching M_0 assumed to be $\mathbb{Z}^2$-periodic. A measure μ on Ω is said to have slope (s, t) if its expected height function is a linear function, with slope (s, t): for all faces f, if f' denotes the translate of f by $(x, y) \in \mathbb{Z}^2$, then $\mu[h(f') - h(f)] = sx + ty$. μ is said to be a Gibbs measure if its conditional distributions on finite sub-graphs are uniform,

$\mu(\cdot|M \in \Omega_{m,G'}) = \pi_{m,G'}(\cdot)$ (*DLR property*). It is ergodic if it is not a linear combination of other Gibbs measures. Ergodic Gibbs measures of fixed slope can be thought of as the natural uniform measures on matchings of G conditioned on their average slopes. The following theorem due to Sheffield [She05] classifies all of them :

Theorem 3.2.3. *There exists a closed, convex polygon N in $\mathbb{R}^2$ such that, for all (s,t) in its interior $\mathring{N}$, there exists a unique ergodic Gibbs measure $\mu_{s,t}$ of slope (s,t). The vertices of N are determined by the slopes of some $\mathbb{Z}^2$-periodic matchings of G (i.e. matchings of the fundamental domain) and thus are integer points. For $(s,t) \in \partial N := N \setminus \mathring{N}$, there exists an ergodic Gibbs measure but it may not be unique.*

N is called the Newton polygon, see Fig. 3.1.

Phase classification

As proved in [KOS06], ergodic Gibbs measures come in three possible phases: solid, liquid and gas, depending on the position of (s,t) in N.

- Solid phases correspond to slopes in ∂N. For any side ℓ of ∂N, there exists at least one infinite periodic path γ on G^* (cf. Definition 3.2.1) such that the configuration of the edges crossed by γ (or by any of its translates) is deterministic and is the same for all measures with slope $(s,t) \in \ell$. The path γ is said to be frozen.

  The asymptotic direction of γ is determined as follows. All the planes with slope in ℓ and containing the origin of $\mathbb{R}^3$ intersect in a straight line. The direction of this line, when projected on the (x,y) plane, is the direction of γ.

  At a vertex of the Newton polygon, which is the intersection of two sides of ∂N, there are two families of frozen paths with different directions, which form so to speak a grid on G^*. The components of the complement of the frozen paths are finite sets of faces. Heights are clearly independent in two distinct components, and the fluctuations of the height difference between two faces f_1, f_2 are bounded deterministically and uniformly in the distance between them.

- Liquid phases correspond to generic points of $\mathring{N}$. In these phases, heights fluctuations behave like a Gaussian free field in the plane. In particular the variance of the height difference between f_1 and f_2 grows like $1/\pi$ times the logarithm of the distance, while edge correlations decay slowly (as the inverse of the square of the distance). Liquid phases are discussed in finer detail in the next section.

- Gaseous phases have exponentially decreasing edge correlations; the height difference fluctuations are not deterministically bounded, but

their variance is bounded, uniformly with the distance of the faces. Gaseous phases may (but do not necessarily) occur when the slope (s,t) is an integer point in $\mathring{\mathrm{N}}$. The condition for the occurrence of a gaseous phase at an integer slope $(s,t) \in \mathring{\mathrm{N}}$ is discussed in Section 3.2.3.

In the example of Fig. 3.1, only the square-octagon graph has a gaseous phase which has slope $(0,0)$.

Edge probabilities

When $(s,t) \in \mathring{\mathrm{N}}$ (i.e. for liquid and gaseous phases) there is an explicit expression of edge probabilities under $\mu_{s,t}$.

Theorem 3.2.4. *[KOS06] Fix $(s,t) \in \mathring{N}$. There exists an infinite periodic matrix $K_{s,t} = \{K_{s,t}(\mathrm{w},\mathrm{b})\}_{\mathrm{w},\mathrm{b}}$ with* b *(resp.* w*) ranging on black (resp. white) vertices of G and an infinite periodic matrix $K_{s,t}^{-1} = \{K_{s,t}^{-1}(\mathrm{b},\mathrm{w})\}_{\mathrm{w},\mathrm{b}}$ satisfying $K_{s,t}K_{s,t}^{-1} = Id$ such that, for any finite subset $\{e_1 = (\mathrm{w}_1,\mathrm{b}_1),\dots,e_l = (\mathrm{w}_l,\mathrm{b}_l)\}$ of edges of G, the $\mu_{s,t}$-probability of seeing all of them occupied is:*

$$\mu_{s,t}(e_1 \in M,\dots,e_l \in M) = \left(\prod_{j=1}^{l} K_{s,t}(\mathrm{w}_j,\mathrm{b}_j)\right) \det\left(K_{s,t}^{-1}(\mathrm{b}_k,\mathrm{w}_i)\right)_{1\le i,k\le l}.$$

$K_{s,t}$ is called a Kasteleyn matrix. It is a weighted and signed version of the adjacency matrix, so in particular $K_{s,t}(\mathrm{w},\mathrm{b})$ can be non-zero only if (b,w) is an edge of G. The signs (which are independent of the slope (s,t)) are chosen so that their product around any face f is -1 if f has $0 \bmod 4$ sides and $+1$ if it has $2 \bmod 4$ sides. We will not need to specify the explicit choice of signs, see [KOS06]. Periodicity means that $K_{s,t}(\mathrm{w}+(x,y),\mathrm{b}+(x,y)) = K_{s,t}(\mathrm{w},\mathrm{b})$ for every $(x,y) \in \mathbb{Z}^2$, and similarly for $K_{s,t}^{-1}$.

Given $K_{s,t}$ and two complex numbers w,z, we define a *finite* matrix $\mathbf{K}_{s,t}(z,w)$ from white to black vertices of the fundamental domain G_1, as follows. Consider G_1 as a weighted periodic bipartite graph on the torus, where the weight of an edge is the one induced by $K_{s,t}$, and note that it can contain multiple edges between two vertices, even if the infinite graph G does not (see e.g. Fig. 3.1). Consider a path γ_x (resp. γ_y) winding once horizontally (resp. vertically) along the torus and multiply by z (resp. $1/z$) the weight of each edge crossed by γ_x with the black vertex on the left (resp. on the right) and similarly by $w, 1/w$ the edges crossed by γ_y. Then, $\mathbf{K}_{s,t}(z,w)$ is the adjacency matrix of G_1, with these modified weights. With the usual graph theory convention, this means that the (w,b) element of $\mathbf{K}_{s,t}(z,w)$ (with w (resp. b) a white (resp. black) vertex of G_1) is the sum of the weights of the edges joining w to b. Let $Q_{s,t}(z,w)$ (a matrix from black to white vertices of G_1) be the adjugate matrix of $\mathbf{K}_{s,t}(z,w)$ so that

$[Q_{s,t}\mathbf{K}_{s,t}](z,w) = P(z,w)\mathrm{Id}$ where $P(z,w) = \det(\mathbf{K}_{s,t}(z,w))$. The (b,w) element of $Q_{s,t}(z,w)$ is denoted $Q_{s,t}^{\mathrm{b},\mathrm{w}}(z,w)$.

We can now give a formula for the inverse infinite Kasteleyn matrix $K_{s,t}^{-1}$:

Theorem 3.2.5. *[KOS06] Let* b *and* w *be a black and a white vertex in* G_1*. The following holds for* $(x,y) \in \mathbb{Z}^2$*:*

$$K_{s,t}^{-1}(\mathrm{b},\mathrm{w}+(x,y)) = \frac{1}{(2i\pi)^2}\int_{\mathbb{T}^2} \frac{Q_{s,t}^{\mathrm{b},\mathrm{w}}(z,w)}{P_{s,t}(z,w)} w^x z^y \frac{\mathrm{d}w}{w}\frac{\mathrm{d}z}{z}$$

where $\mathbb{T}^2 = \{z,w \in \mathbb{C}^2, |z| = |w| = 1\}$ *is the unit complex torus.*

Here, to avoid confusion, it can be useful to emphasize that $\frac{Q_{s,t}}{P_{s,t}}(z,w)$ is the inverse of the finite matrix $\mathbf{K}_{s,t}(z,w)$, while $K_{s,t}^{-1}$ is an inverse of the infinite matrix $K_{s,t}$, with no dependence on z,w (i.e. with the original edge weights).

3.2.3 Asymptotics of $K_{s,t}^{-1}$ and Gaussian fluctuations in the "liquid phase"

It is shown in [KOS06] that, for an integer slope $(s,t) \in \mathring{\mathrm{N}} \cap \mathbb{Z}^2$, the Laurent polynomial $P_{s,t}$ has either no zeros on the unit torus (in which case $\mu_{s,t}$ corresponds to a gaseous phase) or has a unique zero of order two (which corresponds to a liquid phase). For any non-integer slopes in $\mathring{\mathrm{N}} \setminus \mathbb{Z}^2$, instead, $P_{s,t}$ has exactly two conjugate simple zeros. In this case Theorem 3.2.6 gives the asymptotics of $K_{s,t}^{-1}(\mathrm{b},\mathrm{w})$ when the two vertices b,w are far apart. We emphasize that in our applications (i.e. in the proof of Theorem 3.2.8), we will have to consider only cases where the Newton polygon has no integer points in its interior.

Theorem 3.2.6. *[KOS06] Fix* (s,t) *a non-integer slope in* $\mathring{N}$*, so that* $P_{s,t}$ *has two simple zeros* (z_0,w_0) *and* $(\bar{z}_0,\bar{w}_0)$ *on* $\mathbb{T}^2$*. Let* $\alpha = \frac{\partial}{\partial z}P_{s,t}(z_0,w_0)$ *and* $\beta = \frac{\partial}{\partial w}P_{s,t}(z_0,w_0)$ *and define* $\phi(x,y) = x\alpha z_0 - y\beta w_0$*. Then the map* $\phi : \mathbb{R}^2 \mapsto \mathbb{C}$ *is invertible, the matrix* $Q_{s,t}(z_0,w_0)$ *is of rank* 1 *and can be written as* $U_{s,t}V_{s,t}^T$ *where the column vector* $U_{s,t}$ *(resp.* $V_{s,t}$*) is indexed by the black (resp. white) vertices of* G_1*. Moreover, we have*

$$K_{s,t}^{-1}(\mathrm{b},\mathrm{w}+(x,y)) = -\Im\left(\frac{w_0^x z_0^y U_{s,t}(\mathrm{b})V_{s,t}(\mathrm{w})}{\pi\phi(x,y)}\right) + O\left(\frac{1}{x^2+y^2}\right) \qquad (3.5)$$

where $O((x^2+y^2)^{-1})$ *has to be understood as* $\frac{h(x,y)}{x^2+y^2+1}$ *with* h *bounded on* $\mathbb{Z}^2$ *and* $\Im(z)$ *denotes the imaginary part of* z*.*

Remark 3.2.7. *The invertibility of* ϕ *is a consequence of the fact that* αz_0 *is not collinear with* βw_0*. This is not proved explicitly in [KOS06] but the*

argument is simple: Both the torus $\mathbb{T}^2$ *and* $P_{s,t}^{-1}(\{0\})$*, the set of zeros of* $P_{s,t}$*, are two-dimensional manifolds in* $\mathbb{C}^2$ *which contain* (z_0, w_0)*. The tangent space of* $\mathbb{T}^2$ *at* (z_0, w_0) *is given by*

$$p_1 = \{a(iz_0, 0) + b(0, iw_0) + (z_0, w_0), (a, b) \in \mathbb{R}^2\}$$

and the tangent space of $P_{s,t}^{-1}(\{0\})$ *is*

$$p_2 = \{\zeta(\beta, -\alpha) + (z_0, w_0), \zeta \in \mathbb{C}\}.$$

Since (z_0, w_0) *is a simple zero of* $P_{s,t}$ *seen as a function on* $\mathbb{T}^2$*, one necessarily has* $p_1 \cap p_2 = \{(z_0, w_0)\}$ *and it is easy to check that this fails if* $\alpha z_0 = \lambda \beta w_0$ *with* $\lambda \in \mathbb{R}$*.*

The asymptotic expression (3.5) is the main tool for the following result, that is proven in Appendix 3.A:

Theorem 3.2.8. *Fix a non-integer slope* $(s, t) \in \mathring{N}$ *and* $g \in G^*$*. Under the Gibbs measure* $\mu_{s,t}$*, the moments of the variable*

$$\frac{h(f) - h(g) - (\mu_{s,t}(h(f)) - \mu_{s,t}(h(g)))}{\sqrt{\mathrm{Var}_{\mu_{s,t}}(h(f) - h(g))}} \tag{3.6}$$

tend as $|\phi(f) - \phi(g)| \to \infty$ *to those of a standard Gaussian* $\mathcal{N}(0, 1)$*. Furthermore*

$$\mathrm{Var}_{\mu_{s,t}}(h(f) - h(g)) \sim \frac{1}{\pi^2} \log|\phi(f) - \phi(g)| \tag{3.7}$$

Here and later, when we write $\phi(f)$ we mean $\phi(x, y)$ if f is the (x, y) translate of a face in the fundamental domain G_1. The fact that the variance of $h(f) - h(g)$ behaves like $(1/\pi^2) \log|\phi(f) - \phi(g)|$ is proved in [KOS06].

For the hexagonal lattice and under the assumption that f and f_0 are along the same column of hexagons, convergence of the moments is proven in [Ken09]. The general case is qualitatively more difficult and requires nontrivial work (see the discussion at the beginning of Appendix 3.A; our proof uses ideas from [Ken07, Sec. 7] but the setting here is more general and we give a more explicit control of the "error terms").

3.2.4 Almost-planar boundary conditions

A central role will be played by "almost planar" boundary conditions.

We say that $h \in \Omega$ is an almost-planar height function with slope $(s, t) \in \mathring{\mathrm{N}}$ if there exists C such that, for every $f \in G^*$,

$$|h(f) - \mu_{s,t}(h(f))| \leqslant C. \tag{3.8}$$

We will sketch briefly in Section 3.2.5 a proof that almost-planar boundary conditions actually exist for every $(s, t) \in \mathring{\mathrm{N}}$ (even with $C = 1$).

Theorem 3.2.8 implies the following:

Theorem 3.2.9. *Fix a non-integer slope $(s,t) \in \mathring{N}$ and let m be an almost-planar boundary condition with slope (s,t). Let the finite graph G' be as in Definition 3.2.2. One has for every $\varepsilon > 0$ and $n > 0$:*

$$\pi_{m,G'}(\exists f \in G^* : |h(f) - \mu_{s,t}(h(f))| \geqslant L^{\varepsilon}) = O(L^{-n}). \tag{3.9}$$

Remark 3.2.10. *The maximal equilibrium height fluctuation with respect to the average height should be of order* $\log L$ *with high probability, but we will not need such a refined result.*

Proof of Theorem 3.2.9 given Theorem 3.2.8. For the hexagonal lattice this is given in detail in [CMST10] (see Proposition 4 there). For general graphs the proof is almost identical and we recall just the basic principle.

By monotonicity (see Section 3.3.1), the event $E_f = \{h(f) - \mu_{s,t}(h(f)) \geqslant L^{\varepsilon}\}$ is more likely if we change the boundary condition for a higher one, i.e. if we replace m with m' such that $h_{m'}(f') \geqslant h_m(f')$ for every face $f' \notin (G')^*$ adjacent to some face in $(G')^*$ (this set of faces is denoted here $\partial G'$, and $(G')^*$ is the collection of faces of G'). Assume without loss of generality that the reference face f_0 where heights functions are fixed to zero belongs to $\partial G'$. Then choose a *random* boundary condition m' from the measure $\mu_{s,t}$, and this time fix its height at the reference face as $h_{m'}(f_0) = h_m(f_0) + L^{\varepsilon}/2 = L^{\varepsilon}/2$. Thanks to Theorem 3.2.8, one has $h_{m'} \geqslant h_m$ on $\partial G'$, except with probability $O(L^{-n})$ for any given n. Finally, with such random boundary condition, by the DLR property the probability of E_f is nothing but $\mu_{s,t}(h(f) - \mu_{s,t}(h(f)) \geqslant L^{\varepsilon}/2)$, which is also $O(L^{-n})$, again thanks to Theorem 3.2.8. □

3.2.5 Perfect matchings, capacities and maximal configurations

Linear characterization of height functions

The set of height functions corresponding to a perfect matching of a finite subset of G can be characterized by linear inequalities as follows.

Consider as in Definition 3.2.2 a finite sub-graph G' of G and a boundary condition $m \in \Omega$. In this subsection we will use m (even if it is not necessarily periodic) as reference matching for the definition of height functions. For any two neighboring faces f, f' with a common edge e oriented positively (i.e. such that going from f to f' one crosses e leaving the white vertex on the right), let the oriented capacities $d(f,f')$ and $d(f',f)$ be defined as follows:

$$d(f,f') = \begin{cases} 0 \text{ if } e \notin G' \\ 0 \text{ if } e \in G' \text{ and } e \in m \\ 1 \text{ if } e \in G' \text{ and } e \notin m; \end{cases} \qquad d(f',f) = \begin{cases} 0 \text{ if } e \notin G' \\ 1 \text{ if } e \in G' \text{ and } e \in m \\ 0 \text{ if } e \in G' \text{ and } e \notin m \end{cases} \tag{3.10}$$

Now for any pair of faces f, f' (not necessarily neighbors) let $D(f, f')$ be the *minimum* over all paths $f = f_1, \ldots, f_n = f'$ in G^* of the sum of the $d(f_i, f_{i+1})$ (the minimum is well defined, the capacities being non-negative).

Proposition 3.2.11. *An integer-valued function h on G^* is the height function (with reference matching m) of a matching in $\Omega_{m,G'}$ if and only if*

$$D(f, f') \geq h(f') - h(f) \text{ for every } f, f' \in G^*. \tag{3.11}$$

Proof. The proof is in the spirit of [Fou96, Theorem 1]. The "only if" part is trivial since, going back to Section 3.2.1, it is immediate to see that the *maximal* possible height difference $h(f') - h(f)$ between neighboring faces f, f', for any matching in $\Omega_{m,G'}$, does not exceed $d(f, f')$. As for the "if" part, remark first of all that, thanks to (3.11), for every neighboring faces f, f' one has $h(f) - h(f') \in \{-1, 0, 1\}$. Let us "mark" all edges $e \in G'$ between faces f, f' (with e oriented positively from f to f') such that $h(f') - h(f) = d(f, f')$, together with edges $e \in G \setminus G'$ such that $e \in m$. Let M be the union of all marked edges and let us prove it is a matching (note that, automatically, $M \equiv m$ outside of G'). For any white (resp. black) vertex v, let e_v be the unique edge incident to v which belongs to m. From (3.11) and considering paths that turn counterclockwise (resp. clockwise) around v, it is easy to see that:

- either all the faces f sharing vertex v have the same value of $h(f)$ and e_v is the single marked edge around v;
- or there exists a single marked edge $e'_v \neq e_v$, incident to v, such that $h(f') = h(f) - 1$, with f, f' neighboring faces sharing e'_v, such that v is on the left (resp. right) when going from f to f'.

M is thus a matching and by construction $M \equiv m$ outside G'. In conclusion, $M \in \Omega_{m,G'}$ and of course its height function is just h. □

Maximal and minimal configurations

The characterization of height functions provided by Proposition 3.2.11 shows the existence of a unique maximal (resp. minimal) height function h_{max} (resp. h_{min}) in $\Omega_{m,G'}$. "Maximal" means that for any other height function h in $\Omega_{m,G'}$ satisfying $h(f_0) = 0$ (recall from Section 3.2.2 that the height is fixed to zero at some face f_0 outside of G') one has $h(f) \leqslant h_{max}(f)$ for every $f \in G^*$. Indeed, define $h_{max}(f) := D(f_0, f)$ on G^*. This satisfies (3.11) (since $D(\cdot, \cdot)$ satisfies the triangular inequality) and maximality is a consequence of the fact that $d(f, f')$ is the maximal possible height difference between neighboring faces. Similarly, one has $h_{min}(f) = -D(f, f_0)$. Observe that the height functions h_{max}, h_{min} (with respect to the reference configuration m) vanish outside G' as they should (this is because the set of faces of G not belonging to G' is connected, recall Definition 3.2.2).

Free paths and possible rotations

Definition 3.2.12. *Fix a matching $M \in \Omega$. We say that an oriented path γ in G^* is a* free path *(relative to M) if all edges crossed by γ are free (i.e. not occupied) and have the same orientation (i.e. either all of them have their white vertex on the right of γ or all of them on the left). If white vertices are on the right (resp. left) then γ is called a positive (resp. negative) free path.*

See Fig. 3.2.

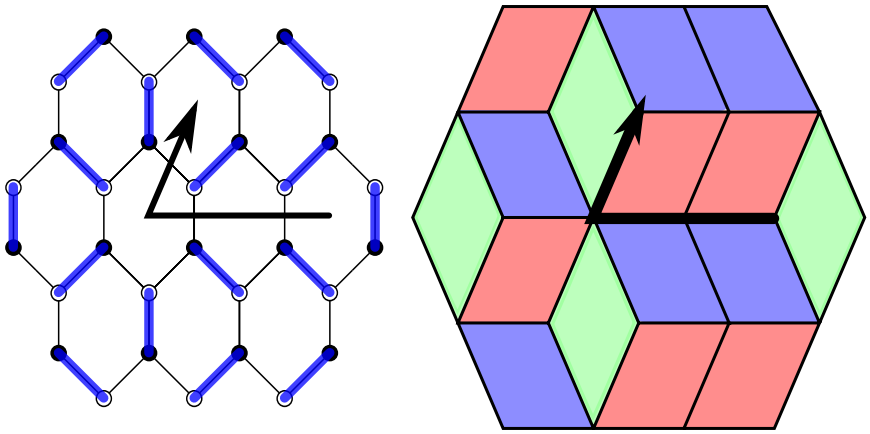

Figure 3.2: The relation between height function and dimer configuration in the case of the honeycomb graph. It is easy to see the right-hand drawing as a stepped surface in 3 dimensions. It should be clear from the right-hand drawing that the positive free path (thick line) moves away at constant speed from the $(1, 1, 1)$ plane; at its endpoint (marked by an arrow) the free path cannot be possibly continued, and a cube can be added there (i.e. a rotation can be performed in the left-hand drawing).

A first observation is that free paths cannot form loops:

Proposition 3.2.13. *Let γ be a free path relative to some $M \in \Omega$, and assume that γ forms a simple loop. Then, for every $M' \in \Omega$ the edges crossed by γ are free.*

Together with Assumption 1, this excludes loops.

Proof of Proposition 3.2.13. Let h be the height function of M', with reference matching M. Let f be a face along γ. By symmetry, suppose γ is a positive path. Since all edges are traversed with the positive orientation, we have

$$\begin{aligned} h(f) = h(f) &+ |\{\text{edges crossed by } \gamma \text{ and occupied in } M'\}| \\ &- |\{\text{edges crossed by } \gamma \text{ and occupied in } M\}|. \end{aligned}$$

Since γ crosses no occupied edge of M by assumption, it crosses no occupied edge of M' either. □

A second observation is that, since only the reference matching (however it is chosen) makes a contribution to the height difference along a free path γ, the height function is non-increasing (resp. non-decreasing) if γ is a positive (resp. negative) free path. An important consequence, that we will need in Section 3.4.2 to upper bound the equilibration time of the dynamics, is the following:

Proposition 3.2.14. *Fix $(s,t) \in \mathring{N}$. Let $M \in \Omega$ be such that the corresponding height function stays between two planes of slope (s,t) and mutual distance H. All free paths relative to M have length at most CH, where the constant C depends only on (s,t).*

Proof of Proposition 3.2.14. Since the graph G is periodic, there exists only a finite number k of types of faces that are not obtained by integer translation of each other. Let γ be a positive free path (if it is a negative free path, the argument is similar) relative to some matching M. We claim that,

$$\begin{gathered}\text{if one walks } n \text{ steps along } \gamma, \text{ the function } f \mapsto h(f) - \mu_{s,t}(h(f)) \\ \text{decreases by at least } -\lfloor n/k \rfloor \varepsilon \text{ for some } \varepsilon = \varepsilon_{s,t} > 0.\end{gathered} \tag{3.12}$$

Then, the proposition follows (with the constant C being inversely proportional to ε/k) because the function $\mu_{s,t}(h(\cdot))$ on G^* is essentially planar with slope (s,t).

To prove (3.12), observe first that the matching M gives no contribution to the variation of h along γ (all crossed edges are free) so that the variation of $h - \mu_{s,t}(h)$ is simply minus the $\mu_{s,t}$-average number of crossed edges which are covered by dimers. Fix some face $f \in \gamma$ and walk along γ until a face f' which is a translate of f is reached (the number of steps is at most k). The $\mu_{s,t}$-average of crossed dimers between f and f' is non-negative and we will actually prove that it is strictly positive and independent of the type of face f, which implies the claim. Indeed, let $\tilde{\gamma}$ be the infinite periodic path on G^* obtained by repeating periodically the finite portion of γ which joins f to f'. If the average of crossed edges is zero, then clearly the slope of the height under the measure $\mu_{s,t}$ along the asymptotic direction of $\tilde{\gamma}$ is extremal, which contradicts the assumption that (s,t) is in the interior of the Newton polygon N. Uniformity w.r.t. the type of the face f is just a consequence of the fact that the number of different face types is finite. □

For any face f of G, there exist exactly two ways to perfectly match its vertices among themselves. Label "+" one of the two matchings, and "−" the other (according to some arbitrary rule). If M is a matching of G such that the vertices of f are matched only among themselves, we call "rotation

around f" the transformation which consists in leaving M unchanged outside of f, and in flipping from "$-$" to "$+$" (or vice-versa) the matching of the edges of f. If some vertices of f are matched to vertices not belonging to f, then the rotation is not possible.

Free paths yield a way to find a face where an elementary rotation is possible. Given $M \in \Omega$, we pick an arbitrary face f_1 and we construct a growing sequence $\{\gamma_n\}_{n\geqslant 1} = \{(f_1, \dots, f_n)\}_{n\geqslant 1}$, of positive free paths, with $\gamma_1 \equiv (f_1)$ (an analogous construction gives a growing sequence of negative free paths). Given γ_n, consider all faces f which are neighbors of f_n and such that going from f_n to f one crosses a free edge with white vertex on the right. Choose f_{n+1} (according to some arbitrary rule) among such faces. If there are no such faces available, we say that the procedure stops at step n. In this case, it means that every second edge around f_n is occupied by a dimer, and this is exactly the condition so that a rotation at f_n is possible. Altogether, we have proven:

Proposition 3.2.15. *Fix $(s,t) \in \mathring{N}$. Let $M \in \Omega$ be such that the corresponding height function stays between two planes of slope (s,t) and mutual distance H. Within distance $C_{s,t}\, H$ from any face f there exists a face f^+ (resp. f^-) where a rotation is possible; such a rotation increases (resp. decreases) the height at f^+ (resp. f^-) by 1 and $h(f^+) \leq h(f) \leq h(f^-)$.*

Almost planar height functions

Here we prove that almost-planar height functions satisfying (3.8) with $C = 1$ do exist (under the assumption that $(s,t) \in \mathring{\mathrm{N}}$ is a non-integer slope). Indeed from Theorem 3.2.8 and Borel-Cantelli we get that, for every fixed $\delta > 0$, almost all configurations from $\mu_{s,t}$ satisfy

$$|h(f) - \mu_{s,t}(h(f))| \leqslant B + \delta |\phi(f) - \phi(f_0)| \tag{3.13}$$

for some random B, where f_0 is the face where the heights are fixed to zero. Take one of these configurations. Let A_n the set of faces at graph-distance at most n from f_0 and suppose that $h(f) - \mu_{s,t}(h(f)) < -1$ (the argument is similar if the difference is > 1) for some $f \in A_n$. The same argument that led to Proposition 3.2.14 shows that, if δ is chosen small enough (say much smaller than the constant $\varepsilon_{s,t}$ in (3.12)), any positive free path γ starting from f is of length $O(\delta n/\varepsilon_{s,t}) \leqslant n$ for n large enough. Therefore, the last face f' of γ is in A_{2n} and (by the properties of positive free paths) one has $h(f') - \mu_{s,t}(h(f')) < -1$. By Proposition 3.2.15, a rotation is possible at f' and it increases $h(f') - \mu_{s,t}(h(f'))$ by 1. The configuration thus obtained clearly still verifies (3.13) with the same B and the quantity

$$\Delta = \sum_{f \in A_{2n}} |h(f) - \mu_{s,t}(h(f))| \mathbf{1}_{|h(f) - \mu_{s,t}(h(f))| > 1}$$

decreased by 1. Since Δ is finite, the procedure can be repeated a finite number of times until there is no point left in A_n with $|h(f)-\mu_{s,t}(h(f))| > 1$. One concludes easily using the fact that n can be taken arbitrarily large. □

3.3 Dynamics and mixing time

The dynamics we consider lives on the set $\Omega_{m,G'}$ of matchings on a finite subset $G' \subset G$ (as in Definition 3.2.2) with boundary condition $m \in \Omega$. Every face f of G' has a mean-one, independent Poisson clock. When the clock at f rings, if the rotation around f is allowed, flip a fair coin: if "head" then choose the "+" matching of the edges of f, if "tail" then choose the "−" matching. In other words, perform the rotation around f with probability $1/2$.

Call μ_t^M the law of the dynamics at time t, started from M.

Proposition 3.3.1. *For $t \to \infty$, μ_t^M converges to the uniform measure $\pi_{m,G'}$.*

Proof. It is obvious that $\pi_{m,G'}$ is invariant and reversible, so one should only check that the dynamics connects all the configurations in $\Omega_{m,G'}$. This is done by using the free paths of Section 3.2.5.

Let $M \in \Omega_{m,G'}$ and let $M_{max} \in \Omega_{m,G'}$ be the matching corresponding to the maximal height function h_{max} introduced in Section 3.2.5. The height function h of M with reference matching M_{max} is clearly non-positive and vanishes outside G'. Pick a face f such as $h(f) \leqslant -1$ and consider a positive free path γ growing from f (as in the proof of Proposition 3.2.15). Along γ the height function h cannot grow and, G' being finite, γ has to stop after a finite number of steps. The last face f' of γ clearly is inside G' (since the height is zero outside) and we have already discussed that a rotation is possible at f' and it increases $h(f')$ by 1. By recursion, M can be transformed into M_{max} by a finite sequence of elementary rotations inside G'. Arbitrariness of M allows to conclude. □

As usual [LPW08], an informative way to quantify the speed of approach to equilibrium is via the mixing time, defined as

$$T_{\text{mix}} = T_{\text{mix}}(m, G') = \inf\{t > 0 : \max_{M \in \Omega_{m,G'}} \|\mu_t^M - \pi_{m,G'}\| < 1/(2e)\} \quad (3.14)$$

where $\|\mu - \nu\|$ is the total variation distance of measures μ, ν and the choice of the value $1/(2e)$ is conventional (any other value smaller than $1/2$ would do). With this choice, one has [LPW08]

$$\max_{M \in \Omega_{m,G'}} \|\mu_t^M - \pi_{m,G'}\| \leqslant e^{-\lfloor t/T_{\text{mix}} \rfloor}. \quad (3.15)$$

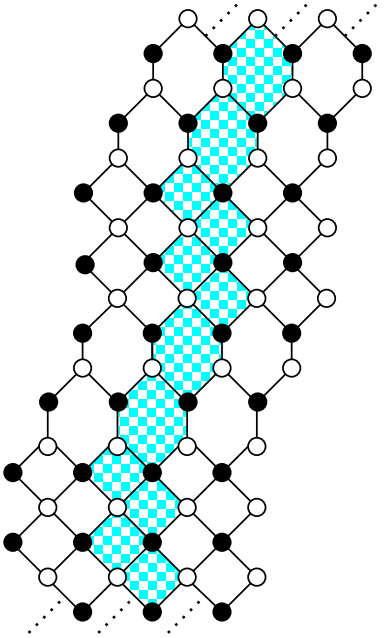

Figure 3.3: An example of the class of graphs where our results could be extended, see Remark 3.3.4. The shaded region is a *thread* (cf. Section 3.4.1). Layers of squares and hexagons can be of arbitrary vertical thickness and the periodicity in the "vertical" direction can be arbitrarily large.

We will study the mixing time when the boundary conditions are almost planar. The following is the main result of this work:

Theorem 3.3.2. *Fix $(s,t) \in \mathring{N}$, m an almost-planar boundary condition of slope (s,t) and let G' be as in Definition 3.2.2. If G is either the square, hexagon or square-hexagon lattice (cf. Fig. 3.1) then there exists some $c > 0$ such that*

$$cL^2 \leqslant T_{\text{mix}} \leqslant L^{2+o(1)}. \quad (3.16)$$

We refer to Section 3.1.1 above for a discussion of previously known results.

Remark 3.3.3. *The proof of the lower bound in* (3.16) *actually shows the following: if the dynamics is started from the maximal configuration, which has an excess volume $c\,L^3$ with respect to the typical (almost flat) equilibrium configuration, it takes a time $c_1 L^2$ before the excess volume becomes smaller than say $(c/2)\,L^3$ (which is still very large w.r.t. typical volume fluctuations). In this sense, the equilibration time lower bound is optimal.*

Remark 3.3.4. *Our result could be extended to a class of graphs obtained by alternating periodically layers of squares and hexagons (see Fig. 3.3). On the other hand, we will explain in Section 3.5.1 why our method does not (and should not!) work for general periodic bipartite graphs G, in particular not for graphs like the square-octagon lattice which possesses a "gaseous phase".*

3.3.1 Monotonicity

It is natural to introduce the following partial order on Ω : $M \geq M'$ if and only if $h_M(f) \geq h_{M'}(f)$ for every $f \in G^*$. As usual, the reference face f_0 is assumed to be fixed once and for all. Note that the partial order does not depend on the reference matching used to define the height. We say that

an event $A \subset \Omega$ is increasing if $M \geq M'$ and $M' \in A$ implies $M \in A$. We define in the usual way stochastic domination: $\mu \succeq \mu'$ if $\mu(A) \geq \mu'(A)$ for every increasing event A.

Proposition 3.3.5. *The dynamics defined in Section 3.3 is monotone, that is $\mu_t^M \succeq \mu_t^{M'}$ for every t and every $M \geqslant M'$.*

Proof. Couple the dynamics started from M and M' by using the same clocks and the same coin tosses. Partial order is preserved along time. Indeed, it suffices to observe that if $h_M(f) = h_{M'}(f)$ and a rotation at f that increases the height by 1 is possible for M', then necessarily the configuration of the edges of f in M is the same as in M', otherwise at some face f' neighboring f one would have $h_M(f') < h_{M'}(f')$. □

Remark 3.3.6. *As in [CMT12, Sec. 2.2], one can realize all the evolutions $M_t^{M_0}$ for all possible initial conditions M_0 on the same probability space, with the property that if $M_0 \leqslant M_0'$ then almost surely $M_t^{M_0} \leqslant M_t^{M_0'}$ for every $t \geqslant 0$. This construction is called* global monotone coupling.

Proposition 3.3.7. *If A is an increasing event, then $\pi_{m,G'}(\cdot|A) \succeq \pi_{m,G'}$.*

Proof. Remark that in the proof of Proposition 3.3.1 we showed that the maximal configuration can be reached from any other by a chain of rotations that increase the height, so $h_{\max} \in A$ and A is connected. Consider the original dynamics started from $h_{\max}$ and the reflected dynamics (again started from $h_{\max}$) where each update that would leave A is canceled. It is clear that they converge to $\pi_{m,G'}$ and $\pi_{m,G'}(\cdot|A)$ respectively and that, when coupled by using the same clocks and coin tosses, the second always dominates the first. □

Monotonicity allows to apply "censoring inequalities" of Peres and Winkler [PW11] which, roughly speaking, say the following: if the dynamics is started from the maximal or minimal configuration, deleting some updates along the evolution in a pre-assigned way (i.e. independently of the actual realization of the dynamics) increases the variation distance from equilibrium. The precise statement we need (cf. Corollary 3.3.9 below) is a bit more general than what is proven in [PW11] but the proof is almost identical, so we will just point out where some modification is needed.

Consider a probability measure π on Ω and $P^{(v)}, v \in \mathcal{V}$ a set of transition kernels that satisfy reversibility ($\pi(\sigma)P^{(v)}(\sigma \to \eta) = \pi(\eta)P^{(v)}(\eta \to \sigma)$) and monotonicity. We define a dynamics on Ω by assigning a Poisson clock of rate c_v to each $v \in \mathcal{V}$ and applying $P^{(v)}$ when v rings. The dynamics of Section 3.3 corresponds to $\mathcal{V} = (G')^*$, $c_v = 1$ and $P^{(f)}$ the kernel that corresponds to a rotation around f with probability 1/2 (if allowed).

Theorem 3.3.8. *Let ν_0 be a probability measure on Ω such that $\frac{\mathrm{d}\nu_0}{\mathrm{d}\pi}$ is increasing. Consider ν_t the law at time t of the dynamics started from ν_0. Then, for every $t \geqslant 0$, $\frac{\mathrm{d}\nu_t}{\mathrm{d}\pi}$ is increasing and, if $\{\mu_t\}_{t\geqslant 0}$ is a family of probability measures such that $\nu_t \preceq \mu_t$ for all t, one has*

$$\|\nu_t - \pi\| \leq \|\mu_t - \pi\|.$$

Corollary 3.3.9. *Let ν_0 be as in Theorem 3.3.8. Suppose that for all $v \in \mathcal{V}$, for all ν such that $\frac{\mathrm{d}\nu}{\mathrm{d}\pi}$ is increasing, we have $P^{(v)}\nu \preceq \nu$. Let μ_t be the law at time t of the dynamics started from ν_0, where the rates c_v of the Poisson clocks are replaced by deterministic time-dependent rates $\tilde{c}_v(s)$, such that $0 \leqslant \tilde{c}_v(s) \leqslant c_v$ for every $0 \leqslant s \leqslant t$. Then,*

$$\text{for every } t \geqslant 0, \quad \nu_t \preceq \mu_t \text{ and } \|\nu_t - \pi\| \leq \|\mu_t - \pi\|.$$

Remark 3.3.10. *The hypothesis of $\mathrm{d}\nu_0/\mathrm{d}\pi$ increasing is immediate if the dynamics is started from the maximal configuration $h_{\max}$, since in that case ν_0 is concentrated on h_{max}.*

As in [PW11], the proof of Theorem 3.3.8 follows directly from the following two lemmas.

Lemma 3.3.11. *With the above definitions, for any probability measure μ, if $\frac{\mathrm{d}\mu}{\mathrm{d}\pi}$ is increasing then $\frac{\mathrm{d}P^{(v)}\mu}{\mathrm{d}\pi}$ is increasing.*

This replaces Lemma 2.1 of [PW11], which uses explicitly the fact that the dynamics is of "heat-bath" type.

Proof.

$$\frac{\mathrm{d}P^{(v)}\mu}{\mathrm{d}\pi}(\sigma) = \frac{1}{\pi(\sigma)}\sum_s \mu(s)P^{(v)}(s\to\sigma) = \frac{1}{\pi(\sigma)}\sum_s \frac{\mu(s)}{\pi(s)}\pi(s)P^{(v)}(s\to\sigma) \tag{3.17}$$

$$= \frac{1}{\pi(\sigma)}\sum_s \frac{\mu(s)}{\pi(s)}\pi(\sigma)P^{(v)}(\sigma\to s) = \mathbb{E}^{(v)}_\sigma[\frac{\mathrm{d}\mu}{\mathrm{d}\pi}(X)] \tag{3.18}$$

where X is the state after one action of $P^{(v)}$, starting from σ. The third equality uses the reversibility and the monotonicity of $P^{(v)}$ shows that the last expression is increasing in σ. □

Lemma 3.3.12. *[PW11, Lemma 2.4] If μ, ν are two probability measures on Ω such that $\frac{\mathrm{d}\nu}{\mathrm{d}\pi}$ is increasing and $\nu \preceq \mu$, then $\|\nu - \pi\| \leq \|\mu - \pi\|$.*

Proof of Corollary 3.3.9. Decompose the Poisson point process (PPP) of density c_v on $\mathbb{R}^+$ as the union of two independent PPPs, X and Y, of non-constant densities $\tilde{c}_v(s)$ and $c_v - \tilde{c}_v(s) \geqslant 0$. The dynamics μ_t is obtained by erasing the updates from the process Y. From Lemma 3.3.11 we get that $\frac{\mathrm{d}\nu_t}{\mathrm{d}\pi}$ is increasing. Censoring an update $P^{(v)}$ at time t conserves the stochastic domination because, by induction, $\nu_t = P^{(v)}\nu_{t^-} \preceq \nu_{t^-} \preceq \mu_{t^-} = \mu_t$. □

3.4 Mapping to a "bead model"

3.4.1 From dimers to "beads"

From this point onward, we will assume that the graph G is either the square, hexagon or square-hexagon graph (see Fig. 3.1) since we will use some of their geometric properties.

The set Ω of matchings of G can be mapped into the configurations of what we call a *bead model*. Such a correspondence is valid for more general graphs than the square, hexagon and square-hexagon, provided that the graph in question possesses a certain "fibration" with fibers (or *threads*) satisfying the properties described below. See Remark 3.3.4 for a more general class of graphs where this construction would work.

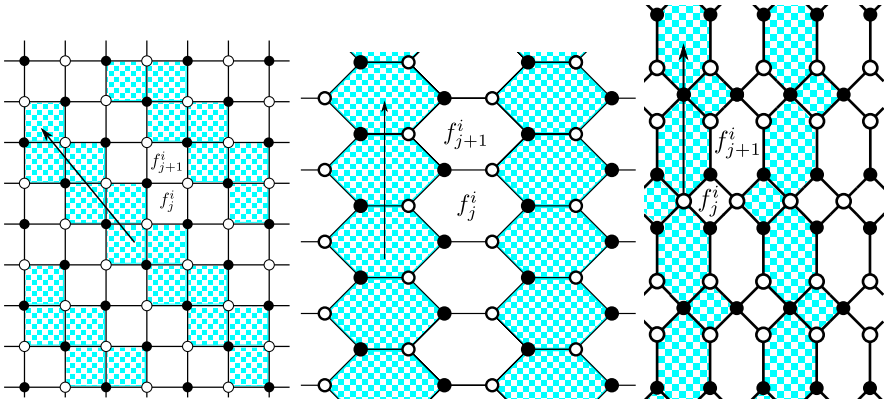

Figure 3.4: The paths called threads and used in the definition of the bead model for the square, hexagon and square hexagon graph. The arrow shows the orientation of the threads.

As is apparent from Fig. 3.4, for the three types of graph we are considering, there exists a family of directed periodic paths $\{\gamma_i\}_{i\in\mathbb{Z}}$ (called *threads*) on G^* such that

(i) labeling the faces along thread γ_i as $\{f^i_j\}_{j\in\mathbb{Z}}$, face f^i_j neighbors only $f^i_{j\pm1}$ and some faces of $\gamma_{i\pm1}$;

(ii) going from the face f^i_j to f^i_{j+1}, one crosses an edge of G (call it e^i_j) which is positively orientated. Such edges are called *transverse edges* and dimers on transverse edges are called *beads*;

(iii) threads γ_i are obtained one from the other by a suitable $\mathbb{Z}^2$ translation and $\cup_i\gamma_i = G^*$.

Proposition 3.4.1. *Consider a finite sub-graph $G' \subset G$ as in Definition 3.2.2 (recall that $G \setminus G'$ is connected) and a boundary condition $m \in \Omega$.*

A matching in $\Omega_{m,G'}$ is uniquely determined by the position of its beads. Furthermore the number of beads in G' on each thread γ_i is the same for every $M \in \Omega_{m,G'}$.

Proof. From the definition of height function and using property (ii) above of threads, which says that transverse edges are all crossed with the same orientation, the height at some $f \in (G')^*$ belonging to thread γ_i is determined by the number of beads on γ_i between the boundary of G' and f. Hence the position of beads uniquely determines the height function and thus the matching. The total number of beads on $\gamma_i \cap (G')^*$ is determined by the height difference between two faces f_1, f_2 of $\gamma_i \setminus (G')^*$, such that the portion of γ_i between f_1 and f_2 includes $\gamma_i \cap (G')^*$. This height difference is clearly independent of the particular chosen matching in $\Omega_{m,G'}$ (because f_1, f_2 are outside G' and $G \setminus G'$ is connected). □

In order to have a complete picture, we have to determine the condition for a set of beads' positions to correspond to a matching of G, that is the kind of constraints beads impose on each other. We first need some notations (see Fig. 3.5).

Definition 3.4.2. *Let as above e^i_j denote the j^{th} transverse edge of the thread γ_i and let b^i_j (resp. w^i_j) denote its black (resp. white) vertex. Let Γ^i be the set of vertices of G which belong both to γ_i and to γ_{i+1}, and order vertices in Γ^i following the same direction as for the faces along the threads. Note that Γ^i contains the white vertices of transverse edges of γ_i and the black vertices of transverse edges of γ_{i+1}. Given transverse edges $e^i_j, e^{i+1}_{j'}$ on γ_i, γ_{i+1}, we write $e^i_j \prec e^{i+1}_{j'}$ (resp $e^i_j \succ e^{i+1}_{j'}$) if w^i_j is below (resp. above) $\mathrm{b}^{i+1}_{j'}$.*

Proposition 3.4.3. *A set of bead positions corresponds to a matching in Ω if and only if, for any two consecutive beads on the same thread (i.e. beads on transverse edges $e^i_a, e^i_b, a < b$ with no bead between them along the same thread γ_i), there is a unique bead in thread γ_{i-1} and a unique bead in thread γ_{i+1} such that their positions e^{i-1}_c, e^{i+1}_d satisfy $e^i_a \prec e^{i-1}_c \prec e^i_b$ and $e^i_a \prec e^{i+1}_d \prec e^i_b$.*

Proof. We advise the reader to keep an eye on Fig. 3.5 while reading this proof.

Proof of the "only if" part. Without loss of generality we can consider threads γ_i and γ_{i+1}. Note that following Γ^i between w^i_a and w^i_b there is necessarily exactly one more black vertex than white vertex (because G is bipartite). Since by assumption there are no beads on γ_i between e^i_a and e^i_b, all the white vertices have to be matched within Γ^i. This leaves exactly a single black vertex which has to be matched along a transverse edge in γ_{i+1}. The corresponding dimer is the unique bead such that its position e^{i+1}_d satisfies $e^i_a \prec e^{i+1}_d \prec e^i_b$.

Proof of the "if" part. Suppose that the bead positions are given and that they satisfy the properties above. This automatically fixes which transverse edges are occupied and which are free. To see that the rest of the matching is also (uniquely) determined, proceed as follows. With the same notations as above, consider the vertices of Γ^i between w_b^i and b_d^{i+1}. These vertices are all matched with each other (because by construction e_d^{i+1} is the "highest" bead in γ_{i+1} such that $e_d^{i+1} \prec e_b^i$) and they form a path with an equal number of alternating white and black vertices, so there is a unique way of matching them. The same goes for vertices between w_a^i and b_d^{i+1}. □

Remark 3.4.4. *Fix $G' \subset G$ and a boundary condition $m \in \Omega$. Under the measure $\pi_{m,G'}$, conditionally on the positions of the beads in $\gamma_{i\pm1}$, the beads of γ_i are independent and each has a* uniform distribution *in a certain finite set of adjacent transverse edges (two transverse edges being adjacent if they are of the form e_j^i, e_{j+1}^i; remark that on the square lattice they can actually share a vertex, while on the hexagonal lattice they cannot). Indeed, given a bead on the transverse edge e_a^i, it is possible to move it up to e_{a+1}^i (resp. down to e_{a-1}^i) via a rotation of the face f_{a+1}^i (resp. f_a^i), provided that f_{a+1}^i (resp. f_a^i) is within G' and that the new position does not violate the ordering properties of Proposition 3.4.3. Uniformity of the distribution is trivial from uniformity of the unconditional measure $\pi_{m,G'}$. Note also that moving a bead up (resp. down) implies changing by -1 (resp. $+1$) the height of the face just above (below) it along the thread.*

3.4.2 Dynamics in terms of beads

The Glauber dynamics defined in Section 3.3 has a simple interpretation in terms of the bead model. As observed in Remark 3.4.4, a rotation is equivalent to moving a bead to an adjacent transverse edge in the same thread (in particular, rotations are possible only at faces adjacent to a bead, and the configuration of beads outside G' is frozen). We can then redefine the dynamics as follows. Each bead in G' has a mean-one independent Poisson clock; when it rings, with probabilities $1/2, 1/2$ move the bead either up or down to the adjacent transverse edge if allowed by the boundary conditions and by the ordering properties.

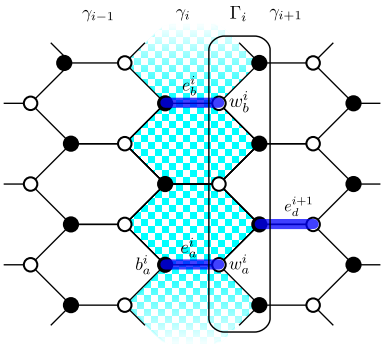

Figure 3.5: An example of the situation in the proof of proposition 3.4.3. Beads on the edges e_a^i and e_b^i are indicated by thick lines.

Fast dynamics

As mentioned in the introduction, we will not work directly with the original Glauber dynamics but rather with an auxiliary one. We will actually need *two* auxiliary dynamics: one, that we call *synchronous fast dynamics*, will be useful to upper bound the mixing time, while the *asynchronous fast dynamics* will provide a lower bound.

Definition 3.4.5.

(i) We define the synchronous fast dynamics *as follows. We have two independent mean-1 Poisson clocks. When the first (resp. second) one rings we resample all the bead positions on even-labelled (resp. odd-labelled) threads following the equilibrium measure $\pi_{m,G'}$ conditioned on the state of beads on odd (resp. even) threads.*

(ii) The asynchronous fast dynamics *is defined instead by giving each bead in G' an independent mean-1 Poisson clock. When a clock rings, the position of the corresponding bead is resampled from $\pi_{m,G'}$ conditioned on the position of all other beads. Note that, by construction, beads outside G' are frozen.*

Thanks to monotonicity of the original Glauber dynamics, one sees easily that both synchronous and asynchronous fast dynamics are monotone.

Remark 3.4.6. *Recall Remark 3.4.4: the positions accessible to a single bead, given the beads of neighboring threads and the boundary conditions, form a segment of the transverse edges of its thread and these segments are mutually non-intersecting. Thus, under both synchronous and asynchronous dynamics each bead is resampled with the uniform law on a finite segment.*

Comparisons of mixing times, and constrained dynamics

As announced, the asynchronous dynamics will provide a mixing time lower bound for the original one.

Proposition 3.4.7. *Fix $G' \subset G$ as in Definition 3.2.2 and a boundary condition m, not necessarily almost planar. Let T_{mix} be the mixing time for the original dynamics and let T^a be the first time such that the law of the asynchronous dynamics, started from the maximal configuration, is within variation distance $1/(2e)$ from equilibrium. Then, $T_{\mathrm{mix}} \geqslant T^a$.*

Proof. Recall the definition (3.14) of mixing time: to get a lower bound, we can just look at the evolution from the maximal configuration h_{max}, which we can therefore assume to be the initial configuration of both original and asynchronous fast dynamics. From the description of the asynchronous fast dynamics in Section 3.4.2, we see that we can couple the two dynamics using

the same Poisson clocks for each bead. To prove that the asynchronous dynamics approaches equilibrium faster than the original one it is enough to show that if $\frac{\mathrm{d}\nu}{\mathrm{d}\pi}$ is increasing then, writing $P^{(b)}$ and $\tilde{P}^{(b)}$ for the kernels corresponding to an update of the bead b according to the original and asynchronous fast dynamics respectively, one has

$$\tilde{P}^{(b)}\nu \preceq P^{(b)}\nu. \tag{3.19}$$

Indeed, together with monotonicity this guarantees that the height function is stochastically lower under the asynchronous dynamics than under the original one and then Theorem 3.3.8 can be applied (with μ_t the law of the original dynamics and ν_t that of the asynchronous one).

By conditioning on all the beads except b, we can assume that ν is a measure on some interval $\{0, \dots, k\}$ and that π is the uniform measure on the same interval (cf. Remark 3.4.4) in which case it is trivial to check (3.19). Indeed, $\tilde{P}^{(b)}\nu = \pi$ for every ν, and $\mathrm{d}P^{(b)}\nu/\mathrm{d}\pi$ is increasing (cf. Lemma 3.3.11 and recall the assumption $\mathrm{d}\nu/\mathrm{d}\pi$ increasing), which implies $\pi \preceq P^{(b)}\nu$. □

Constrained dynamics

Next, we bound T_{mix} from above using the synchronous dynamics: this works well only if the dynamics is constrained between two configurations whose height functions are not too different. Given two matchings $M_- \leqslant M_+$ in $\Omega_{m,G'}$ (M_- will be called "the floor" and M_+ "the ceiling") the constrained dynamics is defined in the subset $\Omega_{m,G'}^{M_\pm} \subset \Omega_{m,G'}$ such that $M_- \leqslant M \leqslant M_+$: it is obtained from the original dynamics, erasing all updates which would exit $\Omega_{m,G'}^{M_\pm}$. It is elementary to check that monotonicity still holds, and the equilibrium measure is of course $\pi_{m,G'}^{M_\pm} := \pi_{m,G'}(\cdot | M_- \leqslant \cdot \leqslant M_+)$. The distance between floor and ceiling is defined as $H = \max_{f \in G^*}(h_{M_+}(f) - h_{M_-}(f))$. To avoid a proliferation of notations, we still call T_{mix} the mixing time of the dynamics constrained between M_- and M_+, and μ_t^M its law at time t, with initial condition M.

To estimate T_{mix} within logarithmic multiplicative errors, we can restrict ourselves to the evolution started from the extreme configurations (see for instance [CMT12, Eq. (6.5)]):

Lemma 3.4.8. *Consider the dynamics constrained between M_- and M_+. For any $t > 0$ and any $M \in \Omega_{m,G'}^{M_\pm}$,*

$$\|\mu_t^M - \pi_{m,G'}^{M_\pm}\| \leq 2H|(G')^*| \max\left[\|\mu_t^{M_+} - \pi_{m,G'}^{M_\pm}\|, \|\mu_t^{M_-} - \pi_{m,G'}^{M_\pm}\|\right]$$

with $|(G')^*|$ the number of faces of G'.

In the next result, T^s_{mix} denotes the mixing time of the synchronous dynamics constrained between M_- and M_+ (just take the Definition 3.4.5 of the synchronous dynamics and replace $\pi_{m,G'}$ by $\pi^{M_\pm}_{m,G'}$ there):

Proposition 3.4.9. *Fix $G' \subset G$ as in Definition 3.2.2 and boundary condition m. Suppose m is almost planar with slope $(s,t) \in \mathring{N}$ and consider floor/ceiling $M_\pm \in \Omega_{m,G'}$, at distance H from each other. We have*

$$T_{\mathrm{mix}} \leq (C_{s,t} H^2 \log^3(H|(G')^*|)) T^s_{\mathrm{mix}}.$$

Proof. A complete proof for the hexagonal graph is given in [CMST10, Section 6.2] and since for the square or square-hexagon graph not much changes, we will be somewhat sketchy.

For simplicity we will write π for $\pi^{M_\pm}_{m,G'}$. One first proves that a single update of the synchronous fast dynamics can be realized by letting the original dynamics evolve for a time $O(H^2(\log H)(\log|(G')^*|))$ while censoring some updates. Indeed, consider the dynamics obtained by starting from M and setting to 0 the rate of updates of beads on, say, odd threads in the original dynamics. It is clear that this auxiliary evolution converges to the uniform measure on configurations of beads on even thread conditioned by the beads on odd threads, which is exactly the measure after one "even update" of the synchronous fast dynamics, and Remark 3.4.6 allows us to easily compute its mixing time. Beads on odd threads are frozen and those on even threads are completely independent so we have to compute the mixing time for a set of independent one-dimensional simple random walks on domains of the type $\{0, \dots, k_i\}$. By Proposition 3.2.14 the k_i are bounded by $C_{s,t}H$ (because, if a bead can be moved n steps up, necessarily there is a length-n free path along the thread) so the mixing time for each walk is $O(H^2 \log H)$ and for $O(|(G')^*|)$ such walks it becomes $O(H^2(\log H)(\log|(G')^*|))$.

It is then clear that the law of the synchronous fast dynamics at time t, call it ν^M_t, coincides (except for a negligible total variation error term), with that of the original dynamics at time $n(t)\Delta$ after censoring suitable updates, where

$$\Delta = C_{s,t} H^2 (\log H)(\log|(G')^*|) \leqslant C_{s,t} H^2 \log^2(H|(G')^*|)$$

and $n(t)$ is a Poisson random variable of average $2t$ (this is the number of updates within time t for the synchronous dynamics). Since we will take t large, we can replace $n(t)$ with its average (we skip details). If Corollary 3.3.9 is applicable (see below), we obtain then that $\|\mu^{M_\pm}_{2t\Delta} - \pi\| \leqslant \|\nu^{M_\pm}_t - \pi\|$. Then, using Lemma 3.4.8 and (3.15),

$$\sup_M \|\mu^M_{2A\Delta T^s_{\mathrm{mix}}} - \pi\| \leqslant 2H|(G')^*| \max\left[\|\mu^{M_+}_{2A\Delta T^s_{\mathrm{mix}}} - \pi\|, \|\mu^{M_-}_{2A\Delta T^s_{\mathrm{mix}}} - \pi\|\right] \tag{3.20}$$

$$\leqslant 2H|(G')^*| \max\left[\|\nu^{M_+}_{AT^s_{\mathrm{mix}}} - \pi\|, \|\nu^{M_-}_{AT^s_{\mathrm{mix}}} - \pi\|\right] \leqslant 2H|(G')^*| e^{-\lfloor A \rfloor} \tag{3.21}$$

which is smaller than $1/(2e)$ for some A of order $\log(H|(G')^*|)$.

To see that Corollary 3.3.9 is applicable, we have to check that $\mathrm{d}\mu/\mathrm{d}\pi$ increasing implies $P^{(b)}\mu \preceq \mu$ with $P^{(b)}$ the kernel of the update of bead b under the original dynamics, where beads move by ± 1 along their respective thread. Conditioning on all other beads, we can assume that μ is a probability on an interval $\{0, \dots, k\}$ and that π is the uniform measure on the same interval. Then, summation by parts shows that

$$P^{(b)}\mu(f) - \mu(f) = -\frac{1}{2}\sum_{x=1}^{k}[\mu(x) - \mu(x-1)][f(x) - f(x-1)]$$

which is negative if f is increasing (μ is also increasing). □

Volume drift

In this section we study the time evolution of the volume between two configurations under the (a)synchronous fast dynamics. This will be the key to evaluate their mixing time and thus, thanks to Propositions 3.4.7 and 3.4.9, the mixing time of the original dynamics. Note that in Proposition 3.4.10 we *do not* require the boundary condition to be almost-planar.

Proposition 3.4.10. *Let $M^1, M^2 \in \Omega_{m,G'}$ be such that $M^1 \leq M^2$ and let $M^i_t, i = 1, 2$ denote the evolution starting from M^i and following the fast dynamics (synchronous or asynchronous: we use the same notation). Letting $\mathcal{F}_t$ denote the filtration induced by $\{M^i_s, i = 1, 2, s \leqslant t\}$ and $V_t = \sum_{f \in G^*}[h_{M^2_t}(f) - h_{M^1_t}(f)]$, then V_t is a supermartingale:*

$$\mathbb{E}[V_t|\mathcal{F}_{t'}] \leq V_{t'} \text{ for every } t \geqslant t'.$$

The same holds if the fast dynamics is constrained between a floor M_- and a ceiling M_+.

Note that, since the volume is expressed as a sum of height differences, it does not matter whether M^1_t evolves independently of M^2_t or not.

Proof. First of all note that the expected drift

$$\lim_{\varepsilon \searrow 0} \frac{1}{\varepsilon}[\mathbb{E}(V_\varepsilon) - V_0] \tag{3.22}$$

is the same for the synchronous and for the asynchronous fast dynamics (as a function of the initial conditions M^1, M^2): this is thanks to the fact that the volume is a sum of height differences over faces, that expectation is linear and that beads in the same thread are updated independently in a step of the synchronous dynamics. (This does not imply that the process V_t itself or even its average is the same for the two dynamics). In the following,

we will therefore assume that we deal with the synchronous dynamics and prove that (3.22) is not positive.

From the proof of Proposition 3.3.1, we see that there exists a sequence of configurations $M_{(0)}, \dots, M_{(k)}$ such that $M_{(0)} = M^2, M_{(k)} = M^1$ and $M_{(i)}$ is obtained by $M_{(i-1)}$ via a rotation that decreases the height at some face f. Writing the volume difference between M^2 and M^1 as a telescopic sum of volume differences between $M_{(i)}$ and $M_{(i-1)}$ and using linearity of the expectation, we see that to prove (3.22) we can restrict to the case where M^1 and M^2 differ only by a rotation on a single face f. We will actually prove that the expected change of V from a single update is 0 except when f is suitably close to the boundary of G', in which case it can be negative (see Remark 3.4.11 for a more precise discussion).

The proof will be given only for the square-hexagon graph since it contains all the difficulties, but the same method works equally well for the hexagon or square graph.

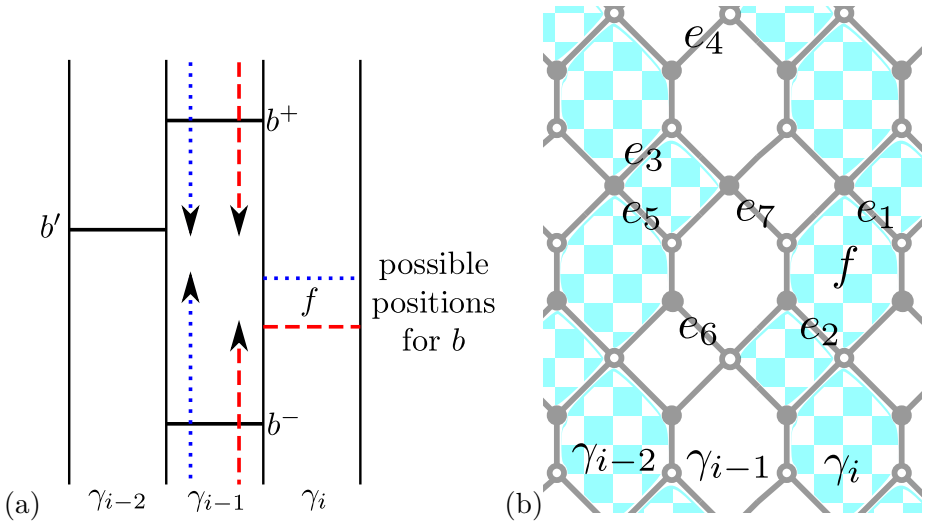

Figure 3.6: Volume drift when f is a hexagon. (a): a schematic representation of threads $\gamma_i, \gamma_{i-1}, \gamma_{i-2}$ with the beads $b, b^{\pm}, b'$. (b): a more detailed view of the three threads in question, with the hexagonal face f and the transverse edges $e_1, \dots, e_7$ mentioned in the proof.

Case 1: f is a hexagon. Suppose that the face f, whose rotation brings M^1 to M^2, is a hexagon on thread γ_i (cf. Fig. 3.6). Then, there is a certain bead b which in the two configurations is on two different adjacent transverse edges of γ_i on the boundary of f (such edges are called e_1 and e_2 in the picture). Now consider a step of the synchronous dynamics. If threads with the same parity as γ_i are updated then clearly the evolved configurations can be coupled in order to coincide, and the volume decreases by -1. We need to show that when threads of the opposite parity are updated the average

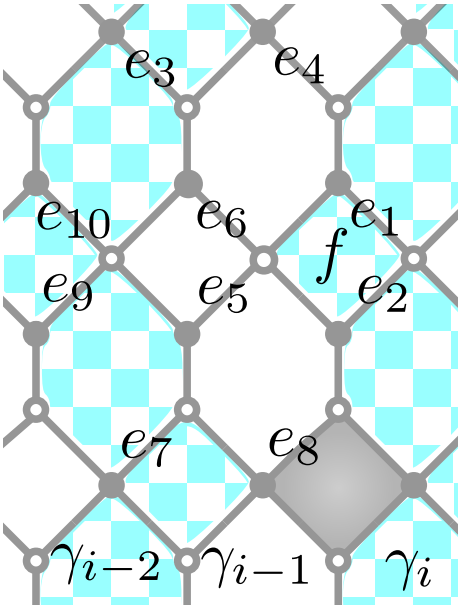

Figure 3.7: Volume drift when f is a square. The threads $\gamma_i, \gamma_{i-1}, \gamma_{i-2}$ with the face f and the transverse edges $e_i, i = 1, \ldots, 10$. A square face like f, which is adjacent to hexagons of the thread to its left, is called a "Type I" square, while a square like the shaded one (adjacent to hexagons of the thread to its right) is called "Type II". Note that if f were a Type II square say again on γ_i, then by symmetry γ_{i-1} would not contribute to the volume change but the thread γ_{i+1} would.

volume increase is at most $+1$. Clearly, only threads $\gamma_{i\pm1}$ contribute to the average change of volume (because there is no discrepancy between M^1 and M^2 on threads $\gamma_{i\pm2}$, which therefore "screen away" $\gamma_{i\pm n}, n \geqslant 3$ from the discrepancy at f) and by symmetry we will just show that γ_{i-1} contributes at most $1/2$.

On γ_{i-1} there are a certain number of beads: call b^+ the lowest bead which is above b (with the ordering convention of Definition 3.4.2) and b^- the highest bead below b. Note that one or both of them could be absent in M^1, M^2 (for instance γ_{i-1} could contain no beads at all): however, suitably changing the dimer configuration outside of G' (which has no effect on the dynamics) we can always assume that such beads do exist (possibly outside G'). Thanks to Proposition 3.4.3, there exists then a unique bead b' in γ_{i-2}, which is lower than b^+ and higher than b^-, see Fig. 3.6(a).

A look at Fig. 3.6(b) and Proposition 3.4.3 suffices to convince that only the following two mutually exclusive cases can occur (Fig. 3.6(a) corresponds to the first one):

- if b' is at or above transverse edge e_3, then b^+ is at or above edge

e_4. Then, the distribution of b^+ given all the other beads does not depend on whether b is at e_1 or e_2, and therefore b^+ (and *a fortiori* beads on γ_{i-1} above b^+) gives no contribution to the average volume change. As for b^-, instead, its set of possible positions (which forms an interval of adjacent transverse edges of γ_{i-1}, recall Remark 3.4.4), includes exactly one edge more (called e_7 in the picture) when b is at e_1 w.r.t when b is at e_2. Since the position of b^- is uniform among the available positions and since the average of a uniform random variable on $\{0, \dots, k\}$ is $k/2$, the average volume change arising from bead b^- is $(k+1)/2 - k/2 = 1/2$ (recall that moving a bead up by one transverse edge results in decreasing the height of a face by -1). It is also clear that beads in γ_{i-1} and below b^- do not contribute to the volume change, since their set of available positions is disjoint from that of b^- (cf. Remark 3.4.6) and does not change when b is moved from e_1 to e_2.

In this discussion, we ignored so far the fact that rotations for the dynamics are allowed only in the sub-graph G'. For the bead b^- to reach (after the update) its new available position e_7 starting from the present one, all the necessary elementary rotations along thread γ_i have to involve faces contained in $(G')^*$. Otherwise, the edge e_7 is actually *not* a possible position for b^-: the set of effectively available positions for b^- is then the same when b is in e_1 or e_2, so the volume change associated to b^- is not $1/2$ but 0. In conclusion, taking into account the fact that G' is not the whole graph, only decreases the average volume change. A similar reasoning shows that the floor/ceiling constraint can only decrease the average volume change. This observation will be picked up again in Remark 3.4.11.

- if instead b' is at or below transverse edge e_5, then b^- is at or below edge e_6. The argument is then similar to the first case (this time b^- does not feel the effect of the discrepancy and b^+ has one more edge available, again e_7, in M^2 than in M^1). As in the first case, constraints from boundary conditions or from floor/ceiling can only decrease the volume change.

Altogether, in both cases the average volume change from γ_{i-1} is either $1/2$ or 0 (depending on the position of f with respect to the boundary of G' and on the presence of floor/ceiling) and, since the same holds for γ_{i+1}, the overall average volume change is at most zero.

Case 2: f is a square (cf. Fig. 3.7). This time assume that the discrepancy between M^1 and M^2 is at a square face f in γ_i, i.e. that a bead b is either on edge e_1 or e_2. Again, when threads with the parity of γ_i are updated the average volume decreases by -1. In this case, it is also clear that the distribution of beads on γ_{i+1} after an update is the same starting

from M^1 or M^2 (because the edges e_1 and e_2 meet on the same vertex of γ_{i+1}), so a non-zero contribution to the average volume change this time can come only from γ_{i-1} and we will show that this contribution is at most $+1$. With the same conventions as in Case 1 for the beads $b^{\pm}$ and b', we distinguish this time three cases (to avoid repetitions, we ignore effects due to floor/ceiling and to the fact that $G' \neq G$: exactly as in Case 1, this can only decrease the average volume change):

- if b' is at or above e_3 then b^+ is at e_4 or higher and does not feel the effect of the discrepancy. At the same time, according to whether b is at e_2 or e_1, the edges e_5, e_6 are available or not for b^-. The average volume change induced by b^- is then $(k+2)/2 - k/2 = 1$.

- similarly, if b' is at or below e_7 then b^- does not feel the discrepancy (it is at or below e_8) and b^+ has two extra available positions (again e_5, e_6) when b is at e_2. Again this gives volume change $+1$.

- finally, when b' is either at e_9 or e_{10}, then both b^+ and b^- feel the discrepancy: indeed, when b is at e_2 then position e_5 is not available for b^- and e_6 is available for b^+, while when b is at e_1 then position e_5 is available for b^- and e_6 is not available for b^+. Again, the average volume change is $+1$.

□

Remark 3.4.11. *It is useful to emphasize that the proof of Proposition 3.4.10 showed the following. Assume for simplicity that there is no floor-ceiling constraint on the dynamics. If M^1 and M^2 differ by a single rotation at $f \in (G')^*$, then the average volume change after an update is between -1 and 0. To decide whether it is zero or non-zero, proceed as follows. The rotation around f changes the set of available positions for a certain number (at most two, actually) of beads in threads neighboring the thread of f: some positions which were not allowed before the rotation of f become allowed and vice-versa. If all the elementary rotations leading such beads along their threads to the new available positions are allowed (i.e. if all the faces corresponding to such elementary rotations are in the finite domain $(G')^*$) then the average volume change is zero. Otherwise, it is different from zero.*

Remark 3.4.12. *From the proof of Proposition 3.4.10 one can also understand why the study of the dynamics on the square or square-hexagon lattice is qualitatively more challenging than on the hexagonal lattice. The basic observation due to D. Wilson in [Wil04] (although it was not formulated in this terms) is the following. Consider the "fast dynamics" for the hexagonal lattice with initial condition given by some matching m, and let $H_t^m(i)$ be average at time t of the sum of the heights of the faces (in $(G')^*$) belonging*

to thread i. Then, for any pair of initial configurations m^1, m^2, the function $\psi_t(\cdot) := H_t^{m^1}(\cdot) - H_t^{m^2}(\cdot)$ satisfies the discrete heat equation

$$\partial_t \psi_t(i) = \frac{1}{2}\Delta\psi_t(i) + R_t = \frac{1}{2}[\psi_t(i+1) - 2\psi_t(i) + \psi_t(i-1)] + R_t \quad (3.23)$$

where the "error term" R_t is due to the boundary of G' and to floor/ceiling constraints (if present) and can be ignored for the sake of this discussion. Call $V_t = \sum_i \psi_t(i)$ the average volume difference between the two evolving configurations. Since there are $O(L)$ threads that intersect G' and the lowest eigenvalue of the discrete Laplacian on $\{1, \dots, L\}$ is of order L^{-2}, one deduces immediately that after a time of order $L^2 \times \log V_0$, the average volume V_t is very small so that the two configurations have coupled with high probability.

That the same kind of argument does not *work for other lattices can be seen as follows. Consider for instance the square-hexagon lattice, and assume that (with the terminology of the caption of Fig. 3.7) m^1 and m^2 differ only by the rotation at a square face f of Type I on thread j. Then, clearly at time zero $\psi_0(j) = 1$ and $\psi_0(j') = 0$, $j' \neq j$. While it is still true that* (3.23) *holds for $t = 0$ and $i = j$ (the initial drift of $\psi(j)$ is $-1 = \frac{1}{2}\Delta\psi_0(j)$), the equation does not hold (even at $t = 0$) for $i = j \pm 1$: indeed, the proof of Proposition 3.4.10 shows that the initial drift of $\psi(j-1)$ is $1 = \nabla\psi_0(j) = \psi_0(j) - \psi_0(j-1)$ (instead of $1/2 = \frac{1}{2}\Delta\psi_0(j-1)$) and that of $\psi(j+1)$ is 0 (instead of $1/2$). If on the contrary the face f were a square of Type II, one would find that the initial drift of $\psi(j-1)$ is 0 and that of $\psi(j+1)$ is $1 = -\nabla\psi_0(j+1)$.*

We believe that, for initial conditions m^1, m^2 such that their height differences are "smooth" on the macroscopic scale, Equation (3.23) *should still (approximately) hold, for L large. Indeed, there are as many Type I as Type II squares in each thread: if each of the two types contributes approximately equally to the height differences $\psi_0(i)$, from the above reasoning one finds that the initial drift of $\psi(j-1)$ is approximately $1/2\nabla\psi_0(j) - 1/2\nabla\psi_0(j-1) = 1/2\Delta\psi_0(j-1)$. However, trying to pursue this route seems quite hard (one should show that "smoothness" is conserved for positive times) and we had to devise an alternative approach instead, based on Proposition 3.4.10 and on Theorem 3.5.1 of next section.*

3.5 Proof of Theorem 3.3.2

3.5.1 Mixing time upper bound

Here we prove the mixing time upper bound of Theorem 3.3.2. The crucial step (Theorem 3.5.1) is to give an almost-optimal estimate when the dynamics is constrained between floor and ceiling of small mutual distance H (in the application, we will take $H = L^\epsilon$ with ϵ small). Then, an argument

developed in [CMT12] allows to deduce the mixing time estimate for the unconstrained dynamics (see Section 3.5.1 for a sketch).

A martingale argument

The basic step is to prove the following:

Theorem 3.5.1. *Consider the same setting as in Theorem 3.3.2, but assume that the height function is constrained between ceiling and floor that are almost-planar configurations of slope* $(s,t) \in \mathring{N}$*, of mutual distance* H*. Then,* $T_{\mathrm{mix}} = O(L^2 H^9 \log^4(HL))$*.*

The main idea will be to apply to the volume between two configurations the following classical bound on the hitting time for a supermartingale:

Lemma 3.5.2. *Let* X_t *be a continuous-time supermartingale such that almost surely* $0 \leq X_t \leq M$ *for every* $t \in \mathbb{R}^+$ *and* $\liminf_{\delta\to 0} \frac{1}{\delta}\mathbb{E}[(X_{t+\delta} - X_t)^2|\mathcal{F}_t] \geq \nu > 0$ *whenever* $X_t > 0$*. Suppose* $X_0 = i > 0$ *almost surely, fix* $0 < m < i$ *and let* $T^{(m)} = \inf\{t : X_t \leq m\}$ *be the hitting time of* $[0, m]$*. Then we have*

$$\mathbb{E}[T^{(m)}] \leq \frac{2Mi}{\nu}.$$

(Just note that if $Z(t) = X_t^2 - 2MX_t - \nu \min(t, T^{(0)})$, then Z_t is a negative sub-martingale and compute the average of $Z(t)$ for $t = T^{(m)}$).

Let V_t denote the volume between the maximal and minimal evolutions M_t^+, M_t^- *under the synchronous fast dynamics*. Proposition 3.4.10 shows that V_t is a super-martingale. Because of the floor and ceiling at distance H, we clearly have $0 \leq V_t \leq |(G')^*|H$ deterministically. To apply Lemma 3.5.2 we only need a lower bound on $\mathbb{E}[(V_{t+\delta} - V_t)^2|\mathcal{F}_t]$. It is important to remark that such a quantity *does depend* on how M_t^+, M_t^- are coupled, while by linearity it is not necessary to specify the coupling to compute the drift $\mathbb{E}[V_{t+\delta} - V_t|\mathcal{F}_t]$.

Lemma 3.5.3. *There exists a global monotone coupling under which*

$$\liminf_{\delta\to 0} \frac{1}{\delta}\mathbb{E}[(V_{t+\delta} - V_t)^2|\mathcal{F}_t] \geq c\frac{V_t}{H^6} \tag{3.24}$$

where c *is a constant depending only on the slope* (s,t)*.*

Proof of Theorem 3.5.1. Applying Proposition 3.4.9, it is enough to give the upper bound

$$T^s_{\mathrm{mix}} \leq \mathrm{cst} L^2 H^7 \log(LH)$$

for the mixing time of the synchronous fast dynamics.

Let $m_i = 2^{-i}H|(G')^*|$ and $T_i = \inf\{t : V_t \leq m_i\}$. Remark that, up to time T_i, V_t satisfies the hypothesis of Lemma 3.5.2 with $M = H|(G')^*|$ and $\nu = cm_i/H^6$. Thus we have

$$\mathbb{E}[T_i - T_{i-1}] \leq H^6 \frac{2Mm_{i-1}}{cm_i} \leq c'|(G')^*|H^7.$$

Finally, since V_t takes integer values, the hitting time of 0 is equal to the hitting time of $[0, 1/2]$ which is T_{i_0} for $i_0 = \lceil \log_2(2H|(G')^*|)\rceil$. We have proved

$$\mathbb{E}T_{i_0} \leq c'|(G')^*|H^7 \log(H|(G')^*|) = c''L^2H^7 \log(LH). \tag{3.25}$$

Therefore, $\mathbb{P}(T_{i_0} > 2ec''L^2H^7 \log(LH)) < 1/(2e)$, which implies

$$T^s_{\text{mix}} \leqslant 2ec''L^2H^7 \log(LH).$$

Indeed, under a global monotone coupling, once maximal and minimal evolutions have coalesced, all the evolutions with arbitrary initial conditions have coalesced too. □

Proof of Lemma 3.5.3. Let $h^{\pm}_t$ be the height functions corresponding to the extremal evolutions $M^{\pm}_t$. Each face contributes at most H to the volume difference, so there are at least V_t/H faces where the height difference $h^+_t(f) - h^-_t(f)$ is at least 1. For each of those, by Proposition 3.2.15 there exists a face f^- at distance at most CH where again $h^+_t(f^-) - h^-_t(f^-) \geqslant 1$ and a rotation in M^+_t that decreases the height is possible. We can thus find at least CV_t/H^3 distinct such faces and each of them is the face directly above a non-frozen bead for M^+_t (i.e. a bead that can be moved upward in M^+_t via an elementary rotation). Call B_t the set of such beads, $|B_t| \geqslant CV_t/H^3$.

The global monotone coupling mentioned in the claim is defined as follows. We take two mean-one independent Poisson clocks: when the first one rings we update the beads in even threads, when the second one rings we update beads in odd threads. The beads are updated as follows. Suppose for instance that the first clock rings. Then, sample independently for each transverse edge e and each bead in each even thread a uniform $[0, 1]$ variable $U_b(e)$ (any continuous law would work the same). A bead b in an even thread then chooses the accessible transverse edge e (given the positions of beads in odd threads) with the lowest value of $U_b(e)$. It is easy to check that this defines a monotone coupling between evolutions with any possible initial condition (we emphasize that each evolution uses *the same realization* of the $U_b(e)$ variables to determine the outcome of an update).

We now turn to the estimate of $\nu_t := \liminf_{\delta\to 0} \frac{1}{\delta}\mathbb{E}[(V_{t+\delta} - V_t)^2|\mathcal{F}_t]$. For any bead b, let $V^{(b)}_t$ denote its contribution to the volume, i.e. the difference of the labels of the transverse edges occupied by b in M^+_t and M^-_t. Finally let $A^{(+)}$ (resp. $A^{(-)}$) denote the event that there is an update of even parity

and no update of odd parity (resp. an update of odd parity and no update of even parity) between time t and $t+\delta$ (each has probability $\delta + o(\delta)$) and for each bead b let $A^{(b)}$ be $A^{(\pm)}$ according to the parity of b. We have (since the occurrence of two updates has probability of order δ^2)

$$\frac{1}{\delta}\mathbb{E}[(V_{t+\delta} - V_t)^2 | \mathcal{F}_t] = \mathbb{E}[(V_{t+\delta} - V_t)^2 | \mathcal{F}_t, A^{(+)}] + \mathbb{E}[(V_{t+\delta} - V_t)^2 | \mathcal{F}_t, A^{(-)}] + o(1) \tag{3.26}$$

$$\geqslant \mathrm{Var}[V_{t+\delta} | \mathcal{F}_t, A^{(+)}] + \mathrm{Var}[V_{t+\delta} | \mathcal{F}_t, A^{(-)}] + o(1) = \sum_b \mathrm{Var}(V^{(b)}_{t+\delta} | \mathcal{F}_t, A^{(b)}) + o(1) \tag{3.27}$$

(in the last step, we used the fact that conditionally on $A^{(+)}$, the variables $(V^{(b)}_{t+\delta} - V^{(b)}_t)$ are independent for different b and are zero for b of odd parity). For each bead b four cases can occur:

(i) The set of transverse edges accessible to b in a single update (given the beads of the other parity) is different in M_t^+ and M_t^- and, at least for one of them, it consists of *strictly more than one* transverse edge. We let $B_t^{\neq}$ be the set of such beads. An elementary computation[1] shows that for such bead $\mathrm{Var}(V^{(b)}_{t+\delta} | \mathcal{F}_t, A^{(b)}) \geq \frac{1}{8}$.

(ii) The accessible domain for b is the same in M_t^+ and M_t^- but its positions in the two configurations are different. Let $B_t^{=}$ be the set of such beads. Remark that if the event $A^{(b)}$ occurs, then $V^{(b)}_{t+\delta} = 0$ almost surely while $V^{(b)}_{t+\delta} = V^{(b)}_t \geqslant 1$ if it does not.

(iii) The accessible domain and the initial position of b are the same in M_t^+ and M_t^-. In this case $V^{(b)}_{t+\delta} = V^{(b)}_t = 0$ conditionally on $A^{(b)}$, so these beads give no contribution to the volume variation.

(iv) The accessible domain for b has only a single edge in both M_t^+ and M_t^-. In this case there is no movement possible for b until threads of the opposite parity are updated, so b makes again no contribution conditionally on $A^{(b)}$.

Remark that the set B_t introduced above is included in $B_t^{\neq} \cup B_t^{=}$, so we have $|B_t^{=}| + |B_t^{\neq}| \geq CV_t/H^3$. Indeed, if $b \in B_t$ than it can be moved in M_t^+, which excludes case (iv), and $V_t^b \neq 0$, which excludes case (iii).

Suppose that $|B_t^{\neq}| \geq |B_t^{=}|/(\alpha_{s,t} H)$, with $\alpha_{s,t}$ a slope-dependent constant to be determined later; for $b \in B_t^{\neq}$ we have $\mathrm{Var}(V^{(b)}_{t+\delta} | \mathcal{F}_t, A^{(b)}) \geq \frac{1}{8}$ so the

[1] One can check that the worst case is when the intervals of transverse edges accessible to b in M_t^+ and M_t^- are of the form $\{a, \dots, a+k-1\}$ and $\{a, \dots, a+k\}$. In this case, after an update $V^{(b)} = 0$ with probability $k/(k+1)$ and its average is $1/2$ so the variance in question is at least $(k/4)/(k+1) \geqslant 1/8$.

right-hand size of (3.27) gives, taking the limit $\delta \to 0$,

$$\nu_t \geq \frac{|B_t^{\neq}|}{8} \geq a_{s,t} \frac{V_t}{H^4}$$

for some positive $a_{s,t}$.

Suppose on the contrary that $|B_t^{\neq}| \leq |B_t^{=}|/(\alpha_{s,t} H)$ and (by symmetry) that at least half the beads $b \in B_t^{=}$ are on even threads. After an even update they each contribute $V_{t+\delta}^{(b)} - V_t^{(b)} \leq -1$ so $V_{t+\delta} - V_t \leq -|B_t^{=}|/2 + c_{s,t} H |B_t^{\neq}| \leq -|B_t^{=}|/4$ (we used the fact that, for every b and in particular for $b \in B_t^{\neq}$, $V_{t+\delta}^{(b)} - V_t^{(b)} \leq c_{s,t}\, H$ due to the floor/ceiling at mutual distance H (cf. Proposition 3.2.14) and we chose $\alpha_{s,t} = 4c_{s,t}$). As a consequence, in the limit $\delta \to 0$ (3.26) gives $\nu_t \geq b_{s,t} V_t^2/H^6$ in this case, for some other positive constant $b_{s,t}$. The conclusion follows from $\min(V_t/H^4, V_t^2/H^6) \geqslant V_t/H^6$. □

Remark 3.5.4. *The power H^6 in the lemma is clearly far from optimal. A finer analysis of the contribution of $B_t^{\neq}$ and $B_t^{=}$ would probably improve the power to H^3. We do not follow this route because ultimately the precision of the upper bound is limited by the equilibrium estimate of Theorem 3.2.8 and also because even the bound $|B_t^{=}| + |B_t^{\neq}| \geq CV/H^3$ is certainly far from optimal for a typical configuration.*

A mean curvature motion approach

Given Theorem 3.5.1 and Theorem 3.2.9 on the equilibrium height fluctuations, the proof of the bound $T_{\text{mix}} \leqslant c(\epsilon) L^{2+\epsilon}$ is essentially identical to the proof that $T_{\text{mix}} = O(L^2 (\log L)^{12})$ for the dynamics on the hexagonal lattice with almost-planar boundary conditions, see [CMT12, Th. 2]. Indeed, Theorem 3.5.1 plays the role of [CMT12, Prop. 3] while Theorem 3.2.9 replaces [CMT12, Th. 1]. Therefore, below we will only recall the main ideas, and we skip all details.

Remark 3.5.5. *The reason why in Theorem 3.3.2 we get the L^{ϵ} correction to the mixing time instead of a factor $(\log L)^{12}$ as in [CMT12] is that the fluctuation estimates of Theorem 3.2.9 are a bit weaker than those of [CMT12, Th. 1]: since anyway the exponent 12 is certainly non-optimal (we conjecture the correct value to be 1, cf. the Introduction), we have not tried to refine Theorem 3.2.9 (for instance, one might try to control the exponential moments of the height fluctuations).*

The first step is the following (cf. [CMT12, Prop. 2]):

Step 1 *If the the height function of the initial condition $\xi \in \Omega_{G',m}$ is within distance $L^{\epsilon/10}$ from the almost-planar configuration m (i.e. if $|\xi(f) - h_m(f)| \leqslant L^{\epsilon/10}$ for every $f \in (G')^*$), then (for any given C) for all times*

smaller than L^C the height function stays within distance $2L^{\epsilon/10}$ from m, except with probability $O(L^{-C})$.

This means that, until time L^C, the dynamics is essentially identical to a dynamics with floor/ceiling at mutual distance $O(L^{\epsilon/10})$. Together with Theorem 3.5.1 this implies:

Step 2 *Again if the initial condition ξ is within distance $L^{\epsilon/10}$ from m, after time $L^{2+\epsilon}$ the law of the configuration has small variation distance from equilibrium.*

Therefore, to prove $T_{\text{mix}} \leqslant c(\epsilon)L^{2+\epsilon}$ it is sufficient to prove:

Claim 3.5.6. *At time $c'(\epsilon)L^{2+\epsilon}$ the evolutions started from maximal/minimal configurations are with high probability within distance $L^{\epsilon/10}$ from m (this is the analog of [CMT12, Prop. 1]).*

Consider for instance the evolution h_t^{max} started from the maximal initial configuration $h_{max} \in \Omega_{m,G'}$ and assume for simplicity of exposition that the slope of the quasi-planar boundary condition m is $(s,t) = (0,0)$. Let C_u be a spherical cap whose height is u and whose base is a disk D of radius $\rho_L = L \log L$ with the finite graph G' approximately at its center (recall that the diameter of G' is of order $L \ll \rho_L$). Call R_u the radius of curvature of C_u, which satisfies $(2R_u - u)u = \rho_L^2$ and let $\psi_u(f)$ denote the height of C_u above a face f which is inside D. Then, the key to Claim 3.5.6 is:

Claim 3.5.7. *With overwhelming probability, the height function on $(G')^*$, $f \mapsto h_t^{max}(f)$ is below the deterministic function $f \mapsto \psi_{u_n}(f)$ for all times $t \in [t_n, L^3]$, where $u_n = \rho_L - n$ and the deterministic time sequence t_n is defined by*

$$t_0 = 0, \quad t_n = t_{n-1} + R_{u_n} L^{\epsilon/2}, \quad n \leqslant M := \rho_L - L^{\epsilon/10}.$$

Indeed, it is easy to verify that $R_{u_n} \sim \rho_L^2/(2u_n)$ and (similarly to [CMT12, Eq. (6.14)]) that $t_M = O(L^{2+\epsilon})$. Therefore, if we show the above claim for n up to M, we deduce that at some time $O(L^{2+\epsilon})$ the configuration is within distance $u_M = L^{\epsilon/10}$ from the flat configuration m, and Claim 3.5.6 follows.

For $n = 0$, the statement of Claim 3.5.7 is true (deterministically, not just with high probability, since the maximal height at a face $f \in G'$ is of order $L \ll \rho_L$). Suppose we want to deduce claim $n+1$ from claim n, and look for definiteness only at a face f at the center of the disk D. Consider a disk D_{n+1} centered at f, of radius $R_{u_n}^{1/2} L^{\lambda\epsilon}$ with λ to be chosen later: by monotonicity, given the claim at step n, we can replace the evolution h_t^{max} restricted to D_{n+1}, in the time interval $[t_n, L^3]$, by an evolution where:

- the configuration outside D_{n+1} is frozen and equals some height function which, on the boundary of D_{n+1}, is within distance $O(1)$ from the function $\psi_{u_n}(\cdot)$; note that for f' at the boundary of D_{n+1} one has $\psi_{u_n}(f') \approx u_n - (1/2)L^{2\lambda\epsilon}$;
- the "initial" height function at time t_n in D_{n+1} approximates within $O(1)$ the function $\psi_{u_n}(\cdot)$.

By Step 2, the time such dynamics takes to reach equilibrium is $O(R_{u_n}L^{20\lambda\epsilon})$, much smaller than $t_{n+1} - t_n$ if $\lambda < 1/40$, so that at time t_{n+1} the configuration is essentially at equilibrium (with the above specified boundary conditions around D_{n+1}). Next, elementary geometry and Theorem 3.2.9 shows that, at equilibrium, the height function at f is with overwhelming probability lower than $u_n - 1 = u_{n+1}$: this is because, as we remarked above, the boundary height around the boundary of D_{n+1} is approximately $u_n - (1/2)L^{2\lambda\epsilon}$. We deduce therefore that, with high probability, $h_t^{max}(f) \leqslant u_{n+1} = \psi_{u_{n+1}}(f)$ for $t \in [t_{n+1}, L^3]$ and a similar argument works for any other face $f \in (G')^*$. The claim at step $n+1$ is then proven.

Gaseous phases and entropic repulsion

Theorem 3.3.2 has been formulated for three specific - though quite natural - graphs. While, as explained in Remark 3.3.4, our method can be extended to a wider class of graphs, there is no hope it works for a general infinite bipartite graph. We would like to convince the reader there is a good reason for this. One of the main steps of our argument (cf. Section 3.4.2) is to prove that, given two height functions $h^1 \leqslant h^2$, after a step of the (fast) dynamics the mutual volume has not increased in average. The proof of Proposition 3.4.10 shows that this is true (for the hexagonal, square and square-hexagon graphs), *independently of the boundary conditions* (in particular, for almost-planar conditions, independently of the slope (s,t)) *and independently also of the presence of floor/ceiling constraints*. While obtaining the mixing time upper bound of order $L^{2+\epsilon}$ requires considerable extra work, the volume decrease result implies rather directly [LRS01] that the mixing time is at most polynomial in L, since (i) the maximal volume difference between two configurations is of order L^3 and (ii) the ratio of mixing times of the fast and original dynamics is at most polynomial in L.

Now take for instance the square-octagon graph, with almost-planar boundary conditions of slope $(0,0)$. As we remarked in Section 3.2.2, in this situation the infinite-volume Gibbs measure $\mu_{0,0}$ corresponds to a "gaseous" (or "rigid") phase: the height $h(f)$ at a face f has bounded variance and the random variables $h(f), h(f')$ are essentially independent for f, f' far away. This is very reminiscent of the situation in the classical $(2+1)$-dimensional Solid-on-Solid (SOS) interface model [Tem52] at low temperature $1/\beta$ [BW82]. Let us just recall that the SOS model describes an

interface with integer heights $\phi(x)$, labelled by $x \in \mathbb{Z}^2$, with measure proportional to $\exp(-\beta \sum_{|x-y|=1} |\phi(x) - \phi(y)|)$ and zero boundary conditions $\phi \equiv 0$ around a $L \times L$ box. Recently, it was proved in [CLM$^+$] that, when a floor at height zero is present (i.e. when heights are constrained to be non-negative) the mixing time of the Glauber dynamics for the SOS model is exponentially large in L. This effect is due to the rigidity of the interface *and* to the presence of the floor, which pushes the interface to a height of order $\log L$ (entropic repulsion [BMF82]). If a "gaseous" phase does behave like a SOS interface, which is very likely, then that the dimer dynamics for the square-octagon graph with almost-planar b.c. of $(0, 0)$ slope and floor at height zero has also a mixing time growing exponentially with L. As a consequence, for the reasons exposed above, the volume decrease cannot hold as stated in proposition 3.4.10 (i.e. for general floor/ceiling constraint and boundary condition) for the square-octagon graph (it cannot be true that the mutual volume between two arbitrary height functions decreases on average, under some reasonable "fast dynamics", for the square-octagon graph with general boundary conditions and floor/ceiling constraints). If on the other hand the volume decrease holds only for particular boundary conditions and floor/ceiling, then the mathematical mechanism for that must be considerably more subtle than in Proposition 3.4.10.

3.5.2 Mixing time lower bound

In this section we establish the mixing time lower bound of Theorem 3.3.2. Thanks to Proposition 3.4.7, it is enough to show that at time $T_0 = \epsilon L^2$ the asynchronous dynamics started from the maximal configuration is still at variation distance at least $1/(2e)$ from equilibrium.

The strategy is the following. First, we define (for each of the three types of graph in question) a special (very non-planar) boundary condition $p \in \Omega$ and finite domain $W_L \subset G$ of diameter of order L for which it is easy to prove that, starting from the maximal configuration, the drift of the volume is lower bounded by $-cL$. Therefore, after time $T_0 = \epsilon L^2$ the eroded volume is at most $c\epsilon L^3$ and the configuration (call it $\tilde{M}_{T_0}$) is still away from its (non-flat) equilibrium shape. Next, a monotonicity/coupling argument allows to deduce that, again at time T_0, the configuration M_{T_0}, evolving this time in our original domain G' with the almost-planar boundary condition m we are interested in, is above $\tilde{M}_{T_0}$ and that it is also far from its typical (flat, this time) equilibrium shape.

Pyramids

For each of the three graphs (square, hexagon, square-hexagon) consider the special matching $p \in \Omega$ ("p" for "pyramid" for reasons to become clear soon) of the whole G, defined through Fig. 3.8. Note that in all three cases

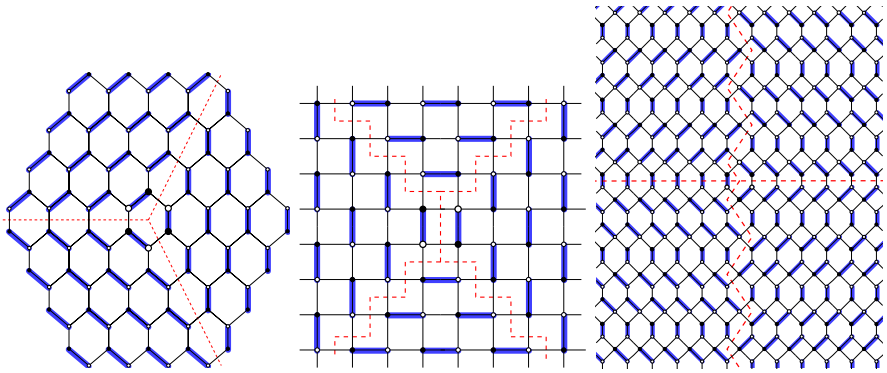

Figure 3.8: "Pyramids" for the square, hexagon and square-hexagon graphs. The matchings are intended to extend over the whole infinite graph. The dotted lines separate the domains tiled with different periodic matchings of extremal slope.

G is divided into a finite number of infinite domains, separated by dotted lines (three domains for the hexagon graph and four for the square and square-hexagon graph): each domain corresponds to a vertex in the Newton polygon N of G and it is tiled with the periodic matching corresponding to that vertex (cf. Fig. 3.1). The central face f_0 is assumed to contain the origin of $\mathbb{R}^2$ and we fix the height there to 0. The large-scale height function $\mathbb{R}^2 \ni x \mapsto H(x)$, obtained by rescaling the lattice spacing and the heights by $1/L \to 0$ while keeping f_0 at the origin of the plane can be described as follows. For each vertex v of N, take the plane of the corresponding slope which contains the origin of $\mathbb{R}^3$, and let s_v be the half-space below it. The intersection of all the s_v with v ranging over the vertices of N is clearly a pyramid Π with vertex at the origin of $\mathbb{R}^3$. The boundary of Π gives the height function $H(\cdot)$. It is possible to prove (but we will not need this directly) that the discrete height function associated to matching p is given by $h(f) = -D(f, f_0)$, cf. Section 3.2.5. This observation could be used to build "pyramids" in a systematic way, for other graphs.

Remark 3.5.8. *For the hexagonal lattice, the pyramid p just corresponds (in terms of stepped surfaces, cf. Fig. 3.2) to the surface of the corner of an infinite cube with vertex at the origin of $\mathbb{R}^3$.*

Next, we need to introduce a finite sub-graph $W_L \subset G$, with the face f_0 in the center. This is defined through Fig. 3.9: for the hexagonal lattice this is the portion of G included in a $(2L+1) \times (2L+1) \times (2L+1)$ hexagon, for the square lattice it is a $(2L+1) \times (2L+1)$ square and for the square-hexagon lattice it is the portion of G contained in a suitable lozenge (delimited by a full line in the picture) whose diagonals contain $2L+1$ hexagons. Note that the maximal configuration in Ω_{p,W_L} is just p: indeed, just observe that none

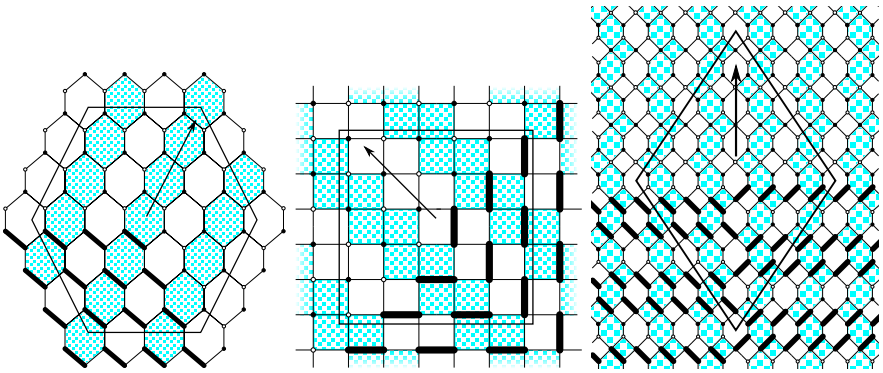

Figure 3.9: The sub-graph W_L and the associated beads of configuration p. Threads are in light blue and white and beads are in solid black. Arrows mark the orientation of threads.

of the beads in W_L can be moved to a lower transverse edge in the same thread.

Proposition 3.5.9. *Consider the asynchronous fast dynamics on the finite graph W_L defined above, with "pyramid" boundary condition p. Let M_t^{max} (resp. M_t^{eq}) denote the state at time t of the dynamics started from the maximal configuration, which is nothing but p (resp. from the equilibrium uniform measure π_{p,W_L}) and let $\mathcal{F}_t$ be the sigma-algebra generated by $\{M_s^{max}, M_s^{eq}, s \leqslant t\}$. Remark that M_t^{eq} is stationary. Let $V_t = \sum_{f\in W_L}[h_{M_t^{max}}(f) - h_{M_t^{eq}}(f)]$. Then, for every $t \geq t'$*

$$\mathbb{E}[V_t - V_{t'}|\mathcal{F}_{t'}] \geq -CL(t-t')$$

for a certain constant C.

Proof. The two evolutions can be coupled so that the one started from p always dominates the stationary one. Therefore, it is sufficient to prove that, given two height functions $h^- \leqslant h^+$, the initial-time drift of their volume difference, see (3.22), is lower bounded by $-CL$. Let $\partial^- W_L$ denote the set of faces in W_L at graph-distance at most r from the exterior of W_L and assume the following

Claim 3.5.10. *There exists some finite r such that the initial-time volume drift is zero whenever h^+ and h^- differ at a single face $f \in W_L \setminus \partial^- W_L$.*

As in the proof of Proposition 3.4.10, take a sequence of configurations $h_{(0)}, \ldots, h_{(k)}$ such that $h_{(0)} = h^+, h_{(k)} = h^-$ and $h_{(i)}$ is obtained by $h_{(i-1)}$ via a rotation that decreases the height at some face f. Along the sequence $\{h_{(i)}\}_i$, each face in $\partial^- W_L$ can be rotated at most a number $c(r)$ of times (since its height difference w.r.t. a face outside W_L at distance r can take at most $c(r) = 2r+1$ values). Then write the volume difference between h^+

and h^- as a telescopic sum of volume differences between $h_{(i)}$ and $h_{(i-1)}$: the terms corresponding to a rotation in $W_L \setminus \partial^- W_L$ give zero drift (cf. Claim 3.5.10) and those with rotation in $\partial^- W_L$ give a contribution lower bounded by -1 (cf. Remark 3.4.11). Then, one gets that the volume drift is lower bounded by $-c(r)$ times the number of faces in $\partial^- W_L$, which is of order L, and Proposition 3.5.9 follows. □

Proof of Claim 3.5.10. In order to follow, the reader should have in mind the proof of Proposition 3.4.10: there we proved that the initial-time volume drift is zero except for "boundary effects", and here we show that indeed the boundary effects are not there sufficiently far away from the boundary. As in the proof of Proposition 3.4.10, we consider for definiteness only the square-hexagon lattice, the other two cases being very similar. Note that there are $2L+1$ threads intersecting W_L (we label them $\gamma_i, i = -L, \dots, L$ from left to right) and that thread γ_i contains $L+1-|i|$ beads in W_L (we label them $b^i_j, j = 1, \dots, L+1-|i|$ from the lowest to the highest with respect to the orientation of the thread, see Fig. 3.10(a) for a schematic drawing). This geometric structure is essential for the proof of the Claim and, as the reader can check from Fig. 3.9, it is common to the "pyramids" of the three types of graphs. The effect of the boundary of W_L is simply that the beads of thread γ_i are constrained to stay strictly below some transverse edge $e^+_i \in \gamma_i$ and strictly above some transverse edge $e^-_i \in \gamma_i$ (such edges are surrounded by circles in Fig. 3.10(a)).

By symmetry, we assume that the face f belongs to γ_i for some $-L+r \leqslant i \leqslant 0$ (the case $-L \leqslant i < -L+r$ is excluded otherwise $f \in \partial^- W_L$) and assume for definiteness that f is a hexagonal face (the argument is essentially identical when f is a square). Then, h^+ is obtained from h^- by moving a bead b^i_j one "transverse edge" lower along thread γ_i (with the notations of the proof of Proposition 3.4.10 (Case 1), $b = b^i_j$ moves from e_1 to e_2). We need to show that, if $f \in W_L \setminus \partial^- W_L$, when threads of the opposite parity than i are updated while the threads with the same parity as i are frozen, thread γ_{i-1} contributes exactly $1/2$ to the change of volume (the same holds for γ_{i+1}).

We distinguish two cases, represented respectively in Figures 3.10(b) and 3.10(c):

- $1 < j < L+1-|i|$. Recall that from Section 3.4.2 that, according to the position of b^{i-2}_{j-1} (which was called b' there), either b^{i-1}_j (which was called b^+) has one more available transverse edge (called e_7) when the configuration before the update is h^+ rather than h^-, or otherwise b^{i-1}_{j-1} (which was called b^-) has one more available transverse edge (again e_7) starting from h^- rather than from h^+. Say that the former is the case. As discussed in Remark 3.4.11, the volume change due to thread γ_{i-1} is $1/2$ unless the boundary conditions prevent b^+ from moving

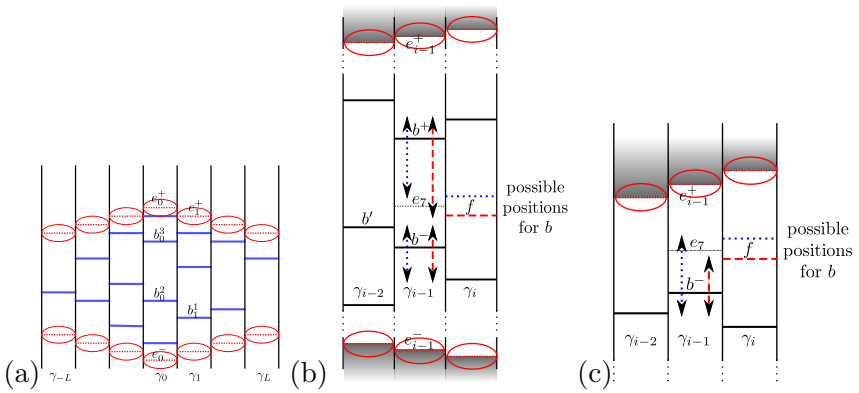

Figure 3.10: (a): A schematic view of the threads and beads in W_L (here, $L = 3$). (b): The case $1 < j < L + 1 - |i|$. Here, $i = 0$ and $j = 3$. Boundary conditions only prevent beads from entering the gray region outside W_L, so they cannot prevent b^+ from moving down to e_7. (c): The case $j = L+1-|i|$. If $f \in \partial^- W_L$ then e_7 can be at e^+_{i-1}, in which case it is not an allowed bead position; otherwise, e_7 is in W_L (since it is at distance of order 1 from f) and b^- can reach such position.

down to e_7, i.e. if e_7 is not higher than e^-_{i-1}: this however cannot be the case, since e_7 is clearly higher than $b^- = b^{i-1}_{j-1}$ which is itself higher than e^-_{i-1} (here we use that $j - 1 \geqslant 1$, i.e. the bead b^{i-1}_{j-1} is in W_L).

- $j = L + 1 - |i|$ (or $j = 1$, by symmetry). The argument is slightly different since this time neither $b^+ = b^{i-1}_j$ nor $b' = b^{i-2}_{j-1}$ exist (since $j > L + 1 - |i - 1|$), or equivalently we can imagine that b^+, b' are higher than e^+_{i-1}, e^+_{i-2} respectively (i.e. they are outside W_L). Since the edge e_3 of Fig. 3.6 is at distance of order 1 from f, we deduce that if f is at distance larger than some finite r from the boundary of W_L then b' is above e_3. In this case, from Section 3.4.2, we get that b^- has one more available position (transverse edge e_7) when the update of γ_{i-1} is performed starting from configuration h^- rather than h^+. It is clear from Fig. 3.9 and 3.6 that, if f is at distance at least r, with r sufficiently large, from the boundary of W_L, the edge e_7 is lower than e^+_{i-1}, so there is no obstruction for b^- to actually reach it.

□

Lower bound on mixing time

Recall Definition 3.2.2: the finite graph G' we are interested in is the portion of G enclosed in LU, where U is a smooth bounded domain of $\mathbb{R}^2$, which without loss of generality we can assume to include the origin in its interior

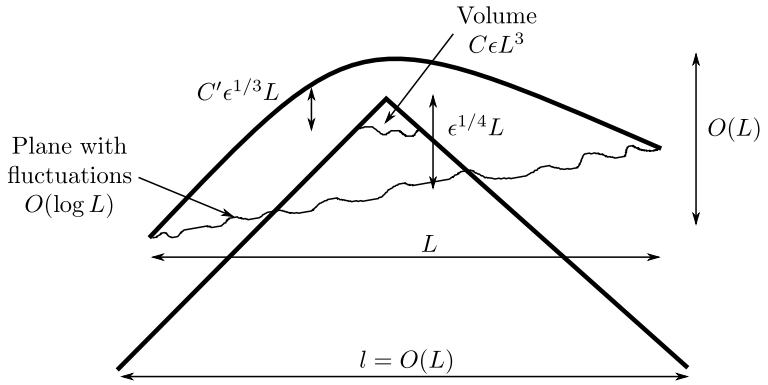

Figure 3.11: An illustration of the proof of the lower bound. The pyramid and, above it, the maximal configuration with planar boundary condition m. The top of the pyramid is $O(L)$ above the typical "almost-planar" equilibrium configuration (wiggled line). After a time ϵL^2, the pyramid has only lost a volume ϵL^3, so its top is still well above the "almost-planar" surface. By stochastic domination, the same holds for the maximal evolution with boundary condition m.

(so that f_0 is at distance of order L from the boundary of G'). Now consider the finite graph $W_\ell \subset G$ defined in Section 3.5.2, and choose ℓ to be the minimal integer such that $W_\ell \supset G'$ (it is clear that $\ell = O(L)$).

Consider first the evolution in W_ℓ with boundary condition p (and started from the maximal configuration p): by Proposition 3.5.9 and Markov's inequality we have that at time $T_0 = \epsilon L^2$,

$$\mathbb{P}(h_{T_0}(f_0) \leqslant -\epsilon^{1/4}L) = O(\epsilon^{1/4}) \tag{3.28}$$

(indeed observe that, if $h(f_0) < -\epsilon^{1/4}L$ then the eroded volume is at least $const \times (\epsilon^{1/4}L)^3 \simeq LT_0\epsilon^{-1/4}$ while the average eroded volume is of order LT_0).

Now recall that the boundary condition m we are interested in is almost-planar of slope (s,t): up to an irrelevant global change of the heights by an additive constant, we can assume that its height function $h_m(\cdot)$ is within $O(1)$ from a plane of slope (s,t) and containing the point $(0,0,-2\epsilon^{1/4}L)$. If $h_p(\cdot)$ is the height function associated to the "pyramid" matching p and if ϵ is sufficiently small, $h_m(f) \geqslant h_p(f)$ for every f along the boundary of G' (the height difference is actually of order L). To see this, just recall that the slope of the height function associated to p is negative and maximal (in absolute value) along any straight line starting from f_0, while the slope (s,t) is in the interior of the Newton polygon, so it is not an extremal slope (see Figure 3.11). Note that ϵ has to be taken very small if the slope (s,t) is very close to ∂N.

We have then that, by monotonicity, the evolution in G', with boundary

condition m and started from the maximal configuration, is stochastically higher than the restriction to G' of the evolution in W_ℓ with boundary condition p. As a consequence, for the former dynamics we have that (3.28) still holds. Thanks to Theorem 3.2.9, at equilibrium (with almost-planar boundary condition m) the typical equilibrium height at f_0 is around $-2L\epsilon^{1/4}$ and the probability that it is higher than $-L\epsilon^{1/4}$ tends to zero with L. This suffices to conclude that at time T_0 the variation distance from equilibrium is still close to 1. □

3.A Gaussian behavior of fluctuations

In this section we prove Theorem 3.2.8. The proof is quite independent of the rest of the paper. The main tools are the results from [KOS06] that were stated in Section 3.2.2. The proof is very similar to that of [Ken07, Section 7] but the setting here is more general and we give a more explicit control of the "error terms".

From the definition of height function, we know that $h(f) - h(g)$ is determined by the dimers crossed by a path from f to g. In particular, for the square, hexagon and square-hexagon graphs, assume that f and g are on the same thread (cf. Section 3.4.1): then, $h(f) - h(g)$ is determined just by the number $N_{f,g}$ of such dimers. Label $e_1, \dots, e_k$ the transverse edges between f and g: it is easy to realize, using Theorem 3.2.4, that the set of occupied edges among the e_i forms a determinantal point process: in other words, the probability $\mu_{s,t}(e_{i_1} \in M, \dots, e_{i_m} \in M)$ can be written as $\det(A(i_a, i_b)_{1 \leqslant a,b \leqslant m})$ for a certain $k \times k$ matrix A directly related to $K_{s,t}^{-1}$. Now, it turns out [Ken09] that for the hexagonal lattice such matrix is Hermitian. In this case, a well-known theorem by Costin and Lebowitz (cf. for instance [Sos00]) implies that $N_{f,g}$ is distributed like the sum of independent Bernoulli random variables, whose parameters are the eigenvalues of A. In particular, if the variance of $N_{f,g}$ diverges as $k \to \infty$, the variable $[N_{f,g} - \mu_{s,t}(N_{f,g})]/\sqrt{\mathrm{Var}(N_{f,g})}$ tends to $\mathcal{N}(0,1)$. Unfortunately, for the square and square-hexagon graph the matrix A is not Hermitian and has complex eigenvalues, the Costin-Lebowitz theorem does not apply and the asymptotic moments have to be computed otherwise.

3.A.1 Choice of paths

Fix an integer k. We are interested in the behavior of

$$\mu_{s,t}\left[M(f,f')^k\right] = \mu_{s,t}\left(\left[\left(h(f) - \mu_{s,t}(h(f))\right) - \left(h(f') - \mu_{s,t}(h(f'))\right)\right]^k\right) \tag{3.29}$$

when the distance between f and f' goes to infinity. Remark that for any path C on G^* from f to f' that only crosses edges in the positive direction[2], $h(f') - h(f)$ is exactly the difference between the number of dimers crossed by the random matching minus those crossed by the reference matching, so $M(f, f') = \sum_e [1_{e \in M} - \mu_{s,t}(e \in M)]$ with the sum over all edges crossed by C. We will compute moments of higher order by taking k such paths $C_1, \dots, C_k$:

$$\mu_{s,t}\left[M(f,f')^k\right] = \mu_{s,t}\Big[\sum_{e_1 \in C_1} (\delta_{e_1} - \mu_{s,t}(\delta_{e_1})) \dots \sum_{e_k \in C_k} (\delta_{e_k} - \mu_{s,t}(\delta_{e_k}))\Big] \tag{3.30}$$

where we write δ_e for $1_{e \in M}$.

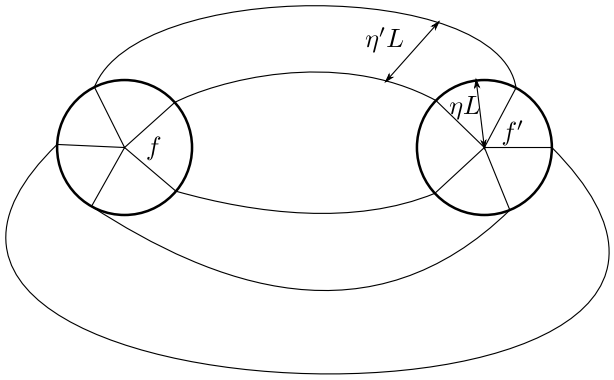

Figure 3.12: The paths $C_1, \dots, C_k$ (here $k = 5$) along which is computed the height, displayed at large scale so that they look like continuous curves. They are macroscopically away from each other except near f and f' where they are periodic (so that on large scale they look linear).

In principle we can choose the paths $C_1 \dots, C_k$ freely as long as they only cross edges in the positive direction. In practice, for reasons that will be clear later we will adopt the following construction, illustrated in Fig. 3.12. Fix $\eta, \eta' > 0$. Inside balls of radius ηL around f and f', the C_i are portions of length ηL of infinite periodic paths (cf. Definition 3.2.1) and have mutually different asymptotic directions. Outside of these balls the paths stay at distance at least $\eta' L$ of each other and their length is of order L. Furthermore η, η' and the infinite periodic paths depend on k but not on L.

3.A.2 Exact simplifications

Fix k edges $e_1 = (\mathrm{w}_1, \mathrm{b}_1) \in C_1, \dots, e_k = (\mathrm{w}_k, \mathrm{b}_k) \in C_k$, and consider the corresponding term (written $\Pi(e_1, \dots, e_k)$) of the sum (3.30).

[2]exercise: prove that such a path exists for every f, f'

We write δ_i for δ_{e_i}, $K_{i,j}^{-1}$ for $K_{s,t}^{-1}(\mathrm{b}_i, \mathrm{w}_j)$ and K_{ij} for $K_{s,t}(\mathrm{w}_i, \mathrm{b}_j)$. We also write S_k the set of permutations of $\{1, \dots, k\}$, $\tilde{S}_k$ the set of permutations without fixed points and $\tilde{S}_k^2$ those of order 2. Given $\sigma \in S_k$, we denote $\epsilon(\sigma)$ it signature.

First we express each term $\Pi(e_1, \dots, e_k)$ of the sum (3.30) as a sum over permutations with no fixed points.

Lemma 3.A.1. *Given edges $e_1, \dots, e_k$ as above, we have*

$$\Pi(e_1, \dots, e_k) \equiv \mu_{s,t}[\prod_{n=1}^{k}(\delta_n - \mu_{s,t}(\delta_n))] = \prod_{n=1}^{k} K_{nn} \sum_{\sigma \in \tilde{S}_k} \epsilon(\sigma) \prod_{n=1}^{k} K^{-1}_{n\sigma(n)}. \tag{3.31}$$

This is exactly like [Ken00, Lemma 21].

Now we replace $K^{-1}_{n\sigma(n)}$ by its asymptotic expression from Theorem 3.2.6. To lighten notations we use the following conventions. Recall that $e_i = (\mathrm{w}_i, \mathrm{b}_i)$ and write (in a unique way) $\mathrm{b}_i = \hat{\mathrm{b}}_i + (x_i, y_i), \mathrm{w}_i = \hat{\mathrm{w}}_i + (x'_i, y'_i)$ with $\hat{\mathrm{b}}_i, \hat{\mathrm{w}}_i$ in the fundamental domain G_1 and $(x_i, y_i) \in \mathbb{Z}^2, (x'_i, y'_i) \in \mathbb{Z}^2$. Note that $(x_i - x'_i, y_i - y'_i)$ is a vector of order 1. Then let $U_i := U_{s,t}(\hat{\mathrm{b}}_i)$, $V_j := V_{s,t}(\hat{\mathrm{w}}_j)$ and $\phi_i := \phi(x_i, y_i)$, $x_{ij} = x'_i - x_j$ and $y_{ij} = y'_i - y_j$. We then get

$$\begin{aligned}\frac{\Pi(e_1, \dots, e_k)}{\prod_{n=1}^{k} K_{nn}} &= \sum_{\sigma \in \tilde{S}_k} \epsilon(\sigma) \prod_{n=1}^{k} \Bigg(i \frac{U_n V_{\sigma(n)} w_0^{x_{n\sigma(n)}} z_0^{y_{n\sigma(n)}}}{2\pi(\phi_n - \phi_{\sigma(n)})} \\ &\qquad + \text{complex conjugate} + O\Big(\frac{1}{x_{n\sigma(n)}^2 + y_{n\sigma(n)}^2}\Big)\Bigg) \qquad (3.32) \\ &\equiv \sum_{\sigma \in \tilde{S}_k} \epsilon(\sigma) \prod_{n=1}^{k} (A_{n,\sigma(n)} + A^*_{n,\sigma(n)} + R_{n,\sigma(n)}).\end{aligned}$$

We then expand the product over n and we call "dominant terms" those such that no R factors appear and, in addition, such that within each cycle of σ either only A terms or only A^* terms appear. All other terms of the expansion are called "error terms". We first show that in the dominant terms we can assume that all cycles of the permutation σ are of order two. This comes from the following result:

Lemma 3.A.2. *If $\tilde{S}_\ell^c$ denotes the set of cyclic permutations of $\{1, \dots, \ell\}$, then*

$$\begin{aligned}\sum_{\sigma \in \tilde{S}_\ell^c} \epsilon(\sigma) \prod_{n=1}^{\ell} A_{n\sigma(n)} &= \sum_{\sigma \in \tilde{S}_\ell^c} \epsilon(\sigma) \prod_{n=1}^{\ell} \frac{i}{2\pi} \frac{U_n V_{\sigma(n)} w_0^{x_{n\sigma(n)}} z_0^{y_{n\sigma(n)}}}{\phi_n - \phi_{\sigma(n)}} \\ &= 0 \left(= \sum_{\sigma \in \tilde{S}_\ell^c} \epsilon(\sigma) \prod_{n=1}^{\ell} A^*_{n\sigma(n)} \right) \qquad (3.33)\end{aligned}$$

if $\ell > 2$.

Proof. Recall that $\epsilon(\sigma)$ is constant for cyclic permutations, thus it is enough to show that

$$\sum_{\sigma\in\tilde{S}_\ell^c}\prod_n \frac{U_nV_{\sigma(n)}w_0^{x_{n\sigma(n)}}z_0^{y_{n\sigma(n)}}}{\phi_n-\phi_{\sigma(n)}} = \prod_n (U_nV_n)\, w_0^{\sum_i(x_i'-x_i)} z_0^{\sum_i(y_i'-y_i)} \sum_{\sigma\in\tilde{S}_\ell^c}\prod_n \frac{1}{\phi_n-\phi_{\sigma(n)}} = 0 \tag{3.34}$$

as soon as $\ell > 2$. The second equality is purely algebraic and is given in [Ken07, Lemma 7.3]. □

Decompose a permutation σ into cycles and remark that in equation (3.31) and (3.32), the sum over permutations with a given cycle structure can be factorized as a product over cycles. Then, Lemma 3.A.2 implies that the dominant terms in

$$\sum_{\sigma\in\tilde{S}_k\setminus\tilde{S}_k^2}\epsilon(\sigma)\prod_{n=1}^k (A_{n,\sigma(n)}+A^*_{n,\sigma(n)}+R_{n,\sigma(n)})$$

exactly cancel each other so only "error terms" are left (recall that $\tilde{S}_k^2$ is the set of permutations without fixed points, and with only cycles of order 2). Altogether, we have proven (cf. (3.32))

$$\mu_{s,t}(M(f,f')^k) = \sum_{e_1,\dots,e_k}\sum_{\sigma\in\tilde{S}_k^2}\epsilon(\sigma)\left(\prod_{n=1}^k K^{-1}_{n\sigma(n)}\right)\left(\prod_{n=1}^k K_{nn}\right) + \text{error terms.} \tag{3.35}$$

In particular, if k is odd then there are only "error terms" because $\tilde{S}_k^2$ is empty, while, using equation (3.31) separately for all pairs,

$$\mu_{s,t}(M(f,f')^{2k}) = \sum_{\sigma\in\tilde{S}_{2k}^2}\mu_{s,t}[M(f,f')^2]^k + \text{error terms} \tag{3.36}$$

$$= g_{2k}\left[\mathrm{Var}_{\mu_{s,t}}(h(f)-h(f'))\right]^k + \text{error terms} \tag{3.37}$$

where $g_{2k} = (2k)!/(2^k k!)$ is the Gaussian moment of order $2k$. We will prove in the following section that the error terms are negligible, i.e. give a contribution to $\mu_{s,t}(M(f,f')^k)$ that is much smaller than $[\mathrm{Var}_{\mu_{s,t}}(h(f)-h(f'))]^{k/2}$.

3.A.3 Controlling the "error terms"

Recall that there are two kinds of "error terms" in the expression (3.35) for the k-th moment of the height fluctuation: those which contain both A and

A^* factors within the same cycle of σ but but no R factor (recall (3.32)), and those which contain R factors. The former will be shown to be "small" because they oscillate and give a negligible contribution when summed over $e_1, \dots, e_k$, while the latter are small because their denominator contains at least one factor $|\phi_j - \phi_{\sigma(j)}|$ more than in the dominant terms. For simplicity purpose we assume in the following that σ contains only a single cycle. The general case is essentially the same since an error term can be factorized as a product over the cycles of σ.

We will need the following elementary estimates:

Lemma 3.A.3. *Define*

$$\begin{aligned} F_k(L) &= \sum_{d_1,\dots,d_k \leqslant L} \frac{1}{(d_1+d_2)\dots(d_k+d_1)}, \\ \tilde{F}_k(L) &= \sum_{d_1,\dots,d_k \leqslant L} \frac{1}{(d_1+d_2)\dots(d_{k-1}+d_k)}. \end{aligned} \tag{3.38}$$

One has $\tilde{F}_k(L) \leqslant LF_{k-1}(L)$ *and* $F_k(L) = O((\log L)^{\lfloor k/2 \rfloor})$.

Proof. To get $\tilde{F}_k(L) \leqslant LF_{k-1}(L)$, writing $F_{k-1}(L)$ either as a sum over $d_1, \dots, d_{k-1}$ or over $d_2, \dots, d_k$ it is not difficult to see that

$$2LF_{k-1}(L) - 2\tilde{F}_k(L) = \sum_{d_1,\dots,d_k} \frac{1}{(d_1+d_2)\dots(d_{k-2}+d_{k-1})} \frac{(d_1-d_k)^2}{(d_1+d_{k-1})(d_2+d_k)(d_{k-1}+d_k)} \geqslant 0$$

(use the fact that the denominator is symmetric under the exchange of d_1 with d_k). As for $F_k(L) = O((\log L)^{\lfloor k/2 \rfloor})$, this is an easy computation if $k = 2$. By induction on k, the proof is concluded if we show that $F_k(2L) - F_k(L) = O(kF_{k-2}(L))$ for $k \geqslant 4$ and $F_k(2L) - F_k(L) = O(1)$ for $k = 3$. To see this, one notes that the dominant contribution to $F_k(2L) - F_k(L)$ comes from the terms where one of the variables is in $[L, 2L]$ while all the others are smaller than L: altogether, this gives

$$\sum_{i=1}^{k} \sum_{d_1,\dots d_k \leq L} \frac{1}{(d_1+d_2)\dots(d_{i-1}+(L+d_i))((L+d_i)+d_{i+1})\dots(d_k+d_1)} \leq kL\tfrac{1}{L^2}\tilde{F}_{k-1}(L).$$

For $k > 3$ use $\tilde{F}_{k-1}(L) \leqslant LF_{k-2}(L)$ and for $k = 3$ note that $\tilde{F}_2(L) = O(L)$. □

The first remark about the computation of $\mu_{s,t}(M(f,f')^k)$ is that we can restrict ourselves to the cases where either all edges e_i are in the ball $B_f(\eta L)$ of radius ηL around either f or in the analogous ball around f'.

Indeed, call d_i the distance of e_i from f and observe that, since the map ϕ is non-degenerate and the paths C_i are almost linear in $B_f(\eta L)$, one can bound $|\phi_i - \phi_j|$, from above and below, by a constant times $(d_i + d_j)$. Then the sum of (3.32) with, for example, $e_1, \dots, e_{k-1}$ in $B_f(\eta L)$ and e_k out of $B_f(\eta L)$ is of order $(1/L)\tilde{F}_{k-1}(\eta L) \leqslant F_{k-2}(\eta L) = O((\log L)^{\lfloor k/2 \rfloor - 1}) \ll [\mathrm{Var}_{\mu_{s,t}}(h(f) - h(f'))]^{k/2}$. Terms with more than one e_i outside of $B_f(\eta L)$ are even smaller. To fix ideas, we will assume that all e_i are in $B_f(\eta L)$.

Consider now an "error term" containing a factor R (if it contains more than one, the argument is similar). Summing over e_i, this gives a contribution of order

$$\begin{aligned}
&\sum_{d_1,\dots,d_k \leq \eta L} \frac{1}{(d_1+d_2)\dots(d_k+d_1)} \frac{1}{d_1+d_2} \\
&\qquad \leq \sum_{d_2,\dots,d_k} \frac{1}{(d_2+d_3)\dots(d_{k-1}+d_k)} \sum_{u=d_2}^{\infty} \frac{1}{d_k u^2} \\
&\qquad \leq \text{const} \times \sum_{d_2,\dots,d_k} \frac{1}{(d_2+d_3)\dots(d_k+d_2)} \frac{d_2+d_k}{d_2 d_k} \qquad (3.39) \\
&\qquad = O(F_{k-1}(\eta L)) \\
&\qquad \ll [\mathrm{Var}_{\mu_{s,t}}(h(f) - h(f'))]^{k/2}.
\end{aligned}$$

We still have to deal with the error terms including no R factors but both A and A^* within the same cycle of σ. Recall that for simplicity of exposition that σ is assumed to have a single cycle. Omitting the product of the factors $\pm i/(2\pi)$, these terms are of the form

$$\sum_{e_1,\dots,e_k} e^{i[r(x_1,\dots,x_k)+s(y_1,\dots,y_k)]} C(e_1,\dots,e_k) \prod_{i \in J} \frac{1}{\phi_i - \phi_{\sigma(i)}} \prod_{i \in J^c} \frac{1}{{\phi^*}_i - {\phi^*}_{\sigma(i)}} \qquad (3.40)$$

where e_j runs over the edges crossed by path C_j and:

- J (resp. J^c) is the set of indices $n \in \{1, \dots, k\}$ for which we take $A_{n\sigma(n)}$ (resp. $A^*_{n\sigma(n)}$) in the expansion of the product (3.32). Note that both J and J^c are non-empty, proper subsets of $\{1, \dots, k\}$;
- $C(e_1, \dots, e_k)$ depends only on the types of the k edges (two edges being of the same type if they are related by a translation of $\mathbb{Z}^2$):

$$C(e_1,\dots,e_k) = \prod_{i \in J} \left(U_i V_{\sigma(i)} w_0^{(x'_i - x_i)} z_0^{(y'_i - y_i)} \right) \prod_{i \in J^c} \left(U_i^* V^*_{\sigma(i)} w_0^{-(x'_i - x_i)} z_0^{-(y'_i - y_i)} \right);$$

- r, s are linear functions: if $J' = \{i \in J : \sigma^{-1}(i) \in J^c\}$ and $J'' = \{i \in J^c : \sigma^{-1}(i) \in J\}$ (remark that $|J'| = |J''| \neq 0$ otherwise σ would have

more than one cycle) and writing $w_0 = \exp(i\theta_w), z_0 = \exp(i\theta_z)$,

$$r(x_1,\dots,x_k)+s(y_1,\dots,y_k) = 2\theta_w(\sum_{a\in J'} x_a - \sum_{a\in J''} x_a)+2\theta_z(\sum_{a\in J'} y_a - \sum_{a\in J''} y_a).$$

Splitting the sum $\sum_{e_1,\dots,e_k}$ over the different types of edges, we can assume without loss of generality that all edges in each path are of the same type (so that $C(e_1,\dots,e_k)$ becomes a constant; edge types can be different in different paths) and that edges in the path j are obtained one from the other via translations by an integer multiple of some $v^{(j)} = (v_1^{(j)}, v_2^{(j)}) \in \mathbb{Z}^2$. The edges in the j-th path will be labeled by an integer d_j, which runs from 1 to $M_j = O(\eta L)$ and $r(x_1,\dots,x_k) + s(y_1,\dots,y_k)$ becomes is a linear function of $d_1,\dots,d_k$.

Assume without loss of generality that $1 \in J'$. From the discussion above we obtain that

$$(r+s)(d_1,\dots,d_k) = (r+s)(0,d_2,\dots,d_k) + 2(\theta_w v_1^{(1)} + \theta_z v_2^{(1)})d_1.$$

Despite the fact that w_0, z_0 are unit complex numbers with phase different from $0, \pi$ it could happen that $\Theta := 2(\theta_w v_1^{(1)} + \theta_z v_2^{(1)})$ is a multiple of 2π, so that $\exp(i(r+s))$ is independent of d_1: this can however be avoided if the asymptotic directions and the period of path C_1 in $B_f(\eta L)$ are chosen suitably (we skip tedious details on this point).

We separate the sum over e_1 from the others and we make a summation by parts to get:

$$\text{const} \times \sum_{e_2,\dots,e_k} \frac{e^{i(r+s)|_{d_1=0}}}{(\tilde\phi_2 - \tilde\phi_3)\dots(\tilde\phi_{k-1} - \tilde\phi_k)} \times \Bigg[\sum_{d_1}\Big(\sum_{d\le d_1} e^{i\Theta d}\Big) \frac{\Delta\tilde\phi_1(\tilde\phi_k + \tilde\phi_2 - 2\tilde\phi_1(d_1) - \Delta\tilde\phi_1)}{(\tilde\phi_1(d_1) - \tilde\phi_2)(\tilde\phi_k - \tilde\phi_1(d_1))(\tilde\phi_1(d_1+1) - \tilde\phi_2)(\tilde\phi_k - \tilde\phi_1(d_1+1))} + O\left(\frac{1}{d_2 d_k}\right)\Bigg] \quad (3.41)$$

where the $O(...)$ comes from boundary terms in the summation by parts (note that $\sum_{d\le d_1} e^{i\Theta d}$ is bounded since $\Theta \neq 0 (\mathrm{mod}\ 2\pi)$), $\Delta\tilde\phi_1 = \tilde\phi_1(d_1 + 1) - \tilde\phi_1(d_1)$ is constant by linearity of ϕ and for simplicity of notation $\tilde\phi_i$ can denote either ϕ_i or its complex conjugate. We can thus bound $|\phi_i - \phi_j|$ by $d_i + d_j$ as before and (up to a constant factor) the absolute value of (3.41) by

$$\sum_{d_2,\dots,d_k} \frac{1}{(d_2+d_3)\dots(d_{k-1}+d_k)}\Big(\sum_{d_1}\frac{2d_1+d_2+d_k}{(d_1+d_2)^2(d_1+d_k)^2}+O\Big(\frac{1}{d_2d_k}\Big)\Big)$$
$$=\sum_{d_2,\dots,d_k}\frac{1}{(d_2+d_3)\dots(d_{k-1}+d_k)(d_2+d_k)}$$
$$\Big(\sum_{d_1}\frac{(2d_1+d_2+d_k)(d_2+d_k)}{(d_1+d_2)^2(d_1+d_k)^2}+O\Big(\frac{d_2+d_k}{d_2d_k}\Big)\Big)$$
$$=O\big(F_{k-1}(\eta L)\big)\ll[\mathrm{Var}_{\mu_{s,t}}(h(f)-h(f'))]^{k/2} \tag{3.42}$$

because the parenthesis in the second line is clearly bounded.

Chapter 4

CLT pour les T-graphes

4.1 Introduction

In [Ken07] and in [KS04], a class of aperiodic graphs called T-graphs was introduced and some deep links between these graphs and both the uniform spanning tree and the dimer or perfect matching model were proved. In particular in [Ken07] they appear as a tool to express correlation functions in the hexagonal dimer model (also known as the lozenge tiling model) see Section 4.4.1 for details. Using this method, one can relate the large scale behavior of dimers, which is one of the main questions on dimer models, to the way discrete harmonic functions approximate a continuous harmonic limit. Here we give a further step in this direction by proving a central limit theorem for the random walk on these graphs, which shows that discrete harmonic functions do indeed resemble continuous harmonic functions on large scale. This is not trivial because T-graphs generically do not have any exact symmetry. We became aware while finishing the writing of this paper of another work on harmonic functions on T-graph [Li13]. Their methods are very different from ours since they do not use a central limit theorem. They work with more general graphs but only obtain convergence of discrete functions to their continuous counterpart along sub-sequences.

Unfortunately the method we use does not provide any speed of convergence so we do not get any accurate estimate on the difference between continuous and discrete harmonic functions. However the result is valuable on its own because our environment is very far from being IID: all the randomness in the T-graph is encoded in a uniform variable λ on the unit circle, and conditionally on λ the graph is deterministic and quasi-periodic. In this framework interesting mathematical challenges arise. Increments of the random walk are highly correlated and some of the important concepts used with random environment, like renewal times, cannot be used. Furthermore the definition of the graph itself is quite involved so even simple facts like connectedness are non trivial. One can refer to [Zei02] for a general overview

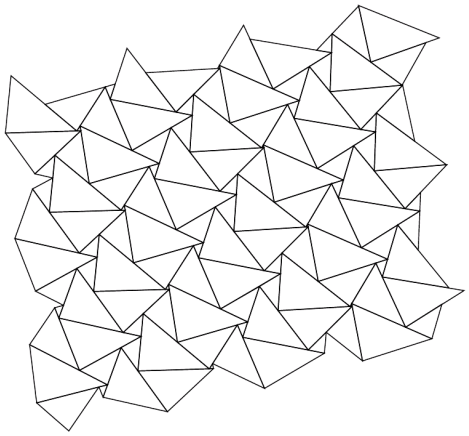

Figure 4.1: A picture of a finite domain inside a T-graph showing clearly the properties of 4.2.14. Image taken from [Ken07].

of random walk in random environment.

Keeping these difficulties in mind, it is striking to see that the ideas of [Law82, Szn02] carry on; the proof is thus also a testimony of the robustness of the method. In particular an important point to note is the role of ergodicity of the graph (i.e. the environment) with respect to translations. Usually one looks at ergodicity with respect to some group. Here on the other hand, the translations that send a vertex to another do *not* form a group (or any usual algebraic structure) so one might think that we cannot use ergodic theory. However we do not need any structure on translations to define ergodicity in the sense that any translation invariant event must have probability 0 or 1. As it will appear later (see Remark 4.3.25) this will give enough information on the (spatial) environment to prove that trajectories of the random walk are ergodic with respect to time shifts (which do form a semi-group) and to use Birkhoff ergodic theorem. This remark might be useful to study the random walk on other kind of environments where translations do not form a group, like random graphs.

The rest of the paper is organised as follows. We first give the construction of the graphs we are interested in (section 4.2.2) and derive some useful properties (section 4.2.3). The random walk we will use is then defined in section 4.2.4, where we also state the main theorem on quenched invariance principle and convergence of discrete harmonic function. The proof of the theorem is divided into two independent parts. In section 4.3 we use ergodicity arguments and the martingale invariance principle to prove almost-sure convergence of the random walk to a brownian motion with an unknown deterministic covariance. Finally in section 4.4 we see that the covariance has to be proportional to the identity, using the a priori knowledge of a harmonic function provided by the mapping with random lozenge tilings

[KOS06, KS04].

4.2 T-graph construction

In this section, we construct the family of graphs and the random walk we will study in the later sections. The specific structure of the graphs produced by the construction will be of key importance in section 4.3.2.

4.2.1 Hexagonal lattice

First of all we define suitable coordinates on the infinite hexagonal lattice. Of course the specific choice we give here plays no essential role so this section is only about fixing notations. However it is still quite important in practice because we will use several explicit formulas that depend on the choice of coordinates.

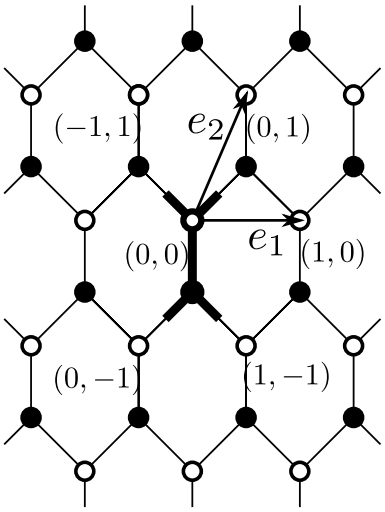

Figure 4.2: An illustration of the coordinates we use on the hexagonal lattice. Near each vertical edge are indicated the (common) coordinates of its two endpoints.

Notation 4.2.1. We embed the hexagonal lattice $\mathcal{H}$ in the plane in the way represented in figure 4.2. We call fundamental domain and write $\mathcal{H}_1$ the two vertices with thicker lines. We let e_1 and e_2 be the two vectors represented. Given v a vertex of $\mathcal{H}$, we call coordinates of v the unique n, m such that $v - me_1 - ne_2 \in \mathcal{H}_1$. Note that given m, n there are exactly two vertices with coordinates (m, n), the top one is called a white vertex, the bottom one is called black.

We will write $m(v)$ and $n(v)$ for the coordinates of the vertex v. We will also write $b(m, n)$ and $w(m, n)$ for the black and white vertices of coordinates (m, n).

Remark 4.2.2. *The three neighbors of a point $b(m, n)$ are $w(m, n)$, $w(m, n-1)$ and $w(m+1, n-1)$ while the three neighbors of $w(m, n)$ are $b(m, n)$, $b(m, n+1)$ and $b(m-1, n+1)$. We will call edges $w(m, n)b(m, n)$* vertical*, edges $w(m, n)b(m, n+1)$* north east-south west *(NE-SW) and edges $w(m, n)b(m-1, n+1)$* north west-south east *(NW-SE).*

Notation 4.2.3. We write $\mathcal{H}^*$ for the dual graph of $\mathcal{H}$. This is a triangular lattice. Each of its faces contains a vertex of $\mathcal{H}$ and it is called black/white

according to the color of that vertex. Vertices of $\mathcal{H}^*$ can be associated to the point in the centre of a face of $\mathcal{H}$. For a vertex v of $\mathcal{H}^*$ we let $(m(v), n(v))$ be the (common) coordinates of the two points just right of v.

4.2.2 Construction

T-graphs are defined by integration of an explicit 1-form on the edges of $\mathcal{H}^*$. In this section we define this form and verify that its primitive is well defined.

Notation 4.2.4. Let λ be a complex number of modulus one and let Δ be a triangle of area one. We let $a\alpha$, $b\beta$ and $c\gamma$ be the complex numbers corresponding to its sides, taken in the counterclockwise order, with a, b, c real positive and α, β, γ complex of modulus one. These parameters will be fixed for the rest of the section and will thus be often omitted from the notations.

The role of λ will be clarified in Proposition 4.2.13 and in Section 4.3.2.

Notation 4.2.5. We define the following functions :

- f is defined on white vertices by $f(w(m,n)) = (\frac{\beta}{\gamma})^m(\frac{\beta}{\alpha})^n$
- g is defined on black vertices by $g(b(m,n)) = \alpha(\frac{\beta}{\gamma})^m(\frac{\beta}{\alpha})^n$
- $K(w,b)$ on edges defined by $K(w,b) = a$ on vertical edges, b on SW-NE edges and c on NW-SE edges.

Remark that the three functions depend on Δ and not on λ. We will write f_Δ, g_Δ and K_Δ if we want to emphasize this dependence.

Remark 4.2.6. *f and g are defined in order to have $\bar{f}(w)g(b)$ equals to α (resp. β, γ) when w and b are the endpoints of a vertical (resp. NE-SW, NW-SE) edge.*

Proposition 4.2.7. *We have :*

- *for any black vertex b, $\sum_{w\sim b} f(w)K(w,b) = 0$*
- *for any white vertex w, $\sum_{b\sim w} K(w,b)g(b) = 0$,*

where $w \sim b$ means that w and b are neighbouring vertices.

Proof. The three terms of the sums are, up to a multiplicative constant, the edge vectors of Δ so they sum to 0. □

Notation 4.2.8. We let $\phi_{\lambda\Delta}$ denote the following flow on oriented edges:

$$\phi(wb) = K(w,b)\Re(\bar{\lambda}\bar{f}(w))\lambda g(b)$$

and $\phi(bw) = -\phi(wb)$, with $\Re(z)$ the real part of z. We let ϕ^* denote the dual flow on oriented edges of $\mathcal{H}^*$ obtained by rotating ϕ by $+\pi/2$ (counter-clockwise). That is, crossing the edge bw with the white vertex on the left gives flow $+K(w,b)\Re(\bar{\lambda}\bar{f}(w))\lambda g(b)$.

By Proposition 4.2.7, ϕ has zero divergence and thus the flow of ϕ^* around any face of $\mathcal{H}^*$ is zero. This implies the existence of a function $\psi_{\lambda\Delta}$ on $\mathcal{H}^*$, unique up to a constant, such that $\forall v, v' \in \mathcal{H}^*$, $\psi(v')-\psi(v) = \phi^*(vv')$. We fix the constant by setting $\psi = 0$ on $v(0,0)$ the vertex of $\mathcal{H}^*$ on the left of the fundamental domain.

We extend ψ linearly to the edges of $\mathcal{H}^*$, so that ψ maps $\mathcal{H}^*$ to a subset of $\mathbb{C}$. We define $T_{\lambda\Delta} = \psi_{\lambda\Delta}(\mathcal{H}^*)$. T is the "T-graph" we are interested in. We will see in Proposition 4.2.13 that the graph so obtained is "quasi-periodic" (or periodic if the angles of the triangle Δ are rational multiples of π).

Remark 4.2.9. *The definition of ϕ might seem strange, especially taking the complex conjugate inside a real part. However we claim that this is the natural definition. Indeed if we remove the real part from the definition of ϕ we get a flow $\tilde{\phi}$ with $\tilde{\phi} = a\alpha$ (resp. $b\beta$,$c\gamma$) on vertical (resp. NW-SW, NW-SE) edges. Its primitive $\tilde{\psi}$ is the linear mapping from $\mathcal{H}^*$ to $\mathbb{C}$ that makes all triangles similar to Δ. In a sense with the real part we get a perturbation of this linear map where all black faces are flattened to segments. This will be made more clear in the next section.*

Remark 4.2.10. *We have not specified how to choose which side of Δ is $a\alpha$ and corresponds to vertical edges, so it may seem that there is an ambiguity in the construction. However this is not the case because T does not depend on this choice. Indeed, making a different choice is equivalent to rotating the hexagonal lattice $\mathcal{H}$ by $2\pi/3$ (which leaves $\mathcal{H}$ invariant) so the new function $\tilde{\psi}$ verifies $\tilde{\psi}(x) = \psi(e^{2i\pi/3}x)$ and we see that $\tilde{T} = \tilde{\psi}(\mathcal{H}^*) = \psi(\mathcal{H}^*) = T$.*

4.2.3 Geometric properties of T-graphs

These properties are given both because they enter the proof of the central limit theorem, and also because they allow to visualize the type of graphs we are working with. The results and some of the proofs are taken from [Ken07] and [KS04] (in the latter a more general class of graphs is studied but full details are only given in the case of a finite graph). We also give explicit formulas when possible.

Proposition 4.2.11. *ψ is almost linear, more precisely if $\ell(m,n) = \frac{a\alpha}{2}m - \frac{c\gamma}{2}n$, then $\psi(v) - \ell(m(v),n(v))$ is bounded.*

Proof. This follows from direct computation. Let v a vertex of $\mathcal{H}^*$: it is on the left of the vertical edge of coordinates (m,n) so, assuming for simplicity

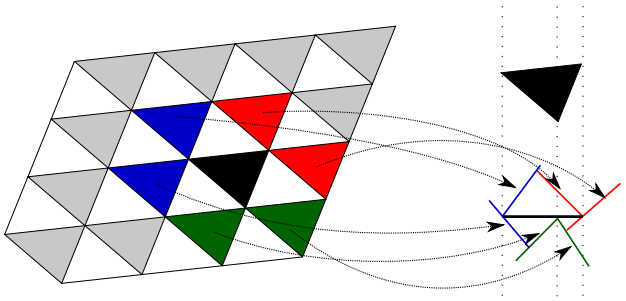

Figure 4.3: A schematic view of the image of a black face and its neighbours in $\mathcal{H}^*$.

both coordinates are positive,

$$\begin{aligned}\psi(v) &= \sum_{j=0}^{m-1} \phi^*(w(0,j)b(0,j)) + \sum_{j=0}^{n-1} \phi^*(w(m,j)b(m-1,j+1)) \\ &= \sum_{j=0}^{m-1} (+a)\frac{1}{2}\left(\bar{\lambda}\left(\frac{\beta}{\gamma}\right)^{-j} + \lambda\left(\frac{\beta}{\gamma}\right)^{j}\right)\alpha\lambda\left(\frac{\beta}{\gamma}\right)^{j} \\ &\quad + \sum_{j=0}^{n-1}(-c)\left(\bar{\lambda}\left(\frac{\beta}{\gamma}\right)^{-m}\left(\frac{\beta}{\alpha}\right)^{-j} + \lambda\left(\frac{\beta}{\gamma}\right)^{m}\left(\frac{\beta}{\alpha}\right)^{j}\right)\lambda\alpha\left(\frac{\beta}{\gamma}\right)^{m-1}\left(\frac{\beta}{\alpha}\right)^{j+1}.\end{aligned}$$

In each sum there are two terms. In the first the powers of α, β, γ cancel out so they give a linear contribution, in the second they add up so these terms oscillate and give bounded geometric sums. Finally

$$\psi(v) = +\frac{a\alpha}{2}m - \frac{c\gamma}{2}n + \text{bounded}.$$

When the coordinates are not positive the same computation holds and we just have to change the signs. □

Remark 4.2.12. *Since α and γ are not collinear, the linear application ℓ is non degenerate and T covers the whole plane: any point of $\mathbb{C}$ is at bounded distance from T.*

The following result shows that T is quasi-periodic, in the sense that translations of the graphs have properties similar to iterates of an irrational rotation, or periodic if the ratios β/α and β/γ are both roots of the unity. Also, it clarifies the role of λ in the construction: a translation of the graph is equivalent to a change of λ.

Proposition 4.2.13. *Let $T_{\lambda\Delta}$ the graph constructed above (recall that we choose $\psi = 0$ on the vertex of $\mathcal{H}^*$ just left of the fundamental domain $\mathcal{H}_1$).*

Let v be the vertex of $\mathcal{H}^*$ of coordinates (m,n) and let T' be the graph constructed in the same way but taking $\psi(v)=0$. Then we have $T'=T_{\lambda'\Delta}$ with $\lambda'=\lambda(\frac{\beta}{\gamma})^m(\frac{\beta}{\alpha})^n$.

Proof. This is immediate from the definition : the change of λ is equivalent to multiplying both f and g by $(\frac{\beta}{\gamma})^m(\frac{\beta}{\alpha})^n$ which in turn corresponds to a translation of the origin. □

Here are collected some geometric facts about T:

Proposition 4.2.14. *T has the following properties (see Figure 4.1):*

1. *The image of the black face of $\mathcal{H}^*$ containing the vertex b of $\mathcal{H}$ is a segment. More precisely, it is a suitable translation of $-\lambda g(b)\Re(\bar{\lambda}\bar{g}(b)\Delta)$ (we use the convention that, for a subset $U\subset\mathbb{C}$, $\Re(U)=\{\Re(z), z\in U\}$);*

2. *The image of the white face containing the vertex w is a triangle similar to Δ and with the same orientation. More precisely, it is a translation of $\lambda f(w)\Re(\bar{\lambda}\bar{f}(w))\Delta$. Remark that multiplication by $\lambda f(w)$ is a rotation and multiplication by $\Re(\bar{\lambda}\bar{f}(w))$ is a contraction;*

3. *The length of segments is uniformly bounded away from zero independently of λ; for generic λ no triangle is degenerate to a point ;*

4. *For any λ (resp. generic λ), for any vertex v of $\mathcal{H}^*$, $\psi(v)$ belongs to at least (resp. exactly) three segments: generically it is an endpoint of two of them and in the interior of the third one. All endpoints of segments are of the above form $\psi(v)$ with v a vertex of $\mathcal{H}^*$;*

5. *The triangular images of white faces cover the plane and do not intersect, that is any x not in a segment belongs to a unique face of the T-graph;*

6. *Segments do not intersect in their interior.*

Proof. Points (1), (2), (3) come directly from the construction. As an example we give the computation that proves (2). Let w be a white vertex of coordinates m,n. Let v_1,v_2,v_3 the vertices of $\mathcal{H}^*$ around w, taken in the counterclockwise order starting from the lower-left one. We have

$$\begin{aligned}\psi(v_2) &= \psi(v_1)+K(w,b(m,n))\Re(\bar{\lambda}\bar{f}(w))\lambda g(b(m,n))\\ &= \psi(v_1)+a\alpha\Re(\bar{\lambda}\bar{f}(w))\lambda f(w)\end{aligned}$$

and similarly

$$\psi(v_3)=\psi(v_2)+b\beta\Re(\bar{\lambda}\bar{f}(w))\lambda f(w).$$

We see that the image of the white face around w is equal to Δ rotated by $\lambda f(w)$ and scaled by $\Re(\bar{\lambda}\bar{f}(w))$.

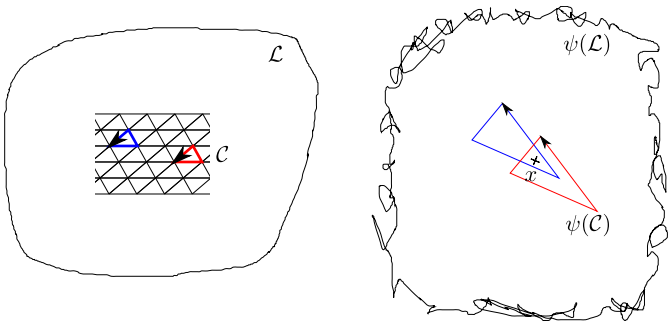

Figure 4.4: An illustration of the proof that faces of T do not overlap. The curve $\psi(\mathcal{C})$ made by the two triangles have winding number 2 around x while the large curve $\psi(\mathcal{L})$ have winding number 1.

For point (4) it is immediate from the construction that $\psi(u)$ is in at least three segments and generically in the interior of one of them (just look at the three segments corresponding to the black faces of $\mathcal{H}^*$ around u). Let S be this segment and let b be the corresponding black face. It is easy to check from the formulas that the image of the three white faces neighboring u cover on side of S, while the other side is covered by the image of the the white face neighboring b and not u (see figure 4.3). By point (5), which does not requires this part of of point (4), no other face cover a neighborhood of $\psi(u)$ and thus $\psi(u)$ is in no other segment.

We turn to point (5) from which point (6) follows easily. The key idea of the proof is to combine almost linearity of ψ with the fact that all faces have the same orientation and to look at winding numbers, see figure 4.4 for an illustration. Let $x \in \mathbb{C}$ and suppose by contradiction that x is in the interior of two faces $\psi(w_1)$ and $\psi(w_2)$ (writing here, with some abuse of notation, w_1 and w_2 for white faces of $\mathcal{H}^*$). Let $\mathcal{C}$ denote the (possibly non-connected) closed curve going once around w_1 and once around w_2 anticlockwise: $\psi(\mathcal{C})$ has winding number $+2$ around x. Consider a simple closed curve $\mathcal{L}$ in $\mathcal{H}^*$ going around both w_1 and w_2 in anticlockwise order. By point (2), the image of a white face of $\mathcal{H}^*$ can only have winding number 0 or $+1$ around a point. The winding number of $\psi(\mathcal{L})$ around x is the sum of the winding numbers around x of all the white faces inside $\mathcal{L}$ so it is at least the winding number of $\psi(\mathcal{C})$, i.e. at least $+2$. On the other hand, suppose that the loop $\mathcal{L}$ is very large and that both w_1 and w_2 are very far from it (but still inside it): then, by almost linearity of ψ, $\psi(\mathcal{L})$ has winding number 1 around x, which leads to a contradiction.

Finally let Ψ be the union of all closed faces, we need to check that $\Psi = \mathbb{C}$. We already said for point (4) that any segment is adjacent to three faces, with two on one side and the last one in the other. Thus segments are never on the boundary of Ψ so Ψ has no boundary and since it is not empty and every point of $\mathbb{C}$ is at finite distance from T, we have $\Psi = \mathbb{C}$. □

Definition 4.2.15. *The image of a white face of $\mathcal{H}^*$ is said to be degenerate if its size is zero. We will call such a point a degenerate face. A segment is said to be degenerate if it has no vertex in its interior. A T-graph is said to be degenerate if any of its segment or face is degenerate. We will say that a face (resp. a segment) is ϵ almost degenerate if its area is smaller than ϵ^2 (resp. has its interior point at distance less than ϵ from its endpoints). Given an almost degenerate edge, we will call the sub-segment connecting the two vertices at distance at most ϵ the "short sub-segment".*

Proposition 4.2.16. *There exists $\epsilon_0, C > 0$, depending only on Δ, such that, for all $\epsilon \in (0, \epsilon_0)$, if S is an ϵ-almost-degenerate segment, then there exists a $C\epsilon$-almost-degenerate face F adjacent to S. Furthermore for any $C\epsilon$-almost-degenerate face F, the three edges of F are the short sub-segments of $C^2\epsilon$-almost-degenerate segments.*

Proof. Let S be an almost degenerate segment and let v_1, v_2 be the endpoints of its small sub-segment . By construction the segment $[v_1, v_2]$ is an edge of some face F. Since all faces are similar to Δ, if one of the edges of F is small then its area is small, with a ratio C depending only on Δ. For the same reason, if F is almost degenerate than the length of its edges is small. However by proposition 4.2.14 point (3), segments have length bounded away from zero. Thus an edge of a small face cannot be a full segment which proves the end of the proposition. □

4.2.4 The random walk and the main theorem

In this section we define the random walk and we state precisely the invariance principle.

Definition 4.2.17. *The random walk $X(t)$ on a non-degenerate graph T is the continuous time Markov process on vertices of T defined by the following jump rates. If the process is at a vertex v of T, call v^+, v^- the endpoints of the unique edge in the interior of which v is contained. Then, the rates of the jumps from v to $v^\pm$ are $1/\|v^\pm - v\|$.*

Note that this random walk is automatically a martingale thanks to the choice of the jump rates.

We can now state our main result:

Theorem 4.2.18 (Quenched central limit theorem)**.** *Let Δ be a triangle of area one and let λ be a generic point in S^1. Let X_t denote the random walk on $T_{\lambda\Delta}$, started from a point v. Then we have*

- *$(\frac{X_{nt}}{\sqrt{n}})_{t\in\mathbb{R}_+}$ converges in law to a Brownian motion*
- *The asymptotic covariance is proportional to the identity and does not depend on λ or v (it may depend on Δ).*

For the initial problem of approximation of continuous harmonic function by discrete harmonic ones, as we said in the introduction, because of the lack of speed of convergence, we do not get precise estimates but we do get convergence, for example:

Corollary 4.2.19 (Dirichlet problem)**.** *Let U denote a smooth open domain in $\mathbb{R}^2$ and let f be an harmonic function on U that extends continuously on the boundary ∂U. Let T a non-degenerate T-graph and let T_n be T rescaled by $1/n$ (its edges are $O(1/n)$). Let $U_n = U \cap T_n$ and let ∂U_n denote the set of vertices adjacent to U_n and not in U_n. Consider f_n the solution to the Dirichlet problem*

- *f_n is discrete harmonic in U_n;*
- *$f_n = f$ on ∂U_n (for points outside of U take the value of the nearest point in U).*

The sequence f_n converges pointwise towards f as n goes to infinity.

Proof. Let v_n a sequence of vertices of U_n such that $v_n \to v_\infty$, a point in U. Let $X_t^{(n)}$ denote the random walk started in v_n and let B_t denote the brownian motion started in v_∞, with the asymptotic covariance. Let τ_n denote the first exist time of $X^{(n)}$ from U_n and let τ_∞ denote the first exit time of B. We have by harmonicity $f_n(v_n) = \mathbb{E}[f(X_{\tau_n}^{(n)})]$ and $f(v_\infty) = \mathbb{E}[f(B_{\tau_\infty})]$. Furthermore the trajectory $(B_t)_{t\geqslant 0}$ is almost surely a continuity point of τ_∞ seen as a function of the trajectory, so convergence of $X^{(n)}$ to B implies convergence in law of $X_{\tau_n}^{(n)}$ to B_{τ_∞} and thus of $f_n(v_n)$ to $f(v_\infty)$. □

Remark 4.2.20. *In [Szn02], the uniform ellipticity of the walk is an important part of the proof of the CLT. Yet for the random walk X_t, the projection of the increment in the direction orthogonal to the segment containing the current position of the walk, is zero. In this sense, the walk lacks uniform ellipticity everywhere. However, if one looks at the position of the walk after some finite time (say 1), ellipticity is recovered. More precisely (see Proposition 4.2.22), the increments of the discrete time random walk $(X_n)_{n\in\mathbb{N}}$ have strictly positive conditional variance in any direction, uniformly in the current position. For this reason we will often look at the position of the random walk at integers times in the rest of the proof.*

Definition 4.2.21. *An* oriented path *on T is a sequence $\psi(v_1), \psi(v_2), \ldots$ with $v_i \in \mathcal{H}^*$ such that, for all i, $\psi(v_i)$ is in the interior of a non degenerate segment and $\psi(v_{i+1})$ is one of the endpoints of this segment (using point (6) of Proposition 4.2.14, $\psi(v_i)$ is in the interior of a unique segment).*

Proposition 4.2.22. *There exists $\epsilon > 0$ (depending continuously on Δ) such that, for any $\mathbf{n} \in \mathbb{S}^1$ and any $x_0 \in T$, writing $(X_t)_{t\geq 0}$ the random walk started at x_0,*

$$1/\epsilon > Var(X_1 \cdot \mathbf{n}) > \epsilon$$

Proof. Since the length of segments is lower bounded (proposition 4.2.14 point (1)), there is a uniform lower bound on the probability to see at least k jumps in the interval $(0,1)$.

Also because the length of segments is bounded, there are only two cases where the variance after a single jump can be lower than ϵ: either the current position is in a segment whose direction is very close to $\mathbf{n}^\perp$ (so that changes of $x \cdot \mathbf{n}$ are small), or the current position is in an almost degenerate segment (so that change of $x \cdot \mathbf{n}$ are almost deterministic and small).

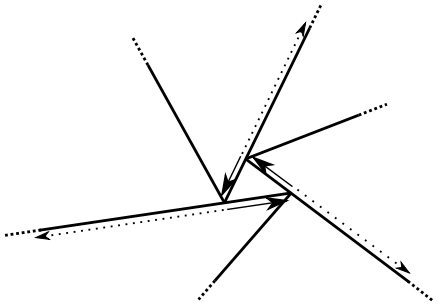

Figure 4.5: The neighborhood of an ϵ almost degenerate face. The arrows give the possible transition of the random walk: the arrows with full line have high rate of order $1/\epsilon$ while the dotted arrows have rates of order one.

In the second case of an almost degenerate segment, the random walk can make either a very small step (with high rate) or a large one (with rate of order one). However making a small jumps brings the walk to another vertex of an almost degenerate face F where the situation is the same. Actually the random walk is trapped inside the vertices of F as long as it does only small jumps (see figure 4.5). Since for each of this vertices a large jump can occur with rate of order one, a large jump will occur before time 1 with probability bounded away from zero. Finally this large jump can happen in either of the three segments (to which the edges of F belong) with probabilities bounded away from zero since the distribution of the time spent in each of the vertices of F depends only on the ratio of the edge lengths, which are fixed. At least two of these segments have direction far from $\mathbf{n}^\perp$ so jumps along them contribute a finite amount to the variance.

In the first case of a segment with "bad" direction, it is clear from the construction that the angles between neighboring segments are given by the angles of Δ. Thus neighboring segments have direction far away from $\mathbf{n}^\perp$. Events with two jumps in the interval $(0,1)$ have finite probability and we just showed that they correspond to large change of $X \cdot \mathbf{n}$ (unless the neighboring segments are almost degenerate where we are back to the above case).

The upper bound is essentially trivial. Small jumps only occur inside the "traps" made by almost degenerate faces so they have a small effect on the position of X_1. As for large jumps, their rate is bounded so the probability to make a large number of large jumps is exponentially decreasing. Overall the increment $X_1 - X_0$ has exponential tails and thus a bounded variance. □

Proposition 4.2.23. *Let T be a non-degenerate graph. For any $\mathbf{n} \in \mathbb{S}^1$*

and any vertex x_0, there exist two infinite oriented path P^+ and P^- starting in x_0 such that the couple $(\mathbf{n}\cdot x, \mathbf{n}^\perp \cdot x)$ is increasing (resp. decreasing) along P^+ (resp. P^-) for the lexicographic order (i.e. at each step either the first coordinate is increasing, or it is constant and the second coordinates is increasing). Furthermore $\mathbf{n}\cdot x$ is increasing (resp. decreasing) at least once every two steps.

There exists $\epsilon > 0$ such that for any x_0 and any $\mathbf{n} \in \mathbb{S}^1$, there exists infinite oriented paths $\tilde{P}^+ = (x_k^+)_k$ (resp. $\tilde{P}^- = (x_k^-)_k$), such that, for all k, $(x_{k+4}^+ - x_k^+)\cdot \mathbf{n} > \epsilon$ (resp. $(x_{k+4}^- - x_k^-)\cdot \mathbf{n} < -\epsilon$).

Proof. By symmetry we will only construct the path P^+ and $\tilde{P}^+$. For the first one, by construction x_0 is in the interior of a segment S_0 and the point x_1 has to be one of the endpoints of S. If S is not orthogonal to $\mathbf{n}$ then moving to one of its endpoints increases $\mathbf{n}\cdot x$. If S is orthogonal to $\mathbf{n}$, we can keep $\mathbf{n}\cdot x$ constant and increase $\mathbf{n}^\perp \cdot x$. Finally by construction the angles between neighboring segments of T are the angles of Δ so they are never aligned and two neighboring segments cannot be both orthogonal to $\mathbf{n}$.

To construct $\tilde{P}^+$ we recall the proof of proposition 4.2.22. The only case where we cannot increase $x\cdot\mathbf{n}$ by ϵ in one step are almost degenerate segments and segments with direction close to $\mathbf{n}^\perp$. In the latter case, one step is enough to arrive to a "good" segment or an almost degenerate one. In the former case, we see that after at most three small steps we can find a segment where we can increase $x\cdot\mathbf{n}$ by a bounded amount. Overall after 4 steps we can increase $x\cdot\mathbf{n}$ by ϵ. □

Remark 4.2.24. *For generic Δ there is no need to distinguish the paths P and $\tilde{P}$, the only problem comes from triangles with one right angle and two irrational ones.*

4.3 Central limit theorem

Here we give the proof of the central limit theorem for the oriented random walk on the T-graph. The identification of the limiting covariance will be achieved in Section 4.4 with a completely different set of ideas: it follows from the knowledge of a specific harmonic function on the graph, which comes from the study of dimer models [Ken07].

The proof of the CLT follows quite closely a proof in the case of random walk in balanced random environment [Law82, Szn02]. It is at first intriguing that we can use arguments from random walk on random environment in our environment that, once the single parameter λ is fixed, is deterministic and quasi-periodic. However the specific structure of T-graphs will allow us to use an ergodicity and a compactness argument that are the core of the proof for a random environment. One can also argue that we lose the

deterministic nature of the graph in the theorem since it applies only to generic λ and we have no explicit condition on λ.

4.3.1 Periodic case

If β/γ and β/α are both roots of the unity then ϕ^* is periodic and thus T is a periodic graph. Even though that case could be dealt with using the same techniques as the general one, the result can be proved with much simpler arguments.

Let T be a periodic T graph and let T_1 be one fundamental domain of T. Given the first point, there is a bijection between random walk trajectories on T and T_1.

The random walk on T_1 is a finite state Markov chain and it is not difficult using proposition 4.2.23 to show that it has only one recurrent set. Let us assume for simplicity that the starting point x_0 is recurrent. Let $\tau_0 = 0, \tau_1, \dots$ be the return times in x_0 of the random walk on T_1; thanks to exponential mixing the $\tau_{i+1} - \tau_i$ are iid and have exponential moments. Going back to the random walk on T, the $X_{\tau_{i+1}} - X_{\tau_i}$ are also iid with exponential moments and the central limit theorem for random walk gives the result.

4.3.2 Topology on graphs

The proof of the central limit theorem consists of two crucial steps. First we construct, using a compactness argument, an invariant measure for the random walk (more precisely for the environment from the point of view of the particle, see notation 4.3.7 and lemma 4.3.16 for precise statements) and then we apply Birkhoff ergodic theorem to get convergence of the variance of the random walk.

In this section we set up the compactness argument by defining a distance on T-graphs and giving the properties of the induced topology we will need.

Definition 4.3.1. *A pointed T-graph is a couple $T^\bullet = (T, v)$ where $T = T_{\lambda\Delta}$ for a certain Δ and λ is a T-graph and v is a vertex of T. We let $\mathcal{T}^\bullet$ denote the set of pointed T-graphs.*

Notation 4.3.2. We will need an explicit correspondence between black vertices of $\mathcal{H}$ and vertices of T. Recall that the image of a black face b of $\mathcal{H}^*$ is a segment where the image of the three vertices of the face are the two endpoints and a third point on the segment (proposition 4.2.14 point (4)). We define $v(b)$ as this third point. Generically $v(b)$ is in the interior of the segment but for exceptional values of λ, when the ψ-images of two vertices of $\mathcal{H}^*$ are equal, $v(b)$ can be one of the endpoints. Except in the non generic graph where this happens, v is a bijection and we define coordinates on vertices of T by using the coordinates of v^{-1}. We write $v(m, n) = v(b(m, n))$ to simplify notations.

Notation 4.3.3. Let $\mathcal{P}$ the set of parameters $\mathcal{P} = \{(\lambda, \Delta) | \lambda \in \mathbb{S}^1, \Delta \text{ area one triangle}\}$. We define the mapping $\mathcal{C} : \mathcal{P} \to \mathcal{T}^\bullet$ by

$$\mathcal{C}(\Delta, \lambda) = (T_{\lambda\Delta}, v(0,0))).$$

Notation 4.3.4. Let d_H denote the Hausdorff distance on closed set of $\mathbb{C}$. We define d on $(\mathcal{T}^\bullet)^2$ by

$$d((T,v),(T',v')) = \inf\{\epsilon | d_H(t_{-v}T \cup \bar{B}(\tfrac{1}{\epsilon}), t_{-v'}T' \cup \bar{B}(\tfrac{1}{\epsilon})) < \epsilon\}$$

where t_x denotes the translation by x and $\bar{B}(r)$ is the closed ball of center 0 and radius r.

Proposition 4.3.5. *d is a pseudo-distance on $\mathcal{T}^\bullet$.*

Remark 4.3.6. *The distance is chosen in order to measure how similar are the neighborhoods of the pointed vertex in different graphs. It is more or less the local distance of Benjamini-Schramm.*

Notation 4.3.7. We let $\mathcal{T}^\bullet/d$ denote the quotient of $\mathcal{T}^\bullet$ by d. We extend trivially functions into $\mathcal{T}^\bullet$ as function into $\mathcal{T}^\bullet/d$ without changing notation.

We can now restate Proposition 4.2.13:

Proposition 4.3.8. *Let $\tau_{m,n}$ the translation defined by $\tau_{m,n}(T, v(m', n')) = (T, v(m+m', n+n'))$. We have*

$$d\left(\tau_{m,n} \circ \mathcal{C}(\Delta, \lambda), \mathcal{C}(\Delta, (\tfrac{\beta}{\gamma})^m (\tfrac{\beta}{\alpha})^n \lambda)\right) = 0,$$

which means that in the set $\mathcal{T}^\bullet/d$ a translation is a special case of changing λ.

Proposition 4.3.9. *$\mathcal{C}$ is continuous and onto from $\mathcal{P}$ to $\mathcal{T}^\bullet/d$.*

Proof. First we prove that $\mathcal{C}$ is onto. By proposition 4.3.8, any pointed graph (T, v) where v is the image of a black vertex is identified in $\mathcal{T}^\bullet/d$ with a graph pointed in 0, which is in the image of $\mathcal{C}$ by construction. Thus we only have to check that any vertex of a T-graph is of the form $v(b)$ for a certain black vertex b.

Fix a graph T, in proposition 4.2.14 point (4) we see that a vertex of T is always an endpoint of (at least) a segment so it is the image of a vertex u of $\mathcal{H}^*$. However this does *not* imply directly that it is of the form $v(b)$. For generic λ each vertex is in the interior of a single segment and thus is trivially of the form $v(b)$. For non generic λ some segments will be degenerate. If the image of a certain b presents such a case, then $v(b)$ is by definition the "double" endpoint so there is no issue with the definition, yet we have to check that no vertex of T is a "simple" endpoint of all the segments it is in. This could be seen from the explicit definition but we give a perturbative

argument (see figure 4.6 for an illustration). Suppose that for some λ_0 and some $x \in \mathcal{H}^*$, $\psi(x)$ is a simple endpoint of the three segments corresponding to the three black vertices around x. For λ close to λ_0 those segments will be almost degenerate with the interior point far away from $\psi(x)$ and thus $\psi(x)$ will not be of the form $v(b)$ which contradicts the results for generic λ.

It is also clear from the explicit formula that ϕ^* is continuous as a function of Δ, λ and thus for fixed $x \in \mathcal{H}^*$, $\psi(x)$ is continuous as a function of Δ, λ. To finish the proof we need to show that we only need to know ψ on a finite number of points to know T in a given ball. This is immediate because we see from Proposition 2 that the scaling factor of adjacent faces cannot be both vanishingly small so there is a finite number of face in any ball. □

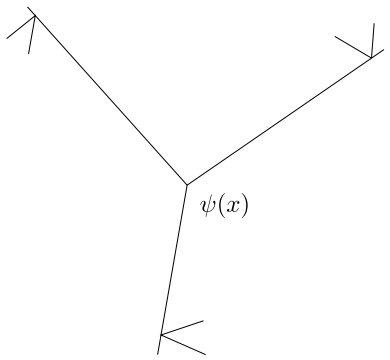

Figure 4.6: The local configuration around $\psi(x)$ with a generic λ close to λ_0. This configuration is impossible by proposition 4.2.14 point (4).

Corollary 4.3.10. *$\mathcal{T}^\bullet/d$ is locally compact. Let $\mathcal{T}^\bullet_\Delta = \{T_{\lambda\Delta} | \lambda \in \mathbb{S}^1\} = \mathcal{C}(\mathbb{S}^1, \delta)$; $\mathcal{T}^\bullet_\Delta/d$ is compact.*

Remark 4.3.11. *The fact that $\mathcal{T}^\bullet/d$ is not compact comes from the very flat triangles. We can recover the compactness easily, for example by adding a condition on the perimeter being bounded (recall that we already fixed the area to be 1).*

4.3.3 Core of the proof

In this section we give the proof of the central limit theorem through compactness and ergodicity arguments. Two key lemmas on absolute continuity of the invariant measure for the environment from the point of view of the particle will be left for the next sections.

Notation 4.3.12. Let Δ a triangle with angles that are not all rational multiples of π. Let λ such that no triangle has size 0 in $T_{\lambda\Delta}$ (any generic λ works). As we said before, we could work with rational multiples of π but our choice will make our statements about ergodicity simpler.

In this section we will only work with the set $\mathcal{T}^\bullet/d$ so functions and measures will always be defined on this set.

Let $\mathbb{U}$ be the uniform measure on the unit circle and let $\mathbb{P} = \mathcal{C}(\Delta, \mathbb{U})$ be its image by the construction. It is clear from Proposition 4.3.8 and ergodicity of irrational rotations that $\mathbb{P}$ is invariant and ergodic for the group

of translations $\{\tau_{mn}|m,n\in\mathbb{N}\}$. $\mathbb{P}$ will replace the law of the environment in the proof of [Szn02].

Notation 4.3.13. We define the environment from the point of view of the particle by $T_t^\bullet=(T,X_t)$ where X_t is the random walk on T. We let W be its generator: W is the operator on functions on $\mathcal{T}^\bullet/d$ defined by $Wf(T,v)=\frac{f(T,v^+)}{\|v^+-v\|}+\frac{f(T,v^-)}{\|v^--v\|}-f(T,v)$. We also define p_t the transition probabilities for the environment from the point of view of the particle, $p_t(T,v)f(T,v)=\mathbb{E}_v[f(T,X_t)]$, with the expectation with respect to the random walk on T started at v.

The main point of the proof will be to construct an invariant ergodic measure for p_t and to show that it is absolutely continuous with respect to $\mathbb{P}$. This is done through approximation of the aperiodic graph $T_{\lambda\Delta}$ by periodic graphs.

Notation 4.3.14. Let Δ_n be a sequence of triangles such that $\Delta_n\to\Delta$ and all the angles of the Δ_n are rational multiple of π. Let $\lambda_n\to\lambda$ such that none of the $T_{\Delta_n\lambda_n}$ has a face of size 0. By construction the $T_{\Delta_n\lambda_n}$ are periodic graphs. Let $\mathbb{P}_n$ the uniform probability measure on $\{(T_{\Delta_n\lambda_n},v),v\in T_{\Delta_n\lambda_n}\}/d$ (which is finite by periodicity) and let $\mathbb{Q}_n$ be an invariant ergodic measure for the random walk on the same set. $\mathbb{Q}_n$ exists by general theorems on finite state Markov chains and $\mathbb{Q}_n$ is clearly p_t invariant.

Lemma 4.3.15. *Let $q_n=\frac{\mathrm{d}\mathbb{Q}_n}{\mathrm{d}\mathbb{P}_n}$, the q_n are uniformly bounded in the $L^2(\mathbb{P}_n)$ norm.*

The proof will be given in the next section 4.3.4.

Lemma 4.3.16. *There exists a measure $\mathbb{Q}$ on $\mathcal{T}_\Delta^\bullet$ which is p_t invariant and absolutely continuous with respect to $\mathbb{P}$.*

Proof. Let K be a uniform (in n) upper bound on the perimeter of the Δ_n and let $\mathcal{T}_K^\bullet$ the set of pointed T-graphs with triangles of perimeter less than K. By corollary 4.3.10, $\mathbb{Q}_n$ is a sequence of probability measures on the compact set $\mathcal{T}_K^\bullet/d$ so, up to extraction, it converges towards a measure $\mathbb{Q}$. It is clear that $\mathbb{Q}$ is supported on $\mathcal{T}_\Delta^\bullet$ because the parameters of the triangle are continuous functions of the graph.

Now we have to verify that $\mathbb{Q}$ is p_t invariant for all t. p_t, the transition kernel of the environment from the point of view of the particle, is by definition an operator on measurable function of pointed T-graphs. Furthermore the jump rates of the random walk and the translations (by bounded amount) are continuous functions of the graph so p_t maps continuous functions to continuous functions. Thus, for any continuous bounded function f, in the equality $\mathbb{E}_{\mathbb{Q}_n}[p_tf(X)]=\mathbb{E}_{\mathbb{Q}_n}[f(X)]$ both sides go to the limit by convergence in law of $\mathbb{Q}_n$ to $\mathbb{Q}$ and:

$$\forall g:\mathcal{T}^\bullet\to\mathbb{R}\text{ continuous bounded},\quad \mathbb{E}_{\mathbb{Q}}[p_tg(X)]=\mathbb{E}_{\mathbb{Q}}[g(X)]$$

This equality means by definition that the measure $\mathbb{Q}p_t$ and $\mathbb{Q}$ are identical on bounded continuous functions and this implies $\mathbb{Q}p_t = \mathbb{Q}$.

Finally we check that $\mathbb{Q}$ is absolutely continuous with respect to $\mathbb{P}$. It is easy to note that $\mathbb{P}_n$ converges to $\mathbb{P}$. Let $q_n = \frac{\mathrm{d}\mathbb{Q}_n}{\mathrm{d}\mathbb{P}_n}$ and let g be a continuous bounded function, we have

$$\begin{aligned}
|\int g\mathrm{d}\mathbb{Q}| &= \lim|\int g\mathrm{d}\mathbb{Q}_n| \text{ by convergence in law} \\
&= \lim|\int gq_n\mathrm{d}\mathbb{P}_n| \\
&\leq \limsup\left(\int |g|^2\mathrm{d}\mathbb{P}_n\right)^{1/2}\left(\int |q_n|^2\mathrm{d}\mathbb{P}_n\right)^{1/2} \\
&\leq C\|g\|_{L^2(\mathbb{P})}
\end{aligned}$$

and thus $\mathbb{Q}$ is absolutely continuous with respect to $\mathbb{P}$. □

Lemma 4.3.17. *$\mathbb{Q}$ is unique and $\mathbb{P} \sim \mathbb{Q}$. Furthermore the stationary measure on trajectories of the environment from the point of view of the particle is ergodic for the semi-group of time shifts.*

The proof is essentially identical to [Szn02] and will be given in section 4.3.5.

Theorem 4.3.18. *Let X_t denote the continuous time random walk on $T_{\lambda\Delta}$ started on $b(0,0)$. For generic λ, there exist a positive definite symmetric matrix M such that $X_{Nt}/\sqrt{N}$ converges in law to the two dimensional brownian motion of covariance M. Furthermore M does not depend on λ (it may depend on Δ).*

Remark that for any direction $\mathbf{n}$, $X_t.\mathbf{n}$ is a square integrable martingale. By the central limit theorem it is asymptotically gaussian so we only have to prove that the variance grows linearly to obtain our result. This is done by the ergodic theorem.

Theorem 4.3.19 (Birkhoff ergodic theorem)**.** *Let $(\mathcal{T}, \mu)$ a measured space and $F : \mathcal{T} \to \mathcal{T}$ a measure preserving transformation. We assume that μ is finite and F invariant and ergodic, then for all $g \in L^1(\mu)$ and μ almost all x we have :*

$$\frac{1}{n}\sum_1^n g \circ F^k(x) \to \int g\mathrm{d}\mu.$$

Proof of theorem 4.3.18. Fix $\mathbf{n} \in \mathbb{S}^1$ a direction and let us prove a one dimensional invariance principle for the random walk $X_t \cdot \mathbf{n}$. Since proposition 4.2.22 was given with an unit time increment, we will work with the discrete time walk $(X_n)_{n\in\mathbb{N}}$. It is clear this is sufficient to get a result in the original continuous time model. Indeed the probability for the random walk to go far away from X_n in the time interval $[n, n+1]$ is exponentially decreasing.

Let $g(T,v) = \mathbb{E}_v[(X_1 \cdot \mathbf{n} - X_0 \cdot \mathbf{n})^2]$ with the expectation taken with respect to the random walk on T started in v. By the Markov property, g gives the conditional variance of any increment, more precisely

$$\forall k,\ \mathbb{E}[(X_{k+1} \cdot \mathbf{n} - X_k \cdot \mathbf{n})^2 | \mathcal{F}_k] = g(T, X_k).$$

Consider now the set of infinite oriented paths of pointed T-graphs (i.e. of environments viewed from the point of view of the particle). On this set, put the measure obtained sampling the environment (pointed T-graph) at time zero using $\mathbb{Q}$. The time shift is a measurable transformation on this set and by lemma 4.3.17 the measure is invariant and ergodic. The function g extends trivially to a function on trajectory and is bounded so we can apply Birkhoff ergodic theorem to get

$$\frac{1}{N}\sum_{k=1}^{N} g(T, X_k) = \int g(T^\bullet) \mathrm{d}\mathbb{Q}(T^\bullet) + o(1)$$

where the equality holds for $\mathbb{Q}$ almost all graphs and almost all trajectories. Since $\mathbb{Q} \sim \mathbb{P}$, it is also valid for $\mathbb{P}$ almost all graphs.

The left hand side can be rewritten

$$\frac{1}{N}\sum_{k} \mathbb{E}[(X_{k+1} \cdot \mathbf{n} - X_k \cdot \mathbf{n})^2 | \mathcal{F}_k];$$

the right hand side is deterministic so by taking expectation on both sides we get, for $\mathbb{P}$ almost all graph,

$$\frac{1}{N}\mathbb{E}[(X_N \cdot \mathbf{n} - X_0 \cdot \mathbf{n})^2] = \int g(T^\bullet) \mathrm{d}\mathbb{Q}(T^\bullet) + o(1).$$

Remark that the limit is given by some fixed integral and does not depend on the starting point or λ.

Finally the invariance principle for martingales applies because $X_k \cdot \mathbf{n}$ has L^2 increments and we just proved that its variance grows linearly so we have that $(\frac{X_{\lfloor Nt \rfloor}}{\sqrt{N}} \cdot \mathbf{n})_{t \geq 0}$ converges to a Brownian motion (with some unknown variance). Now this is true for any direction $\mathbf{n}$ so by definition $X_{\lfloor Nt \rfloor}/\sqrt{N}$ converges to a two dimensional brownian motion (again with an unspecified covariance matrix). As we said above, this is enough to conclude for the original continuous time process. □

4.3.4 L^2 estimates of invariant measure

In this section we prove lemma 4.3.15. The proof is very similar to the one in [Szn02] (with the notable exception that there they work with an underlying graph $\mathbb{Z}^2$) and is included here for the sake of completeness. This proof is slightly different from the one in [Law82] and it uses the approach of [KT90] (see Theorem 2.1 there).

We write the proof as a sequence of two lemmas. In the first one the structure of the graph appears so, since T-graphs are very different from $\mathbb{Z}^2$, we give a detailed proof. In the second one, on the other hand, the structure of the underlying does not appear so we only give a basic idea of the proof which is completely identical to [Szn02].

Notation 4.3.20. Recall the notation 4.3.14 and write $T^{(n)} = T_{\lambda_n \Delta n}$. The $T^{(n)}$ is a sequence of periodic non-degenerate T-graphs with parameters converging to some (λ, Δ) such that $T_{\lambda\Delta}$ is aperiodic and non degenerate. We assume here that the period of the $T^{(n)}$ are of order n in both directions. We let $T_1^{(n)}$ denote the fundamental domain of $T^{(n)}$, seen as a finite graph embedded on the plane.

Lemma 4.3.21. *Let X_t^x denote the random walk on $T^{(n)}$ started in x and let ν be the time of the first exist of $T_1^{(n)}$, and for a function f on $T_1^{(n)}$ let $Qf(x) = \mathbb{E}\sum_{0\leq k<\nu} f(X_k^x)$. We have*

$$\|Qf\|_\infty \leq Cn^2 \|f\|_{L^2(\mathbb{P}_n)}.$$

Proof. We write $Qf = u$ and we drop the superscript n to simplify notations. We let δT_1 denote the neighbours of T_1 (in the periodic graph). The first exit of T_1 is by definition the hitting time of δT_1. Remark that for all $x \in T_1$, $\mathbb{E}[u(X_1^x) - u(x)] = -f(x)$ (we define by convention $u = 0$ on δT_1).

Let $s(x) = \{\mathbf{v} \in \mathbb{R}^2 | \forall x' \in T_1 \cup \delta T_1, u(x') \leq u(x) + \mathbf{v}\cdot(x'-x)\}$ and let $S = \cup_{x\in T_1} s(x)$. We start by giving a lower bound on the volume of S.

Let D be the diameter of $T_1 \cup \delta T_1$, let $\mathbf{v} \in \mathbb{R}^2$ such that $|\mathbf{v}| < \max(u)/D$ and let $x_0 \in T_1$ be a point where $\max(u)$ is attained. By definition of the diameter, for all $x \in T_1 \cup \delta T_1$,

$$u(x_0) + \mathbf{v}\cdot(x - x_0) > 0.$$

Thus the function $x \to u(x_0) + \mathbf{v}\cdot(x-x_0) - u(x)$ is strictly positive on δT_1 (recall $u(x) = 0$ on δT_1) while its minimum is negative or zero so it reach its minimum in a certain $x' \in T_1$. We see immediately that $\mathbf{v} \in s(x')$ and so $\mathbf{v} \in S$. We just proved $\{\mathbf{v} \in \mathbb{R}^2 \text{ s.t. } |\mathbf{v}| < \max(u)/D\} \subset S$ so S has a volume at least $\max(u)^2/D^2$.

Now we will upper bound the volume of S by giving an upper bound on the volume of each $s(x)$. Let $x \in T_1$, $\mathbf{v} \in s(x)$ and x' such that $\mathbb{P}(X_1^x = x') = p > 0$. Since $\mathbf{v} \in s(x)$, the random variable $u(x) - u(X_1^x) + \mathbf{v}\cdot(X_1 - x)$ is positive and thus

$$\mathbb{E}[u(x) - u(X_1^x) + \mathbf{v}\cdot(X_1 - x)] \geq p\left(u(x) - u(x') + \mathbf{v}\cdot(x'-x)\right).$$

The walk is balanced $\mathbb{E}[\mathbf{v}\cdot(X_1^x - x)] = 0$ and by definition $\mathbb{E}[u(X_1^x) - u(x)] = -f(x)$ so we can rewrite

$$\mathbf{v}\cdot(x'-x) \leq u(x') - u(x) + f(x)/p.$$

We also have by applying directly the definition of $s(x)$ to x' :

$$\mathbf{v} \cdot (x' - x) \geq u(x') - u(x).$$

Finally, by uniform ellipticity we have a lower bound on p so each $s(x)$ has volume at most $Cf^2(x)$. Since we already found a subset of volume $(\|u\|_\infty/D)^2$ we get the inequality :

$$\|u\|_\infty \leq CD(\sum f^2(x))^{\frac{1}{2}} \leq C'n^2(\tfrac{1}{|T_1|}\sum f^2(x))^{\frac{1}{2}}$$

which proves the lemma. □

Lemma 4.3.22. *[Szn02] Let X_t^x denote the random walk on $T^{(n)}$ started at x and let τ be a geometric time of mean n^2 independent of the walk. We have for any function f on $T_1^{(n)}$ (lifted as a periodic function on $T^{(n)}$):*

$$\sup_{x \in T^{(n)}} \mathbb{E}[f(X_\tau^x)] \leq cn^2 \|f\|_{L^2(\mathbb{P}_n)}.$$

This lemma is about going from "Dirichlet boundary conditions" to "periodic boundary conditions". The main idea is to introduce iterates of the stopping time $\inf\{t > 0 \text{ s.t } \|X_t - X_0\| \geq n\}$ and to use lemma 4.3.21 between each time.

Finally for the proof of Lemma 4.3.15, we first see that lemma 4.3.22 implies the same kind of bound for the expectation with respect to $\mathbb{Q}_n$. Then by duality we get the bound we wanted on $\|\frac{d\mathbb{Q}_n}{d\mathbb{P}_n}\|_{L^2(\mathbb{P}_n)}$.

4.3.5 Ergodicity of $\mathbb{Q}$

In [Szn02] it is proved, for a random walk in ergodic random environment on $\mathbb{Z}^d$, that if there exist a invariant measure $\mathbb{Q}$ for the environment seen by the particle, absolutely continuous with respect to the law of the environment $\mathbb{P}$, then:

- $\mathbb{Q} \sim \mathbb{P}$
- $\mathbb{Q}$ is unique
- the stationary random walk with initial law $\mathbb{Q}$ is ergodic (for the time shifts semi-group).

The proof translates almost identically to our setting once we have lemma 4.3.23 (which was trivial in the $\mathbb{Z}^d$ case). However we will still give the proof of the first point to emphasize where we need lemma 4.3.23 and also why we do *not* need the graph translations to form a group.

Lemma 4.3.23. *Let T denote a non-degenerate T-graph and let v, v' be two of its vertices. There exists an oriented path going from v to v'.*

Proof. Let T_v be the set of points accessible by some oriented path starting in v. In this proof we emphasize that we will not only work with connections by oriented paths but also with connections by any non necessarily oriented path. We will use the term "connected" and associated definition of simple connectedness and connected component only for the latter, i.e. the usual definition when T is seen as a non oriented graph.

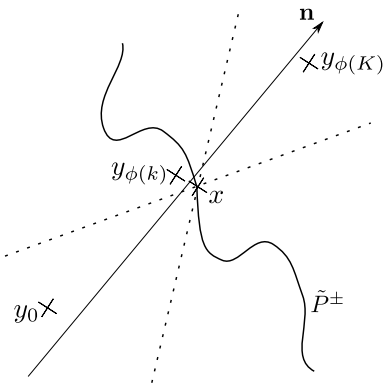

Figure 4.7: An illustration of the proof that there is no infinite connected component in $T \setminus T_v$. Points y_0, $y_{\phi(k)}$ and $y_{\phi(K)}$ are in $T \setminus T_v$ and all in a direction close to $\mathbf{n}$. x is a point in T_v close to $y_{\phi(k)}$. The path $\tilde{P}^{\pm}$, which is known to stay inside the cone delimited by doted lines, separates y_0 from $y_{\phi(K)}$

First we prove that T_v is simply connected. Indeed if it is not the case let G denote a finite connected component of its complement. Remark that any edge connecting G to T_v is oriented from G to T_v. Let y be a vertex of G. By the properties of T-graph, there exist exactly two vertices y_1^- and y_2^- that can be its predecessor in an oriented path and by definition of G both are in G. By going through all vertices of G this way we count each edge with both ends in G exactly once so we have $|\{\text{edges of } G\}| = 2|\{\text{vertices of } G\}|$. However we can also count edges of G by looking at their starting point. We also have two edges going out of each vertex but some of them lead to vertices of T_v so $2|\{\text{vertices of } G\}| = |\{\text{edges from } G \text{ to } T_v\}| + |\{\text{edges of } G\}|$. Finally by proposition 4.2.23 there are at least two edges going from G to T_v and we have found a contradiction.

To conclude we have to show that there are no infinite connected components in the complement of T_v. Again by contradiction suppose there is one called G and let y_k be an infinite path in G that stays at distance $O(1)$ of the boundary. By compactness we can extract a subsequence $y_{\phi(k)}$ such that $y_{\phi(k)}/|y_{\phi(k)}|$ converges to a direction $\mathbf{n}$. Now remark that the paths $\tilde{P}^{\pm}$ constructed by proposition 4.2.23 for the direction $\mathbf{n}^{\perp}$ have increments (every four steps) whose directions are bounded away from $\mathbf{n}$. In particular such a path lies completely in a cone of direction $\mathbf{n}^{\perp}$ and of angle $\pi - O(\epsilon)$, with $\epsilon > 0$ given in proposition 4.2.23. Now consider k large enough and x a point in T_v close to $y_{\phi(k)}$ and define two paths $\tilde{P}^+$ and $\tilde{P}^-$ starting from x. All points of $\tilde{P}^+ \cup \tilde{P}^-$ are in T_v and $\tilde{P}^+ \cup \tilde{P}^-$ separates the plane in two infinite connected components. By construction these connected components each include one of the connected component of the cone of direction $\mathbf{n}$ and

angle $O(\epsilon)$. By taking k large enough y_0 will be in one of them while $y_{\phi(K)}$ will be in the other for $K \geq k$ large enough. This is a contradiction with the fact all y are in the same connected component G. □

Lemma 4.3.24. *Let $\mathbb{Q}$ an invariant measure for the environment from the point of view of the particle. If $\mathbb{Q} \ll \mathbb{P}$, then $\mathbb{Q} \sim \mathbb{P}$.*

Proof. We write $f = \frac{d\mathbb{Q}}{d\mathbb{P}}$ and we let $E = \{f = 0\}$. Recall that p_t denote the probability transition function of the environment from the point of view of the particle, by construction we have $\mathbb{Q}p_t = \mathbb{Q}$

In particular $\mathbb{Q}p_t 1_E = \mathbb{Q}1_E = \int 1_{\{f=0\}} f d\mathbb{P} = 0$. However we also have $\mathbb{Q}p_t 1_E = \int p_t 1_E f d\mathbb{P}$ so $p_t 1_E = 0$ on $\{f \neq 0\} = E^c$ and thus, since $p_t 1_E \leq 1$, we get for $\mathbb{P}$ almost all pointed graph T:

$$\forall t > 0\,, 1_E(T) \geq p_t 1_E(T) = \sum_{T' \text{ translate of } T} p_t(T \to T') 1_E(T').$$

This implies by lemma 4.3.23

$$\forall T' \text{ translate of } T, 1_E(T) \geq 1_E(T')$$

and by symmetry between T and T', E is invariant by translations (up to a negligible set).

Now remark that this implies that E is invariant for the τ_{mn} which form a group for which $\mathbb{P}$ is ergodic so we have $\mathbb{P}(E) = 0$ or 1. Since $\int f d\mathbb{P} = 1$, $\mathbb{P}(E) = 1$ is impossible. □

Remark 4.3.25. *The use of the ergodic theorem here is not as straightforward as it may seem. The set of translations of the plane that send one vertex to another does* not *form a group for the composition. Even worse, we cannot see a translation of the plane as a function on pointed graphs. The functions τ_{mn} on the other hand are well defined on T-graphs but are not usual translations. Indeed for fixed pointed graph T, $\tau_{mn}T$ is a translate of T but the translation vector depends on T. In the ergodicity argument we need well defined functions so we have to use the τ_{mn} but the only thing we really use is the idea of a translation invariant event which does not depend on the existence of a group on the set of translation.*

4.4 Identification of the covariance

In this section we show that the covariance in the above central limit theorem is proportional to the identity. We use an approach completely different from the one above. The main idea of the proof can be summarized in the following way. We know from the connection between T-graph and dimer model one specific discrete harmonic function on T (see [Ken07]). However on large scale the random walk on T is similar to a brownian motion with

some limit covariance matrix M so discrete harmonic functions should be almost continuous harmonic function for the Laplacian associated to M. To identify the covariance it it thus enough to find the only Laplacian for which our specific discrete harmonic function is almost continuous harmonic.

According to the previous sketch, the first step is the construction a specific discrete harmonic function. We will actually only construct a function harmonic except for a unit discontinuity along a line, similar to $\arg(z)$.

4.4.1 Dimer model

We give a few background informations about the hexagonal dimer model for the reader to be able to see where our harmonic function comes from.

Definition 4.4.1. *A* dimer covering *or perfect matching of $\mathcal{H}$ is a subset D of edges of $\mathcal{H}$ such that each vertex is in one and only one edge of D. Dimer coverings of $\mathcal{H}$ can also be seen as lozenge tilings of the plane.*

Theorem 4.4.2. *[She05] For all p_a, p_b, p_c in $(0,1)$ such that $p_a+p_b+p_c = 1$, there exists a unique ergodic Gibbs measure μ on dimer coverings such that :*

- *the conditional measure on any finite subgraph of $\mathcal{H}$ is uniform;*
- *vertical (resp. NE-SW, NW-SE) edges appear with probability p_a (resp. p_b, p_c).*

The distribution of dimers in these measures are given by determinantal process whose kernels are the inverses of the infinite matrix K which was defined in Section 4.2.2.

Theorem 4.4.3. *[KOS06] Let μ be an ergodic Gibbs measure on dimer coverings of $\mathcal{H}$. There exists an infinite matrix K^{-1}, indexed by white and black vertices of $\mathcal{H}$ such that, for all sets of edges $(w_1b_1), \dots, (w_nb_n)$,*

$$\mu(\forall i, w_ib_i \in D) = \prod_i K(w_i, b_i) \det\left(K^{-1}(b_k, w_l)\right)_{1\leq k,l\leq n}$$

Remark 4.4.4. *The notation K^{-1} for the kernel is justified because it is indeed an inverse of K, as can be seen from the compatibility condition around single vertices. K being an infinite matrix there is no contradiction with it having many inverses. However only one of them is bounded, and for this inverse we have the following expression.*

Proposition 4.4.5. *[KOS06] The only bounded inverse of K has the asymptotic expansion*

$$K^{-1}(b,w) = \frac{1}{2\pi}\Im\left(\frac{\bar{f}(b)g(w)}{\ell(m(w),n(w)) - \ell(m(b),n(b))}\right) + O\left(\frac{1}{\|w-b\|^2}\right)$$

where $O(\|w-b\|^{-2})$ has to be understood as $\frac{h(b,w)}{\|w-b\|^2}$ with h bounded on $\mathbb{Z}^2$ and $\Im(z)$ denotes the imaginary part of z. Recall that ℓ is an explicit linear map, $\ell(m,n) = \frac{a\alpha}{2}m - \frac{c\gamma}{2}n$.

4.4.2 Covariance

In all this section we work with a fixed graph and we will omit the parameters λ, Δ.

Definition 4.4.6. *A function h on T is discrete harmonic if and only if, for all $x \in T$,*

$$\mathbb{E}_x[h(X_1)] = h(x)$$

Notation 4.4.7. We define $K_T(w,b) = \Re(\bar{\lambda}\bar{f}(b))\lambda g(w)K(b,w)$. We let K^{-1} denote the only bounded inverse of K defined above. It is easy to see that K_T is also invertible and that the matrix $K_T^{-1}(b,w) = \frac{1}{\Re(\bar{\lambda}\bar{f}(b))\lambda g(w)}K^{-1}(b,w)$ is an inverse of K_T.

Remark 4.4.8. *We have $K_T(w,b) = \phi(wb)$ so we have only reinterpreted a flow on edges as a matrix.*

Our harmonic function will be the primitive of K_T^{-1}.

Proposition 4.4.9. *Let w be a face of T and let d be a half line from the interior of w to infinity that avoids all vertices of T. There exists an unique (up to a constant) function $G^*_{wd} : T \to \mathbb{C}$ such that:*

- *G^*_{wd} is continuous except for -1 discontinuity when crossing d counterclockwise.*
- *G^*_{wd} is linear on edges of T (on edges where it is discontinuous it is linear plus an Heaviside function)*
- *for any segment with endpoints x^+ and x^-, $G^*_{wd}(x^+) - G^*_{wd}(x^-) = K_T^{-1}(b,w)(x^+ - x^-)$ (with a additional $+1$ on discontinuous edges)*

Proof. It is clear that the properties define G^*_{wd} completely, the only thing we have to check is that the definition is consistent. It is enough to check that the increments of G^*_{wd} around any face sum to 0.

Given w' a face of T, we write x_1, x_2, x_3 its vertices and b_i the segment between x_i and x_{i+1} (with convention $x_4 = x_1$), we have :

$$\begin{aligned} G^*_{wd}(x_{i+1}) - G^*_{wd}(x_i) &= K_T^{-1}(b_i,w)(x_{i+1} - x_i) \\ &= K_T^{-1}(b_i,w)\phi^*(w',b_i) \text{ by definition of } T \\ &= K_T^{-1}(b_i,w)K_T(w',b_i) \end{aligned}$$

on edges where G^*_{wd} is continuous. On edges where G^*_{wd} is discontinous the same holds with a $+1$.

Finally $K_T K_T^{-1} = Id$ so the above terms sum to 0 on faces that are not w since either all edges are continuous or there are exactly one $+1$ and one -1 discontinuity. Around the face w there is a -1 discontinuity and the $K^{-1}K$ sum to 1 so in the end G^*_{wd} is well defined. □

Remark 4.4.10. *G^*_{wd} is discrete harmonic except on edges where it is discontinuous.*

The asymptotic formula for K^{-1} allows us to get an asymptotic expansion of G^*_{wd} :

Proposition 4.4.11. *We have,*

$$G^*_{wd}(\psi(b)) = \frac{1}{2\pi}\Big(\arg_d(\psi(b)-w)+\frac{\Im(\bar\lambda\bar f(w_0))}{\Re(\bar\lambda\bar f(w_0))}\log|\psi(b)-w|\Big)+C+O(\frac{1}{\psi(b)-w})$$

where $\arg_d$ *denotes the determination of the argument with a* 2π *discontinuity on the half line* d *and* C *is a suitable constant.*

Proof. The proof is a direct computation. We pull back G^*_{wd} as a function on $\mathcal{H}^*$ where we can explicitly integrate K_T^{-1} and then we use the almost linearity of the mapping ψ to go back to T.

Before we start with the formulas, a word about the discontinuity of G^*. When we consider a linear path $P_{\mathcal{H}^*}$ on $\mathcal{H}^*$, it corresponds to a path $P_T = \psi(P_{\mathcal{H}^*})$ in T which is not linear and might cross the half line d a number of time. However by almost linearity we see that P_T can only make a finite number of loops around w. Thus, taking $P_{\mathcal{H}^*}$ far enough from 0 we can make sure P_T does not make any loop around w. For such a path the discontinuity of G^*_{wd} give exactly the same contribution as the discontinuity of $\arg_d$ so we can drop it from the computation.

Fix b a black vertex of coordinates $(m,0)$, we compute $G^*_{wd}(\psi(b)) - G^*_{wd}(\psi(b(0,0)))$. For simplicity, we assume, since G^*_{wd} is defined up to a constant, that $G^*_{wd}(\psi(b(0,0))) = 0$. We have, writing $b_j = b(j,0)$ and $w_j = w(j,0)$:

$$\begin{aligned}
G^*_{wd}(\psi(b)) &= \sum_{j=0}^{m-1} K_T(w_j,b_j)K_T^{-1}(b_j,w_0)\\
&= \sum_{j=0}^{m-1} K(w_j,b_j)\Re(\bar\lambda\bar f(w_j))\lambda g(b_j)\frac{1}{\Re(\bar\lambda f(w_0))}\frac{1}{\lambda g(b_j)}K^{-1}(b_j,w_0)\\
&= \sum_{j=0}^{m-1} K(w_j,b_j)\frac{\Re(\bar\lambda\bar f(w_j))}{\Re(\bar\lambda\bar f(w_0))}\Im\left(\frac{\bar f(w_0)g(b_j)}{2\pi\ell(j,0)}\right)+\frac{h(j)}{j^2+1}
\end{aligned}$$

Expanding the real and imaginary parts and replacing $K(w_j, b_j) = a$

$$\begin{aligned} G^*_{wd}(\psi(b)) &= \frac{a}{8i\pi\Re(\bar\lambda\bar f(w_0))}\times \\ &\quad \sum_{j=0}^{m-1}(\bar\lambda\bar f(w_j)+\lambda f(w_j))(\frac{\bar f(w_0)g(b_j)}{\ell(j,0)}-\frac{f(w_0)\bar g(b_j)}{\bar\ell(j,0)})+\frac{h(j)}{j^2+1} \\ &= \frac{a}{8i\pi\Re(\bar\lambda\bar f(w_0))}\sum_{j=0}^{m-1}\Big(\frac{\bar f(w_0)g(b_j)\bar\lambda\bar f(w_j)}{\ell(j,0)}-\frac{f(w_0)\bar g(b_j)\lambda f(w_j)}{\bar\ell(j,0)} \\ &\qquad +\frac{\bar f(w_0)g(b_j)\lambda f(w_j)}{\ell(j,0)}-\frac{f(w_0)\bar g(b_j)\bar\lambda\bar f(w_j)}{\bar\ell(j,0)}\Big)+\frac{h(j)}{j^2+1}. \end{aligned}$$

Thanks to the definition of f and g, the product $\bar f(w_j)g(b_j)$ does not depend on j (it is actually α, see remark 4.2.2) so the first two terms give harmonic sums. On the other hand the two last terms have an oscillating factor so they converge and the remainder of their sum is of order $1/m$. Finally the $O(1/j^2)$ terms also converge with a $1/m$ remainder. Overall we get, for black vertices of the form $b(m,0)$:

$$\begin{aligned} G^*_{wd}(\psi(b)) &= \frac{a}{8i\pi\Re(\bar\lambda\bar f(w_0))}\sum_{j=0}^{m-1}2i\Im\frac{\alpha\bar\lambda\bar f(w_0)}{\ell(j,0)}+C+O(1/m) \\ &= \frac{1}{2\pi}\frac{\Im(\bar\lambda\bar f(w_0))}{\Re(\bar\lambda\bar f(w_0))}\log(m)+C+O(1/m) \end{aligned}$$

where in the last line we replaced $\ell(j,0) = a\alpha j/2$ (see section 4.2.2).

We still have to check what happens in the n direction in order to identify the bounded dependence on the argument. The most natural way to do this would be to compute G^*_{wd} along a circle, however for technical reason we will compute it along a parallelogram.

We first compute $G^*_{wd}(\psi(b(m,n))) - G^*_{wd}(\psi(b(m,0))$ for $|n| \le m$. It is also equal to a sum of n terms along a straight path but this time in the y direction. The computations above are still valid except that we have to replace w_j and b_j by the black and white vertices of the edges crossed by a path in the y directions. For these NW-SE edges (recall section 4.2.1 and remark 4.2.2), the coordinates of w_j are (m, j), the coordinates of b_j are $(m-1, j+1)$, $K(w_j, b_j) = c$ and $\bar f(w_j)g(b_j) = \gamma$. Going back to the

expression of G^*_{wd} we get

$$G^*_{wd}(\psi(b(m,n))) - G^*_{wd}(\psi(b(m,0)) = \frac{c}{8i\pi\Re(\bar\lambda\bar f(w_0))}\sum_{j=0}^{n-1}(\bar\lambda\bar f(w_j) + \lambda f(w_j))$$
$$\times\,(\frac{\bar f(w_0)g(w_j)}{\ell(m-1,j+1)} - \frac{f(w_0)\bar g(b_j)}{\bar\ell(m-1,j+1)}) + \frac{h(j)}{m^2+j^2+1}$$
$$= \frac{1}{8i\pi\Re(\bar\lambda\bar f(w_0))}\sum_j 2i\Im(\frac{c\gamma\bar\lambda\bar f(w_0)}{\ell(m-1,j+1)})+$$
$$\sum_j 2i\Im(\frac{c\gamma\bar\lambda f(w_0)}{\ell(m-1,j+1)}(\frac{\beta}{\gamma})^{2m}(\frac{\beta}{\alpha})^{2j}) + \sum_j \frac{h(j)}{m^2+j^2+1}.$$

The last sum is of order $O(1/m)$ because it contains at most m terms of order $1/m^2$, the second one is an oscillating sum of terms of order $1/m$ and is thus also $O(1/m)$, so we have :

$$G^*_{wd}(\psi(b(m,n))) - G^*_{wd}(\psi(b(m,0)) =$$
$$\frac{1}{4\pi\Re(\bar\lambda\bar f(w_0))}\Im\Big(\sum_j \frac{\bar\lambda\bar f(w_0)c\gamma}{-\frac{a\alpha}{2}(m-1)+\frac{c\gamma}{2}(j+1)}\Big) + O(\frac{1}{m}).$$

The sum is approximately (up to $O(1/m)$) the integral of $2/z$ between $\psi(b(m,0))$ and $\psi(b(m,n))$ so it gives $2\log(|\psi(b(m,n))|)+2i\arg_d(\psi(b(m,n)))-2\log(|\psi(b(m,0)|)) - 2i\arg_d(\psi(b(m,0)))$. Finally we have

$$\Im(\bar\lambda\bar f(w_0)\sum_j \frac{c\gamma}{-\frac{a\alpha}{2}m+\frac{c\gamma}{2}j}) = 2\Re(\bar\lambda\bar f(w_0))(\arg_d(b(m,n)) - \arg_d(b(m,0)))$$
$$+ 2\Im(\bar\lambda\bar f(w_0))(\log(|b(m,n)|) - \log(|b(m,0)|))$$

and together with the previous estimate on $G^*_{wd}(\psi(b(m,0))$ we find, for any point with $|n| \le m$,

$$G^*_{wd}(\psi(b(m,n)) =$$
$$\frac{1}{2\pi}\Big(\arg_d(\psi(b)-w) + \frac{\Im(\bar\lambda\bar f(w_0))}{\Re(\bar\lambda\bar f(w_0))}\log|\psi(b)-w|\Big) + C + O(1/(\psi(b)-w))$$

with a constant that does not depend on (m,n).

We can obtain the value of G^*_{wd} on the other sides of the parallelogram $\|(m',n')\|_\infty = m$ using exactly the same computation.

□

The above proposition is already almost a proof that the covariance in the central limit theorem is proportional to the identity. Indeed the only thing left to say is that the large scale behavior of G^*_{wd} has to be harmonic for

the Laplacian corresponding to the limit covariance. We turn this result into a precise statement now. This requires some cumbersome integral expression but it is really only straightforward calculus.

Proposition 4.4.12. *The covariance matrix in theorem 4.3.18 is proportional to the identity.*

Proof. Fix v a vertex of T. To simplify notations we will assume that v has coordinates $(0,0)$ in the plane where lies T and is on the segment of coordinates $(0,0)$.

We can assume by rotating the axes that M is diagonal with coefficients $M_{11} \leq M_{22}$. Fix $\epsilon > 0$ and D large enough. Let w_n be a sequence of faces of T with $w_n - v \sim Dn\mathbf{e_y}$. Let d_n be a sequence of almost vertical half lines from w_n going up and that avoid all vertices. To simplify notations, let G_n^* denote $G^*_{w_n d_n}$.

Let τ_n be the minimum between n^2 and the first exit of X_t from the ball of radius $nD/2$ and of center $(0,0) = X_0$. Let B_t denote the brownian motion of covariance M and let τ_∞ be the minimum between 1 and the exit time of B_t from the ball of radius $D/2$. Remark that B_t is almost surely a continuity point of τ_∞, seen as a function of the trajectory $(B_t)_{t\in[0,1]}$ so X_{τ_n}/n converges in distribution to B_{τ_∞}. Note also that the probability that $\tau_n \neq n^2$ is of order $e^{-D^2/8}$.

By discrete harmonicity, we have $\mathbb{E}_v(G_n^*(X_{\tau_n})) = G_n^*(v)$. On the other hand using the asymptotic formula, where we write c_n for $\frac{\Im\bar{\lambda}\bar{f}(w_n)}{\Re\bar{\lambda}\bar{f}(w_n)}$:

$$\begin{aligned}
\mathbb{E}_v(G_n(X_{\tau_n})) &= \mathbb{E}_v\left[\frac{1}{2\pi}\Big(\arg_{d_n}(X_{\tau_n} - w_n) + c_n \log|X_{\tau_n} - w_n|\Big) + \frac{h(X_{\tau_n})}{|X_{\tau_n} - w|}\right] \\
&= \frac{c_n}{2\pi}\log(Dn) + \frac{1}{2\pi}\mathbb{E}\Big[\arg_{d_n}(\frac{X_{\tau_n} - w_n}{n})\Big] \\
&\quad + \frac{c_n}{2\pi}\mathbb{E}\Big[\log|\frac{X_{\tau_n} - w_n}{Dn}|\Big] + O(\frac{1}{nD}) \\
&= G_n^*(v) + \frac{c_n}{2\pi}\mathbb{E}\Big[\log|\frac{X_{\tau_n} - w_n}{Dn}|\Big] + o(1) + O(e^{-D^2/8}).
\end{aligned}$$

In the last line, we first replaced τ_n by n^2 which gives an error $O(e^{-D^2/8})$ then we used the central limit theorem to replace the first expectation by $1/2 + o(1)$ (remark that with our choice $\arg_{d_n}(v) = \pi$) and finally we used the asymptotic formula $G_n^*(v) = \frac{c_n}{2\pi}\log(Dn) + 1/2 + O(\frac{1}{nD})$. To finish the proof we just have to prove that $\frac{c_n}{2\pi}\mathbb{E}\Big[\log|\frac{X_{\tau_n} - w_n}{Dn}|\Big]$ does not vanish with n and is bigger than $O(e^{-D^2/8})$.

We can choose w_n such that c_n converges to a non zero value. For the expectation, the central limit theorem gives the limit

$$\mathbb{E}\Big[\log|\frac{X_{\tau_n} - w_n}{Dn}|\Big] \to \mathbb{E}[\log|\frac{B_{\tau_\infty}}{D} - i|].$$

In the limit of large D, the integral on the right hand side becomes

$$\begin{aligned}
\mathbb{E}[\log|\frac{B_{\tau_\infty}}{D} - i|] &= \int \log|\frac{x}{D} - i|\mathrm{d}N(0,C) + O(e^{-D^2/8}) \\
&= \int \tfrac{1}{2}\log\Big(M_{11}\frac{x^2}{D^2} + (1-\sqrt{M_{22}}\frac{y}{D})^2\Big)\frac{e^{-\frac{x^2}{2}}e^{-\frac{y^2}{2}}}{2\pi}\mathrm{d}x\mathrm{d}y \\
&\qquad + O(e^{-D^2/8}) \\
&= \tfrac{1}{2}\int \log\Big(1 - 2\sqrt{M_{22}}\frac{y}{D} + M_{11}\frac{x^2}{D^2} + M_{22}\frac{y^2}{D^2}\Big) \\
&\qquad \frac{e^{-\frac{x^2}{2}}e^{-\frac{y^2}{2}}}{2\pi}\mathrm{d}x\mathrm{d}y + O(e^{-D^2/8}) \\
&= \tfrac{1}{2}\int \left(-2\sqrt{M_{22}}\frac{y}{D} + M_{11}\frac{x^2}{D^2} + M_{22}\frac{y^2}{D^2} - \tfrac{1}{2}(\sqrt{M_{22}}\frac{2y}{D})^2\right) \\
&\qquad \frac{e^{-\frac{x^2}{2}}e^{-\frac{y^2}{2}}}{2\pi}\mathrm{d}x\mathrm{d}y + O(\frac{1}{D^3}) \\
&= \tfrac{1}{2D^2}(M_{11} - M_{22})\int y^2\frac{e^{-\frac{y^2}{2}}}{\sqrt{2\pi}}\mathrm{d}x + O(\frac{1}{D^3}).
\end{aligned}$$

The expansion of log is legal in the fourth line by dominated convergence. In the last line we just remark that we can separate the integrals over x and y and that both give the same term. For $M_{11} \neq M_{22}$ the integral is of order $1/D^2$ and we have the contradiction we were looking for. □

Bibliography

[BMF82] J. Bricmont, A. El Mellouki, and J. Fröhhlich. Random surfaces in statistical mechanics: roughening, rounding, wetting... *J. Statist. Phys.*, 29:193–203, 1982.

[Bou09] Cédric Boutillier. The bead model and limit behaviors of dimer models. *Annals of Probability*, 37,No.1:107–142, 2009.

[BP93] Robert Burton and Robin Pemantle. Local characteristics, entropy and limit theorems for spanning trees and domino tilings via transfer-impedances. *Ann. Prob.,*, 21,:1329–1371, 1993.

[BW82] R. Brandenberger and C. E. Wayne. Decay of correlations in surface models. *J. Statist. Phys*, 27:425–440, 1982.

[CEP96] Henry Cohn, Noam Elkies, and James Propp. Local statistics for random domino tilings of the Aztec diamond. *Duke Math. J.*, 85(1):117–166, 1996.

[CKP01] Henry Cohn, Richard Kenyon, and James Propp. A variational principle for domino tilings. *Journal of the AMS*, 14:,297–346, 2001.

[CLM$^+$] P. Caputo, E. Lubetzky, F. Martinelli, A. Sly, and F. L. Toninelli. Dynamics of 2+1 dimensional sos surfaces above a wall: slow mixing induced by entropic repulsion. to appear on Ann. Probab. arXiv:1205.6884.

[CLP98] Henry Cohn, Michael Larsen, and James Propp. The shape of a typical boxed plane partition. *New York Journal of Mathematics*, 4:137–165, 1998.

[CMST10] P. Caputo, F. Martinelli, F. Simenhaus, and F.L. Toninelli. Zero temperature stochastic 3d ising model and dimer covering fluctuations: A first step towards interface mean curvature motion. *Communications on Pure and Applied Mathematics*, 64:778–831, 2010.

[CMT12] Pietro Caputo, Fabio Martinelli, and Fabio Lucio Toninelli. Mixing times of monotone surfaces and sos interfaces: a mean curvature approach. *Comm. Math. Phys.*, 311:157–189, January 2012.

[Des02] N. Destainville. Flip dynamics in octagonal rhombus tiling sets. *Phys. Rev. Lett.*, 88:030601, Jan 2002.

[DSC93] P. Diaconis and L. Saloff-Coste. Comparison theorems for reversible markov chains. *Annals of Applied Probability*, 3:696–730, 1993.

[Fou96] J.C Fournier. Pavage des figures planes sans trous par des dominos: Fondement graphique de l'algorithme de thurston, parallélisation, unicité et décomposition. *Theoretical Computer Science*, 159(1):105 – 128, 1996.

[FS97] T. Funaki and Herbert Spohn. Motion by mean curvature from the ginzburg-landau $\nabla\phi$ interface model. *Communication in Mathematical Physics*, 185:1–36, 1997.

[Fun03] Tadahisa Funaki. *École d'été de probabilité de Saint-Flour XXXIII-2003*, chapter Stochastic interface models, pages 103–274. Lectures on Probability Theory and Statistics. Springer, 2003.

[Gia83] M. Giaquinta. *Multiple integrals in the calculus of variations and nonlinear elliptic systems*, volume 105. Princeton University Press, 1983.

[Gor72] W. B. Gordon. On the diffeomorphisms of euclidean space. *Amer. Math. Monthly*, 79:755–759, 1972.

[Had06] J. Hadamard. Sur les tranformations ponctuelles. *Bull. Soc. Math. France*, 34:71–94, 1906. Oeuvres, pp. 349–363 and pp. 383–384.

[Hen97] C. L. Henley. Relaxation time for a dimer covering with height representation. *J. Statist. Phys.*, 89:483–507, 1997.

[JPS95] William Jockusch, James Propp, and Peter Shor. Random domino tilings and the arctic circle theorem. http://arxiv.org/abs/math/9801068, 1995.

[Kas61] P. W. Kasteleyn. The statistics of dimers on a lattice, i. the number of dimer arrangements on a quadratic lattice. *Physica*, 27:1209–1225, 1961.

[Ken00] Richard Kenyon. Conformal invariance of domino tiling. *Annals of Probability*, 28:759–795, 2000.

[Ken01] R. Kenyon. Dominos and the gaussian free field. *Ann. Prob.*, 29:1128–1137, 2001.

[Ken07] Richard Kenyon. Height fluctuations in the honeycomb dimer model. *Communications in Mathematical Physics*, 281(3):675–709, 2007.

[Ken09] Richard Kenyon. Lectures on dimers, October 2009.

[KO07] Richard Kenyon and Andrei Okounkov. Limit shapes and the complex burgers equation. *Acta Mathematica*, 199:263–302, 2007.

[KOS06] Richard Kenyon, Andrei Okounkov, and Scott Sheffield. Dimers and amoebae. *Annals of Mathematics*, 163:1019–1056, 2006.

[KPW00] Richard Kenyon, James G. Propp, and David B. Wilson. Trees and matchings. *Electronic Journal of Combinatorics*, 7(1):R25,, 2000.

[KS04] Richard Kenyon and Scott Sheffield. Dimers, tilings and trees. *Journal combinatorial theory B*, 92:295–317, 2004.

[KT90] Hung-Ju Kuo and Neil S. Trudinger. Linear elliptic difference inequalities with random coefficients. *Mathematics of computation*, 55:37–58, 1990.

[Las13] Benoit Laslier. Central limit theorem for the random walks on T-graphs. http://arxiv.org/abs/1312.3177, 2013.

[Law82] Gregory F. Lawler. Weak convergence of a random walk in a random environment. *Communications in Mathematical Physics*, 87(1):81–87, 1982.

[Li13] Zhongyang Li. Discrete complex analysis and t-graphs. http://www.statslab.cam.ac.uk/ zl296/dctg.pdf, 2013.

[LPW08] David A. Levin, Yuval Peres, and Elizabeth L. Wilmer. *Markov Chains and Mixing times*. American Mathematical Society, 2008.

[LRS01] Michael Luby, Dana Randall, and Alistair Sinclair. Markov chain algorithms for planar lattice structures. *SIAM journal on Computing*, 31(1):167–192, 2001.

[LST11] H. Lacoin, F. Simenhaus, and F. L. Toninelli. Zero-temperature 2d ising model and anisotropic curve-shortening flow. to appear on J. Eur. Math Soc., December 2011.

[LST13] H. Lacoin, F. Simenhaus, and F. L. Toninelli. The heat equation shrinks ising droplets to points. to appear on Comm. Pure Appl. Math., June 2013.

[LT12] Benoit Laslier and Fabio Toninelli. How quickly can we sample a uniform domino tiling of the 2l x 2l square via gauber dynamics? http://arxiv.org/abs/1210.5456, to appear in Prob. Th. Rel. Fields, October 2012.

[LT13] Benoit Laslier and Fabio Lucio Toninelli. Lozenge tilings, glauber dynamics and macroscopic shape. http://arxiv.org/abs/1310.5844, 2013.

[Mac15] Percy Alexander MacMahon. *Combinatorial Analysis*. Cambridge University Press, 1915.

[MS06] M. Mucha and P. Sankowski. Maximum matchings in planar graph via gaussian elimination. *Algorithmica*, 45:3–20, 2006.

[Pet12a] Leonid Petrov. Asymptotics of random lozenge tilings via gelfand-tsetlin schemes. http://arxiv.org/abs/1202.3901, February 2012.

[Pet12b] Leonid Petrov. Asymptotics of uniformly random lozenge tilings of polygons. gaussian free field. http://arxiv.org/abs/1206.5123, June 2012.

[Pro03] J. Propp. Generalized domino-shuffling. *Theoret. Comput. Sci.*, 303:267–301, 2003.

[PW11] Yuval Peres and Peter Winkler. Can extra updates delay mixing?, December 2011. arXiv:1112.0603.

[RT00] Dana Randall and Prasad Tetali. Analyzing glauber dynamics by comparison of markov chains. *Journal of Mathematical Physics*, 41:1598–1615, 2000.

[She05] Scott Sheffield. *Random Surfaces*, volume 304. Société mathématique de France, Asterisque, 2005.

[Sos00] A. Soshnikov. Determinantal random point fields. *Russ. Math. Surv.*, 55:923–975, 2000.

[Spo93] Herbert Spohn. Interface motion in models with stochastic dynamics. *Journal of Statistical Physics*, 71(5-6):1081–1132, 1993.

[Szn02] Alain-Sol Sznitman. *Ten Lectures on Random Media*, volume 32 of *Oberwolfach Seminars*, chapter 1 and 2, pages 9–22. Birkhäuser, 2002.

[Tem52] H. N. V. Temperley. Statistical mechanics and the partition of numbers. ii. the form of crystal surfaces. *Proc. Cambridge Philos. Soc.*, 48:683–697, 1952.

[Tem74] H. Temperley. In *Combinatorics: Proceedings of the British Combinatorial Conference 1973*, number 13 in Lecture Notes Series, pages 202–204. London Math. Soc., 1974.

[TF61] W. Temperley and M. Fisher. Dimer problem in statistical mechanics–an exact result. *Philosophical Magazine*, 68:1061–1063, 1961.

[Wil96] D. B. Wilson. Generating random spanning trees more quickly than the cover time. In *Proc. of the 28th annual ACM symposium on Theory of computing (STOC '96)*, pages 296–303, 1996.

[Wil97] D. B. Wilson. Determinant algorithms for random planar structures. In *Proc. Eighth Annual ACM-SIAM Symposium on Discrete Algorithms*, pages 258–267, 1997.

[Wil04] David B. Wilson. Mixing times of lozenge tiling and card shuffling markov chains. *Annals of Applied Probability*, 14:274–325, 2004.

[Zei02] Ofer Zeitouni. Random walks in random environments. *Proceedings of the ICM, Beijing*, 3:117–130, 2002.